Available online at www.sciencedirect.com

SciVerse ScienceDirect

Nuclear Data Sheets 112 (2011) 2887–2996

Nuclear Data Sheets

www.elsevier.com/locate/nds

ENDF/B-VII.1 Nuclear Data for Science and Technology: Cross Sections, Covariances, Fission Product Yields and Decay Data

M.B. Chadwick,[1,*] M. Herman,[2] P. Obložinský,[2] M.E. Dunn,[3] Y. Danon,[4] A.C. Kahler,[1] D.L. Smith,[5] B. Pritychenko,[2] G. Arbanas,[3] R. Arcilla,[2] R. Brewer,[1] D.A. Brown,[2,6] R. Capote,[7] A.D. Carlson,[8] Y.S. Cho,[13] H. Derrien,[3] K. Guber,[3] G.M. Hale,[1] S. Hoblit,[2] S. Holloway,[1] T.D. Johnson,[2] T. Kawano,[1] B.C. Kiedrowski,[1] H. Kim,[13] S. Kunieda,[1,15] N.M. Larson,[3] L. Leal,[3] J.P. Lestone,[1] R.C. Little,[1] E.A. McCutchan,[2] R.E. MacFarlane,[1] M. MacInnes,[1] C.M. Mattoon,[6] R.D. McKnight,[5] S.F. Mughabghab,[2] G.P.A. Nobre,[2] G. Palmiotti,[14] A. Palumbo,[2] M.T. Pigni,[3] V.G. Pronyaev,[9] R.O. Sayer,[3] A.A. Sonzogni,[2] N.C. Summers,[6] P. Talou,[1] I.J. Thompson,[6] A. Trkov,[10] R.L. Vogt,[6] S.C. van der Marck,[11] A. Wallner, [12] M.C. White,[1] D. Wiarda,[3] P.G. Young[1]

[1] *Los Alamos National Laboratory, Los Alamos, NM 87545, USA*
[2] *Brookhaven National Laboratory, Upton, NY 11973-5000, USA*
[3] *Oak Ridge National Laboratory, Oak Ridge, TN 37831-6171, USA*
[4] *Rensselaer Polytechnic Institute, Troy, NY 12180, USA*
[5] *Argonne National Laboratory, Argonne, IL 60439-4842 USA*
[6] *Lawrence Livermore National Laboratory, Livermore, CA 94551-0808, USA*
[7] *International Atomic Energy Agency, Vienna-A-1400, PO Box 100, Austria*
[8] *National Institute of Standards and Technology, Gaithersburg, MD 20899-8463, USA*
[9] *Institute of Physics and Power Engineering, Obninsk, Russian Federation*
[10] *Jozef Stefan Institute, Jamova 39, 1000 Ljubljana, Slovenia*
[11] *Nuclear Research and Consultancy Group, P.O. Box 25, NL-1755, ZG Petten, The Netherlands*
[12] *Faculty of Physics, University of Vienna, Waehringer Strasse 17, A-1090 Vienna, Austria*
[13] *Korea Atomic Energy Research Institute, Daejeon, Korea*
[14] *Idaho National Laboratory, Idaho Falls, ID 83415, USA and*
[15] *Japan Atomic Energy Agency, Tokai-mura Naka-gun, Ibaraki 319-1195, Japan*

(Received 12 July 2011; revised received 22 September 2011; accepted 17 October 2011)

The ENDF/B-VII.1 library is our latest recommended evaluated nuclear data file for use in nuclear science and technology applications, and incorporates advances made in the five years since the release of ENDF/B-VII.0. These advances focus on neutron cross sections, covariances, fission product yields and decay data, and represent work by the US Cross Section Evaluation Working Group (CSEWG) in nuclear data evaluation that utilizes developments in nuclear theory, modeling, simulation, and experiment.

The principal advances in the new library are: (1) An increase in the breadth of neutron reaction cross section coverage, extending from 393 nuclides to 423 nuclides; (2) Covariance uncertainty data for 190 of the most important nuclides, as documented in companion papers in this edition; (3) R-matrix analyses of neutron reactions on light nuclei, including isotopes of He, Li, and Be; (4) Resonance parameter analyses at lower energies and statistical high energy reactions for isotopes of Cl, K, Ti, V, Mn, Cr, Ni, Zr and W; (5) Modifications to thermal neutron reactions on fission products (isotopes of Mo, Tc, Rh, Ag, Cs, Nd, Sm, Eu) and neutron absorber materials (Cd, Gd); (6) Improved minor actinide evaluations for isotopes of U, Np, Pu, and Am (we are not making changes to the major actinides ^{235,238}U and ^{239}Pu at this point, except for delayed neutron data and covariances, and instead we intend to update them after a further period of research in experiment and theory), and our adoption of JENDL-4.0 evaluations for isotopes of Cm, Bk, Cf, Es, Fm, and some other minor actinides; (7) Fission energy release evaluations; (8) Fission product yield advances for fission-spectrum neutrons and 14 MeV neutrons incident on ^{239}Pu; and (9) A new decay data sublibrary.

Integral validation testing of the ENDF/B-VII.1 library is provided for a variety of quantities: For nuclear criticality, the VII.1 library maintains the generally-good performance seen for VII.0 for a wide range of MCNP simulations of criticality benchmarks, with improved performance coming from new structural material evaluations, especially for Ti, Mn, Cr, Zr and W. For Be we see some improvements although the fast assembly data appear to be mutually inconsistent. Actinide cross section updates are also assessed through comparisons of fission and capture reaction rate measurements in critical assemblies and fast reactors, and improvements are evident. Maxwellian-averaged capture cross sections at 30 keV are also provided for astrophysics applications.

We describe the cross section evaluations that have been updated for ENDF/B-VII.1 and the measured data and calculations that motivated the changes, and therefore this paper augments the ENDF/B-VII.0 publication [1].

*) Electronic address: mbchadwick@lanl.gov

doi:10.1016/j.nds.2011.11.002

Contents

I. INTRODUCTION

The previous ENDF/B-VII.0 database was released in 2006 [1] and has been widely adopted by researchers in nuclear science and technology. It represented the culmination of many years of work by the US nuclear data evaluation, simulation, theory and modeling, and experimental research communities, and benefited from international collaborations, especially for the standards and for the integral data validation testing. As a measure of its impact, in the 5 years since the release of the library it has been referred to 1400 times in articles and proceedings according to Google Scholar, with over 450 citations to our reference paper [1]. A detailed document on the processing of ENDF/B-VII.0 for applications, using the NJOY code, has also been written [2], together with follow-on papers that described the actinide and radiochemical dosimetry cross section evaluations in ENDF/B-VII.0 in more detail [3, 4, 5], and that summarized integral validation testing [6]. The ENDF/B-VII.0 neutron cross section standards were documented in a comprehensive paper by Carlson *et al.* [7].

Our new ENDF/B-VII.1 library described in the present paper integrates the community's research efforts over the last few years, and builds on the earlier ENDF/B-VII.0 library in various ways: Extensive nuclear reaction data on uncertainties (covariance data evaluations) are provided for 190 isotopes that are particularly important in nuclear technology applications. Minor actinide cross section evaluations are improved. Structural material evaluations have been advanced through use of recent resolved and unresolved resonance analyses of new measured data. New light nucleus R-matrix evaluations have been developed for the nuclides ^{3}He, ^{9}Be, and ^{6}Li. Certain neutron capture cross sections on fission products have been updated. Fission product data for fast and 14 MeV neutrons incident on plutonium are developed, including details of the neutron energy dependence over the fast neutron range from 0.5–2.0 MeV. New data for fission energy release are provided, and a new decay data library has been created. In all, 229 ENDF/B-VII.0 evaluations have been updated, and 30 added, for ENDF/B-VII.1.

But for all the nuclear data evaluation upgrades described above, ENDF/B-VII.1 still preserves much of the ENDF/B-VII.0 library capabilities. We are only modifying the neutron, fission product yield, and decay data sublibraries and we have not changed the proton, photonuclear, charged particle, *etc.* databases. The ENDF/B-VII.0 standards evaluation [7] remains unchanged over their defined energy ranges for H(n,p), ^{3}He(n,p), ^{6}Li(n,t), ^{10}B(n,α), ^{12}C(n,n) (elastic), ^{197}Au(n,γ), ^{235}U(n,f) and ^{238}U(n,f). And we are not changing the major actinide ^{235,238}U and ^{239}Pu evaluations (except for delayed neutrons and covariances), although later in Section XI we summarize ongoing work in these areas that will be likely incorporated into future library releases. We have sought to preserve, and improve

upon, the generally good integral data validation criticality testing seen in ENDF/B-VII.0 [1, 6], and this is summarized in Section X and described in greater detail in a companion paper in this edition [8].

The ENDF/B-VII.1 database has not been developed in isolation, but rather, it continues to evolve through close interactions with parallel organizations around the world, most notably with Europe (JEFF), Japan (JENDL), and with South Korea. Organizations such as the International Atomic Energy Agency (IAEA) and the Organization for Economic Cooperation and Development (OECD)'s Nuclear Energy Agency (NEA) provide valuable forums for exchanging developments in evaluation, measurement, and theory from laboratories across the world, including Russia, China, and India. The recent impressive JENDL-4.0 database has been documented by Shibata *et al.* and G. Chiba *et al.* [9, 10], as has the excellent JEFF-3.1.1 database [11].

Our ENDF/B-VII.1 library has borrowed many minor actinide evaluations from JENDL-4.0, as discussed further in this paper. Such a borrowing reflects our recognition of the significant amount of recent work devoted to these isotopes by our Japanese colleagues – many of the previous ENDF evaluations dated back many decades, and the US has not had the resources to improve these evaluations. Other national evaluation projects have historically been much influenced by US capabilities in various areas, such as: R-matrix light nucleus evaluations (*e.g* hydrogen, oxygen); thermal scattering constants, photoatomic, electroatomic, and photonuclear data; resonance data and analyses; fission product yields, and delayed neutron spectra. We have also had close collaborations with JEFF on actinide evaluations, notably in the resonance region (Oak Ridge and CEA/Cadarache), and in the fast region (LANL and CEA/Bruyères-le-Châtel).

This paper is organized as follows. Section II gives some perspectives on reasons for our release cycle of the ENDF/B library. Section III describes some notable deficiencies in the previous ENDF/B-VII.0 library that have motivated work on the present ENDF/B-VII.1 library. Section IV provides an overview of the contents of the ENDF/B-VII.1 library. Section V describes the covariance data (with companion papers in this edition adding many more details). Section VI gives detailed documentation on the new evaluations in ENDF/B-VII.1. Section VII describes the standards evaluations (unchanged from VII.0). Section VIII summarizes the new fission product yields we are recommending for fast and 14 MeV neutrons on plutonium. Section IX describes our new decay data sublibrary, which is largely derived from data from the Evaluated Nuclear Structure Data File (ENSDF). Section X provides a summary of integral validation data testing, with a companion paper in this edition by Kahler [8] giving more details. Section XI provides a summary of ongoing work that is not incorporated into ENDF/B-VII.1 but will most likely impact future ENDF library releases. Our conclusions are given in Section XII.

II. PERSPECTIVES ON UPDATING ENDF

Some readers might wonder why CSEWG is releasing ENDF updates so rarely — this update is five years since the previous ENDF/B-VII.0 library release. And in contrast, in the 1990s the releases of ENDF/B-VI occurred at a faster rate, occurring nearly every year on average for ENDF/B-VI.1 through VI.8.

The release schedule of a nuclear data library is set by a number of competing factors. New advances in nuclear data evaluations are being continually made and we have a desire to make these available to the broader user community promptly. But this must be balanced by our desire to ensure that the database has undergone a thorough validation testing process, and this can take more time. Also, since the impact of many of the evaluations tend to perform in concert in integral simulations of nuclear criticality it is important that we test the ensemble of data files together in our integral validation testing. Informal releases of updated evaluations are made available to sponsors more promptly than the official ENDF releases.

The cautious rate that we have adopted for library releases reflects the limited resources we have to devote to this work. It is true that all the efforts that have contributed to the ENDF/B-VII.1 release have been funded by a variety of US nuclear research and development programs (mainly the DOE), as well as contributions from some international funding agencies. Nevertheless, the integration of these various efforts into a single database only occurs because of the devotion that the CSEWG community has to the concept of ENDF — a freely available database that reflects our best understanding of nuclear reaction phenomena. We note that, as for ENDF/B-VII.0, we have benefited from the willingness of numerous retirees who are renowned experts in their disciplines to continue to contribute to ENDF, and to help mentor the new generation (who themselves are not as young as they used to be!).

We note that the majority of our users — whether in national security, nonproliferation, nuclear criticality safety, reactor design, medical applications, or fundamental science — are not particularly keen to move to new ENDF releases on a fast timetable. In many user communities it takes significant resources to update and rebenchmark and validate integrated neutronics simulation capabilities to a new ENDF database. Such users typically only want to do this when they are convinced that the new database has a sufficient number of advances to warrant the investment of such an effort. We believe that the new ENDF/B-VII.1 database should indeed warrant our user communities' attention.

III. DEFICIENCIES IN THE PREVIOUS ENDF/B-VII.0 LIBRARY

It is useful to summarize some of the weaknesses of the previous ENDF/B-VII.0 library that we aim to remove in this new VII.1 release. Some were known at the time of the release in 2006, whilst others have become evident in the intervening years through valuable feedback from users of the library. We itemize the most important of these issues below.

- **^{238,240}Pu**
  The previous evaluations for isotopes were quite old. We have developed new evaluations at higher energies based on modern GNASH model calculations and usage of experimental data, some only recently measured.

- **Minor actinide isotopes of U, Np, Am**
  Through validation studies using MCNP simulations compared with measured reaction rates of capture and fission in critical assemblies, we determined that some of the evaluations needed to be updated, and changes were made for ^{237}Np, ^{241,243}Am, ^{236,237}U and ^{242}Pu isotopes. ^{239}U was also upgraded to use new Livermore surrogate data for fission.

- **Minor actinide isotopes of Ac, Th, Pa, U, Np, Pu, Am, Cm, Bk, Cf, Es, Fm**
  In the ENDF/B-VII.0 release we were well aware that many of the minor actinide evaluations were of questionable quality and dated back to work done many decades ago. Such deficiencies were noted by some of our colleagues[12], but we have lacked the resources to work on upgrading these evaluations. To address this deficiency we have adopted 59 evaluations from the Japanese nuclear data community's recent work in JENDL-4.0, which appears to us to be of good quality.

- **Structural materials: Ti, V, Mn, Cr, Ni, W**
  The criticality safety program in the US recognized that nuclear data in the resolved and unresolved resonance region and the fast region need upgrading, and this was also reflected in the poor performance of the modeling of some critical assemblies, for example the ANL ZPR assemblies, using ENDF/B-VII.0. This has led to new evaluations that take advantage of new measured data from ORNL together with higher energy evaluations from LANL and abroad.

- **Fission product thermal capture**
  C. Dean wrote a paper that described some integral data testing sensitive to thermal capture cross sections of certain important fission products [13]. We have studied this and concluded that these experiments point to changes that need to be made in the underlying capture cross sections.

- **Fission product yields (FPY) from ^{239}Pu**
  A study on fission spectrum neutron FPY for plutonium identified that the England and Rider (ENDF/B-VI) data are too low by 4% for ^{99}Mo, an important reference fission product [14, 15]. Our new evaluation corrects this, and introduces information on the neutron incident energy dependence of FPY over the fast region from 0.5–2 MeV for the first time, which is needed for high-accuracy determinations of fission burnup in fast systems. In the course of this work we also have noted that we feel the previous evaluations in use at Livermore dating back to 1985 [16], JEFF [17, 18, 19, 20], and the CEA (Laurec's work [21]) are too low by typically 5–10% for the important dosimetry fission products ^{95}Zr, ^{99}Mo, ^{137}Cs, ^{140}Ba ^{141,144}Ce, and ^{147}Nd, for fission-spectrum neutrons incident on plutonium.

- **Delayed neutron data**
  We made changes in ENDF/B-VII.0 for delayed neutrons (DN), replacing the earlier ENDF/B-VI data with new results that were based on model calculations as well as measured data. The initial integral validation testing appeared to be generally benign, and favorable in some cases [6]. But we have received valuable feedback in recent years from many users, particularly B. Kiedrowski, C. Wemple, and Y. Yedvab, that the data are problematic. There is a lesson here: one should be wary of analyses that overly rely on theory predictions for cases where theory's predictive power is weak, and where insufficient attention is paid to experimental phenomenology. To correct this we are returning to ENDF/B-VI 6-group precursor yields and decay constants until we can solve this problem.

- **Major actinides ^{235,238}U and ^{239}Pu**
  Although our evaluations for ^{235,238}U and ^{239}Pu are performing relatively well in many applications, there are deficiencies that we are aware of. But our view has been that we are not going to change these evaluations until a larger body of work has been completed, and until good integral performance can be re-established in criticality simulations. In our ENDF/B-VII.0 documentation [1] we noted the poor performance of ^{239}Pu in the thermal range for solutions, and this has not yet been resolved. There is also a major ongoing effort in experiment and theory to better understand the fission neutron spectra emission energy-dependence at thermal and at higher incident neutron energies, an effort that will take a number of years to complete. We also note concerns raised by the Japanese nuclear data community that the ^{235}U capture cross section may be too high by $\sim$25% or more in the 1-keV region. These issues are discussed in more detail later in this paper.

IV. OVERVIEW OF ENDF/B-VII.1 LIBRARY

A. Contents of ENDF/B-VII.1

The ENDF/B-VII.1 library contains 14 sublibraries as summarized in Table I. They are ordered according to NSUB, the identification number of the sublibrary. The number of materials (isotopes or elements) are given for both the new (VII.1) and previous (VII.0) versions of the ENDF/B library.

TABLE I: Contents of the ENDF/B-VII.1 library, with ENDF/B-VII.0 and ENDF/B-VI.8 shown for comparison. NSUB stands for the sublibrary number in the ENDF-6 format. Given in the last three columns are the number of materials (isotopes or elements).

No.	NSUB	Sublibrary name	Short name	VII.1	VII.0	VI.8
1	0	Photonuclear	g	163	163	-
2	3	Photo-atomic	photo	100	100	100
3	4	Radioactive decay	decay	3817	3838	979
4	5	Spont. fis. yields	s/fpy	9	9	9
5	6	Atomic relaxation	ard	100	100	100
6	10	Neutron	n	423	393	328
7	11	Neutron fis.yields	n/fpy	31	31	31
8	12	Thermal scattering	tsl	20	20	15
9	19	Standards	std	8	8	8
10	113	Electro-atomic	e	100	100	100
11	10010	Proton	p	48	48	35
12	10020	Deuteron	d	5	5	2
13	10030	Triton	t	3	3	1
14	20030	^{3}He	he3	2	2	1

The major US laboratory contributors to the ENDF/B-VII.1 library are summarized in Table II. Below we give a summary of the sublibraries.

TABLE II: Major US laboratory contributors to the ENDF/B-VII.1 library.

Sublibrary/activity	Major US contributors
Neutron sublibrary	LANL, BNL, ORNL, LLNL
Thermal scattering sublibrary	LANL
Standards sublibrary	NIST, LANL
Photonuclear sublibrary	LANL
Decay data sublibrary	BNL
Proton sublibrary	LANL
d, t, ^{3}He sublibraries	LANL
Fission yield sublibraries	LANL
Atomic data sublibraries	LLNL
Data verification	BNL
Data validation	LANL, KAPL, Bettis, ANL, INL, BNL
Archival and dissemination	BNL

1. The photonuclear sublibrary was carried over unchanged from ENDF/B-VII.0. It contains evaluated cross sections for 163 materials (all isotopes) mostly up to 140 MeV. The sublibrary was supplied by Los Alamos National Laboratory (LANL) and it is largely based on the IAEA-coordinated collaboration completed in 2000.

2. The photo-atomic sublibrary was taken over from ENDF/B-VII.0=ENDF/B-VI.8. It contains data for photons from 10 eV up to 100 GeV interacting with atoms for 100 materials (all elements). The sublibrary was supplied by Lawrence Livermore National Laboratory (LLNL).

3. The decay data sublibrary has been re-evaluated and considerably improved by the Brookhaven National Laboratory (BNL).

4. The spontaneous fission yields were taken over from ENDF/B-VII.0=ENDF/B-VI.8. The data were supplied by LANL.

5. The atomic relaxation sublibrary was taken over from ENDF/B-VII.0=ENDF/B-VI.8. It contains data for 100 materials (all elements) supplied by LLNL.

6. The neutron reaction sublibrary represents the heart of the ENDF/B-VII.1 library. The sublibrary has been updated and extended, it contains 423 materials, including 422 isotopic and 1 elemental evaluation. A brief summary of the neutron evaluations, particularly changes compared to the previous ENDF/B-VII.0 database, is given in Table III. Altogether 234 materials have been changed in ENDF/B-VII.1 compared to ENDF/B-VII.0.

7. Neutron fission yields were reevaluated for ^{239}Pu (fast and 14 MeV) by Los Alamos; others were taken over from ENDF/B-VII.0=ENDF/B-VI.8, having been supplied by LANL.

8. The thermal neutron scattering sublibrary was carried over unchanged from ENDF/B-VII.0. It contains thermal scattering-law data, largely supplied by LANL.

9. The neutron cross section standards sublibrary was carried over from ENDF/B-VII.0 unchanged [7]. Therefore, as for VII.0, the VII.0 standard cross sections were completely adopted by the VII.1 neutron reaction sublibrary except for the thermal cross section for ^{235}U(n,f) where a slight difference occurs to satisfy thermal data testing, and some very small differences for ^{235}U(n,f) and ^{238}U(n,γ) in the keV–MeV region.

10. The electro-atomic sublibrary was taken over from ENDF/B-VII.0=ENDF/B-VI.8. It contains data for 100 materials (all elements) supplied by LLNL.

11. The proton-induced reactions were carried over unchanged from ENDF/B-VII.0, supplied by LANL, the data being mostly to 150 MeV.

12. The deuteron-induced reactions were supplied by LANL, carried over unchanged from ENDF/B-VII.0. This sublibrary contains 5 evaluations.

13. The triton-induced reactions were supplied by LANL, carried over unchanged from ENDF/B-VII.0. This sublibrary contains 3 evaluations.

14. Reactions induced with ^{3}He were supplied by LANL, carried over unchanged from ENDF/B-VII.0. This sublibrary contains 2 evaluations.

TABLE III: An overview of the changes made in the neutron cross section sublibrary between ENDF/B-VII.0 and ENDF/B-VII.1. Not listed are minor format changes and changes in MT458 fission energy release.

Material	Description of changes and their authors
H-001	R. Little's fix for ACE library. AFCI covariance data added, BNL.
H-002	AFCI covariance data added, BNL.
H-003	Inserted (n,2n) cross sections from ENDF/B-VI.8, BNL; D. Cullen's fix.
He-003	New R-matrix analysis by Hale (Sep. 2010). New capture cross sections, adjusted total and kept elastic, LANL.
He-004	New R-matrix analysis. Hale, LANL.
Li-006	New R-matrix evaluation above 1 MeV, based in part on new LANSCE/WNR (n,t) cross section and angular distribution data, Hale, LANL; New standards evaluations, Pronyaev, IPPE.
Be-009	New R-matrix evaluation for cross sections (but not angular distributions), also using new RPI total cross section data, Hale, LANL; capture cross sections updated, total and non-elastic (MT1,3) adjusted accordingly, LANL.
B-010	New standards evaluations, Pronyaev, IPPE.
B-011	Added AFCI covariance data, BNL.
C-000	Added AFCI covariance data, BNL. Replaced capture cross sections by JENDL-4.0 < 20 MeV. Total and non-elastic (MT1,3) adjusted accordingly, LANL.
N-014	Fixed total cross section balance, BNL.
N-015	Added AFCI covariance data, BNL.
O-016	Capture cross section taken from JENDL-4.0, LANL. In MF14, MT103 the wrong parent state was corrected, LLNL. AFCI covariance data added, BNL.
Na-022	Modifications to resonance total width. Mughabghab, BNL.
Mg-024	In MF12, MT58 the final level for the first gamma was incorrect, LLNL. Added AFCI covariance data, BNL.
Mg-025	Added AFCI covariance data, BNL.
Mg-026	Added AFCI covariance data, BNL.
Al-027	AFCI MF33 covariances added, BNL.
Si-028	AFCI MF33 covariances added, BNL.
Si-029	Removing extra 0-energy gamma, LLNL. AFCI MF33 covariances added, BNL.
Si-030	AFCI MF33 covariances added, BNL.
P-031	Adjusted capture and made redundant cross sections consistent. Trkov, BNL.
S-034	Fix of zero background in MF3/MT1, Lin interpolation to 4th point, fix NDIGIT and ISR in MF32, BNL.
Cl-035	New R-Matrix Limited MF2/32 evaluation by ORNL, (LRF=7, LCOMP=2), 16 proton widths 133<E<954 keV increased to 400 meV, ORNL.
Cl-037	New MF2/32 evaluation, ORNL.
K-039	New MF2/32 evaluation, ORNL.
K-041	New MF2/32 evaluation, ORNL.
Sc-045	R. Little's fix for ACE library.
Ti-046	New fast region neutron evaluation, LANL; new MF32, ORNL. Covariances added. Kawano, Oh, Kahler, LANL; Leal, ORNL. MF6,12,14 updated to fix E balance, LANL.
Ti-047	New fast region neutron evaluation, LANL; new MF32, ORNL. Covariances added. Kawano, Oh, Kahler, LANL; Leal, ORNL. MF6,12,14 updated to fix E balance, LANL.
Ti-048	New fast region neutron evaluation, LANL; new MF32, ORNL. Covariances added. Kawano, Oh, Kahler, LANL; Leal, ORNL. MF6,12,14 updated to fix E balance, LANL.
Ti-049	New fast region neutron evaluation, LANL; new MF32, ORNL. Covariances added. Kawano, Oh, Kahler, LANL; Leal, ORNL. MF6,12,14 updated to fix E balance, LANL.
Ti-050	New fast region neutron evaluation, LANL; new MF32, ORNL. Covariances added. Kawano, Oh, Kahler, LANL; Leal, ORNL. MF6,12,14 updated to fix E balance, LANL.
V-050	JENDL-4.0 adopted (replacing elemental in ENDF/B-VII.0).
V-051	New fast neutron region, LANL; MF2 from JENDL-4.0 (replacing elemental in ENDF/B-VII.0.
Cr-050	New MF2/MF32 resonance parameters, ORNL. AFCI covariances added, MF33/MT2 LB1 section for scattering radius uncertainty, BNL. (n,α) production cross sections and spectra from 20-150 MeV updated by Kunieda, Kawano, to better match Haight LANSCE data.
Cr-052	New MF2/MF32 resonance parameters, ORNL. AFCI covariances added. MF33/MT2 LB1 section for scattering radius uncertainty, BNL. (n,α) production cross sections and spectra from 20-150 MeV updated by Kunieda, Kawano, to better match Haight LANSCE data.

TABLE III: An overview of the changes made in the neutron cross section sublibrary between ENDF/B-VII.0 and ENDF/B-VII.1. Not listed are minor format changes and changes in MT458 fission energy release.

Material	Description of changes and their authors
Cr-053	New MF2/MF32 resonance parameters, ORNL. AFCI covariances added. MF33/MT2 LB1 section for scattering radius uncertainty, BNL. (n,α) production cross sections and spectra from 20-150 MeV updated by Kunieda, Kawano, to better match Haight LANSCE data.
Cr-054	New MF2/MF32 resonance parameters, ORNL. (n,α) production cross sections and spectra from 20-150 MeV updated by Kunieda, Kawano, to better match Haight LANSCE data.
Mn-055	New MF2/32 evaluation,ORNL; New fast neutron region and covariances, IAEA.
Fe-054	AFCI covariances added, BNL. (n,α) production cross sections and spectra from 20-150 MeV updated by Kunieda, Kawano, to better match Haight LANSCE data.
Fe-056	AFCI covariances added, BNL. (n,α) production cross sections and spectra from 20-150 MeV updated by Kunieda, Kawano, to better match Haight LANSCE data.
Fe-057	(n,α) production cross sections and spectra from 20-150 MeV updated by Kunieda, Kawano, to better match Haight LANSCE data.
Fe-058	AFCI covariances added, BNL.
Co-058	New BNL evaluation, Mughabghab and H.I. Kim, BNL.
Co-059	(n,α) production cross sections and spectra from 20-150 MeV updated by Kunieda, Kawano, to better match Haight LANSCE data.
Ni-058	New MF2/32 evaluation by ORNL, updated α-production, various corrections, AFCI MF33 covariances added, MF33/MT2 LB1 for scattering radius uncertainties, capture uncertainties, BNL. (n,α) production cross sections and spectra from 20-150 MeV updated by Kunieda, Kawano, to better match Haight LANSCE data.
Ni-060	AFCI covariance data added to file. MF33/MT1,2,102 unmodified. (n,α) production cross sections and spectra from 20-150 MeV updated by Kunieda, Kawano, to better match Haight LANSCE data.
Ni-061	MF2 replaced with JENDL-4.0 by BNL to improve agreement with Grenoble lead-slowing-down benchmark. Trkov, BNL.
Ni-062	New MF2 evaluation. The capture width of the 4.5 keV resonance and the scattering widths of the p-wave resonances below 100 keV increased to achieve agreement with recent LANL differential capture measurement and recent 30 keV Maxwellian capture cross section measurements. Mughabghab, BNL, fix total widths for resonance parameters.
Ni-064	MF2 replaced with JENDL-4.0 to improve agreement with Grenoble lead-slowing-down benchmark. Trkov, BNL.
Zn-064	Replaced Zn-0 elemental evaluation with JENDL-4.0.
Zn-065	Replaced Zn-0 elemental evaluation with JENDL-4.0.
Zn-066	Replaced Zn-0 elemental evaluation with JENDL-4.0.
Zn-067	Replaced Zn-0 elemental evaluation with JENDL-4.0.
Zn-068	Replaced Zn-0 elemental evaluation with JENDL-4.0; MF9 MT102 added, Zn-68 MF8 added, MF9/MT102 from EAF-2010 > 516 eV res, zero-distribution removed from MF6/MT22,32. Trkov, BNL.
Zn-070	Replaced Zn-0 elemental evaluation with JENDL-4.0, zero-distributions removed from MF6/MT22,32. Trkov, BNL.
As-075	LANL updated cross sections, building on work from LLNL (Kawano, LANL). Problems in total and inelastic cross sections fixed.
Kr-078	New fast neutron region by LLNL merged with MF2 from ENDF/B-VII.0.
Rb-086	Corrected total width for first resonance to sum of partial widths. Hoblit, BNL.
Rb-087	D.Cullen's fix.
Y-089	New evaluation for total and capture. Kawano, LANL.
Zr-090	New MF2, bound level at -234 keV removed. New BNL fast region evaluation Kim, Mughabghab, BNL.
Zr-091	Parameters of the bound level changed to reproduce new measurement of the thermal capture cross section. New BNL fast region evaluation Kim, Mughabghab, BNL, AFCI MF33 covariances.
Zr-092	New BNL fast region evaluation Kim, BNL. AFCI MF33 covariances added, BNL.
Zr-093	New BNL fast region evaluation Kim, BNL. AFCI MF33 covariances added, BNL.
Zr-094	New BNL fast region evaluation Kim, BNL. AFCI MF33 covariances added, BNL.
Zr-095	New BNL fast region evaluation Kim, BNL. AFCI MF33 covariances added, BNL.
Zr-096	New BNL fast region evaluation Kim, BNL. AFCI MF33 covariances added, BNL.
Nb-095	AFCI MF33 covariances added, BNL.
Mo-092	AFCI MF33 covariances added, updated thermal, resonance, unresolved resonance regions, BNL.
Mo-094	AFCI MF33 covariances added, BNL.
Mo-095	Capture width of the 45 eV resonance changed following Dean's reactivity worth measurements. Mughabghab, BNL, AFCI MF33 covariances added, BNL. Fix total widths for resonance parameters.
Mo-096	AFCI MF33 covariances added, BNL.
Mo-097	R. Little's fixes for ACE library, AFCI MF33 covariances added, BNL.
Mo-098	AFCI MF33 covariances added, BNL.
Mo-100	AFCI MF33 covariances added, BNL.
Tc-099	Thermal and resonance region modified. The thermal capture cross section and the capture resonance resonance integral were decreased to achieve agreement with Dean's reactivity worth measurements. Mughabghab, BNL.
Ru-101	AFCI MF33 covariances added, BNL.
Ru-102	AFCI MF33 covariances added, BNL.
Ru-103	AFCI MF33 covariances added, BNL.
Ru-104	AFCI MF33 covariances added, BNL.
Ru-106	AFCI MF33 covariances added, BNL.

TABLE III: An overview of the changes made in the neutron cross section sublibrary between ENDF/B-VII.0 and ENDF/B-VII.1. Not listed are minor format changes and changes in MT458 fission energy release.

Material	Description of changes and their authors
Rh-103	Thermal, resonance,URR regions modified. The parameters of the first resonance were modified on the basis of Dean's reactivity worth measurements. Mughabghab, BNL, AFCI MF33 covariance data added.
Pd-105	AFCI MF33 covariances added, elastic uncertainty capped, BNL.
Pd-106	AFCI MF33 covariances added, elastic uncertainty capped, BNL.
Pd-107	AFCI MF33 covariances added, elastic uncertainty capped, BNL.
Pd-108	AFCI MF33 covariances added, elastic uncertainty capped, BNL.
Ag-109	Thermal and resonance region modified. The thermal capture cross section was slightly decreased and the resonance region extended up to 7 keV. Mughabghab, BNL, AFCI MF33 covariances added, BNL.
Cd-106	New MF2 from IRMM.
Cd-108	New MF2 from IRMM.
Cd-110	New MF2 from IRMM.
Cd-111	New MF2 from IRMM.
Cd-112	New MF2 from IRMM.
Cd-113	Thermal and resonance region modified. The thermal capture cross section was re-evaluated on the basis of thermal capture cross section measurements of Cd and criticality measurements. This results in changes in the resonance parameters at 0.178 eV. Mughabghab, BNL.
Cd-114	New MF2 from IRMM.
Cd-116	New MF2 from IRMM.
Sn-115	Corrected total width for first resonance to be sum of partial widths. Hoblit, BNL, fix total widths for resonance parameters.
Sn-125	Photon yield, total width for the first resonance. Trkov, BNL.
Te-124	Corrected total width for first resonance to be sum of partial widths. Hoblit, BNL.
Te-126	Corrected total width for first resonance to be sum of partial widths. Hoblit, BNL.
Te-132	Corrected gamma multiplicity and Q-values. Trkov, BNL.
I-127	LANL added excitation energies in MF8 MT103 and 107, AFCI MF33 covariances added, BNL.
I-129	AFCI MF33 covariances added, elastic uncertainty capped, BNL.
Xe-123	New fast neutron region by LLNL. MF2 AWR corrected, various fixes. Trkov, BNL.
Xe-124	New fast neutron region by LLNL, corrected total width for the first resonance, AWR in MF2, small deficiencies. Trkov, BNL.
Xe-131	AFCI MF33 covariances added, elastic uncertainty capped, BNL. fix total widths for resonance parameters.
Xe-132	AFCI MF33 covariances added, elastic uncertainty capped, BNL.
Xe-134	AFCI MF33 covariances added, elastic capped, BNL.
Cs-133	Thermal, resonance, and URR regions modified. Following Dean's reactivity worth measurements, the resonance parameters of the first resonance at 5.86 eV were modified. Mughabghab, BNL, AFCI MF33 covariances added, BNL.
Cs-135	AFCI MF33 covariances added, BNL.
La-139	AFCI MF33 covariances added, elastic uncertainty capped, BNL.
Ce-141	Correct total width for first resonance to be sum of partial widths. Hoblit, BNL, AFCI MF33 covariances added, elastic uncertainty capped at 20%, BNL.
Pr-141	AFCI MF33 covariances added, BNL.
Nd-143	AFCI MF33 covariances added, BNL.
Nd-145	Thermal, resonance, and URR regions modified. Thermal capture cross section was decreased from 49.8 to 39.7 b by changing parameters of the bound level to account for Dean's reactivity worth measurements. Mughabghab, BNL, AFCI MF33 covariances added. New evaluation of unresolved resonance region.
Nd-146	AFCI MF33 covariances added, BNL.
Nd-148	AFCI MF33 covariances added, BNL.
Pm-147	AFCI MF33 covariances added, elastic uncertainty capped, BNL.
Sm-149	AFCI MF33 covariances added, elastic uncertainty capped, BNL.
Sm-151	AFCI MF33 covariances added, elastic uncertainty capped, BNL.
Sm-152	AFCI MF33 covariances added, elastic uncertainty capped, BNL.
Eu-153	Thermal, resonance, and URR regions modified. Thermal capture cross section is increased by about 11% to account for Dean's reactivity worth measurements. Mughabghab, BNL, thermal capture upgraded to include recent Widder data, AFCI MF33 covariances added, BNL.
Eu-155	AFCI MF33 covariances added, elastic uncertainty capped, BNL.
Gd-155	Replace MF33 covariance data with AFCI covariances, BNL.
Gd-156	Replace MF33 covariance data with AFCI covariances, BNL.
Gd-157	On the basis of integral measurements the capture cross section remains about the same as in ENDF/B-VII.0. Mughabghab, BNL, replaced MF33 covariance data with AFCI covariances, BNL.
Gd-158	Replaced MF33 covariance data with AFCI covariances, BNL.
Gd-160	Replaced MF33 covariance data with AFCI covariances, add 4% relative LB=1 MF33 uncertainty to elastic between 1-100 keV, BNL.
Er-166	AFCI MF33 covariances added, BNL.
Er-167	AFCI MF33 covariances added, elastic uncertainty capped, BNL.
Er-168	AFCI MF33 covariances added, BNL.
Er-170	AFCI MF33 covariances added, elastic uncertainty capped, BNL.
Tm-168	New evaluation in the resonance and fast neutron regions, BNL. MT16,102 by LANL.
Tm-169	New evaluation in the resonance and fast neutron regions, BNL. MT102 by LANL.
Tm-170	New evaluation in the resonance and fast neutron regions, BNL. MT16,102 by LANL.
Hf-174	JEFF-3.1 modified. Wright, ORNL.
Hf-176	JEFF-3.1 modified. Wright, ORNL.
Hf-177	JENDL-3.3 modified. Wright, ORNL.
Hf-178	JEFF-3.1 modified by Wright, ORNL. AWR in MF2 corrected by Trkov, BNL.

TABLE III: An overview of the changes made in the neutron cross section sublibrary between ENDF/B-VII.0 and ENDF/B-VII.1. Not listed are minor format changes and changes in MT458 fission energy release.

Material	Description of changes and their authors
Hf-179	JENDL-3.3 modified. Wright, ORNL.
Hf-180	JEFF-3.1 modified by Wright, AWR in MF2 corrected by Trkov, BNL.
Ta-180	New fast neutron region by LLNL, various fixes by BNL.
Ta-181	New fast neutron region by LLNL. AWR in MF2, small deficiencies. Trkov, BNL, various fixes, resonance background MF3 fixed.
W-180	New MF2/32 by ORNL. New fast neutron region. Covariances included. Capote, IAEA, Correct max number of Legendre coefficients for MF4/MT2.
W-182	New MF2/32 by ORNL. New fast neutron region. Covariances included. Leal, ORNL; Trkov, Capote, IAEA, Correct max number of Legendre coefficients for MF4/MT2.
W-183	New MF2/32 by ORNL. New fast neutron region. Covariances included. Leal, ORNL; Trkov, Capote, IAEA.
W-184	New MF2/32 by ORNL. New fast neutron region. Covariances included. Leal, ORNL; Trkov, Capote, IAEA, Correct max number of Legendre coefficients for MF4/MT2.
W-186	New MF2/32 by ORNL. New fast neutron region. Covariances included. Leal, ORNL; Trkov, Capote, IAEA, Correct max number of Legendre coefficients for MF4/MT2.
Re-185	New fast neutron region by LLNL with BNL fixes.
Re-187	New fast neutron region by LLNL with BNL fixes.
Au-197	Standard covariances included, Pronyaev, IPPE.
Tl-203	New evaluation in the fast and resonance regions, BNL.
Tl-205	New evaluation in the fast and resonance regions, BNL.
Pb-204	AFCI MF33 covariances added, BNL.
Pb-206	Eliminated duplicated energy in MF4/MT2. Trkov, BNL; AFCI MF33 covariances added, BNL.
Pb-207	Eliminated duplicated energy in MF4/MT2. Trkov, BNL; AFCI MF33 covariances added, BNL.
Pb-208	Scaled down (n,d) MT 650,651, 652 below 12 MeV. Trkov, BNL, AFCI MF33 covariances added. Added MEND line.
Bi-209	AFCI MF33 covariances added, BNL.
Ac-225	JENDL-4.0 adopted. The ENDF/B-VII.0 evaluation was taken from JENDL-3.3, which in turn was taken from JENDL-3.2. JENDL-4.0 updates JENDL-3.3.
Ac-226	JENDL-4.0 adopted. The ENDF/B-VII.0 evaluation was taken from JENDL-3.3, which in turn was taken from JENDL-3.2. JENDL-4.0 updates JENDL-3.3.
Ac-227	JENDL-4.0 adopted. The ENDF/B-VII.0 evaluation was taken from JENDL-3.3, which in turn was taken from JENDL-3.2. JENDL-4.0 updates JENDL-3.3.
Th-227	JENDL-4.0 adopted. The ENDF/B-VII.0 evaluation was taken from JENDL-3.3, which in turn was taken from JENDL-3.2. JENDL-4.0 updates JENDL-3.3.
Th-228	JENDL-4.0 adopted. The ENDF/B-VII.0 evaluation was taken from JENDL-3.3, which in turn was based on JENDL-3.2 but includes some fixes applied by Wright (ORNL). JENDL-4.0 fits the (n,f) data, including correcting the data in EXFOR subentry 40155002 which apparently has a normalization error.
Th-229	JENDL-4.0 adopted. The ENDF/B-VII.0 evaluation was taken from JENDL-3.3, which in turn was based on JENDL-3.2 but includes some fixes applied by Wright (ORNL). JENDL-4.0 fits the (n,f) data, including correcting the data in EXFOR subentry 22647004 which apparently has a normalization error.
Th-230	JENDL-4.0 adopted. The ENDF/B-VII.0 evaluation is the 1977 evaluation by Mann and it has an unphysical (n,f) cross section around 1 keV. The JENDL-4.0 evaluation fits 3 more (n,f) sets that were not available to Mann.
Th-231	JENDL-4.0 adopted. JENDL-4.0 is the only library that contains an evaluation on this isotope.
Th-232	Fixed small deficiencies, negative gamma yields in MF6, MT18. Trkov, BNL.
Th-233	JENDL-4.0 adopted. The ENDF/B-VII.0 evaluation was taken from JENDL-3.3. JENDL-4.0 updates JENDL-3.3.
Th-234	JENDL-4.0 adopted. The ENDF/B-VII.0 evaluation was taken from JENDL-3.3. JENDL-4.0 updates JENDL-3.3.
Pa-229	JENDL-4.0 adopted. JENDL-4.0 is the only library that contains an evaluation on this isotope.
Pa-230	JENDL-4.0 adopted. JENDL-4.0 is the only library that contains an evaluation on this isotope.
Pa-232	JENDL-4.0 adopted. ENDF/B-VII.0 adopted JENDL-3.3 after applying fixes made by Wright. The JENDL-4.0 evaluation matches the (n,f) data in EXFOR entry 13602002, the only usable cross section data taken on this isotope.
U-230	JENDL-4.0 adopted. JENDL-4.0 is the only library that contains an evaluation on this isotope.
U-231	JENDL-4.0 adopted. JENDL-4.0 is the only library that contains an evaluation on this isotope.
U-232	JENDL-4.0 adopted. Both the ENDF/B-VII.0 and JENDL-4.0 evaluations are new and use the same experimental data. JENDL-4.0 has a significantly better χ^2 when compared to both the (n,f) and (n,tot) cross section data.
U-233	LANL reverted delayed neutron 6-grp to ENDF/B-VI.8 and replaced URR covariances by LANL MF33, MT2. Covariances added. Talou, Holloway, LANL; Leal, ORNL. MF33/MT2, MAT number incorrect for seq. 2-7, correction applied to cross sections and angular distributions.
U-234	LANL reverted delayed neutrons 6-grp to ENDF/B-VI.8. Holloway, LANL.
U-235	LANL reverted delayed neutrons 6-grp to ENDF/B-VI.8, new MF33 evaluation by ORNL/LANL, PFNS (MF5,MT18) on finer grid, updated with energy-dependent fission release data based on Madland2006. Covariances added. Talou, Holloway, LANL; Leal, ORNL; Standard covariances included, Pronyaev, IPPE.

TABLE III: An overview of the changes made in the neutron cross section sublibrary between ENDF/B-VII.0 and ENDF/B-VII.1. Not listed are minor format changes and changes in MT458 fission energy release.

Material	Description of changes and their authors
U-236	LANL reverted delayed neutrons 6-grp to ENDF/B-VI.8. Capture cross section increased 10% to better match critical assembly capture data. Kawano, Chadwick, Kahler, LANL, AFCI MF33 covariances added. Range in MF5/MT455 corrected.
U-237	New fast neutron region updated to better match critical assembly ^{237}U fission rate data of Barr and Behrens fission systematics; Unresolved and resolved resonances taken from JENDL-3.3; delayed neutrons 6-grp reverted to ENDF/B-VI.8. Young, Chadwick, Holloway, LANL, MF5/MT455 range correction from 20 to 30 MeV.
U-238	LANL reverted delayed neutrons 6-grp to ENDF/B-VI.8, standard covariances included, capture retained at VII.1-beta2, Pronyaev, IPPE. PFNS (MF5,MT18) on finer grid, updated with energy-dependent fission release data based on Madland2006.
U-239	New fast neutron region by LLNL that updates previous LANL evaluation to match new surrogate fission data. Resonances and unresolved resonances estimated by A. Trkov, BNL.
Np-234	JENDL-4.0 adopted. JENDL-4.0 is the only library that contains an evaluation on this isotope.
Np-235	JENDL-4.0 adopted. The ENDF/B-VII.0 evaluation is taken from JENDL-3.2 which is in turn based on a combination of results from the STAPRE and CASTHY Hauser-Feshbach codes. JENDL-4.0 replaces these with a single calculation using CCONE using solid systematics.
Np-236	JENDL-4.0 adopted. ENDF/B-VII.0 uses the JENDL-3.2 evaluation, modified by Wright. JENDL-4.0 updates this evaluation.
Np-237	LANL reverted delayed neutrons 6-grp to ENDF/B-VI.8. Thermal capture updated. Updated (n,2n) and (n,3n) using Maslov's evaluation. Holloway, Kawano, Chadwick, LANL. Obsolete MATP set to zero in MF8, AFCI MF33 covariances added, BNL.
Np-238	JENDL-4.0 adopted. ENDF/B-VII.0 uses the JENDL-3.3 evaluation which is in turn taken from JENDL-3.2. JENDL-4.0 updates this evaluation and achieves a better χ^2 when compared to the (n,f) data in EXFOR entry 13602003.
Np-239	JENDL-4.0 adopted. The ENDF/B-VII.0 evaluation is the 1987 evaluation of R. Q. Wright. The (n,f) cross section has a severe unphysical drop at the fission threshold. JENDL-4.0 uses modern systematics and has better matching onto the resonance region.
Pu-236	JENDL-4.0 adopted. ENDF/B-VII.0 adopted the JENDL-3.3 evaluation. JENDL-4.0 updates the JENDL-3.3 evaluation and has a better χ^2 compared to existing (n,f) data.
Pu-237	JENDL-4.0 adopted. ENDF/B-VII.0 uses the 1978 Mann and Schenter evaluation. This evaluation has unphysical (n,2n) and (n,3n) cross sections.
Pu-238	New fast neutron region by LANL. P.G.Young, P. Talou, Multiplicities in MT 16,17, and 37 fixed, fission cross sections section modified.
Pu-239	LANL reverted delayed neutrons 6-grp to ENDF/B-VI.8, standard covariances included, Pronyaev, IPPE. PFNS (MF5,MT18) on finer grid. Updated with energy-dependent fission release data based on Madland2006.
Pu-240	New fast neutron region evaluation, including MF31,33,35. Young, Talou, LANL, reverted RRR and URR evaluation to VII.0, comments updated.
Pu-241	LANL added covariance matrix for fission (MF33 MT18) to VII.0 file. Talou, LANL.
Pu-242	BNL MF2 added. The fast capture of JENDL-4.0 was decreased by 20%, Mughabghab, BNL.
Pu-244	JENDL-4.0 adopted. ENDF/B-VII.0 is the 1978 evaluation from Mann, Schenter, Benjamin and McCrossen *et al.* JENDL-4.0 fits the 3 (n,f) sets taken since 1978.
Pu-246	JENDL-4.0 adopted. The ENDF/B-VII.0 evaluation was taken from JENDL-3.3. JENDL-4.0 updates JENDL-3.3.
Am-240	JENDL-4.0 adopted. Replace LLNL evaluation with the one from JENDL-4.0 It is consistent with the Younes, Britt and Becker surrogate data analysis (Lawrence Livermore National Lab inter report UCRL-TR-201913) and does not use parts from 242Am. As a bonus, it actually has covariances.
Am-241	Updated fission cross section. Capture updated to use new DANCE data and better match critical assembly capture data. New evaluation and covariance matrices. Kawano, Chadwick, Kahler, LANL.
Am-242	R. Little's LANL fix for ACE library, LANL fixed multiplicities in MT 16,17, and 37.
Am-242m1	R. Little's LANL fix for ACE library, LANL fixed multiplicities in MT 16,17, and 37, AFCI MF33 covariances added.
Am-243	Fixed MF1, MT452 for missing energy points, new (n,2n) isomeric ratio, LANL. New evaluation in the thermal, resonance, URR regions. The fast capture was decreased 16.6 %. AFCI MF33 covariances added, Mughabghab, BNL.
Cm-240	JENDL-4.0 adopted. JENDL-4.0 is the only library that contains an evaluation on this isotope.
Cm-241	JENDL-4.0 adopted. ENDF/B-VII.0 is a 1978 evaluation from Mann and Schenter. It possesses an unphysically large (n,3n) cross section and therefore an unphysically small (n,2n) cross section. The other cross sections are comparable to the JENDL-4.0 evaluation.
Cm-242	JENDL-4.0 adopted. ENDF/B-VII.0 is a 1978 evaluation from Mann, Benjamin, Howerton, *et al.*. JENDL-4.0 fits the (n,f) data in EXFOR 129912 which was taken after the ENDF/B-VII.0 evaluation was compiled.
Cm-243	JENDL-4.0 adopted. ENDF/B-VII.0 is the 1995 evaluation of V.M. Maslov, *et al.* JENDL-4.0 uses the same resolved resonances, $\bar{\nu}$ and fission neutron spectrum as ENDF/B-VII.0, but improves it with newer systematics and a fit to the available (n,f) data.

TABLE III: An overview of the changes made in the neutron cross section sublibrary between ENDF/B-VII.0 and ENDF/B-VII.1. Not listed are minor format changes and changes in MT458 fission energy release.

Material	Description of changes and their authors
Cm-244	JENDL-4.0 adopted. ENDF/B-VII.0 adopted the JENDL-3.3 evaluation. JENDL-4.0 uses the JENDL-3.3 resonance parameters but supplements it with better fits and systematics for the higher energy part of the evaluation.
Cm-245	JENDL-4.0 adopted. ENDF/B-VII.0 adopted the JENDL-3.3 evaluation which is in turn an improvement of the Maslov *et al.* evaluation. JENDL-4.0 uses the same resolved resonances, $\bar{\nu}$ and fission neutron spectrum as ENDF/B-VII.0, but improves it with newer systematics and a fit to the available (n,f) data.
Cm-246	JENDL-4.0 adopted. ENDF/B-VII.0 adopted the JENDL-3.3 evaluation which is in turn an improvement of the Maslov *et al.* evaluation. JENDL-4.0 uses the same resolved resonances, $\bar{\nu}$ and fission neutron spectrum as ENDF/B-VII.0, but improves it with newer systematics and a fit to the available (n,f) data.
Cm-247	JENDL-4.0 adopted. ENDF/B-VII.0 is a modification of the JENDL-3.3 evaluation, made by Wright. JENDL-4.0 uses the same resolved resonance parameters, but improves the evaluation with new unresolved resonance parameters and better fits to higher energy data.
Cm-248	JENDL-4.0 adopted. ENDF/B-VII.0 is the 1978 evaluation of Mann, Benjamin, Howerton, *et al.* JENDL-4.0 uses the resolved resonance parameters from ENDF/B-VII.0, supplementing it with fits to (n,f) data including 3 sets taken after ENDF/B-VII.0 was compiled (EXFOR subentries 12788004, 41336016, and 41343011).
Cm-249	JENDL-4.0 adopted. ENDF/B-VII.0 adopted the JENDL-3.3 evaluation as repaired by R.Q. Wright. These repairs consisted of fixing the J^{π} assignments of the fake resonances in the resolved resonance region. JENDL-4.0 replaced the resolved resonance region.
Cm-250	JENDL-4.0 adopted. ENDF/B-VII.0 adopted the JENDL-3.3. The JENDL-3.3 resolved resonances are fake, but have reasonable average parameters. JENDL-4.0 replaced the resolved resonance region.
Bk-245	JENDL-4.0 adopted. JENDL-4.0 is the only library that contains an evaluation on this isotope.
Bk-246	JENDL-4.0 adopted. JENDL-4.0 is the only library that contains an evaluation on this isotope.
Bk-247	JENDL-4.0 adopted. JENDL-4.0 is the only library that contains an evaluation on this isotope.
Bk-248	JENDL-4.0 adopted. JENDL-4.0 is the only library that contains an evaluation on this isotope.
Bk-249	JENDL-4.0 adopted. ENDF/B-VII.0 and JENDL-4.0 have comparable quality resonance regions and comparable χ^2 for (n,f) and (n,tot), so cannot be distinguished on these bases alone. However, JENDL-4.0 is based on thorough systematics, which cannot be said about the ENDF/B-VII.0 evaluation.
Bk-250	JENDL-4.0 adopted. The ENDF/B-VII.0 evaluation was taken from JENDL-3.3. JENDL-4.0 updates JENDL-3.3.
Cf-246	JENDL-4.0 adopted. JENDL-4.0 is the only library that contains an evaluation on this isotope.
Cf-248	JENDL-4.0 adopted. JENDL-4.0 is the only library that contains an evaluation on this isotope.
Cf-249	JENDL-4.0 adopted. ENDF/B-VII.0 is a 1989 evaluation from Zhou Delin, Su Zhongdi, *et al.* possibly from the CENDL library. There is a large amount of (n,tot) data, but much of it suffers from normalization errors. Both ENDF/B-VII.0 and JENDL-4.0 evaluations match the (n,f) data, but JENDL-4.0 possesses a much better (i.e. lower) χ^2.
Cf-250	JENDL-4.0 adopted. ENDF/B-VII.0 is a 1976 evaluation from Benjamin, McCrosson and Howerton. This evaluation uses a picket fence set of resolved resonance parameters and possesses unphysical (n,f), (n,2n) and (n,3n) cross sections. JENDL-4.0 fits data taken on the (n,f) cross section.
Cf-251	JENDL-4.0 adopted. ENDF/B-VII.0 is a 1976 evaluation from Benjamin, McCrosson and Howerton. This evaluation uses a picket fence set of resolved resonance parameters and possesses unphysical (n,2n) and (n,3n) cross sections.
Cf-252	JENDL-4.0 adopted. ENDF/B-VII.0 is a 1976 evaluation from Benjamin, McCrosson and Howerton. This evaluation uses a picket fence set of resolved resonance parameters and possesses unphysical (n,2n) and (n,3n) cross sections. JENDL-4.0 fits data taken on the (n,f) cross section.
Cf-253	JENDL-4.0 adopted. ENDF/B-VII.0 is a 1975 evaluation from Benjamin and McCrosson. This evaluation uses a picket fence set of resolved resonance parameters and possesses an unphysical (n,f) cross section.
Cf-254	JENDL-4.0 adopted. The ENDF/B-VII.0 evaluation was taken from JENDL-3.3. JENDL-4.0 updates JENDL-3.3.
Es-251	JENDL-4.0 adopted. JENDL-4.0 is the only library that contains an evaluation on this isotope.
Es-252	JENDL-4.0 adopted. JENDL-4.0 is the only library that contains an evaluation on this isotope.
Es-253	JENDL-4.0 adopted. The ENDF/B-VII.0 evaluation was taken from JENDL-3.3. JENDL-4.0 updates JENDL-3.3.
Es-254	JENDL-4.0 adopted. The ENDF/B-VII.0 evaluation was taken from JENDL-3.3. JENDL-4.0 updates JENDL-3.3, fitting (n,f) data in EXFOR subentries 13197008, 12933004, 13646004 and 13197004.
Es-254m1	JENDL-4.0 adopted. JENDL-4.0 is the only library that contains an evaluation on this isotope.
Es-255	JENDL-4.0 adopted. The ENDF/B-VII.0 evaluation was taken from JENDL-3.3. JENDL-4.0 updates JENDL-3.3.
Fm-255	JENDL-4.0 adopted. The ENDF/B-VII.0 evaluation was taken from JENDL-3.3. JENDL-4.0 updates JENDL-3.3.

B. Processing, Testing and Dissemination

The ENDF/B-VII.1 library was issued in its basic format defined by the ENDF-6 Formats Manual [22]. For practical applications the library must be processed so that basic data are converted into formats suitable as input for applied codes such as the Monte Carlo transport code MCNP [23] and the reactor licensing code SCALE. The major processing codes for the ENDF/B-VII.1 library are:

- LANL processing code NJOY-99 (in FORTRAN77) as well as NJOY2010 (in FORTRAN95) which offer also full covariance processing capabilities [2]. These codes can be obtained from RSICC, and also from NEA Data Bank, while patches are available at the LANL T-2 webpage http://t2.lanl.gov.
- ORNL processing code AMPX-6 which includes the PUFF-IV module for covariance processing.

Several testing versions of the new library were issued, see Table IV. The last beta5 testing version was declared to be the official ENDF/B-VII.1 library. Each beta version was subject to two-step data testing: Phase 1 testing (data verification), and Phase 2 testing (integral data validation).

TABLE IV: Testing versions of the ENDF/B-VII.1 library.

Version	Date	Comment
beta0	Oct 2010	Initial release for testing
beta1	Jan 2011	Discarded and replaced by beta2
beta2	Feb 2011	Neutron sublibrary completed
beta3	May 2011	Many covariances added
beta4	Sep 2011	Version extensively tested
beta5	Oct 2011	Became ENDF/B-VII.1 in Dec 2011

Data verification was performed by the National Nuclear Data Center, BNL as follows:

- Checking the whole library by a suite of ENDF-6 utility codes (CHECKR, FIZCON, PSYCHE) for formatting problems and inconsistencies in physics.
- Processing of neutron sublibrary by NJOY-99.368 to ensure that a processed library suitable for neutronics calculations can be produced.
- Use of the processed files by the Monte Carlo code MCNP5 [23] in simple neutronics test calculations to ensure that neutronics calculations can be performed.
- Processing of covariance data to ensure that multigroup data for applied calculations can be produced. Additional checkings following CSEWG covariance criteria were performed.

The ENDF/B-VII.1 library was officially released in December 2011. Users should use the present document and Ref. [1] as the ENDF/B-VII.1 reference, as well as other documents in this issue. The library is archived by the National Nuclear Data Center (NNDC) at BNL which also disseminates these data and provides support [24].

V. NEUTRON REACTION COVARIANCES

The work on covariances for ENDF/B-VII.1 involves contributions from many laboratories, with coordination by Obložinský and Smith. Covariances in ENDF/B-VII.1 can be found in three sublibraries: the neutron reaction sublibrary, discussed below, contains covariances for nearly 45% of the materials; the neutron standards sublibrary provides covariances for 9 reactions (8 materials) [7]; and the decay data sublibrary has a covariance matrix for a single material, ^{252}Cf [1].

Neutron cross section covariances represent one of the major advances in the new ENDF/B-VII.1 library. For illustration, ENDF/B-VII.0 contains neutron cross section covariances for 26 materials, of which only 14 were complete [1], while the new ENDF/B-VII.1 library contains covariances for 190 materials. Of these covariances the majority are complete, meaning that the full energy range is covered and that data are provided for essentially all major reaction channels.

The present Chapter provides a short summary of ENDF/B-VII.1 covariances in the neutron reaction sublibrary. More details can be found in several dedicated papers published mostly in the present issue of Nuclear Data Sheets [25, 26, 27, 28, 29].

A. Preparatory Covariance Libraries

In the period of 2006-2011, three covariance projects have been completed which can be viewed as useful predecessors of ENDF/B-VII.1 covariances. A summary of these libraries is given in Table V, together with brief descriptions given below.

- BOLNA. A covariance library created by five laboratories (BOLNA = Brookhaven-Oak Ridge-Los Alamos-NRG Petten-Argonne) for the purposes of the international project WPEC Subgroup 26 [30]. The library contains covariances for 52 materials, of which 45 were supplied by BNL, put together on a short timetable. Contributing parties either selected covariances from sources deemed suitable for the purpose or used simple estimates. The library represents an *ad hoc* collection of covariances not tied to any specific evaluated nuclear data library.
- Low-fidelity. A library created in 2007-2008 by four US National Laboratories under a DOE project for testing nuclear criticality safety methods [31]. The aim was to produce a library for a full set of materials included in ENDF/B-VII.0 using simple, yet

TABLE V: Summary of three covariance libraries preceding ENDF/B-VII.1 release. Shown is name of the library, year of completion, number of materials, sponsor, principal application and relevance to ENDF/B-VII.1.

Name	Year	Materials	Sponsor	Application	Relevance to ENDF/B-VII.1
BOLNA	2007	52	WPEC	Data adjustment methods	Low: correlations for minor actinides adopted
Low-fidelity	2008	387	DOE	Criticality safety methods	Medium: some low priority materials adopted
COMMARA-2.0	2011	110	DOE	Data adjustment, fast reactors	Major: many priority materials adopted

not unreasonable, methods. The emphasis was on completeness rather than quality, hence the name "low-fidelity".

- COMMARA-2.0 (*Covariance Multigroup Matrix for Advanced Reactor Applications* is the official name for the final product which is sometimes also referred to as the AFCI-2.0 library). A library produced by a BNL-LANL collaboration during 2008-2011 [32, 33]. The goal was to develop a covariance library for 110 materials of importance for the Advanced Fuel Cycle Initiative, with a specific objective being the facilitation of data adjustment (i.e., a calibration process) for fast reactor systems. The library is strictly tied to central values of ENDF/B-VII.0. Since many of these central values were adopted by ENDF/B-VII.1 the COMMARA-2.0 library constitutes the backbone of ENDF/B-VII.1's covariances.

B. Covariance Methodology

A wide range of methods was used in producing the evaluations/estimates of neutron cross section covariances included in the ENDF/B-VII.1 library. As discussed in Ref. [25], the adopted covariance evaluation methods differ considerably depending on the mass range of materials, the incident neutron energy, the priority given to an evaluation, and the type of cross section data.

1. Atomic mass
   - Light nuclei: sophisticated evaluation by R-matrix method; and simple estimate based on comparison with experimental data and their uncertainties.
   - Structural materials: EMPIRE/KALMAN and EMPIRE/GANDR methods using nuclear reaction models as *priors* and data from EXFOR to get *posteriors*; dispersion methods; and error propagation of nuclear model parameters. See Ref. [28] for more details.
   - Fission products: mostly error propagation of nuclear reaction model uncertainties was deemed to be sufficient in view of the low priority given to these materials [28].
   - Actinides: sophisticated methods for major actinides requiring full scale simultaneous evaluation of both central values and covariances; and simple estimates for low priority minor actinides. See Ref. [26] for more details.
2. Energy of incident neutrons
   - Resonance region: full scale simultaneous evaluation by SAMMY and retroactive evaluation by SAMMY [27]; medium complexity method based on a kernel approximation to propagate resonance parameter uncertainties from the Atlas of Neutron Resonances; estimate using the low-fidelity integral method [28].
   - Fast neutron region: EMPIRE/KALMAN and EMPIRE/GANDR methods; dispersion method; error propagation of model parameter uncertainties. See Ref. [28] for more details.
3. Priority of evaluation
   - High priority: requires full scale simultaneous evaluation including both central values and covariances.
   - Medium priority: retroactive evaluation using simplified methods.
   - Low priority: estimates based on nuclear reaction model parameters in the fast region and integral quantities in the resonance region.
4. Type of data
   - Cross sections: nuclear reaction models combined with experimental data.
   - Average neutron multiplicity, $\bar{\nu}$: detailed analysis of experimental data and fit to these data.
   - Fission neutron spectra: detailed analysis of data combined with model predictions.
   - Average scattering cosines, $\bar{\mu}$: analysis of data (^{23}Na, ^{56}Fe in COMMARA-2.0); propagation of optical model parameter uncertainties (59 minor actinides adopted from JENDL-4.0).

C. Contents of ENDF/B-VII.1 Covariances

The neutron sublibrary of ENDF/B-VII.1 provides covariances for 190 materials. Most of these materials were adopted from the COMMARA-2.0 covariance library including light nuclei, actinides, structural materials and fission products. This was augmented by 59

minor actinides adopted from the JENDL-4.0 library [9]. A smaller number of evaluations was produced for nuclear criticality safety and other applications.

A summary of ENDF/B-VII.1 covariances is given in Table VI. More than 100 materials were taken directly from the COMMARA-2.0 covariance library which includes 6 priority minor actinides, ^{242}Pu and ^{242,243,244,245,246}Cm, adopted from JENDL-4.0. The latter library also supplied additional 53 minor actinides.

There were no changes made to the standards cross sections (MF3 file) in the ENDF/B-VII.1 neutron sublibrary, because no new standards evaluations have been released, but full standards covariances for the standards [7] have been inserted in the MF33 files after adjusting them to account for the difference between standards and VII.1 cross sections if applicable. These covariances include not only cross-energy but also cross-reaction and cross-material correlations in cases where they are not negligible (*e.g.* the correlations between ^{235}U and ^{238}U fission cross sections that are present because of the use of cross section ratio measurements in the evaluation of the standards).

TABLE VI: Summary of neutron cross section covariances in ENDF/B-VII.1. Data are available for 190 materials, including 6 priority and 53 minor actinides taken over from JENDL-4.0.

Category	Materials	Comment
Light nuclei	12	6 evaluated by R-matrix 6 low-fidelity estimates
Structural + FPs	105	38 evaluated for COMMARA-2.0 40 updated low-fi estimates 15 eval for crit safety 12 eval for other purposes
Priority actinides	20	13 evaluated for COMMARA-2.0 1 mat from ENDF/B-VII.0 6 materials from JENDL-4.0
Minor Actinides	53	Low priority, all JENDL-4.0

D. Plots by Sigma Covariance QA System

The covariance quality assurance (QA) system recently developed by the NNDC is based on the Sigma Retrieval & Plotting Web interface for nuclear reaction data [34]. A particularly powerful part of the system is comparison of integral cross section values probing various segments of covariances as a function of neutron energy. Currently, Sigma offers integral quantities using the following weighting spectra: thermal energy, resonance integral (RI, 1/E spectrum), 30 keV Maxwellian spectrum (MACS), ^{252}Cf spectrum, and 14 MeV neutron energy, as illustrated in Fig. 1.

The idea is to compare integral cross sections between major evaluated nuclear data libraries, including data from the Atlas of Neutron Resonances [35] and the Karlsruhe astrophysics database KADoNiS [36]. Dispersion between these quantities sheds light on the quality of ENDF/B-VII.1 covariances. As an example, Fig. 2 shows

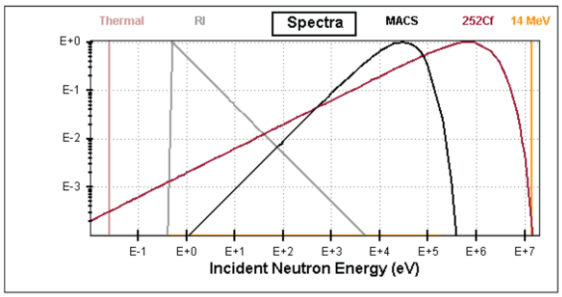

FIG. 1: Weighting neutron spectra used by Sigma covariance QA system developed by the NNDC.

(n,γ) and (n,f) integral cross sections with available uncertainties for ^{235}U, for ^{238}U and also for ^{239}Pu. One can see that in most instances our results look plausible. In several cases, however, such as ^{235}U(n,γ) ENDF/B-VII.1 MACS uncertainty seems to be perhaps too large, showing a potential issue to be addressed in the future. The figure also shows that VII.1's ^{239}Pu(n,γ) cross section lies significantly below other evaluations in the fast range - a topic requiring future attention. Also, it is evident that the fission cross section uncertainties are thought to be very small.

E. Discussion

It should be emphasized that even though an impressive amount of progress has been achieved in covariance evaluations since the release of ENDF/B-VII.0 library in 2006, a non-negligible fraction of our results suffer from inherent limitations. There are several reasons for this:

Due to limited resources, CSEWG decided to address the specific needs of a single user – the AFCI data adjustment project (as well as the Criticality Safety program to a lesser extent). For this reason the backbone of ENDF/B-VII.1 covariances is the COMMARA-2.0 library containing data for 110 materials which were developed and tested in a 33-energy group representation. It should be understood that the production of covariances for this amount of materials, under both time and funding constraints, was not possible without our resorting to simplified procedures in many instances. This, naturally, can be subject to criticism, and is also reason for caution when applying our covariances beyond their intended application. For example, in many cases, covariances were not developed within a consistent simultaneous approach but added "a posteriori". The issue of discrepancy between central values was taken into account by retrofitting (enlarging) uncertainties whenever necessary to embrace the difference. On the other hand, it should be emphasized that the strength of the AFCI covariance effort was the close collaboration of BNL and LANL evaluators with ANL and INL reactor analysts led

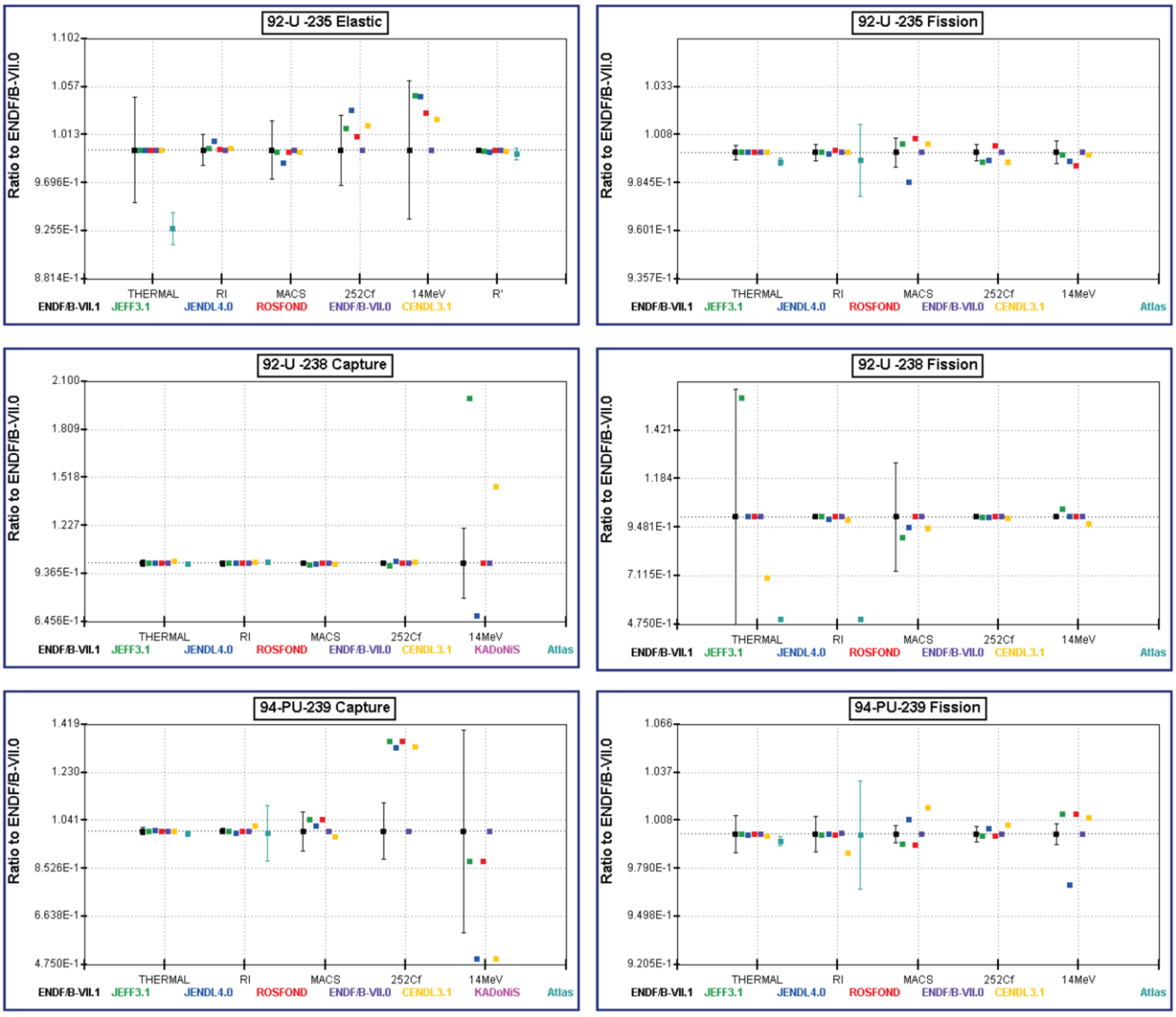

FIG. 2: Screen-shot from the Sigma covariance QA system showing (n,γ) and (n,f) integral cross sections for ^{235}U (top), ^{238}U (middle) and ^{239}Pu (bottom). Shown are thermal cross sections, resonance integrals (RI), 30 keV Maxwellian averages (MACS), averages over ^{252}Cf spectrum, and 14 MeV cross section for major evaluated data libraries relative to ENDF/B-VII.0. Also shown are data from the Atlas of Neutron Resonances; note that nuclear astrophysics database KADoNiS does not cover the actinide mass region. See *http://www.nndc.bnl.gov/sigma/endf71b4.jsp*.

by M. Salvatores and G. Palmiotti. These analysts tested four consecutive versions of the library, allowing evaluators to resolve step-by-step all identified issues and gradually improve their data. As a consequence, the resulting COMMARA-2.0 library, despite its limitations, is considered by both evaluators and reactor analysts to be fairly well tested and of plausible quality.

Second, current evaluation methodologies continue to be a research project and are subject to debate, and a consensus within the nuclear data evaluation community on the relative merits has not been reached. As a consequence, considerable differences in covariances produced by various evaluators are not uncommon. Perhaps the most important single issue is an inadequate treatment of systematic uncertainties, which often boils down to observation that "uncertainties are too low." Years ago, Fröhner pointed out that a covariance evaluation requires knowledge of the data reduction process [37]. This can be seen by considering a typical data reduction process involving subtraction of a background $b \pm \Delta b$ and multiplication by a calibration factor $c \pm \Delta c$. This implies that the data reduction method to obtain counts α_j from the

raw counts a_j is

$$\alpha_j = (a_j - b)c. \quad (1)$$

By neglecting weak cross-correlation terms and computing sensitivities one gets covariance matrix elements

$$\langle \delta\alpha_j \delta\alpha_k \rangle = \left[\delta_{jk}(\Delta a_j)^2 + (\Delta b)^2\right] \langle c \rangle^2 + \alpha_j \alpha_k (\Delta c)^2 \quad (2)$$

where δ_{jk} is Kronecker delta, Δa_j is the statistical uncertainty, and Δb and Δc are systematic uncertainties. Eq. (2) makes it clear that an enhancement of covariances due to systematic uncertainties can be substantial. In practice, however, systematic uncertainties are difficult to trace and they are often not properly accounted for despite the fact that their impact on multigroup uncertainties can be dramatic. A rare attempt to demonstrate this point and to address this issue can be found in the evaluation of ^{239}Pu fission and capture in the resonance region by Derrien *et al.* [38].

Third, covariance quality assurance methods are not yet fully established, even though CSEWG made a serious attempt to address them [25]. A dedicated future effort in the development of ENDF is needed that includes the broad international community of evaluators, experimentalists, and users, to firmly establish such procedures.

In conclusion, a considerable amount of further work is needed to produce robust covariances that could be used with confidence in a broad range of applications. We are aware that this stage has not yet been reached, and we expect that another release of the ENDF/B-VII library will be required to get us there.

VI. NEUTRON REACTION SUBLIBRARY FOR UPDATED NUCLIDES

A. Light Nuclei R-Matrix Evaluations

The following sections describe the updated light-isotope evaluations done for ENDF/B-VII.1. As is the case for all the light-element evaluations done at Los Alamos, these are based on multichannel R-matrix analyses of experimental data for the neutron plus target compound system, using the LANL Energy Dependent Analysis code, EDA (in some cases, though, the capture channel is not obtained from an R-matrix analysis). A flow-chart of the code's operation is shown in Fig. 3. It accommodates any number of two-body channels having particles with arbitrary spins, masses, and charges. The formulation is relativistic, so that even zero-mass particles, such as photons, are treated correctly. General scattering observables are calculated using the Wolfenstein trace formalism. Experimental data can be modified by the use of adjustable normalizations and energy shifts, and the calculations can fold in the effects of beam energy resolution/spread.

Sections VI A 1–VI A 6 describe the analyses done for reactions in the ^{4}He,^{5}He,^{7}Li, ^{10}Be, and ^{17}O compound

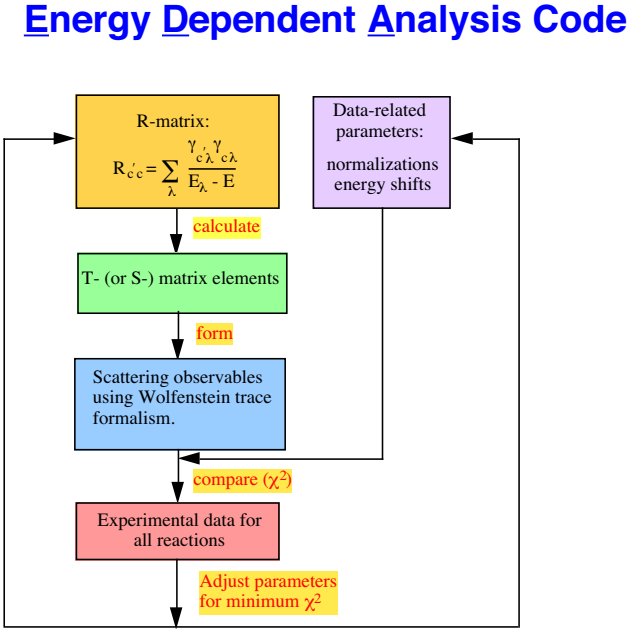

FIG. 3: Schematic of the EDA code.

systems that were used wholly, or in part, to produce the evaluations for neutrons on ^{3}He, ^{4}He, ^{6}Li, ^{9}Be, ^{nat}C, and ^{16}O. In addition, covariances were added for the existing (VII.0) light-element standards evaluations for ^{1}H, ^{6}Li, and ^{10}B, but those will be discussed in a separate paper.

1. ^{3}He

We have used the results of a relatively new R-matrix analysis of reactions in the ^{4}He system to upgrade the neutron capture cross section for ^{3}He over the whole energy range. The analysis includes gamma-ray channels, and data for both capture and photodisintegration reactions in this system. The new capture cross section, shown in figure 4 compared to the old evaluated cross section and to the experimental data, has a very different thermal value and much different behavior at the higher energies. The resonance at 2.2 MeV comes from a $J^{\pi} = 1^{-}$ resonance at about 22.6 MeV excitation energy in ^{4}He. Above about 100 keV, the calculations tend to agree more with the scale of the photodisintegration measurements (blue points) than with that of the capture measurements (green points), which are considerably lower. These revisions give a much better match to the KADONIS data for ^{3}He at 30 keV temperature, which should result in improved performance in astrophysical applications.

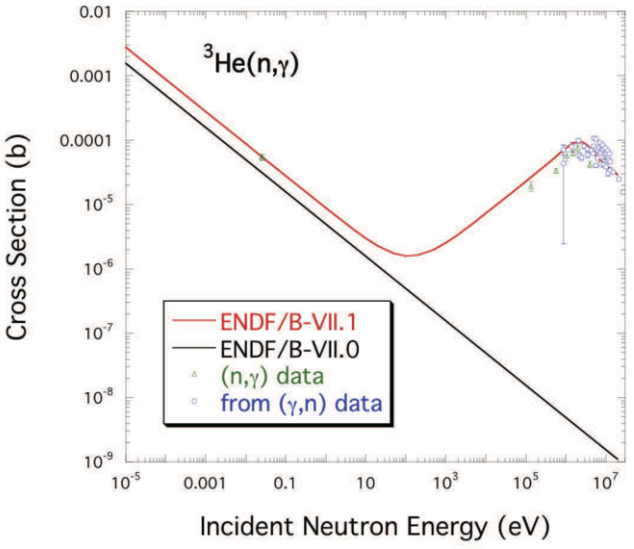

FIG. 4: Neutron capture on ^{3}He. Compared are cross sections in ENDF/B-VII.1 (red curve) with those in ENDF/B-VII.0 (black line), and with experimental data from n+^{3}He capture (green triangles) and inverted γ+^{4}He photodisintegration (blue circles).

2. ^4He

The recent cross-section evaluation for neutrons on ^{4}He came from an R-matrix analysis of reactions in the ^{5}He system that has been used for many years at Los Alamos to provide data for thermonuclear applications. For that reason, the analysis extends to neutron energies well above 20 MeV, but for simplicity, the new evaluation is truncated there to keep it single-channel. A summary of the channel structure and data included in the analysis is given in Table VII. More than 2700 data points are fitted with 117 parameters, giving a chi-square per degree of freedom of 1.5. The $n-\alpha$ scattering data, including the total cross section, are in excellent agreement with calculations from the fit parameters. The fit to the total cross section is shown in Fig. 5.

3. ^6Li

The R-matrix analysis of the ^{7}Li system contains data for all possible reactions among t+^{4}He and n+^{6}Li at energies extending from the t+^{4}He threshold (well below the n+^{6}Li threshold) up to energies corresponding to 4-MeV incident neutrons. Also included are n+^{6}Li* channels to simulate the effects of $n+d+\alpha$ breakup. This is summarized in Table VIII. One sees that a very good fit is obtained to the more than 3900 data points included, with a chi-square per degree of freedom of 1.80.

The fit to the t+^{4}He scattering data, which have very small uncertainties, is quite good. Examples are given

TABLE VII: Channel configuration (top) and data summary (bottom) for each reaction in the ^{5}He system R-matrix analysis.

Channel	a_c (fm)	$l_{\max}$
n+^{4}He	3.0	5
γ+^{5}He	6.0	1
d+^{3}H	5.1	5
n+^{4}He*	5.0	1

Reaction	Range (MeV)	# Data Types	# Data Pts.
^{4}He$(n,n)^4$He	$E_n = 0-28$	2	817
^{3}H$(d,d)^3$H	$E_d = 0-8.6$	6	700
^{3}H$(d,n)^4$He	$E_d = 0-11$	14	1185
^{3}H$(d,\gamma)^5$He	$E_d = 0-8.6$	2	17
^{3}H$(d,n)^4$He*	$E_d = 4.8-8.3$	1	10
Total		25	2729

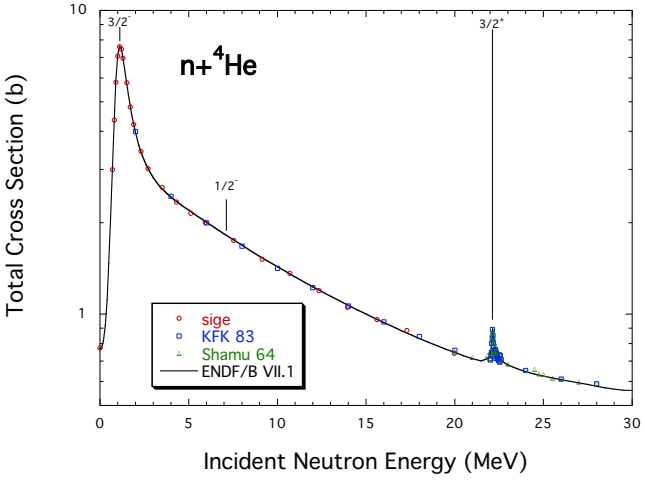

FIG. 5: R-matrix analysis for ^{4}He.

in Figure 6 at triton energies of 8 and 12 MeV, which are near the obvious resonance structure in the ^{6}Li(n,t) reaction at $E_n = 0.24$ and 2.2 MeV (see Fig. 7). These high-precision charged-particle elastic scattering measurements [39] put stringent constraints on fitting the neutron data through properties of multichannel R-matrix theory, such as the unitarity of the scattering matrix.

Another important set of measurements in this analysis are the relatively recent absolute differential cross section measurements for the ^{6}Li$(n,t)^4$He reaction done at the LANSCE/WNR facility at Los Alamos. These measurements confirmed the angular distributions measured at lower energies, and gave additional evidence for the presence of a $3/2^-$ resonance near E_n=2.2 MeV that had been seen in other data. They also indicated somewhat higher integrated cross sections for the reaction in the MeV region up to about 8 MeV than had been obtained in previous ENDF (and ENDL) evaluations.

TABLE VIII: Channel configuration (top) and data summary (bottom) for each reaction in the ^{7}Li system R-matrix analysis.

Channel	a_c (fm)	$l_{\max}$
t+^{4}He	4.02	5
n+^{6}Li	5.0	3
n+^{6}Li*	4.5	1
d+^{5}He	6.0	0

Reaction	Range (MeV)	# Data Pts.	χ^2/Pt.
^{4}He$(t,t)^4$He	$E_t = 0 - 14$ MeV	1649	1.31
^{4}He$(t,n)^6$Li	$E_t = 8.75 - 14.4$ MeV	39	3.35
^{4}He$(t,n)^6$Li*	$E_t = 12.9$ MeV	4	8.65
^{6}Li$(n,t)^4$He	$E_n = 0 - 4$ MeV	1445	2.24
^{6}Li$(n,n)^6$Li	$E_n = 0 - 4$ MeV	805	1.43
Total	χ^2/d.o.f.	3942	1.80

Figure 7 shows the evaluated ^{6}Li(n,t) integrated cross section at energies between 100 keV and 10 MeV. The cross section for ENDF/B-VII.1 was not changed from ENDF/B-VII.0 at energies below 1 MeV, since it is a neutron standard cross section in that energy range. However, above that energy, it follows the R-matrix fit in better agreement with the data of Macklin [40] and of Drosg [41]. These data represent only a small portion of the measurements of the integrated cross section included in the analysis, but they are considered to be the best measurements in this energy range. Above about 3.7 MeV, the evaluation follows the integrated cross sections obtained from the absolute differential cross sections measured at WNR [42], which indicate possible additional structure in the MeV range. The evaluated cross section then joins smoothly with the previous one (VII.0) at around 9 MeV, and is continued to 20 MeV without change.

Figure 8 shows a selection of the fitted ^{6}Li(n,t) differential cross cross sections compared with the measurements [43, 44, 45, 46]. One sees that, although over the years there has been considerable scatter in the measurements at a given energy, especially in MeV region, they tend to indicate resonant structure in the angular distribution as it transitions from the shape of the $5/2^-$ resonance at 240 keV to that of the $3/2^-$ resonance at 2.2 MeV, and possibly that of a higher-energy resonance above 3.7 MeV. The relatively new WNR measurements have been a welcome addition to the data base in that respect, clarifying resonance structure that the earlier data have only hinted at.

4. ^9Be

The evaluation in ENDF/B-VII.1 is only a single-channel fit the total cross section data at energies up to 14 MeV, including new low-energy measurements from RPI at the "iron windows" [47]. These calculations, shown in Fig. 9, also removed a "glitch" in the ENDF/B-VII.0 total cross section at around 425 eV. Improved analyses are underway that also include data for enumerated reactions (elastic scattering, multi-body breakup, and angular distributions) that may be completed in time to include in early revisions of the evaluation.

We have also upgraded the neutron capture cross section over the whole energy range, from below thermal to 20 MeV, taking into account a high-precision thermal value and an additional point near 38 keV. These are important changes for nuclear astrophysics applications. See Fig. 10. The thermal value is just over 10 mb, corresponding to the most accurate experimental value.

Future work on this system will include extension of our R-matrix analyses to include multi-body breakup (*e.g. (n,2n)* and angular distributions, but for now the information on these processes has been carried over from earlier ENDF analyses that are based on the measured data.

5. ^{nat}C

We have upgraded the neutron capture cross section from below thermal to higher energies by using JENDL-4.0, to better match data near 30 keV. This is important in nuclear astrophysics applications, see Fig. 11.

6. ^{16}O

Apart from the capture cross section, we have not changed the other data from ENDF/B-VII.0. We have upgraded the neutron capture cross section from below thermal to higher energies by using JENDL-4.0, to better match data near 30 keV. This is important in nuclear astrophysics applications, see Fig. 12.

Ongoing work is being done by G.M. Hale on a new R-matrix evaluation for oxygen, and a preliminary version of this was tested in the beta2 preliminary testing library for VII.1; it performed well against integral criticality tests, with a comparable level of agreement to our VII.1 final evaluated file (which was the same as VII.0 apart from capture). However, this preliminary beta2 evaluation gave a (n,α) cross section about 30% higher than that in VII.1=VII.0 in the 3-6 MeV range in agreement with the original scale of the Bair and Haas data (prior to their recommended 20% decrease), and in contradiction to new data reported by Georginis (IRMM, Geel) and by Khryachkov (IPPE). We decided to delay the release of a new R-matrix-based evaluation for oxygen until this discrepancy is better understood.

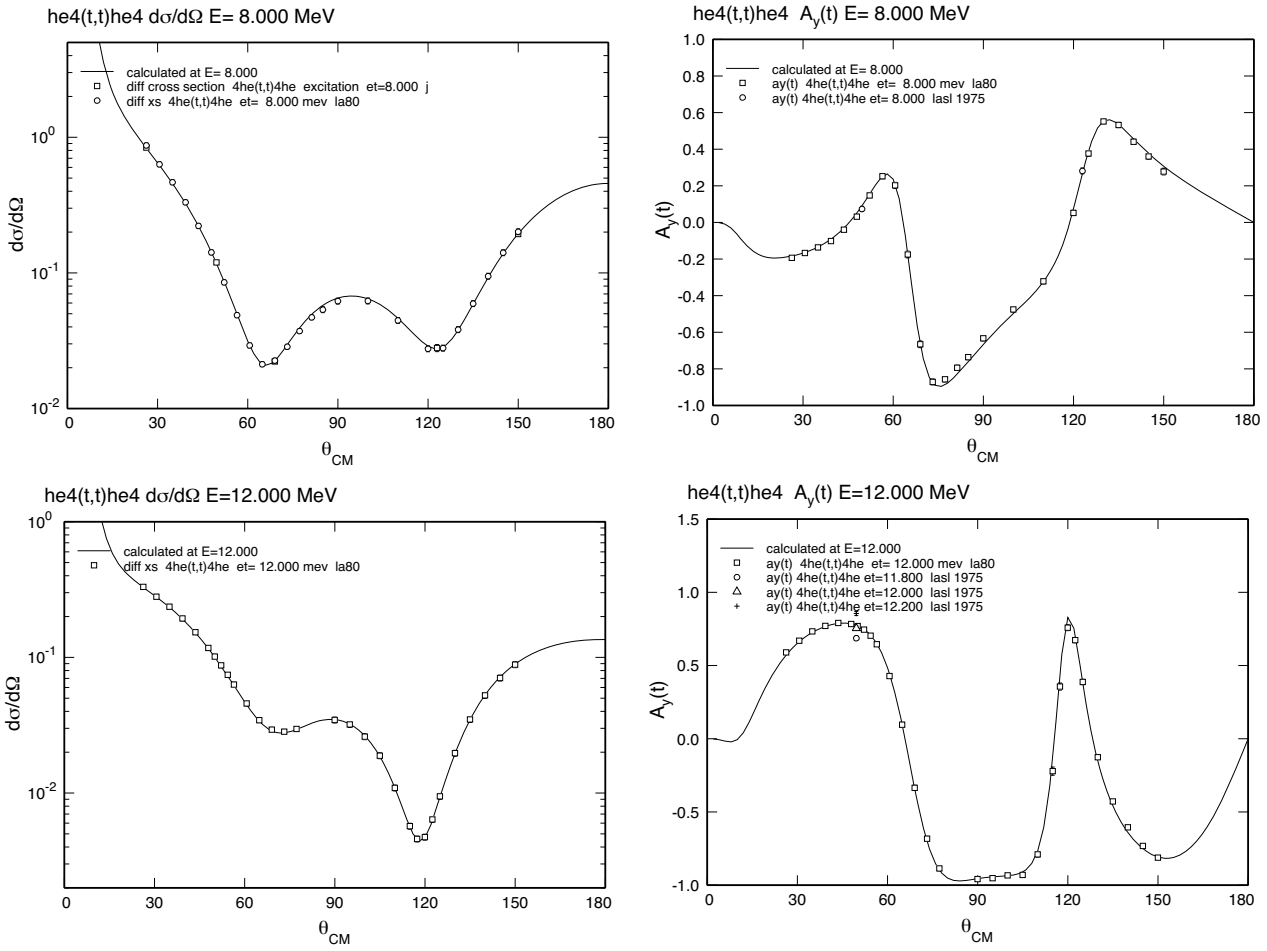

FIG. 6: Calculations of the differential cross section (left) and triton analyzing power (right), compared to the high-precision measurements from Los Alamos for t+^{4}He elastic scattering at E_t = 8 (top) and 12 (bottom) MeV [39].

B. Halogens & Alkali Metals

1. $^{35,37}Cl$

Resonance evaluations for ^{35}Cl and ^{37}Cl were carried out in the energy region from thermal to 1.2 MeV [49]. The expansion of the ENDF-6 format with the LRF=7 option allowed to include charged particle exit channels in the evaluation for ^{35}Cl. The evaluation for both ^{35}Cl and ^{37}Cl include resonance parameters and resonance parameter covariances. Since the proton exit channel for ^{35}Cl is open everywhere, *i.e.*, Q = +0.61522 MeV, the LRF=7 option for the resonance parameters were used. Also the compact formalism was used for covariance representation (LCOMP=1). The Reich-Moore format with LRF=3 was utilized for ^{37}Cl and LCOMP=1 for the covariance representation. The Cl evaluations were based on fits of many data sets with the SAMMY code. A detailed discussion of the analysis methods used to determine parameter values and uncertainties is given in Ref. [49]. For capture and neutron width uncertainties, for example, several SAMMY calculations with different width values for each resonance were overlaid with the data. Both the overlay plots and χ^2 changes with width variation were used to determine final uncertainties that were, in most cases, significantly larger than the SAMMY values.

At the time of the Cl evaluation, SAMMY did not incorporate the now available "Prior Uncertainty Parameter", or PUP procedure. Thus, some normalization and background uncertainties were not propagated properly through the sequential analysis of multiple data sets. Although uncertainties in resonance energies and widths are felt to be realistic, the uncertainties in computed cross sections in valleys between resonances were underestimated. Furthermore, File 32 is

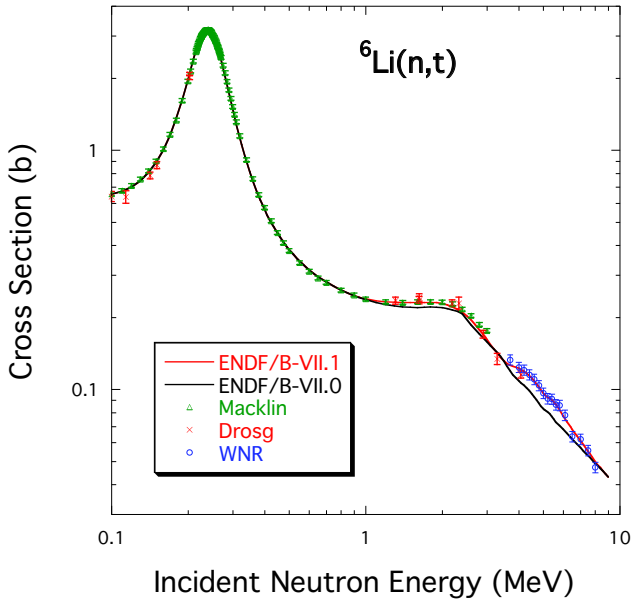

FIG. 7: Integrated cross section for the ^{6}Li$(n,t)^4$He reaction at energies between 0.1 and 10 MeV, showing ENDF/B-VII.1 (red curve), ENDF/B-VII.0 (black curve), and the experimental data of Macklin [40] (green triangles), Drosg [41] (red crosses), and WNR [42] (blue circles).

limited by the ENDF-6 format to resonance parameter uncertainties and correlations while uncertainties in nuclear radii cannot be treated directly. The "normalization/background/radius" effects were represented approximately by adjusting the File 32 uncertainties for the external RPs and for selected resonances in the energy range of the evaluation. Since the resonance parameter representation does not include the direct capture (DC) part of the capture cross section, the DC component was included as a "background" $1/v$ cross section in File 3, sections 1 and 102. At $E = 0.0253$ eV, the ^{35}Cl (^{37}Cl) DC cross section is 0.16 (0.31) b, which is a small (large) fraction of the overall capture cross section of 43.60 (0.433) b. The upper energy limit for the DC cross section is estimated to be 10 (100) keV for ^{35}Cl (^{37}Cl). The $1/v$ cross section was extended to 1.0 MeV to ensure continuity in the evaluation range. Cross section at the thermal values for ^{35}Cl and ^{37}Cl calculated at room temperature are displayed on Table IX. The uncertainties in the thermal cross sections were calculated with PUFF-IV using the resonance parameter covariance data.

2. $^{39,41}K$

Evaluations of ^{39}K and ^{41}K neutron cross sections in the resolved resonance region were done with the multilevel Reich-Moore R-matrix formalism of the SAMMY code. The evaluation incorporates recent high-resolution

TABLE IX: Thermal cross sections and their uncertainties for ^{35,37}Cl+n in barns.

Isotope	Cross Section	VII.1	VII.0	Atlas
^{35}Cl	Capture	43.60±0.52	43.67	43.60±0.40
	Total	64.76±0.68	65.12	64.70±0.50
	Scattering	20.68±0.35	20.97	20.60±0.30
	(n,p)	0.480±0.029	0.48	0.48±0.014
^{37}Cl	Capture	0.433±0.006	0.433	0.433±0.006
	Total	1.583±0.050	1.593	1.583±0.050
	Scattering	1.15±0.05	1.16	1.15±0.05

capture and transmission measurements made at ORELA to extend the resolved resonance energy range up to 1.0 MeV with a much more accurate representation of the data than previous evaluations. The data include transmission measurements by Guber *et al.* [50] and Harvey, *et al.* [51] on the 80-m flight path at ORELA; total cross section data of Cierjacks *et al.* [52] on a 57-m flight path performed at the Karlsruhe Isochronous Cyclotron; and measurements of Singh, et al. [53] done at the 200-m flight path at the Columbia synchrocyclotron. Also included in the evaluation were the high-resolution capture cross section of Guber *et al.* measured in the energy range of 0.1 keV to 600 keV and an older low resolution capture data of Joki, *et al.* [54] done in the energy region from 0.02 eV to 10 eV. We have included resonance parameters (RPs) in File 2, MT151, and the corresponding resonance parameter covariances in File 32, MT15. The Reich-Moore format with LRF=3 and LCOMP=1 was utilized. The applicable energy range is 10^{-5} eV to 1.0 MeV. At 1.0 MeV the File 3 total and elastic cross section values for the previous ENDF evaluations were adjusted slightly to join smoothly with the resonance parameter values. For capture cross sections above 1 MeV, the previous ENDF ^{39}K theoretical values were normalized to 0.436 mb at 1 MeV, and the ^{41}K values were normalized to match the data of reference [55] at 1 MeV. Since the resonance parameter representation does not include the direct capture (DC) part of the capture cross section, the DC component was included as a "background" $1/v$ cross section in File 3, sections 1 and 102. At E = 0.0253 eV, the calculated DC cross section for ^{39}K (^{41}K) is 0.80 (0.52) b, which is a large fraction of the overall capture cross section of 2.10 (1.46) b. The upper energy limit for the DC cross section is estimated to be 100 keV. Therefore, the "background" $1/v$ cross section was terminated at this energy value.

Table X gives a comparison of the thermal elastic, capture and total cross sections at room temperature with the data listed in the Atlas. Also shown in Table X are the thermal values calculated with ENDF/B-VII.0. The quoted uncertainties, obtained from File 32, reflect the rather large experimental uncertainties in the thermal values. The thermal scattering cross-section for ^{41}K in the Atlas is almost 3 times smaller than that of the present evaluation. The reasons for the discrepancies are not known.

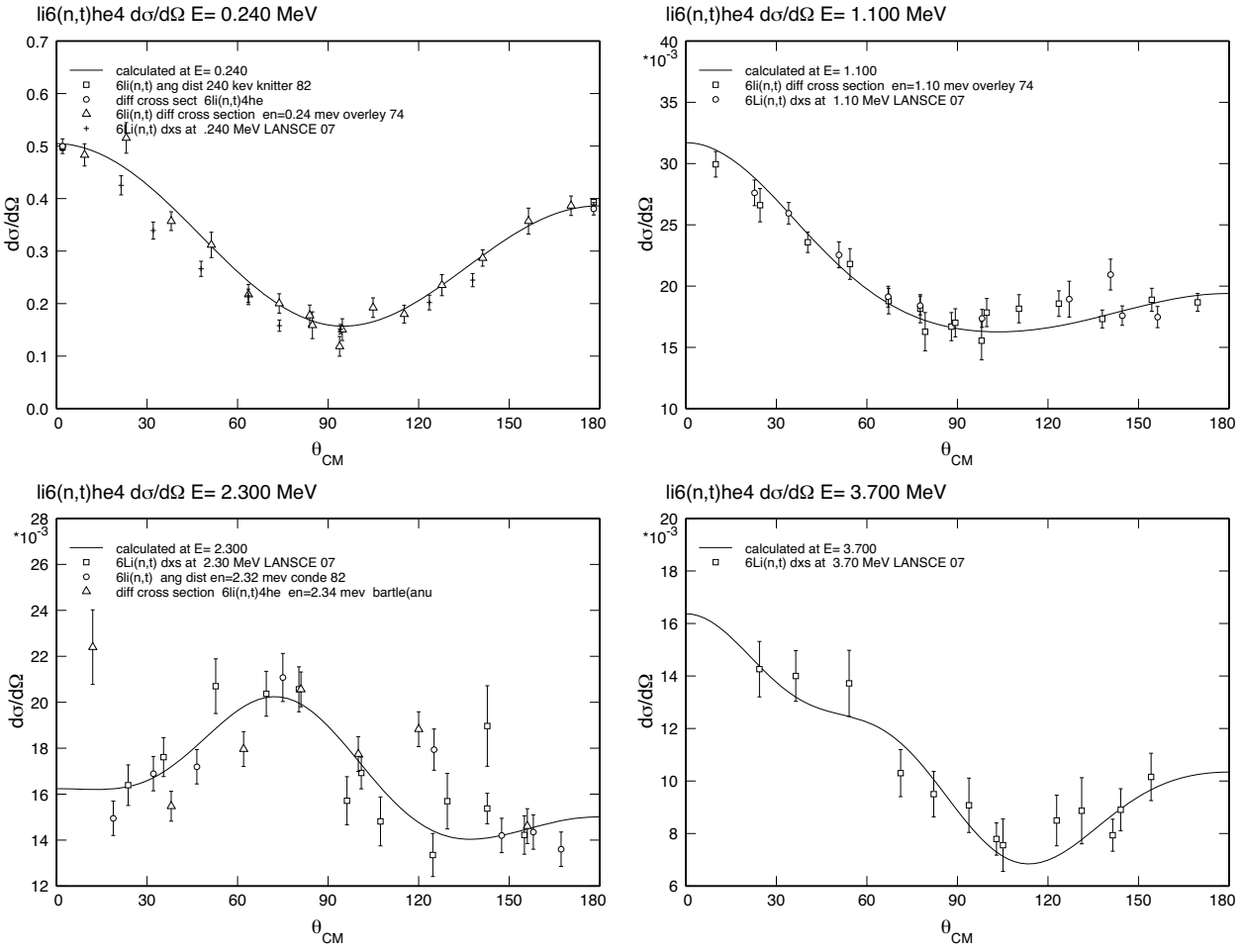

FIG. 8: Differential cross sections for the ^{6}Li$(n,t)^4$He reaction at energies between 0.24 and 3.7 MeV, showing ENDF/B-VII.1 (solid curve) compared to the experimental data of WNR, Knitter, Overley, Conde, and Bartle [42, 43, 44, 45, 46].

TABLE X: Thermal cross sections and their uncertainties for ^{39,41}K+n in barns.

Isotope	Cross Section	VII.1	VII.0	Atlas
^{39}K	Capture	2.13±0.10	2.10	2.10±0.20
	Total	4.19±0.14	4.19	-
	Scattering	2.06±0.10	2.09	1.99±0.17
^{41}K	Capture	1.46±0.09	1.46	1.46±0.03
	Total	4.03±0.14	4.06	-
	Scattering	2.56±0.10	2.60	0.92±0.20

C. Structural Material Evaluations

1. Ti

Titanium is an effective absorbent that serves as baseline material for separation in high-activity waste solutions. Titanium has not been considered for use in nuclear applications such as reactor design and analysis. Rather, it normally appears as a structural material that may be present in fuel cycle facilities or canisters for transport and disposition of nuclear waste. Criticality safety evaluations of systems in which titanium is present require an understanding of the nuclear data and its uncertainty.

ENDF/B-VII.0 had previously adopted the evaluations for ^{46,47,48,49,50}Ti from JENDL-3.3 [56]. These data files were replaced by new evaluations at LANL and ORNL, because of two issues concerning the titanium evaluations reported in the past, namely a $k_{\rm eff}$ bias problem for highly-enriched critical assemblies with a titanium reflector, and an energy balance problem. We also considered new experimental results for (n,n') and (n,2n) cross sections on ^{48}Ti at LANSCE, taken with the GEANIE detector [57].

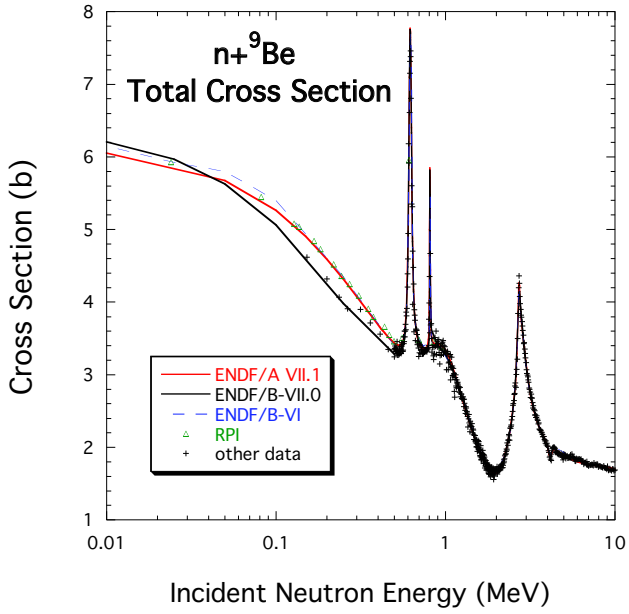

FIG. 9: Total cross section for n+^{9}Be, showing ENDF/B-VII.1 (red curve), ENDF/B-VII.0 (black curve), and the data from Danon (green triangles) and others (black crosses).

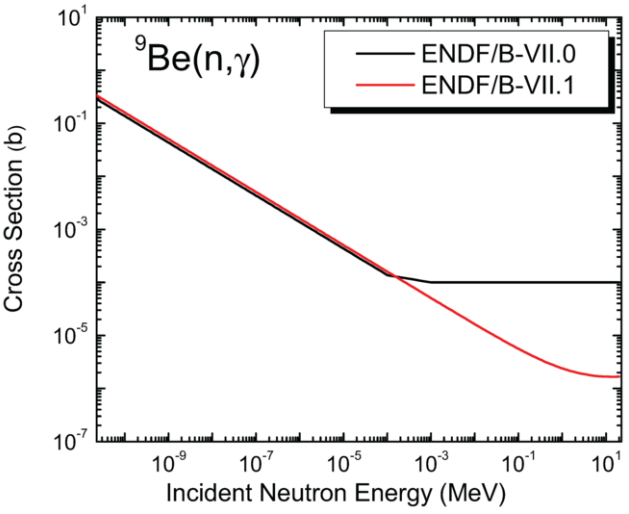

FIG. 10: Neutron capture on ^{9}Be. The red curve is ENDF/B-VII.1, the black curve is ENDF/B-VII.0, and the circles are measured values.

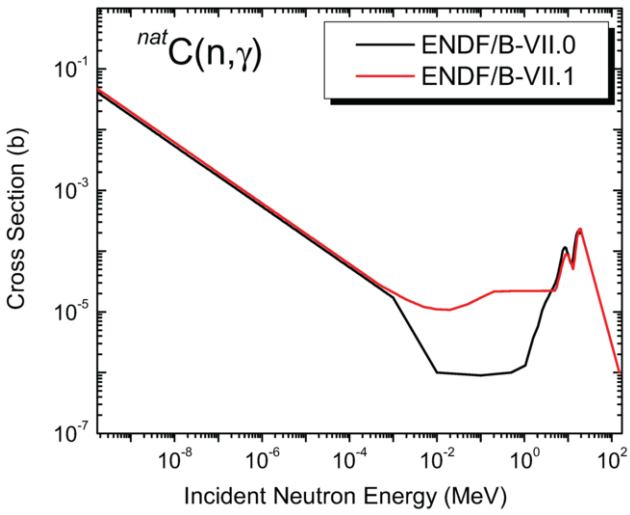

FIG. 11: Neutron capture on ^{nat}C. Compared are cross sections in ENDF/B-VII.1 with ENDF/B-VII.0.

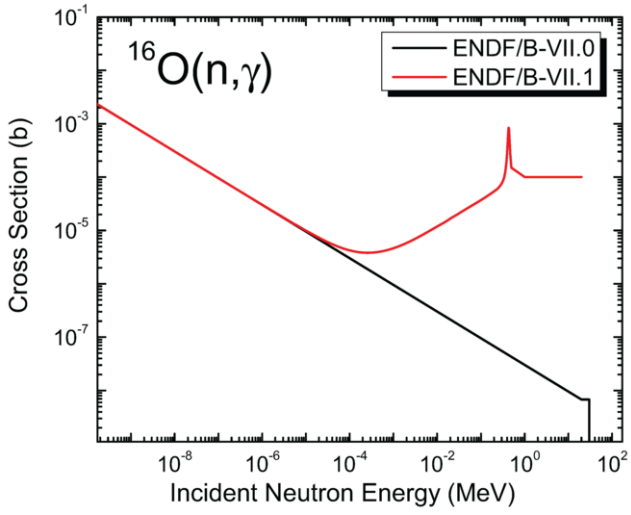

FIG. 12: Neutron capture on ^{16}O. Compared are cross sections in ENDF/B-VII.1 with ENDF/B-VII.0.

Resonance region

To improve the cross section data and uncertainty for titanium in the thermal and epithermal energy regions a resolved resonance parameter and covariance evaluation for ^{48}Ti was done with the SAMMY [58] code. New capture and transmission measurements for enriched ^{48}Ti and natural titanium were made at the ORELA. The neutron transmission and capture data were measured in the energy range from 10 eV to 500 keV. The transmission data were measured with an 80-meter flight-path length, whereas a 40-meter flight-path length was used for the capture cross-section measurements. Since there are no previous capture cross-section measurements available in the resonance region, the ORELA data were vital for determining the shape and the uncertainty in the capture cross section. The resonance evaluation for ^{48}Ti was done in the energy range from 10^{-5} eV to 400 keV. Thermal cross section data available in the EXFOR database [59] were also used in the evaluation.

TABLE XI: Thermal cross sections and their uncertainties for ^{48}Ti+n in barns.

Isotope	Cross Section	VII.1	VII.0	Atlas
^{48}Ti	Capture	8.32±0.23	7.84	8.32±0.16
	Total	12.35±0.30	12.16	12.42±0.25
	Scattering	4.03±0.17	4.32	4.10±0.20

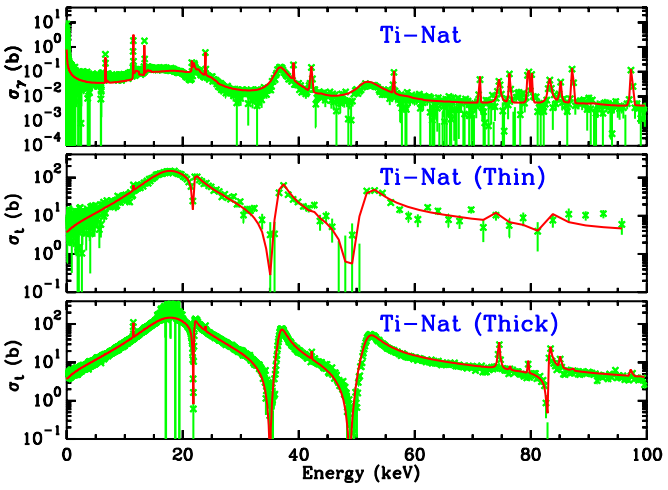

FIG. 13: Comparisons of SAMMY calculations with the resonance parameters of the total and capture cross-sections of natural titanium in the energy region 10 eV to 100 keV.

Fig. 13 displays the results of the SAMMY fitting of the total and capture cross-sections from 10 eV to 100 keV. A resonance parameter covariance was generated for ^{48}Ti as a result of the evaluation with SAMMY. In the SAMMY fit of the experimental data systematic uncertainties such as data normalization, background, *etc.* were propagated into the final resonance parameter covariance. The resonance parameter covariance were converted in the ENDF format using the LCOMP=1 option and processed with PUFF-IV module of AMPX-6. No resonance evaluation was done for ^{46}Ti, ^{47}Ti, ^{49}Ti, and ^{50}Ti. Consequently, the covariances for these isotopes were generated based on the retroactive approach. The uncertainty in the total, capture, and scattering cross sections at the thermal energy for ^{48}Ti are displayed in Table XI. Also listed in Table XI are the Atlas results and that of the ENDF/B-VII.0. The capture resonance integral and uncertainty calculated with the resonance parameter covariance is 3.78±0.17 barns, for the Atlas the value is 3.90±0.25 barns whereas for ENDF/B-VII.0 the value is 3.68 barns. Comparisons of the ENDF/B-VII.0 and ENDF/B-VII.1 capture cross-sections for ^{48}Ti are shown in Fig. 14. Several new resonances have been identified which were not present in the ENDF/B-VII.0 evaluation. The data resolution allowed the identification of these resonances. Benchmark calculations using the titanium ENDF/B-VII.1 evaluation have shown improvements over calculations done with ENDF/B-VII.0, as discussed in more detail by Kahler [8].

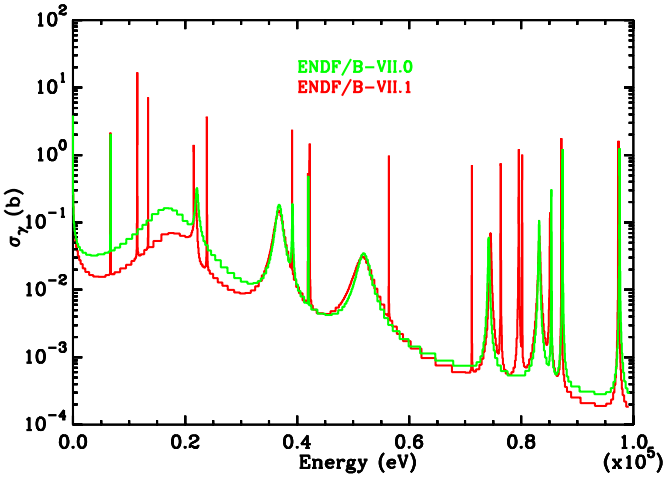

FIG. 14: Comparisons of the capture cross-section of ^{48}Ti calculated with ENDF/B-VII.0 and ENDF/B-VII.1.

Higher energy region

Above the resonance regions, all the cross sections were calculated with the GNASH and CoH_3 [60] codes, where the model parameters were adjusted to optimize agreement with the available experimental data, including the γ-ray production cross section data measured at GEANIE [57]. We have also produced covariance matrices for the cross sections from the nuclear reaction model calculations with the KALMAN code.

The energy balance problem in the earlier ENDF/B-VII.0 Ti evaluations, which were taken from JENDL-3.3, arose due to a bug in a code when neutron and γ-ray energy spectra were calculated. The energy spectra were recalculated with the CoH_3 code, and we confirmed energy conservation was properly accounted for by using the HEATR module in NJOY.

An important modification to the ^{48}Ti was elastic scattering angular distributions at low energies. In ENDF/B-VII.0 the elastic scattering angular distributions are calculated with the optical model and the Hauser-Feshbach statistical model. We found that the calculated P_1 (the $L = 1$ component of the Legendre expansion coefficients) for the differential elastic scattering tends to overestimate the reflection of neutrons in the critical assemblies with a Ti reflector, and adjustment of the optical potential parameters does not solve this problem. This was finally resolved by replacing the elastic scattering angular distributions of ^{48}Ti up to 4 MeV by those in ENDF/B-VI (in fact they are the same as ENDF/B-V by C. Philis, A.B. Smith, and R. Howerton in 1977), in which the angular distributions were evaluated based on experimental data of Langsdorf *et al.* [61], Barnard *et al.* [62] and Guenther *et al.* [63]. The evaluated P_1's in ENDF/B-VII.0 and ENDF/B-VII.1 are compared in Fig. 15. The larger P_1 values in ENDF/B-VII.1 in the fast energy range give more neutron scattering in the forward angles, which re-

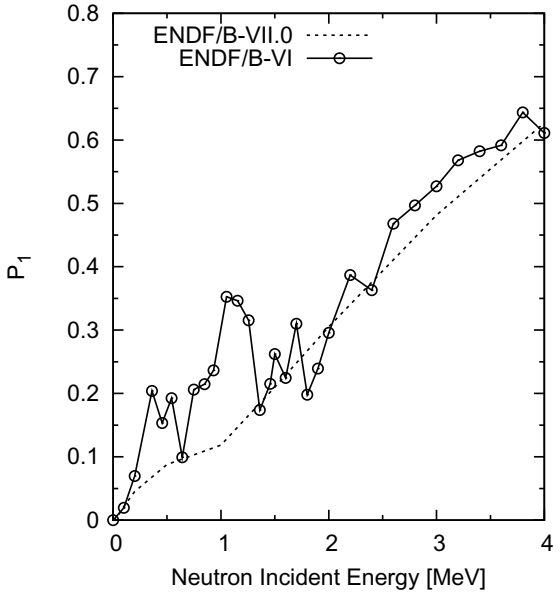

FIG. 15: The $L = 1$ component of the Legendre expansion coefficients for the differential elastic scattering from ^{48}Ti, as a function of neutron incident energy.

sults in less reflection of neutrons inside the reflector, and consequently improved agreement with critical assembly data [8].

2. V

An elemental vanadium evaluation was previously given in ENDF/B-VII.0. For ENDF/B-VII.1 we provide a new ^{51}V evaluation; the ^{50}V was taken from JENDL-4.0 (its isotopic abundance is very small, 0.25%).

The motivation of our re-evaluation of vanadium data is given below. The original ENDF/B-VI evaluation was developed by Smith *et al.* in the late 80's [64, 65]. In 1999, the importance of gas production data on vanadium was studied [66], leading to the (n,np) and (n,t) reaction cross sections being updated by Rochman *et al.* in 2005 [67]. The changes in the (n,np) and (n,t) channels were absorbed by adjusting the continuum inelastic scattering cross sections, which does not preserve consistency in the model calculations. For ENDF/B-VII.1, LANL performed statistical model calculations with the CoH_3 code, maintaining the quality of the evaluations by Rochman *et al.*, and replaced all the reaction cross sections in ENDF/B-VII.0 by these new calculations.

As an example, the evaluated capture cross section is shown in Fig. 16. In this plot, the experimental data of Dudey *et al.* [68] and Sahota *et al.* [69] are shown by the filled-squares and open-circles, and all the other data are shown by the filled-circles. The experimental data of Sahota et al. [69] were corrected by using the recent evaluated cross section of ^{127}I capture reaction as a monitor, as well as the updated γ-ray branching ratio.

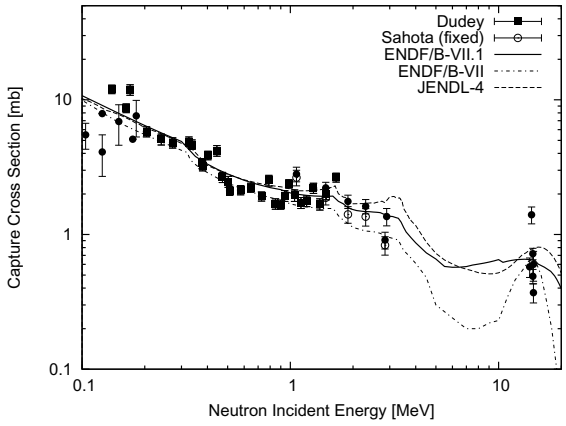

FIG. 16: The evaluated ^{51}V capture cross sections, compared with available experimental data. We have selected two experimental data sets — Dudey *et al.* and Sahota *et al.*, and all the other data were shown by the filled circles.

Because vanadium is an important structural material for nuclear technology, the total and elastic scattering cross sections in the fast energy range play a key role in the neutron shielding calculations. The fluctuating behavior in the total cross section in the MeV energy range cannot be reproduced by an optical model calculation, and we often reproduce the experimental total cross section by a least-squares method. The total cross sections in ENDF/B-VII.0 (same as ENDF/B-VI) and JENDL-4.0 were evaluated in that way, hence basically they follow a tendency of experimental data in the MeV region. We compared these evaluations, and concluded that the more recent JENDL-4.0 evaluation gives a better agreement with the experimental data. Therefore the JENDL-4.0 total cross section was adopted up to 5 MeV, and a new optical model calculation was used above this energy.

3. ^{55}Mn

Accurate neutron capture cross-sections of ^{55}Mn are important for fission and fusion reactor designs in view of its use as an alloy structural material. It is also a well known neutron dosimeter. Furthermore, accurate cross-section data are needed to support criticality safety analyses.

The previous ENDF/B-VII.0 evaluation for ^{55}Mn neutron induced reactions dates back to 1988 [70]. The important ^{55}Mn(n,2n) reaction has been recently reevaluated from threshold up to 40 MeV for neutron dosimetry applications [71]. Deficiencies of the dosimetric evaluation of the ^{55}Mn(n,γ) reaction have been often reported. The availability of new experimental capture data [72, 73] in the resonance range, and of a new dosimetric evaluation, motivated the work presented herein.

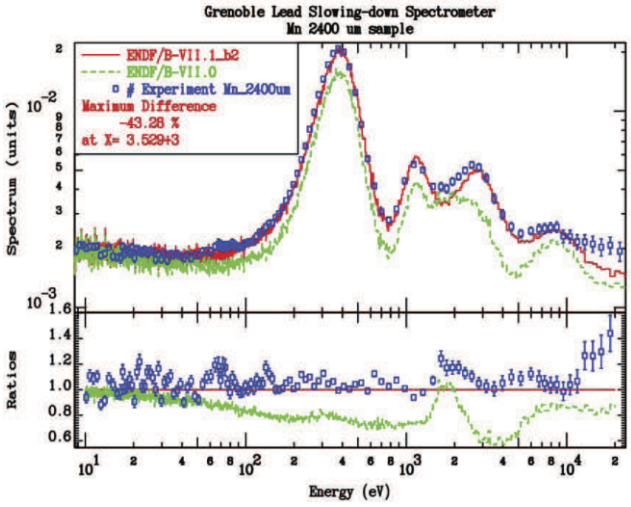

FIG. 17: Grenoble lead-slowing down benchmark data for ^{55}Mn sample (blue squares) [75] vs calculations using ENDF/B-VII.0 (green line) and ENDF/B-VII.1 (red line).

Resonance range

Resonance parameters for ^{55}Mn in the ENDF/B-VII.0 evaluated data files are mainly based on the work performed by Garg *et al.* and by Macklin [74]. The work by Macklin was aimed to meet 10% accuracy in the lowest energy resonances and 20% accuracy up to 100 keV. But measurements done by Perrot *et al.* [75] using a lead slowing-down-spectrometer and simulations have shown that the previously evaluated ^{55}Mn-capture cross sections are inadequate in the energy range of 50 eV to 30 keV as shown in Fig.17. A suggestion was made in 2008 to re-evaluate the ^{55}Mn cross section [76]. A new resonance evaluation of ^{55}Mn was carried out with the SAMMY code [58] including recent experimental transmission and capture data measured at ORELA and GELINA facilities. The evaluation was undertaken in attempt to obtain more accurate resonance parameters in the thermal energy range to 125 keV, below the first inelastic channel.

For the evaluation of the cross sections in the thermal energy range, earlier measurements were added to the experimental data base: total cross section from Coté *et al.* [77] and Rainwater *et al.* [78], and capture cross section from Widder *et al.* [79]. The thermal capture cross section was normalized at the 0.0253 eV value of 13.27 b which is an average of the available experimental values, consistent with the 13.10 b value recommended by IUPAC for neutron activation analysis [80]. The uncertainty of the capture cross section in the thermal region was reduced for consistency with Mughabghab [35] and the IUPAC database [80].

Thermal cross sections for this evaluation are listed in Table XII along with the uncertainty. Also shown in Table XII are the Atlas [35] and the ENDF/B-VII.0 values. The infinite dilute resonance integral calculated from this evaluation is 13.52 ± 0.30 b compared to 13.4 ± 0.5b recommended by the Atlas. The IUPAC recommended ratio $Q_0 = 1.053 \pm 0.032$ [80] of the resonance integral to the thermal cross section is also in excellent agreement with the ENDF/B-VII.1 value of 0.998 ± 0.036. The Q_0 value of the ENDF/B-VII.0 evaluation equal to 0.867 was discrepant.

TABLE XII: ^{55}Mn+n thermal cross sections and their uncertainties in barns.

Cross Section	VII.1	VII.0	Atlas [35]
Capture	13.27±0.11	13.41	13.36±0.05
Total	15.39±0.20	15.58	-
Scattering	2.12±0.04	2.17	2.06±0.03

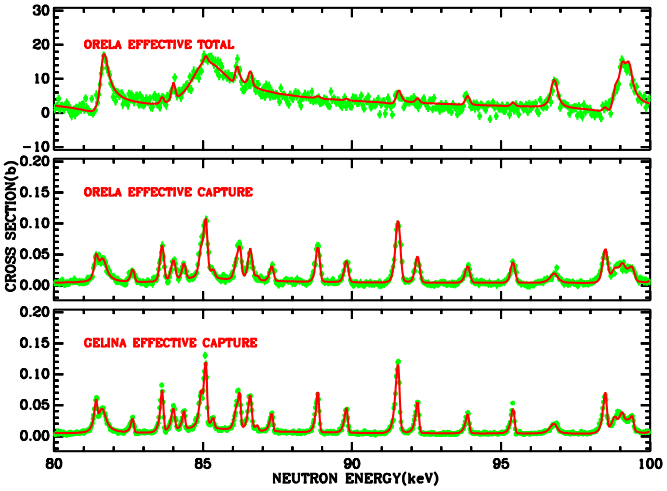

FIG. 18: SAMMY fit of the ^{55}Mn experimental total cross-sections and of the experimental capture cross-section in the energy range of 80 to 100 keV. The solid line represents the cross section calculated by the resonance parameters.

The experimental database in the resonance region includes the 1988 neutron transmission measurement of Harvey *et al.* [81], the 2005 GELINA capture cross section measurement of Aerts *et al.* [73] and the ORELA capture measurement of Guber [72]. The experimental resolution of the capture data allowed a good separation of the resonances up to about 120 keV neutron energy. The sample used in GELINA and ORELA capture measurements had thicknesses of 0.0190 at/b and 0.0178 at/b, respectively, resulting in large self-shielding and multiple-scattering effects. The updated version of SAMMY [58] allowed an accurate correction for these experimental effects. An example of SAMMY fit is given in Fig. 18, showing the total cross section obtained from the experimental transmission and the GELINA effective capture cross sections, in the energy range 80 to 100 keV.

The ^{55}Mn resonance parameters and the corresponding covariance matrix derived in the evaluation were converted to the ENDF-6 format. Comparison of the ENDF/B-VII.0 and ENDF/B-VII.1 capture cross-sections for ^{55}Mn are shown in Fig. 19. There is considerable discrepancy in the new capture cross section

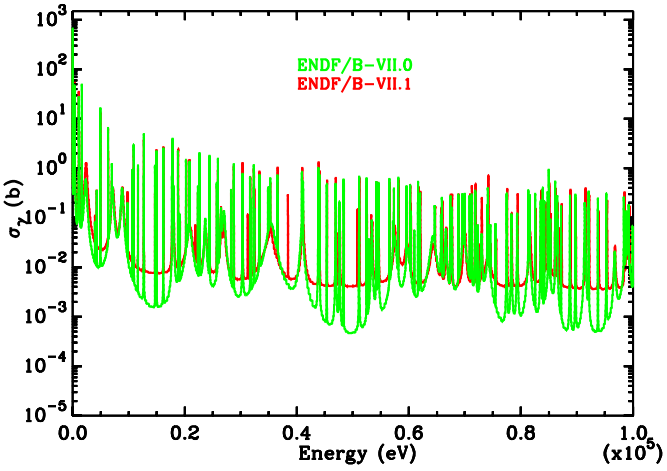

FIG. 19: Comparisons of the capture cross-section of ^{55}Mn calculated with ENDF/B-VII.0 and ENDF/B-VII.1.

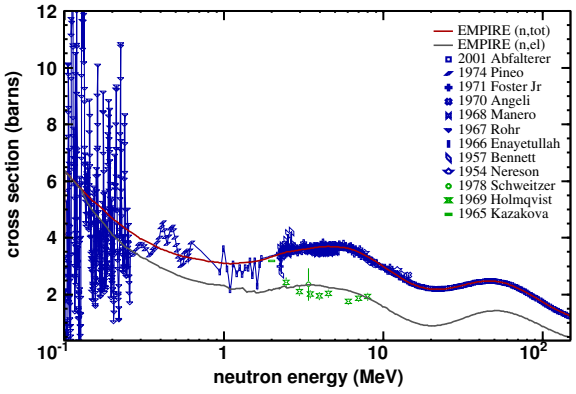

FIG. 20: Experimental total and elastic cross sections on ^{55}Mn nucleus vs. EMPIRE=VII.1 calculations with rigid-rotor dispersive coupled-channel neutron OMP (RIPL 1484). GANDR least-squares results are not shown.

compared to ENDF/B-VII.0 data in the resonance range, but the new evaluation is strongly supported by the analysis of the Grenoble Lead-Slowing-Down benchmark [75] as previously shown in Fig. 17; a major improvement is clearly seen compared to ENDF/B-VII.0 data.

Evaluation methodology in the fast neutron range

The employed evaluation methodology in the fast neutron range developed at the IAEA Nuclear Data Section (R. Capote and A. Trkov) combines theoretical modeling of relevant reactions using the EMPIRE model code [82] with a Bayesian generalized least-squares fitting to include experimental data as implemented in the GANDR code [83]. Modeling results define a theoretical prior that includes both average quantities and corresponding covariance matrices. The raw experimental data retrieved from the EXFOR database [59] are corrected to the latest standards, data correlations are assessed, and discrepant data are either modified or discarded. The calculated modeling prior and selected experimental data are fed into the GANDR system to produce intermediate evaluation results. These fitting results are combined with a selected evaluation of resonance parameters to assemble a full evaluated nuclear data file.

Model calculations in the fast energy range for all IAEA evaluations were based on nuclear model calculations using the EMPIRE code [82], and based on newly derived coupled-channel optical model potentials using dispersion relations (see Refs. [58, 84] and references therein). Starting values for nuclear model parameters were taken from the RIPL recommendations [85, 86]. All the optical model calculations were performed with the ECIS code [87] that is incorporated into the EMPIRE system. The incident channel OMP was always used to calculate direct excitation of the collective levels in the continuum by the DWBA method, which is important for a proper description of double differential cross sections and emission spectra above 5 MeV for all evaluated nuclei. Pre-equilibrium emission was considered using a one-component exciton model (PCROSS), which includes nucleon, gamma and cluster emission. Hauser-Feshbach [88] and Hofmann-Richert-Tepel-Weidenmüller [89] versions of the statistical model were used for the compound nucleus cross section calculations. Both approaches account for the multiple-particle emission and the full gamma-cascade. Level densities were described by the "EMPIRE specific" formalism (EGSM), which uses the superfluid model below the critical excitation energy and the Fermi gas model above [82, 85].

Fast energy range

For the ^{55}Mn evaluation we selected a recently derived OMP of Soukhovitskii and Capote (RIPL catalogue number 1484, see Table 6, p. 3137 of Ref.[85]). This is a dispersive coupled-channel OMP reproducing all available nucleon scattering data on ^{55}Mn nucleus from 100 keV up to 150 MeV, including also low-energy observables like the neutron strength functions and the scattering radius. Using this model, the agreement of calculated total and elastic cross sections with measurements is very good, as shown in Fig. 20.

A modified Lorenzian (MLO) radiative-strength function was taken as recommended by Plujko [85] and resulted in excellent agreement with the experimental neutron capture database in the fast neutron range. The evaluated total inelastic cross section differs significantly from the ENDF/B-VII.0 evaluation, but is in good agreement with Lashuk (n,n'γ) measurements of the excitation of first and second inelastic levels in ^{55}Mn nucleus [90] as can be seen from Fig. 21.

Benchmarks

A comprehensive analysis of criticality benchmarks' results and data verification can be found in a companion paper by Kahler *et al.* in this edition [8]; some favorable improvements are discussed for manganese.

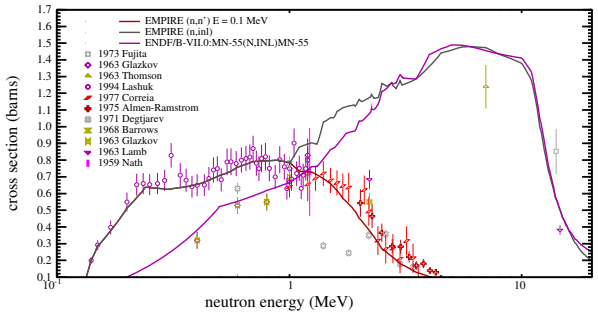

FIG. 21: Experimental inelastic cross sections on ^{55}Mn nucleus vs EMPIRE=VII.1 calculations (red,gray) and ENDF/B-VII.0 evaluation (magenta). GANDR least-squares results are not shown.

4. $^{50,52,53,54}Cr$

Resolved resonance parameter evaluations for chromium isotopes[91], namely ^{50}Cr, ^{52}Cr, ^{53}Cr, and ^{54}Cr, were done with the SAMMY[92] code. The descriptions of the measured data used in the evaluation are indicated in Table XIII. The determination of the resolved resonance parameters for the chromium isotope below 100 keV relied mainly on the recent ORELA measurements. The ORELA capture cross-section data were essential in the evaluation since there are no capture cross section data available in the literature. In addition to the new ORELA measurements, existing high-resolution transmission data for enriched nuclides were also included in the evaluation. Thermal cross section data available in the EXFOR database were also included in the evaluation.

The resonance regions for each chromium isotope were extended by taking advantage of the new ORELA high-resolution data and existing transmission data. The energy ranges for the evaluation done for ENDF/B-VII.1 compared with ENDF/B-VII.0 are shown in Table XIV. Comparisons of the SAMMY R-matrix fit to the data of Guber for natural chromium up to 100 keV are shown in Fig. 22 and Fig. 23, respectively. The top curve represents the capture cross section whereas the two other curves are the total cross sections corresponding to two transmission with thickness of 0.026269 at/b (thin sample) and 0.053103 at/b (thick sample), respectively. Below 100 keV the evaluation relied on the transmission and capture data measurements done by Guber *et al.* at ORELA.

For each of the chromium resonance evaluation with the SAMMY code resonance parameters covariances were generated as a result of the evaluation. In the SAMMY fit of the experimental data systematic uncertainties such as data normalization, background, *etc.* were propagated into the final resonance parameter covariance. The resonance parameter covariances were converted in the ENDF

TABLE XIII: Experimental ORELA transmission and capture.

Data Set	Author	Energy Range (keV)	Flight Path (m)	Density (at/b)
Natural Chromium				
Transmission	Guber	0.01 - 600	79.827	0.053103
Transmission	Guber	0.01 - 600	79.827	0.026269
Capture	Guber	0.01 - 600	38.414	0.0262696
^{50}Cr				
Transmission	Harvey	90 - 800	201.575	0.0606907
^{52}Cr				
Transmission	Harvey	80 - 1450	201.575	0.0605925
Transmission	Harvey	80 - 1450	201.575	0.0394804
^{53}Cr				
Transmission	Guber	0.01 - 600	79.827	0.0056181
Transmission	Guber	0.01 - 600	79.827	0.0179843
Capture	Guber	0.01 - 600	40.116	0.0137050
Transmission	Harvey	60 - 600	201.575	0.0593000
^{54}Cr				
Transmission	Harvey	13 - 850	201.575	0.0541125

TABLE XIV: Range of energies for existing and new evaluations.

Isotope	VII.1	VII.0
^{50}Cr	10^{-5} eV – 600 keV	10^{-5} eV – 783 keV
^{52}Cr	10^{-5} eV – 1.2 MeV	10^{-5} eV – 1.43 MeV
^{53}Cr	10^{-5} eV – 245 keV	10^{-5} eV – 564 keV
^{54}Cr	10^{-5} eV – 750 keV	10^{-5} eV – 834 keV

TABLE XV: Thermal cross sections and their uncertainties for ^{52,53}Cr+n in barns.

Isotope	Cross Section	VII.1	VII.0	Atlas
^{52}Cr	Capture	0.86 ± 0.02	0.75	0.86 ± 0.02
	Total	3.93 ± 0.01	3.73	3.82 ± 0.03
	Scattering	3.07 ± 0.42	2.99	2.96 ± 0.02
^{53}Cr	Capture	18.41±0.51	18.06	18.60±0.60
	Total	26.39±0.28	25.99	26.38±0.62
	Scattering	7.98±0.28	7.92	7.78±0.20

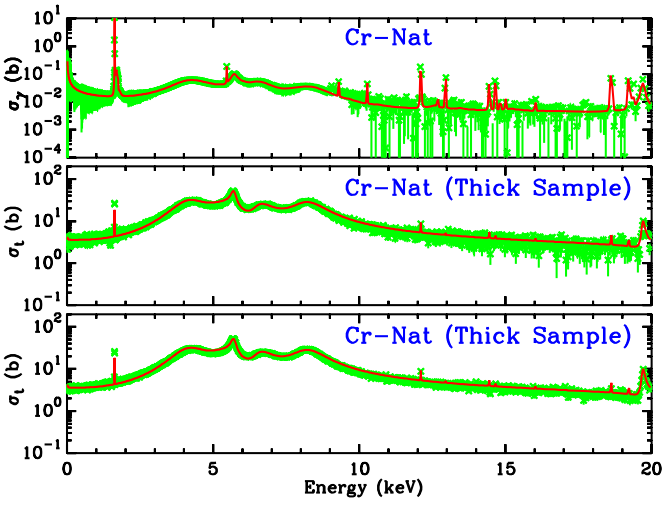

FIG. 22: Comparisons of SAMMY calculations with the resonance parameter (solid line) of the total and capture cross-sections of natural chromium in the energy region 10^{-5} eV to 20 keV.

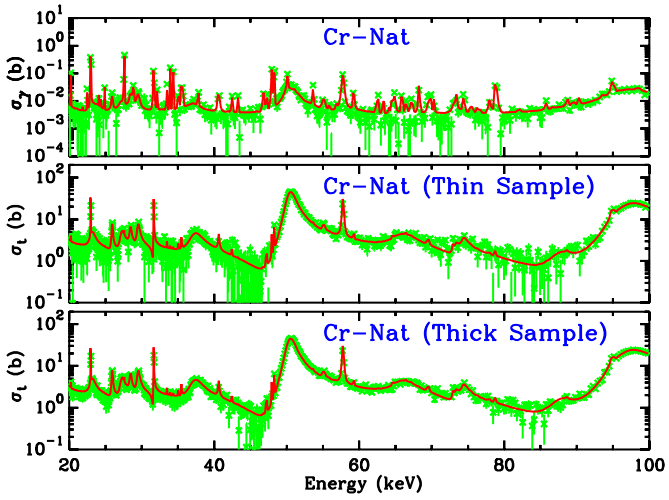

FIG. 23: Comparisons of SAMMY calculations with the resonance parameter (solid line) of the total and capture cross-sections of natural chromium in the energy region 20 keV to 100 keV.

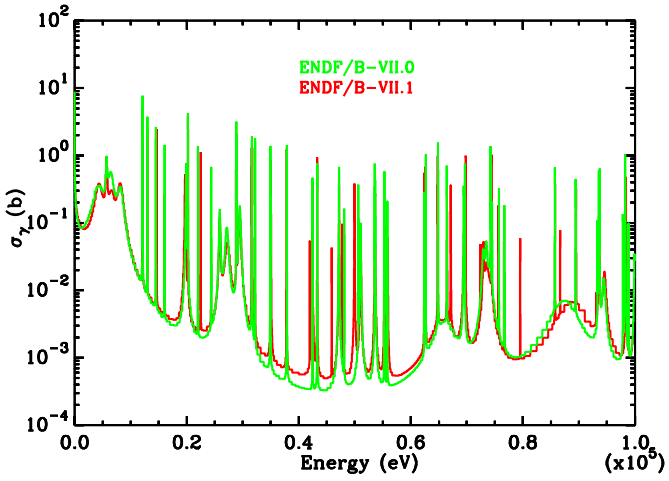

FIG. 24: Comparisons of the capture cross-section of ^{53}Cr calculated with ENDF/B-VII.0 and ENDF/B-VII.1.

format using the LCOMP=1 option and processed with PUFF-IV[93] module of AMPX-6[84]. To illustrate the use of the resonance parameter covariance, the uncertainty in the total, capture, and scattering cross section at the thermal energy for ^{52}Cr and ^{53}Cr are displayed in Table XV. Also listed in Table XV are the results of ENDF/B-VII.0 and those of the Atlas of Neutron Resonances (Atlas)[35]. Comparison of the ENDF/B-VII.0 and ENDF/B-VII.1 capture cross-sections for ^{53}Cr are shown in Fig. 24. New resonances, not present in the ENDF/B-VII.0 evaluation have been found (*e.g.*, the resonance around 50 keV). The data resolution allowed the identification of these resonances.

5. ^{58,60}Ni

Resonance region evaluations of the ^{58}Ni and ^{60}Ni were performed with the code SAMMY [94]. The SAMMY analysis was started with the ENDF/B-VII.0 resonance parameters as prior values, in neutron energy ranges thermal to 812 keV for ^{58}Ni, and thermal to 450 keV for ^{60}Ni. The high experimental resolution of the transmission data of Brusegan permitted us to extend the energy range for ^{60}Ni up to 800 keV. The direct capture cross sections were calculated from direct-semi-direct capture model.

1. ^{58}Ni

   All the neutron transmission data of the experimental database were consistent within 1% for the normalization and within less than 0.002 for the background. In order to fit the ORELA effective capture cross-sections a background contribution not described by the resonance parameters was needed. Part of this background could be explained by the direct capture component, and by the contribution of non-identified *d*-wave resonances in the high neutron energy range of the data. An example of SAMMY fit of the experimental data is shown on Fig. 25. A total number of 487 resonances were used to fit the experimental database in the energy range thermal to 812 keV with 61 *s*-wave, 204 *p*-wave, and 222 *d*-wave resonances. By comparison with the Porter-Thomas distribution of the reduced neutron widths, an excess of *p*-wave resonances was found in the Perey evaluation. In the present evaluation, 43 *p*-wave resonances of Perey evaluation were changed to *d*-wave resonances; all of them had an uncertain angular momentum and spin determination in Perey evaluation. The repartitioning of the resonances in the different angular momentum of the present evaluation is consistent with the spin and energy dependence of the level density. The average level spacing of the *s*-wave resonances (spin J=0.5) is 12.65 ± 0.70 eV. An estimation of the neutron strength functions from the distribution of the reduced neutron widths gives the following results: for *s*-wave S0 = (3.38 ± 0.61)x10^{-4}, *p*-wave S1 = (0.48 ± 0.05)x10^{-4}, and *d*-wave S2 = (2.27 ± 0.30)x10^{-4}.

2. ^{60}Ni

   The ORELA low energy range transmission data (Li-6 glass detector) were consistent within 1% of the normalization, with small background correction. The data at higher energy (NE-110 proton recoil detector) need a large normalization and background correction in the energy range below about 200 keV. Above 200 keV the corrections were very small, and the data were consistent compared to the GELINA transmission in the energy range above 500 keV. The ORELA effective capture cross sections could not be fitted without a residual back-

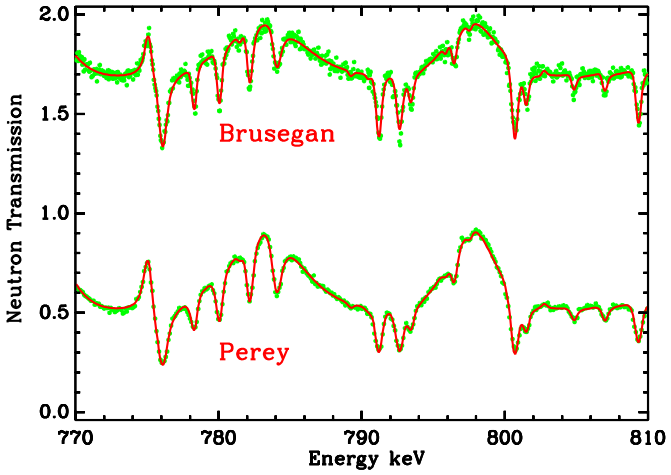

FIG. 25: ^{58}Ni neutron transmission in the energy range of 770 keV to 810 keV from Brusegan *et al.* (upper part), and Perey *et al.* (lower part). The smooth curve represents the transmission calculated by SAMMY. The data of Brusegan were multiplied by a factor of 2 for clarity of the display.

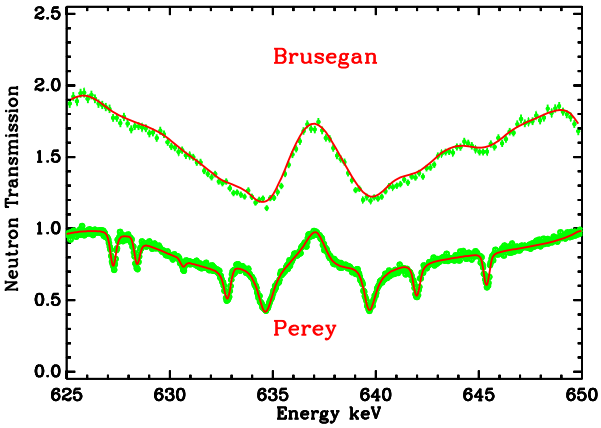

FIG. 26: ^{60}Ni neutron transmission in the energy range of 625 keV to 650 keV from Brusegan *et al.* (upper part), and Perey *et al.* (lower part). The smooth curve represents the transmission calculated by SAMMY. Brusegan data were multiplied by a factor of 2 for clarity of the figure.

TABLE XVI: Thermal cross sections and their uncertainties for ^{58,60}Ni+n in barns.

Isotope	Cross Section	VII.1	VII.0	Atlas
^{58}Ni	Capture	4.27±0.15	4.62	4.37±0.10
	Total	29.32±0.48	29.64	29. 67±0.50
	Scattering	25.05±0.50	25.02	25.30±0.40
^{60}Ni	Capture	2.40±0.06	2.76	2.50±0.06
	Total	3.50±0.10	3.74	3.49±0.09
	Scattering	1.10±0.03	0.98	0.98±0.07

ground varying from 10 mb at 5 keV to about 0.5 mb at 400 keV. Part of this background was explained by the direct capture component and by the contribution of missing p-wave or d-wave resonances. An example of SAMMY fits is given in Fig. 26. A total number of 458 resonances was used to represent the experimental data in the energy rage thermal to 812 keV, including 61 s-wave, 236 p-wave, and 161 d-wave. The average spacing of the s-wave resonances is 11.94 ± 0.66 keV, by taking into account 7 missing levels in the energy range thermal to 812 keV. An estimation of the strength function from the Porter-Thomas distribution of the reduced neutron widths in the energy range from thermal to 450 keV are (2.64 ± 0.64)x10^{-4}, (0.68 ± 0.09)x10^{-4}, and (0.83 ± 0.20)x10^{-4} for s-wave, p-wave, and d-wave, respectively.

The thermal cross-sections and their uncertainties calculated with the ENDF/B-VII.1 are shown in Table XVI for ^{58}Ni and ^{60}Ni, respectively. Listed also in Table XVI are the Atlas values and ENDF/B-VII.0 values.

6. ^{181}Ta

The evaluation for ^{181}Ta was developed by I. Thompson, with the methods described below. We compare measured data with the existing evaluations, with Hauser-Feshbach calculations employing TALYS, version 1.2, with all default parameters, and also with TALYS calculations where some parameters have been tuned to important experimental cross sections. In practice, this is to use (n, tot), $(n, 2n)$ and (n, γ) cross sections to guide parameter adjustments. All the Hauser-Feshbach models here used a Kopecky-Uhl model for the E1 strength function, and M1 parameters from the RIPL-2 database [86]. The Koning-Delaroche optical potential was used for neutrons within a coupled-channels model that included two rotational excited states.

Resonances regions are evaluated separately, to be combined with the predictions of Hauser-Feshbach models.

Resonance data are available up to 2 keV only for ^{181}Ta since it is the only stable tantalum isotope. Because ^{180}Ta has a ground state lifetime of 8.2 hours as well as a long-lived 9^- isomeric state at 77.1 keV (10^{15} years), it may be possible to make a ^{180}Ta isomeric target in the future. Meanwhile, only ^{181}Ta data is available to fix model parameters.

The current n+^{181}Ta evaluations are sufficient for the total cross section. Since there are discrepant $(n, 2n)$ data between 13–15 MeV, we adopt a mean which is very close to (or within) all error bars. Fitting the ^{181}Ta(n, γ) rate is, however, more difficult. Most evaluations agree with experiment up to 1 MeV. There is additional data up to 3 MeV and also at 15 MeV. The TALYS default calculation is close to the 15 MeV data, but overestimates it between 1.5 and 3 MeV. The TALYS normalization can be adjusted in this region by scaling the parameter G_{norm} to

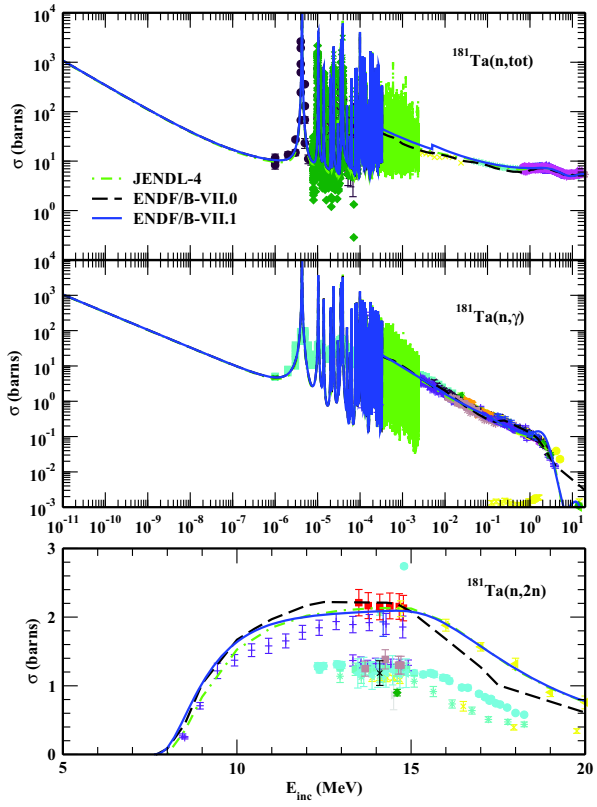

FIG. 27: Experimental data and evaluations for the total, neutron capture and $(n, 2n)$ cross sections for n+^{181}Ta. The ENDF/B-VII.1 and ENDF/B-VII.0 evaluations are in blue and black, respectively. The lower data points in the bottom figure are for the production of the ^{180}Ta^m isomeric state.

adjust the input Γ_γ in TALYS to better match the data. In this case, we rescale to $\Gamma_\gamma = 0.057$ eV, by setting $G_{\rm norm} = 1.7$. The same factor gives $\Gamma_\gamma = 0.051$ eV for ^{180}Ta. We used the experimental resonance spacing D_0 of 1.2 and 4.2 eV for the two nuclei, respectively. The TALYS calculation agrees well with the available data in other respects, and is therefore used in the current evaluation. The only resonance data is for ^{181}Ta.

7. ^{185,187}*Re*

The evaluations for ^{185,187}Re were developed by I. Thompson, with the same methods summarized in the description of the ^{181}Ta evaluation.

The ^{185,187}Re are the only stable isotopes of rhenium. While there is very little $(n, \rm tot)$ data on either isotope, there are useful (n, γ) cross sections. These cross sections are well reproduced by a calculation with the default TALYS parameters, as shown in Figs. 28 and 29. We used the experimental resonance spacing D_0 of 3.1 and 4.1 eV for the two nuclei, respectively. The complete reaction set with these parameters are used to produce

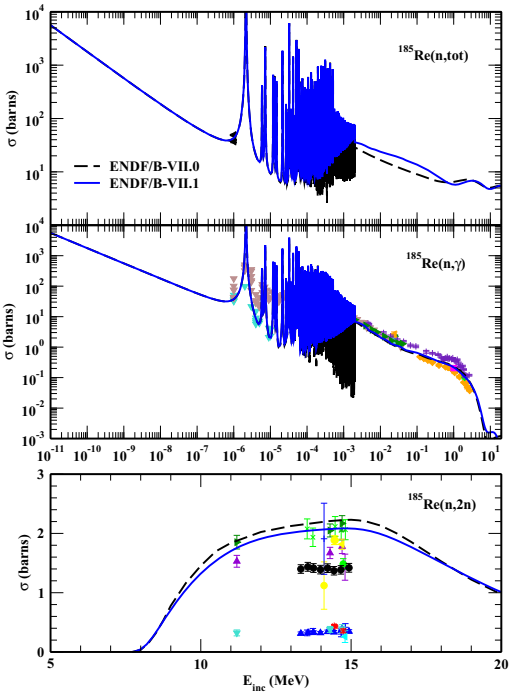

FIG. 28: Measurements and evaluations of the total, neutron capture, and $(n, 2n)$ cross sections for n+^{185}Re. The solid blue line is the default TALYS calculation, which we adopt for ENDF/B-VII.1.

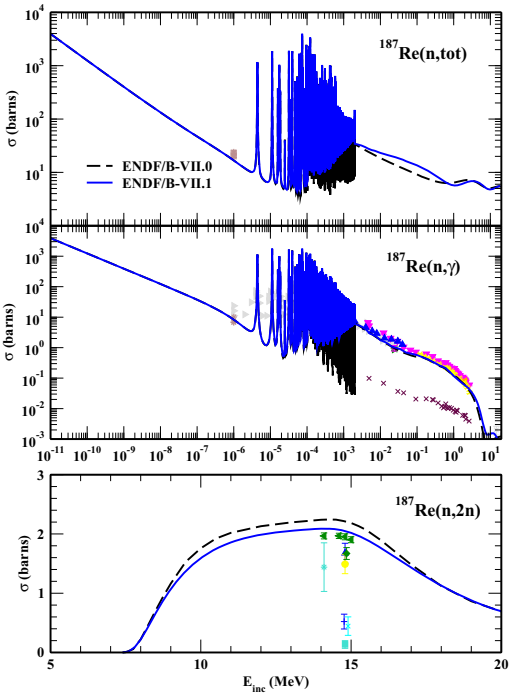

FIG. 29: Measurements and evaluations of the total, neutron capture, and $(n, 2n)$ cross sections for n+^{187}Re. The solid blue line is the default TALYS calculation, which we adopt for ENDF/B-VII.1.

our evaluation.

8. Hf

The original ENDF/B-VII.0 hafnium isotopic evaluations (^{174}Hf, ^{176}Hf, ^{177}Hf, ^{178}Hf, ^{179}Hf, and ^{180}Hf) were completed in 1976. In the 1991 to 1992 timeframe, the resolved and unresolved resonance region evaluations below 90 keV were revised by R. Q. Wright. In preparation for the release of ENDF/B-VII.1, Wright noted the ENDF/B-VII.0 hafnium evaluations are out of date and in need of revision. In addition, newer evaluations are available in the JEFF and JENDL data projects that represent improved evaluations, and these newer data files were recommended for ENDF/B-VII.1. Specifically, the JENDL-3.3 hafnium evaluations were completed in 2001 and include gamma production data. After the release of JENDL-3.3, the JENDL evaluations were revised to include the JEFF-3.1 resonance parameters up to 200 eV. For ENDF/B-VII.1, the hafnium update effort started with the JENDL-3.3/JEFF-3.1 evaluations, and minor modifications were made to the resonance evaluations in accordance with information from the literature as noted in the subsequent discussion.

All of the ENDF/B-VII.1 hafnium isotope evaluations utilize the multi-level Breit-Wigner (MLBW) formalism in the resolved resonance range. For ^{174}Hf, the resolved resonance parameters have been updated. Specifically, the first 9 positive resonances are taken from Ref. [95], and two bound levels are included. The top of the resolved resonance region has been changed from 220 eV to 168 eV. Regarding ^{176}Hf, the resolved resonance range is from 10^{-5} eV to 700 eV, and the first 6 positive resonances are taken from Ref. [95]. The unresolved resonance region extends from 700 eV to 50 keV. The ^{177}Hf resolved resonance evaluation has been extended from 250 eV to 510 eV, and no bound levels are included in the resolved resonance range. The unresolved resonance range extends from 510 eV to 50 keV. For ^{178}Hf, the resolved resonance region extends from 10^{-5} eV to 1600 eV, and the first three positive resonances are revised per Ref. [96], and one bound level is included. The unresolved resonance range extends from 1.6 to 50 keV. Regarding ^{179}Hf, the resolved resonance range extends from 10^{-5} eV to 510 eV, and no bound levels are included. The unresolved resonance range extends from 510 eV to 50 keV. For ^{180}Hf, the top of the resolved resonance range has been extended from 2.5 keV to 4.992 keV, and the first two positive resonances have been revised per Ref. [96]. Moreover, there are 90 *s*-wave and 66 *p*-wave resonances. The unresolved resonance range extends from 4.992 keV to 50 keV. Comparisons between the ENDF/B-VII.0 and ENDF/B-VII.1 evaluations and the JENDL-3.3/JEFF-3.1 evaluation for the thermal capture cross section and the capture resonance integrals are provided in Tables XVII and XIV, respectively.

With regard to the impact on systems with natural hafnium, the ENDF/B-VII.1 thermal capture is 0.3% higher relative to ENDF/B-VII.0. Likewise, the ENDF/B-VII.1 capture resonance integral for natural hafnium is 0.4% higher relative to ENDF/B-VII.0. As a result, the ENDF/B-VII.1 hafnium evaluations should not exhibit a large impact for thermal systems. For fast systems sensitive to natural hafnium, the impact of using ENDF/B-VII.1 may be significant relative to ENDF/B-VII.0; however, the impact should be small relative to the JENDL-3.3 & JEFF-3.1 evaluations. As noted previously, the ENDF/B-VII.1 evaluation now includes gamma production data, and the previous ENDF/B-VII.0 hafnium evaluations do not include gamma production data. Overall, the ENDF/B-VII.1 hafnium isotope evaluations are improved relative to ENDF/B-VII.0.

TABLE XVII: Thermal capture cross section data for $^{174,176-180}$Hf+n in barns.

Isotope	VII.0	JENDL-3.3 & JEFF-3.1	VII.1	Ref. [96]
^{174}Hf	561.8	549.5	549.1	549 ±7
^{176}Hf	13.8	21.3	21.4	23.5±3.1
^{177}Hf	373.5	373.5	373.5	375±10
^{178}Hf	84.0	83.9	83.9	84±4
^{179}Hf	43.6	42.8	42.8	41±3
^{180}Hf	13.01	13.10	13.06	13.04±0.07

TABLE XVIII: Capture resonance integrals for $^{174,176-180}$Hf+n in barns.

Isotope	VII.0	JENDL-3.3 & JEFF-3.1	VII.1	Ref. [96]
^{174}Hf	355.0	442.3	345.0	307±15
^{176}Hf	401.3	694.3	691.3	708±15
^{177}Hf	7175	7197	7197	7200±200
^{178}Hf	1905	1872	1879	1882±20
^{179}Hf	548	522	523	527±30
^{180}Hf	34.5	29.7	33.5	33±1

9. W

Accurate nuclear data for tungsten isotopes are required because tungsten is a candidate material for first-wall components in fusion devices, target and beam window material for spallation neutron sources based on high-current accelerators, as well as neutron dosimetry using the ^{186}W(n,γ) reaction. Evaluations of tungsten isotopes available in ENDF-B/VII.0 [1] go back to work carried out in 1980 by Arthur *et al.* within a LANL-ANL-CEA/BRC collaboration for neutron incident energies below 20 MeV [97, 98]; original evaluations were released for the ENDF-B/V library. A consistent description of scattering data and (n,2n) measurements [99] was very challenging as pointed out by evaluators at the time [97]. ENDF-B/V evaluations were later extended up to 150 MeV incident energy by Chadwick *et al.* in 1996 [100] and adopted for ENDF-B/VI [101]; only minor revisions were carried out in 2001 and 2006.

However, the previous VII.0 data were considered unsatisfactory during recent data validation and assessments: systematic discrepancies were observed in criticality safety benchmarks containing tungsten [6], fusion neutronics benchmarks [102], and measured constants for neutron activation [103]. In addition, new experimental data have been measured (*e.g.* total cross section data for natural tungsten measured by Abfalterer *et al.* in 2001 [104], total cross section data for separated tungsten isotopes measured by Dietrich *et al.* in 2003 [105], and several sets of charged-particle emission cross sections). Finally, there was no evaluation available for neutron induced reactions on the ^{180}W isotope. These deficiencies, together with the availability of new data in the fast neutron range, motivated the work presented herein. Results of comprehensive experimental data analysis and VII.1 evaluations for neutron interactions on tungsten isotopes ^{180,182,183,184,186}W in the neutron energy range up to 150 MeV [106, 107] are described below.

Resonance range

Our review of the resonance parameters of tungsten isotopes showed that no significant improvement in quality is possible without new measurements. Minor adjustments to existing resonance parameters of ^{182}W were made by L. Leal. The sources of other resonance parameters were: Atlas [35] for ^{180}W, IRDF-2002 [108] for ^{186}W and ENDF/B-VII.0 [1] for ^{183}W and ^{184}W isotopes. The unresolved resonance parameters were flagged for the calculation of self-shielding only. The error in the exponent of the gamma-width of the resonance at 1132 eV of ^{184}W was corrected. The capture background was increased from 1.2 to 2.2 keV neutron energy in ^{183}W. Reconstructed capture cross sections had an unusual dip in this energy region, that corresponds to the upper range of the resolved resonance range. The Perrot benchmark [75] shows a dip in the reaction rate corresponding to the same energy region which motivated the undertaken correction. All evaluations include covariance information obtained by a retroactive method, but the details of evaluating the covariances are given elsewhere [27].

Fast energy range

The evaluation methodology was previously described for the ^{55}Mn evaluation, see subsection VI C 3. A comprehensive description of the theoretical modeling based on the EMPIRE code was also given there.

The employed evaluation methodology combines EMPIRE [82] theoretical modeling of relevant reactions with a Bayesian generalized least-squares fitting to include experimental data as implemented in the GANDR code [83]. GANDR fitting results are then combined with a selected evaluation of resonance parameters to assemble a full evaluated nuclear data file.

Selected benchmarks covering both criticality and 14 MeV fusion domains are calculated for the assembled evaluated data file; benchmark results are analysed to further constrain the theoretical modeling and model parameters. Then, the whole process is repeated starting from a new theoretical calculation and concluding with a new GANDR least-squares fitting that produces a new evaluated data file. Iterations are continued until the benchmarks' performance does not improve anymore. We consider this iterative feedback process an important step for improving the tungsten evaluations. This process required a close interaction between the reaction cross section modelers and the benchmark evaluators.

The direct interaction cross sections and transmission coefficients for the incident channel on ^{180,182,183,184,186}W nuclei were obtained from rigid-rotor dispersive coupled-channel optical model potential especially derived for this evaluation (RIPL catalogue numbers 1480,1481,1482; see Table 1 at p.15 of the NEMEA-3 proceedings [109, 110]). The quality of the derived OM potentials can be assessed by calculating the difference of the total cross sections (divided by the average total cross section) of ^{182}W and ^{186}W isotopes measured by Guenther *et al.* [111] and Dietrich *et al.* [105]. Calculated results are compared with measured data in the Fig. 30. Guenther *et al.* [111] experimental data were shifted down by -0.008, while the OMP calculations were shifted up by +0.006, values well within the estimated uncertainty of the vertical scale (around 0.02) [105, 111] which arises from uncertainties in the areal densities of the tungsten targets. The measurements are very well reproduced by the OMP calculations; similar agreement was obtained for the ratio of other tungsten isotopes.

The selection of, and corrections to, the raw EXFOR data have been documented in Ref. [107] and are not repeated here. A modified Lorenzian (MLO) radiative-strength function for all tungsten isotopes was taken as recommended by Plujko [85] and resulted in excellent agreement with the selected experimental neutron capture database in the fast neutron range. Total, capture, secondary emission cross sections of neutrons and charged particles, average resonance parameters, and angular distributions of neutron and proton scattering on all tungsten isotopes were in fairly good agreement with the available differential experimental data. An example of the evaluated cross sections for selected neutron induced reactions on ^{182}W and ^{186}W isotopes in comparison with experimental data is shown in Fig. 31.

Benchmark calculations

Results of the integral validation testing are only discussed here when they were used as a constraint in the iterative evaluation process. A comprehensive analysis of benchmarks' results and data verification can be found in the companion paper by Kahler *et al.* in this edition [8].

Validation of the theoretical model and model parameters was performed by systematically comparing available experimental data in the EXFOR database for the natural element with equivalent quantities reconstructed from the evaluated isotopic data files. For these purposes, the

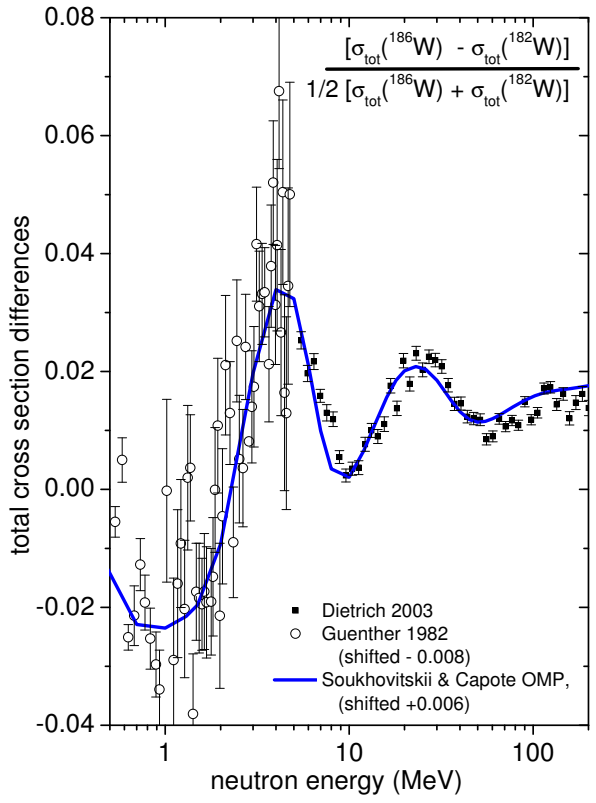

FIG. 30: Energy dependence of the measured ratio $[\sigma_{tot}(^{186}W) - \sigma_{tot}(^{182}W)]/\{[\sigma_{tot}(^{186}W) + \sigma_{tot}(^{182}W)]/2\}$ [105] vs. calculated values (blue line) using dispersive coupled-channel OMP (RIPL 1480-1482) [109, 110].

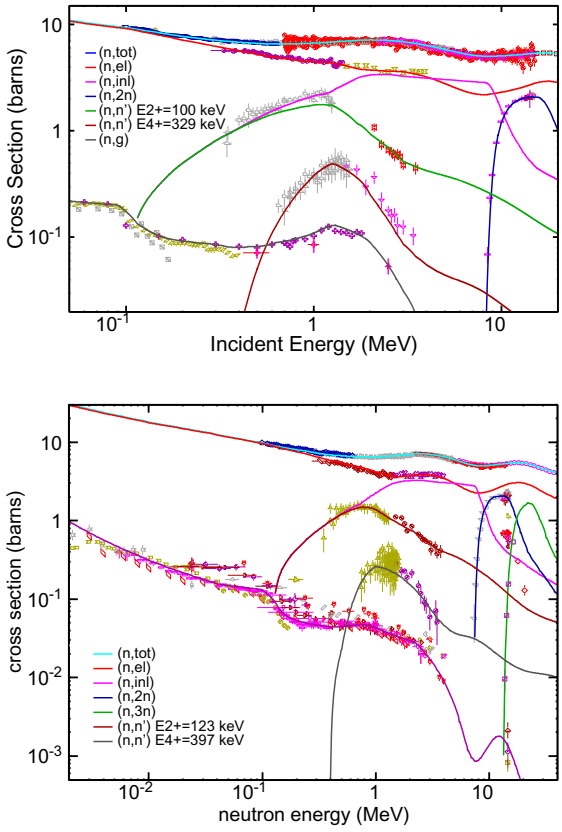

FIG. 31: Neutron induced reactions on ^{182}W (top panel) and ^{186}W (bottom panel) nuclei: EMPIRE=VII.1 calculations (lines) vs experimental data (symbols).

FNG-W benchmark [112] was modeled, which involves a deep penetration of 14 MeV neutrons into a large tungsten block and is sensitive to tungsten data in the fast neutron energy range. Flux attenuation was measured by a number of activation monitors. The predicted activity is within two-sigma for all monitors at all depths, without any systematic shifts that increase as a function of the penetration depth, as shown in Fig. 32.

The analysis was extended to criticality benchmarks from the ICSBEP Handbook [113], namely the ZPR-9 series of benchmarks from Argonne, and the tungsten-reflected plutonium sphere and the tungsten-reflected uranium assemblies from the Elsie facility at Los Alamos. Originally, there was very little improvement in the results for the criticality benchmarks with the new evaluated data. To remedy the situation, a fine-tuning of the model parameters was made (within estimated model parameter uncertainty). Such adjustment had an impact on the calculated capture cross sections below 1 MeV, but had little effect on the previously analysed FNG benchmark. However, there is some contradiction between the criticality benchmarks, which would suggest an increase of the capture cross section below 1 MeV down to about 4 keV, and the activation measurements for gold in the

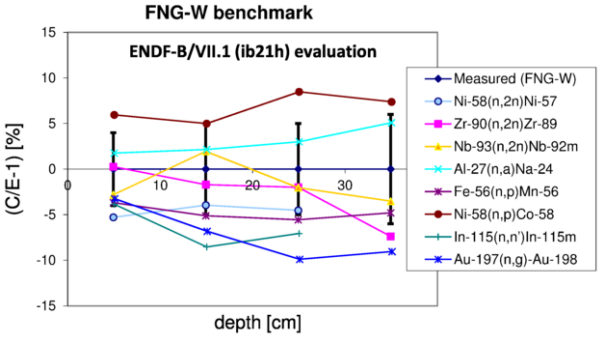

FIG. 32: Measured activation rates at different depths for the FNG-W experiment [112] compared to calculated values using the ENDF/B-VII.1 evaluation.

FNG-W benchmark (see Fig. 32), which would require a decrease. Since there are several independent criticality benchmarks using fast-neutron assemblies, which indicate the same trend, the decision was to retain the higher value of the capture cross sections, resulting in about a 10% underprediction of the activation of gold at a depth of about 35 cm into the tungsten block as measured in

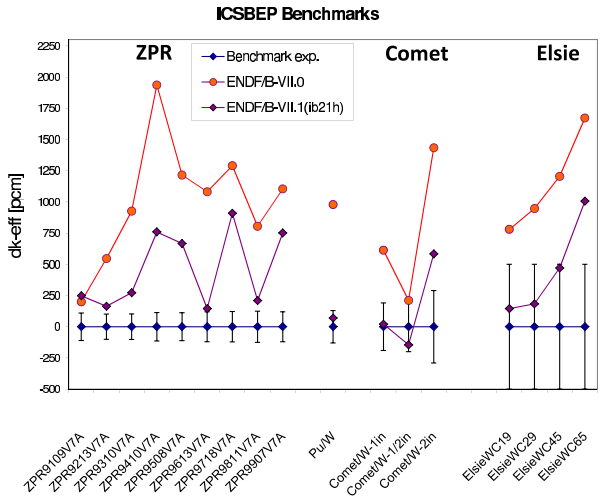

FIG. 33: ICSBEP criticality benchmarks containing tungsten [113] vs calculations using ENDF/B-VII.0 (orange symbols) and ENDF/B-VII.1 (magenta symbols) evaluations, respectively. Connecting lines draw for orientation.

the FNG benchmark. Several iterations were needed to find a satisfactory solution. Some discrepancies in the predicted neutron multiplication factor k_{eff} remain, but overall the discrepancies were reduced by more than a factor of two compared to ENDF/V-VII.0 evaluations as can be seen in Fig. 33. Further improvements to the data will be possible once the recently performed total and capture cross-section measurements on tungsten isotopes at IRMM (Geel) in the resonance energy range are analyzed [114].

10. (n,α) from 20–150 MeV for Cr, Fe, Ni

Haight *et al.* have measured the cross section for production of alpha particles for neutrons with energies that extend up to many tens of MeV on structural materials. These measurements were made at the LANSCE facility at Los Alamos. These data are important for understanding gas production and radiation damage effects in accelerator-driven applications.

Over a decade ago, a first high-energy cross section database was created [100], "LA150", that modeled and represented these processes in ENDF format. The representations were included into the ENDF/B-VII.0 database up to 150 MeV. However, the new Haight *et al.* data enable an improvement in our higher energy alpha-production cross sections for VII.1. Kunieda *et al.* [115] have developed GNASH code calculations that treat the alpha emission in the preequilibrium phase using a cluster exciton model proposed by Iwamoto and Harada. The model calculations were optimized to best match the measured data, and were then used to create alpha production cross sections and secondary energy spectra for ENDF/B-VII.1.

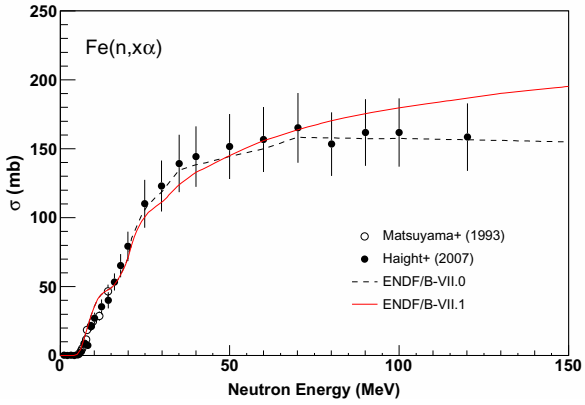

FIG. 34: Calculated alpha production cross section for neutrons on iron, compared to Haight's data from LANSCE.

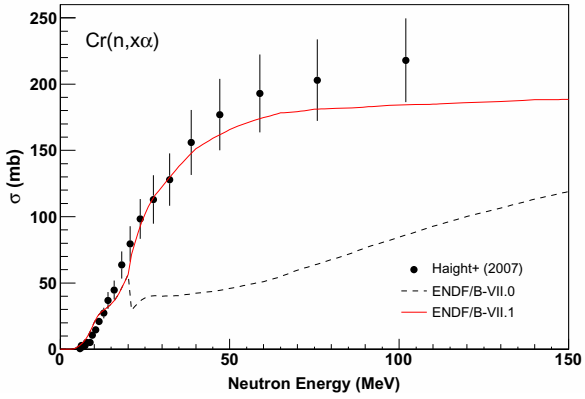

FIG. 35: Calculated alpha production cross section for neutrons on chromium, compared to Haight's data from LANSCE.

Upgrades for VII.1 have been made for ^{50,52,53,54}Cr, ^{54,56,57}Fe, and ^{58,60}Ni, based on measurements for ^{nat}Cr, ^{nat}Fe, and ^{58,60}Ni. Results are shown in Fig. 34, 35, 36, 37. An example of the improved representations of emitted alpha particle spectra is shown in Fig. 38

D. Dosimetry cross sections

1. ^{75}As

Cross sections for ^{75}As above the resonance range were calculated with the CoH_3 code. The total cross section was also calculated by considering a strong oblate deformation of arsenic isotopes, typically $\beta_2 = -0.25$.

The total cross section was calculated with the coupled-channels method implemented in CoH_3. Because the coupling scheme of As is not so clear, the ground state and the first possible rotational band member are only

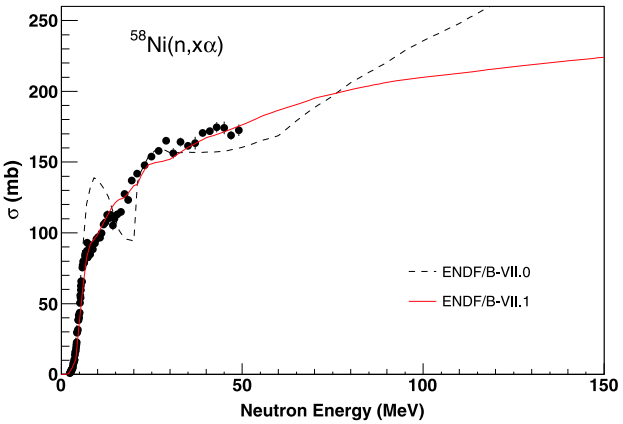

FIG. 36: Calculated alpha production cross section for neutrons on ^{58}Ni, compared to Haight's data from LANSCE.

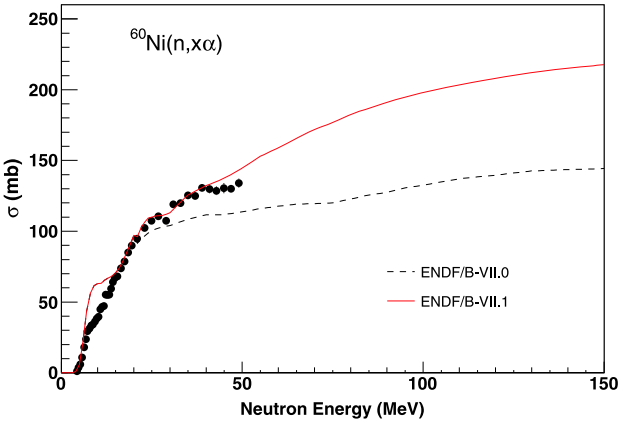

FIG. 37: Calculated alpha production cross section for neutrons on ^{60}Ni, compared to Haight's data from LANSCE.

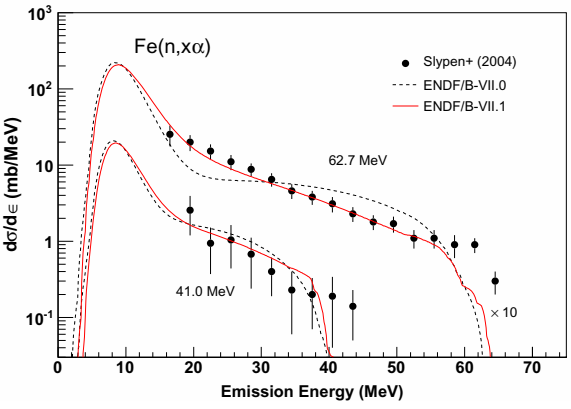

FIG. 38: Calculated alpha production energy spectra for neutrons on iron compared to Haight's data from LANSCE.

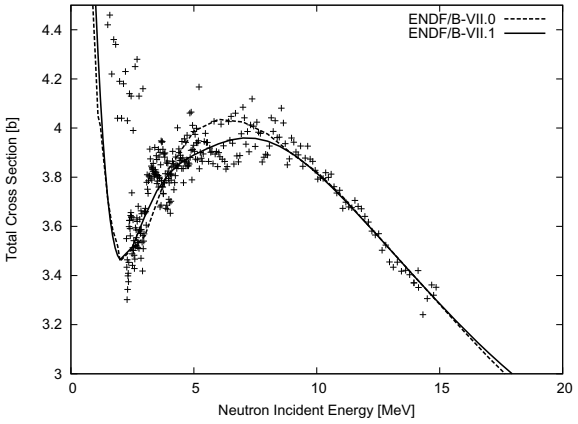

FIG. 39: Calculated ^{75}As total cross section, compared with ENDF/B-VII.0 and experimental data.

coupled. Starting with the Koning-Delaroche spherical global optical potential, an imaginary part was reduced, which effectively accounts for the direct channel coupling. The calculated total cross sections show better reproduction of the experimental data in the 4–8 MeV region, as shown in Fig. 39.

The calculated (n,p), (n,np), (n,α), (n,nα), and (n,2n) cross sections were tuned by adjusting the model parameters to reproduce the ^{75}As experimental data. The (n,2n) and (n,α) cross sections were obtained with very modest parameter adjustment. However, a relatively strong modification to the proton emission channel was needed in order to reproduce the experimental (n,p) cross sections. The result is not still satisfactory, as a large overestimation is seen above 15 MeV, and the difference between ENDF/B-VII.0 and the current evaluation is considerably large there. This problem has not been resolved yet. However the same problem was reported by Shibata *et al.* [116], even though they used a different model code for their arsenic evaluation. The $(n, 2n)$ cross section is shown in Fig. 40.

2. ^{78}Kr

^{78}Kr is the lightest of the stable Kr isotopes with a natural abundance of 0.35%. It is a fission fragment that is used as a radiochemical tracer in NIF gas targets and in dosimetry. The ENDF/B-VII.0 evaluation was carried out by WPEC Subgroup 23 in 2004-2005, as part of the international library of fission product evaluations. That evaluation was obtained by merging the resolved resonance region from Ref [35], with the JENDL-3.3 evaluation for the unresolved resonances and fast neutron region. The JENDL-3.3 evaluation was from 1990, but was based on an evaluation from 1987. Since then (1989) new data for the (n,2n) reaction have been measured [117]. The new data suggest a larger (n,2n) cross section. With this in mind, the cross section in the fast neutron region

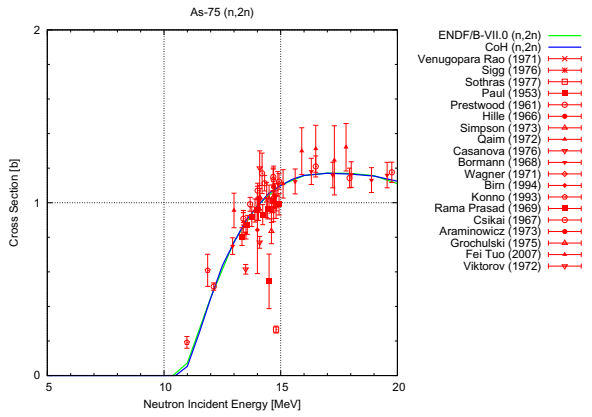

FIG. 40: Calculated ^{75}As$(n, 2n)$ using the CoH code used for ENDF/B-VII.1, compared with ENDF/B-VII.0 and experimental data.

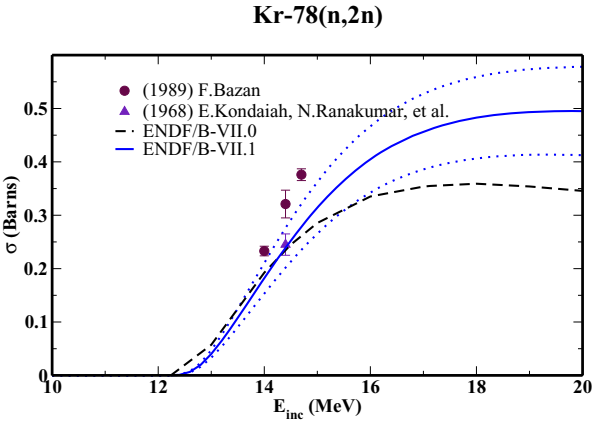

FIG. 41: Comparison of the new ENDF/B-VII.1 (blue solid line) and ENDF/B-VII.0 (black dashed line) ^{78}Kr(n,2n) cross sections with experimental data from EXFOR. The uncertainty in the ENDF/B-VII.1 cross section is shown by the blue dotted lines.

has been re-evaluated and combined with the resolved and unsolved resonance regions from the WPEC 23 evaluation in ENDF/B-VII.0.

The fast region was evaluated using the TALYS code [118]. The approach was to choose a set of model parameters and vary the parameters within realistic bounds. One hundred realizations of the model parameters were calculated using the TALYS code and the cross sections averaged to obtain the evaluation central values. The spherical optical model of Koning and Delaroche [119] was employed, and the parameters of the optical potential varied in order to reproduce the spread of the reaction cross section (roughly 5% for incident neutron energies greater than 10 MeV and $\sim 8-10\%$ for energies less than 10 MeV). The pre-equilibrium model was a single component exciton model, with the overall scaling factor and stripping parameters varied by 25%. The complex particle pre-equilibrium model parameter was reduced to 75% and varied by 20%. It was found that this parameter was probably overestimated in the region of ^{78}Kr due to the very low proton and alpha thresholds [120]. The level density parameters varied from 2-5%, in line with uncertainties from RIPL [85].

In Fig. 41, the TALYS results are shown for (n,2n) reaction compared to the experimental data from EXFOR. The new evaluation follows the trend of the new experimental data, although it is systematically lower than the data. It lies more than one sigma from the Bazan data, but unrealistic pre-equilibrium parameters would have been required in order to fit these data. Uncertainties shown in the figure are from Ref. [120], but covariances are not included in ENDF/B-VII.1 evaluation. Experimental data exists for the (n,γ) channel in the unresolved resonance region, but the evaluation remains unchanged in this region.

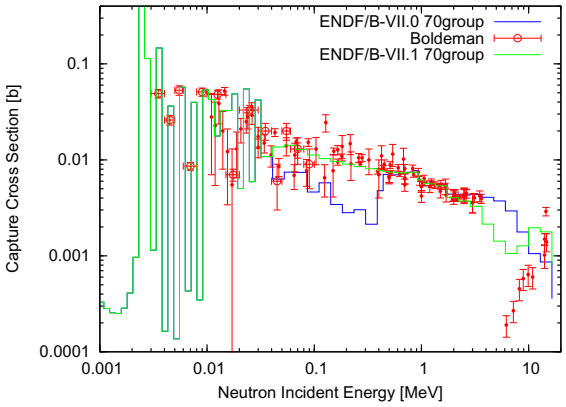

FIG. 42: Calculated ^{89}Y(n, γ) used for ENDF/B-VII.1, compared with ENDF/B-VII.0 and experimental data.

3. ^{89}Y

In ENDF/B-VII.0 the energy upper boundary of the resolved resonance region was 409 keV. This resulted in a significantly low capture cross section in the 100-keV range, due to missing higher partial wave contributions. In ENDF/B-VII.1 the upper-limit of the resolved resonance region was lowered to 45 keV, and the energy gap 45–409 keV was filled by newly evaluated point-wise cross sections.

In the energy range 45 – 650 keV, the total cross section was evaluated with the SOK code [121] based on available experimental data. The capture cross section was calculated with the CoH_3 code in the entire energy range, using the same optical potentials as in the BNL evaluation in ENDF/B-VII.0, see Fig. 42.

4. ^{168,169,170}*Tm and* ^{203,205}*Tl*

New evaluations for ^{168,169,170}Tm and ^{203,205}Tl were performed at BNL to extend LANL radchem files [5] to enable full-scale transport calculations. We used the reaction model code EMPIRE [82] with input parameters adjusted to reproduce experimental data. In the case of Tm, we also aimed to match the LANL evaluations for (n,2n) and (n,γ) so that these could be incorporated in the final files replacing EMPIRE calculations, except for the ^{169}Tm(n,2n) for which the Zolotarev evaluation [122] was adopted (it agrees well with the LANL (n,2n) evaluation [5]). This evaluation, as shown by Capote *et al.* [123], agrees very well with reaction rates measured in the ^{252}Cf spontaneous fission neutron spectrum and in the ^{235}U thermal fission spectrum. The LANL capture on ^{169}Tm was reduced by 10% following feedback from integral validation [5].

For Tm isotopes, the coupled-channels E.D. Arthur optical potential [124] was used. The Koning-Delaroche spherical optical potential was used for both ^{203,205}Tl. For the more deformed ^{205}Tl, however, we used coupled-channel calculations with the imaginary parts reduced by fifteen percent. Although a number of experimental data sets exist for ^{203}Tl, the calculations were matched to those of Bayhurst *et al.* [125]. Empire-specific level densities were used in all cases, except ^{205}Tl, for which microscopic Hartree-Fock-Bogoliubov predictions were adopted. Resonance region evaluations were obtained using the Atlas of Neutron Resonances [35] for all five isotopes.

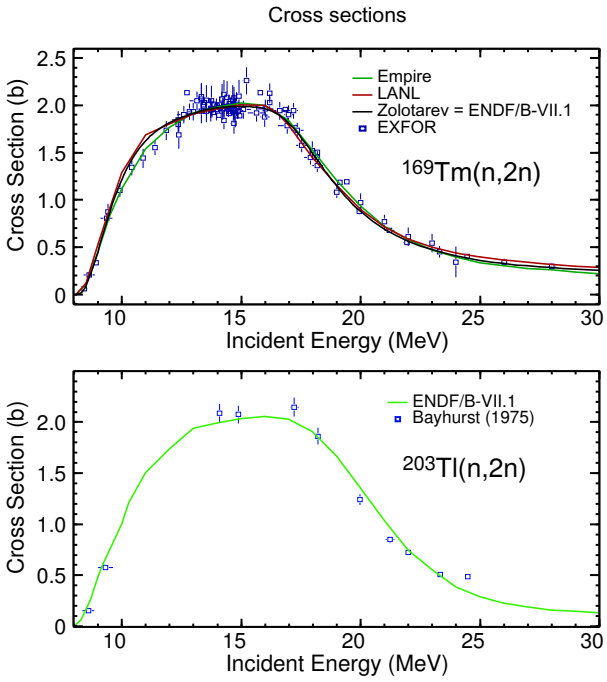

FIG. 43: Results for the ^{169}Tm(n,2n) (top) and ^{203}Tl(n,2n) (bottom) evaluations. In the case of ^{169}Tm(n,2n) we also compare the calculations also with the previous Los Alamos evaluation [5].

E. Fission Products and Other Evaluations

The ENDF work on fission products is summarized here, with more details to be provided in a future publication by Mughabghab.

As pointed out earlier, Dean *et al.* [13] carried out measurements of 12 important fission products with high enrichments to determine their reactivity-worth at two irradiation positions in the Dimple reactor, one resembling a soft neutron spectrum (SOFT); the other a PWR spectrum. These benchmarks were modeled and reactivity-worth calculations were carried out based on JEF-2.2, JEFF-3.1 and WPEC23 evaluated libraries [13]. We note that for these particular fission products, the Working Party on Evaluation Collaboration (WPEC23), borrowed the evaluations of these fission products from ENDF/B-VII.0, meaning that these benchmarks are simultaneously tests of the latter evaluated data files. A summary of the discrepancies between measurements and calculations based on the WPEC23 [ENDF/B-VII.0] evaluated files is shown in Table XIX. According to Dean *et al.* [13] the accuracy of these measurements is assessed at the level of 4 %. In view of these significant results, it was imperative to re-examine the ENDF/B-VII.0 evaluated files of these FP nuclei to find out what possible adjustments in the thermal capture cross and/or the parameters of the first s-wave resonance could be made to resolve these discrepancies. In the following, we discuss in some detail what changes were made for each of these FP nuclei in the ENDF/B-VII.0 in the thermal and low energy regions. In addition, because of the availability of recent measurements and integral benchmark measurements, we examined the following materials: ^{58}Co, ^{62}Ni, ^{90,91}Zr, ^{113}Cd, and ^{157}Gd. At this point, the reader is referred to previous studies dealing with the general evaluation methodology followed in the resonance and unresolved energy regions [126], [127], [128], and [129].

1. ^{95}*Mo*

The reactivity-worth measurements in a thermalized neutron spectrum [13] (Table XIX) indicates that the ENDF/B-VII.0 thermal capture cross section of ^{95}Mo, σ_γ = 13.56 b, is large by about 9%. In contrast, good agreement, within 4%, is observed between the measured and calculated values for the case of the PWR neutron spectrum, denoting good representation for the parameters of the first resonance at 44.9 eV. On the other hand, the latest accurate measurement of the capture cross section at 0.0253 eV, $\sigma_\gamma = 13.4 \pm 0.3$ b by Koester et al.[130] does not allow much adjustment in this quantity. Because of this situation and to partially address this discrepancy,

TABLE XIX: Percentage discrepancy in reactivity worth of important fission products irradiated in two positions in the DIMPLE reactor, characterized as a SOFT or a PWR neutron spectrum [13]. The calculations of the discrepancies are based on WPEC23 (= ENDF/B-VII.0). See text for details.

Nucleus	Discrepancy-SOFT %	Discrepancy-PWR %
^{95}Mo	+9	0
^{99}Tc	+10	+10
^{103}Rh	+12	+8
^{109}Ag	+5	+2
^{133}Cs	+11	+10
^{143}Nd	-2	-6
^{145}Nd	+13	+11
^{147}Sm	+3	0
^{149}Sm	0	-6
^{152}Sm	-1	0
^{153}Eu	-11	-6
^{155}Gd	+4	+3

we adopted 13.1 b for this cross section.

2. ^{92}Mo

The ^{92}Mo ENDF/B-VII.0 evaluation was originally taken from JENDL-3.3, but the thermal capture cross section and capture resonance integral are inconsistent with the Atlas recommendation. The Atlas value for the thermal capture cross section is based on two measurements, whilst that of JENDL-3.3 is calculated from the positive energy resonances. Because of this information, a new evaluation for ENDF/B-VII.1 below the fast region was carried out. The individual and average resonance parameters were carried over from the Atlas compilation. In addition, a bound level was invoked to describe the thermal data. A comparison with ENDF/B-VII.0 (JENDL-3.3) for the thermal capture cross section and capture resonance integral is shown in the Table XXI.

3. ^{99}Tc

The thermal capture cross section of the ENDF/B-VII.0 for ^{99}Tc is based on the measurement of Furutaka *et al.* [131], $\sigma_\gamma = 22.8 \pm 1.8$ b, as well as a consideration of the result of Molnar *et al.* [132]. In contrast, the Dean et al. results [13] (Table XIX), show that this value is over-estimated by about 10 %. This conclusion is in agreement with a previous recommendation for this capture cross section, $\sigma_\gamma = 20 \pm 1$ b [133], suggesting possible problems with the recent measurements. On the basis of the results [13] and previous measurements [133], a thermal capture cross section of 20 ± 1 b is adopted for ENDF/B-VII.1. In view of this conclusion, the parameters of the resonance at 5.58 eV were modified by adopting basically the scattering width of Gunsing *et al.* [134]; the capture width is derived by fitting the thermal capture data. The calculated ENDF/B-VII.1 capture resonance integral gives 322 b, a reduction of 12 % from the ENDF/B-VII.0 value.

4. ^{103}Rh

Measurement of the ^{103}Rh reactivity-worth in a thermalized neutron spectrum [13] indicates that the 2200 m/s capture cross section of ENDF/B-VII.0 may have to be decreased by about 12 %, bringing it down to 132 b from a previous value of 144.9 b. This seems to be apparently supported by the measurements of Lee *et al.* [135] who reported $\sigma_\gamma = 133.0 \pm 0.93$ b. However, this value is not in agreement with the result of Brusegan *et al.* [136], $\sigma_\gamma = 142.0 \pm 1.5$ b and earlier measurements reporting values ranging from 147 ± 4 b to 164 ± 11 b. A detailed examination of the various measured thermal capture cross sections showed that the major contribution to the discrepancy can be attributed to the parameters of the resonance at 1.25 eV and not the evaluated thermal capture cross section. On the basis of this information, the Geel results for the resonance parameters below 290 eV, as well as their thermal capture cross section [136], were adopted in the present evaluation. In addition a bound level was invoked to describe a recommended coherent amplitude [35]. With these modified resonance parameters, the calculated capture resonance integral is 967.5 b, as compared with a previous ENDF/B-VII.0 value of 1034 b, a decrease of 6.9%, confirming the discrepancy of the reactivity-worth measurement of ^{103}Rh for the PWR spectrum; refer to Table XIX. Since the capture resonance integral is quite large in this case, most of which is attributed to the 1.259 eV resonance, the 6.9% change in its value will also influence the SOFT discrepancy results assuming the SOFT spectrum contains a non-negligible epi-cadmium component.

5. ^{109}Ag

As reported by Dean *et al.* [13], the discrepancies between the reactivity worth measurements for ^{109}Ag and the WPEC evaluated file are +5% and +2% for a thermalized and PWR neutron spectra, respectively. Even though these values are comparable to the 4% uncertainty of the measurements [13], we decided, nevertheless, to examine the ENDF/B-VII.0 file for possible improvements below the fast neutron region in view of new measurements and analysis.

A recent activation measurement by De Corte and Van Lierde [137] disclosed that the thermal capture cross section for the ground state transition of ^{110g}Ag is 76.8 ± 1.0 b. Since the isomeric cross section contribution is 3.95 ± 0.05 b [35], then it follows that the total thermal capture cross section is 80.7 ± 1.0 b. The isomeric transition decays by 1.38% to the ground state. This result

is significantly inconsistent with the recommended thermal value 91.0 ± 1.0 b, which was obtained from three independent measurements, as well as consistency checks of the elemental and isotopic values. A possible explanation for this large discrepancy may lie in a lack of precise knowledge for the branching of the 657.5 keV gamma-ray, adopted in this measurement. For these reasons, a 2200 m/s capture cross section of 90.23 b is obtained, based on a Westcott capture factor of 1.00852 for ^{109}Ag, calculated from the present evaluation.

Thus, we have only made small changes to the ENDF/B-VII.0 evaluation and it is unlikely that the calculated SOFT or PWR values will change for ^{109}Ag. But, as noted earlier, the original results were not discrepant with the measured data when one considers the integral experiment's 4% uncertainties.

6. ^{133}Cs

Table XIX shows that the thermal capture cross section and/or the resonance capture integral of ^{133}Cs require changes by about 10 % in the ENDF/B-VII.0 corresponding values. On a detailed examination of the several measured values of thermal capture cross sections and capture resonance integral, it was realized that the discrepancy can be attributed to the parameters of the first resonance at 5.86 eV; there is no room for adjustment in the thermal value. The resonance parameters recommended in the Atlas [35] were adopted with two minor changes: i) The scattering width of the resonance at 5.86 eV, reduced by three standard deviations, is based on the work of Nakajima *et al.* [138], and ii) the energies of the two bound levels in [35] were corrected due to a decimal-point typo-graphical error. With these changes, the capture resonance integral is calculated as 366 b for ENDF/B-VII.1. This is compared with a previous value of 420 b for the ENDF/B-VII.0, a reduction of 11.5 %, explaining quantitatively the reactivity-worth discrepancy of ^{133}Cs. In addition, this is consistent, within the uncertainty limits, with a measurement of Heft who reported 348.2 ± 20.1 b [139] for the total capture resonance integral.

7. ^{143}Nd

Since the SOFT discrepancy is smaller than the experimental uncertainty, no change was carried out for this material.

8. ^{145}Nd

To resolve the 13% dicrepancy between the measured reactivity-worth value and that calculated on the basis of ENDF/B-VII.0 for ^{145}Nd, a new evaluation for the thermal, resonance and URR regions was carried out. This discrepancy for the case of a thermalized neutron spectrum indicated that the thermal capture cross section was over-estimated by about 13 %. This is partly due to the fact that paramagnetic scattering, water absorption and impurities in the samples were not taken into account by the authors in a few of these measurements. Since the mass-spectra measurements of Cabell and Wilkens [140] did not suffer from these effects, the thermal capture cross section of ^{145}Nd, 42.0 ± 2.0 b recalculated from the information provided by these authors, was adopted for the ENDF/B-VII.1. The resolved resonance parameters were borrowed from the Atlas [35]. In addition, the recent RPI results of Barry *et al.* [141] were considered. A bound level was invoked to reproduce this modified thermal capture cross section, as well as the bound coherent scattering amplitude recommended in the Atlas [35]. The computed capture resonance integral is then 220 b as contrasted with 245 b for ENDF/B-VII.0, a reduction of 10 %.

9. ^{147}Nd

We are not changing ^{147}Nd relative to ENDF/B-VII.0, but note that the thermal capture in ENDF is 440 b, based on an experiment at Grenoble, but the value adopted by JENDL-4.0 was based on a burnup measurement creating ^{148}Nd.

10. ^{147}Sm

Since both the SOFT and PWR discrepancies are smaller than the experimental uncertainty, no change was carried out for this material.

11. ^{149}Sm

Since the SOFT discrepancy is smaller than the experimental uncertainty, no change was carried out for this material.

12. ^{152}Sm

Since both the SOFT and PWR discrepancies are smaller than the experimental uncertainty, no change was carried out for this material.

13. ^{153}Eu

This is a new evaluation which takes into account the -11% reactivity-worth discrepancy between the integral measurement and the value calculated using the ENDF/B-VII.0 file [13]. This discrepancy is traced to an under-estimated value of the ENDF/B-VII.0 thermal

capture cross section, 312 b. To resolve this discrepancy, it was necessary to stipulate a 2200 m/s capture cross section of 358 b which was obtained recently from a least-squares fit analysis of the capture data in the low energy region, for ENDF/B-VII.1. Since more than 82% of the thermal capture cross section is attributed to a bound level, its parameters were then altered to describe this new thermal capture cross section, as well as the coherent scattering cross section. The resolved resonance parameters, as well as an effective scattering radius of 8.2 fm, were adopted from the Atlas [35].

Other evaluations:

14. ^{58}*Co*

The previous ENDF/B-VII.0 ^{58}Co evaluation was taken from the NEA's WPEC collaboration. Since there were discrepancies with the Atlas thermal values, as well as huge negative cross sections, presumably background cross sections, we decided to carry out a complete evaluation for this nucleus. The thermal, resonance and unresolved energy regions were treated by the methodology developed for the Atlas [35], while the fast region was computed by the EMPIRE code. The only measured neutron cross sections available for ^{58}Co are the thermal capture cross section and the capture resonance integral. Since the (n,p) threshold is 3.090 MeV below the neutron separation energy for the compound nucleus, a knowledge of the thermal (n,p) cross section is required. To obtain an estimate for this cross section, two methods were called upon: (1) The reciprocity theorem was applied to the inverse reaction, ^{58}Fe(p,n)^{58}Co. The (n,p) values thus obtained in the low keV region were extrapolated to the thermal region; (2) The ratio of the (n,p) cross section of ^{58}Co to that of ^{59}Ni in the low keV region is calculated by EMPIRE and then normalized to the known ^{59}Ni thermal (n,p) cross section of 1.43 ± 0.13 b. of Harvey *et al.* [142]. In spite of the crude assumptions made, both methods surprisingly yielded the same value, 101 b. This result is in disagreement with previous evaluations which reported a cross section of 1707 b at thermal energy. Note that the thermal capture cross section and associated resonance integral in the present evaluation are 1855 b and 6519 b, respectively. These are in excellent agreement with the corresponding Atlas values 1900 ± 200 and 7000 ± 1000 b.

15. ^{62}*Ni*

Because of its importance in astrophysical calculations (the stellar ^{62}Ni problem) and a constituent of structural materials, we present in some detail the evaluation procedure for this nucleus. This is a new updated resonance parameter evaluation for neutron energies below 1.0 MeV. The thermal capture and scattering cross sections, as well as the resonance parameters up to 600 keV recommended in the Atlas [35] are adopted for this ENDF/B-VII.1 evaluation. In addition, recent LANL capture measurements [143] clearly demonstrated that the capture width, Γ_γ = 0.76 eV, for the 4.54 keV resonance which was adopted in the previous evaluation and recommended in [35] was under-estimated. Also the recommended thermal capture cross section and coherent scattering length [35] denote that a bound level is not required to describe the thermal data. On the basis of this information and the resonance data [35], a Γ_γ = 2.6008 eV was derived for the 4.54 keV resonance. With the exception of two p-wave resonances below neutron energy of 94 keV, the scattering widths of these p-wave resonances are not known; only capture kernels are recommended in the Atlas. For this evaluation, an average p-wave capture width, 0.46 eV, and associated spin values are assumed in order to derive the scattering widths for these p-wave resonances. To validate these results, a Maxwellian capture cross section for a temperature of 30 keV is calculated as 24.16 mb. This is compared with measured values of 23.4 ± 4.6 mb [144], 25.9 ± 2.6 mb [138], and 25.8 ± 2.6 mb [143].

A comparison of the ENDF/B-VII.1 evaluation and LANL measurements [143] is made in Fig 44. For clarity, the data points were thinned.

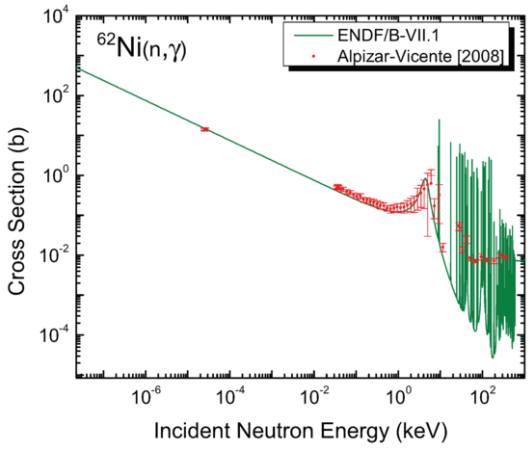

FIG. 44: Comparison of the ENDF/B-VII.1 capture data for ^{62}Ni with the LANL experimental data of Alpizar-Vicente *et al.* [143].

16. Zr

Rationale for new evaluation

Zirconium is used in the cladding of fuel rods due to its corrosion-resistance and low thermal neutron absorption cross-section. It is also considered in advanced reactor design studies as a moderator (in the form of zirconium hydride) and as inert matrix fuel material. The

ENDF/B-VI.8 files evaluated in the 1970's relied heavily on experimental data and lacked quantities such as double-differential cross sections and gamma production. Therefore the preliminary version of ENDF/B-VII.0 followed recommendations of the WPEC Subgroup 23 (but this was not finally adopted for VII.0); in most cases CSEWG adopted neutron resonances recommended by Mughabghab [35] and JENDL-3.3 evaluations in the fast neutron range, except ^{90}Zr where CSEWG favored the BROND-2 evaluation. These evaluations turned out to perform worse than ENDF/B-VI.8, showing an undesirable drop in the reactivity when tested by KAPL and Bettis [145]. Sensitivity studies indicated that this shortage could be counteracted by increasing the elastic cross section in ^{90}Zr. The NNDC (BNL) performed a new evaluation of the fast neutron region in ^{90}Zr using the EMPIRE code and dispersive optical model potential (OMP) based on rigid-rotor couplings for ^{103}Rh [85], which provided an acceptable description of the total cross section on ^{90}Zr and confirmed the higher elastic scattering cross section, however rigid rotor is not a good approximation for the structure of even-even Zr isotopes, and a better OMP treatment was needed. This evaluation was accepted by KAPL and Bettis and adopted by CSEWG for the final release of ENDF/B-VII.0.

Integral testing of ENDF/B-VII.0 performed after its release revealed that the new set of Zr evaluations over predicts reactivity in the TRIGA C132 and C133 benchmarks by more than 500 pcm. In addition, new not yet published measurements of the total cross section on natural Zr performed by RPI indicated that ENDF/B-VI.8 values were much closer to the new data than those of ENDF/B-VII.0. Finally, continued testing at KAPL showed that ENDF/B-VI.8 performance was still superior compared to all modern libraries. This can be viewed as a clear case in which a dated evaluation using little theory, but tuned to the experimental data, is better than more recent evaluations that used far more advanced modeling but that pay less attention to the measurements.

In the old ENDF/B-VI.8 evaluation and in the experimental data, there are pronounced fluctuations in the total and elastic cross sections below 1 MeV indicating either resonance structure or potentially insufficient level density for statistical model treatment, most likely related to the closed neutron shell in ^{90}Zr. In the new evaluations we describe below, we attempt to preserve the completeness of the model based evaluations without losing the experimental information that cannot be reproduced within statistical reaction theory. While doing this, we make use of advanced approaches such as coupled-channel soft-rotor optical potential and microscopic, parity dependent level densities.

Resonance region

New resonance region evaluations were developed for ^{90}Zr and ^{91}Zr. Table XX summarizes the thermal cross section and resonance integrals for the two evaluations.

^{90}Zr: We are changing the recommended ^{90}Zr thermal capture cross section significantly, but we note that since we change both ^{90,91}Zr capture cross sections the overall effect on ^{nat}Zr thermal capture is approximately unchanged for ENDF/B-VII.1 (190 mb) compared to ENDF/B-VII.0 (182 mb) - (the Atlas recommended elemental value is 185±3 mb). The ENDF/B.VII.0 thermal capture cross section, 77 mb, was taken from the Atlas recommendations [35]. This value was obtained by the subtraction method, so a thermal capture cross section of 0.830 ± 0.083 b for ^{91}Zr was adopted, based on the measurements of Lone [146]. A more recent measurement by Nakaruma *et al.* [147] reported a low limit of 1.30±0.04 b for the thermal capture cross section of ^{91}Zr indicating that the derived thermal capture cross section for ^{90}Zr is over-estimated. Therefore, we removed the bound level at -234 eV but otherwise adopted the ENDF/B-VII.0 resonances. The computed thermal capture cross section from the positive-energy resonances is 10 mb, which is in good agreement within the uncertainty limits with a measured value of 14^{+8}_{-4} mb [146]. We truncated the resolved resonance region at 53.5 keV.

TABLE XX: Calculated thermal cross sections (σ_T) and resonance integrals (I_γ) for ^{90}Zr and ^{91}Zr.

	^{90}Zr		^{91}Zr	
Reaction	σ_T **(barn)**	I_γ **(barn)**	σ_T **(barn)**	I_γ **(barn)**
Total	5.50762	-	11.0729	-
Elastic	5.49765	-	9.85728	-
Capture	9.97256×10^{-3}	0.132506	1.21566	6.0062

^{91}Zr: See the note at the beginning of the previous subsection on our essentially not changing the elemental capture cross section. As mentioned above, to be consistent with the natural zirconium capture cross section, we derived a thermal capture cross section of 1.216 b using two bound levels to describe the thermal capture cross section and bound coherent and incoherent scattering lengths [35]. This is consistent within two standard deviations of [147]. We also adopted resonance parameters below 20 keV and an effective scattering radius of 7.2 fm from Mughabghab [35]. We assume average radiative widths of 127 meV and 223 meV for those s- and p-wave resonances, respectively, for whose widths were not determined from measurements [35, 127, 148]. We assigned ℓ values that had not been determined from measurements by applying the Bayesian approach while undetermined J values were assigned randomly to follow the 2J+1 rule. With these parameters, we compute the Westcott factor for capture as $g_w = 1.0031$. In the unresolved resonance region, we deduce an average level spacing and strength functions for s-wave by fitting of reduced widths of resolved resonances to the Porter-Thomas distribution. We adopted the strength function for p-wave from [148] and the average radiative widths for s- and p-wave neutrons of 127 meV and 223 meV, respectively were obtained from [35, 127, 148]. For d-wave neutrons, we obtain a capture width of 148.6 meV from the geometric mean of the s- and p-wave

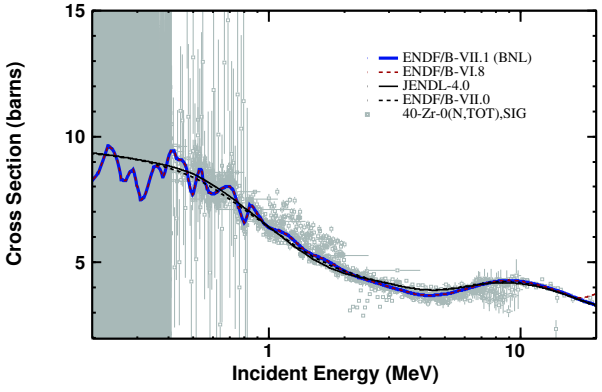

FIG. 45: ^{nat}Zr(n,tot) cross section. The ENDF/B-VII.1 evaluation preserves the data-driven fluctuations present in the older ENDF/B-VI.8 evaluation.

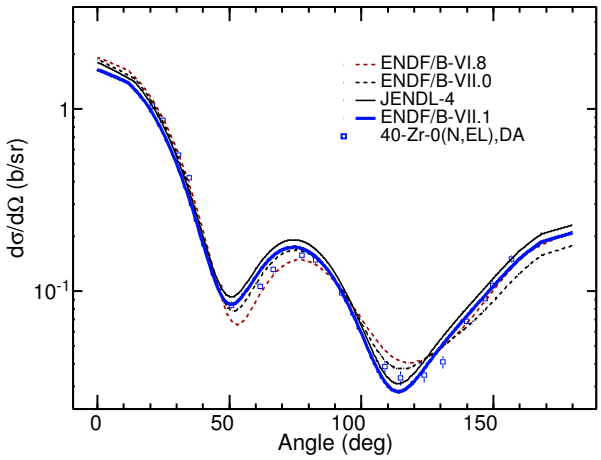

FIG. 46: ^{nat}Zr(n,el) double differential cross section for neutrons with incident energy 3.6 MeV. The ENDF/B-VII.1 evaluation tracks the shape of JENDL-4.0, but with the normalization controlled by the fluctuations in Fig. 45.

components. We took the energy-dependence of the level spacing to be the Gilbert-Cameron level density formula with associated parameters from Mughabghab [35, 126]. Further, we took the energy-dependence of capture widths to be the generalized Fermi liquid model [126] with associated parameters from [35]. We use an effective scattering radius of 7.2 fm in the URR.

Fast neutron region

Because the Zr isotopes are so close to a closed shell, the total and elastic cross sections exhibit pronounced fluctuations up to nearly 1 MeV. To preserve these fluctuations, which were present in the original ENDF/B-VII.8 evaluation and integral testing suggests are important, we used EMPIRE's ability to tune cross sections to data to match ^{nat}Zr(n,tot) (see Fig. 45). Total cross sections in all of the Zr isotopes were tuned with the same factors while elastic cross sections were obtained subtracting non-elastic channels from the total. Whilst strictly speaking this is not correct, it preserves the transport cross section for ^{nat}Zr while leaving the activation cross sections for the individual isotopes unchanged. Model calculations in the fast energy range were based on nuclear model calculations using the EMPIRE code [82]. Starting values for nuclear model parameters were taken from the RIPL recommendations [85]. A dispersive OMP (RIPL 609) [85] based on soft rotor couplings was used to describe the incident channel on even-even targets; the same potential with rigid-rotor couplings (RIPL 611) was employed to describe the incident channel for even-odd isotopes. The optical model calculations for the incident channel of even-even Zr isotopes were performed with the OPTMAN code [149], which is capable of including soft-rotor couplings. All other optical model calculations were performed with the ECIS code [87] that is incorporated into the EMPIRE system. TUL multistep direct and the Heidelberg multistep compound models were employed to describe the preequilibrium neutron emission; proton, gamma and cluster pre-equilibrium emission was calculated using a one-component exciton model (PCROSS). Hauser-Feshbach [88] and Hofmann-Richert-Tepel-Weidenmüller [89] versions of the statistical model were used for the compound nucleus cross section calculations. Both approaches account for the multiple-particle emission and the full gamma-cascade. Level densities were described by the (semi)-microscopic parity dependent Hartree-Fock-Bogoliubov level densities [85].

Extensive comparison of the calculated elastic angular distributions with the wealthy amount of experimental data (about 150 plots) demonstrated that JENDL-4.0 using the Walter-Guss OMP below 6 MeV, and Koning-Delaroche OMP above 6 MeV describes measurements better, especially at low incident energies. Since KAPL sensitivity studies indicated that elastic angular distributions might be of importance for their integral testing we adopted the (n,el) angular distributions from JENDL-4.0. A sample angular distribution is given in Fig. 46. It can be seen that our tuning of the elastic cross sections slightly improves agreement with the experimental data. Benchmarking performed with the suite of 22 integral experiments (see accompanying validation paper [8]) confirmed that switching to the JENDL angular distributions reduces over prediction of the TRIGA 132 and 133 reactivities by 50% bringing our results well within the experimental uncertainties.

Covariance data

We added the Zr point-wise covariance data which were used to produce group-wise COMMARA-2.0 [150] library to the evaluations. In the thermal and resolved resonance region we made use of the covariance formalism based on the kernel approximation along with data in the Atlas of Neutron Resonances. In the fast neutron region covariance estimates were calculated using

the nuclear reaction code EMPIRE and the Bayesian code KALMAN taking into account experimental results.

Future work
In spite of the fact that the new set of evaluations presents a net improvement compared to ENDF/B-VII.0 we consider it an intermediate result on the way to a fully consistent suite of evaluations for zirconium isotopes. We plan to reevaluate the resonance region and fine tune the dispersive soft-rotor OM potential in order to achieve a complete description of neutron induced reactions for the full chain of zirconium isotopes.

17. ^{113}Cd

Analysis of integral measurements by Mosteller *et al.* [151], as well as capture and transmission data carried out by Danon *et al.* [152] below the first resonance at 0.178 eV, showed that the thermal capture cross section of ^{113}Cd in ENDF/B-VII.0 and the Atlas [35] was overestimated. A thermal capture cross section of 19860 ± 250 b is then derived for ^{113}Cd from the natural cadmium and the other isotopic capture cross sections by the subtraction method. The capture width of the 0.178 eV resonance, 113.5 ±1 meV, is adopted from the Gelina result [153] and the scattering width was then adjusted to describe this new evaluated thermal capture cross section.

18. ^{157}Gd

Previously two measurements, carried out by Rauch *et al.* [154] and Leinweber *et al.* [155], suggested that the accepted thermal capture cross section of ^{157}Gd at that time is large by about 10 % [35]. Additional supportive data came from integral measurements of Perret *et al.* [156].

The ultracold neutron measurements in gadolinium by Rauch *et al.* [154] may appear to support the RPI measurements [155]. Rauch *et al.* reported a capture cross section of 49.7±1.6 Mb at 10 m/s for ^{157}Gd and compared it with a value of 55.9±1.5 Mb, obtained by extrapolating the 2200 m/s capture cross section of 254000±815 b [96] using the 1/v law. However, because of the proximity of the 0.0314 eV resonance of ^{157}Gd to the thermal energy, the 1/v law does not hold in this case. In fact, applying the Breit-Wigner formula and the ENDF/B-VII.1 parameters of the 0.0314 eV resonance one obtains a capture cross section of 42.0±1.0 Mb at 10 m/s, instead of the extrapolated value of 55.9±1.5 Mb.

Besides, several simulations of ICSBEP (International Criticality Safety Evaluation Project) benchmarks, carried out for the present project, showed that the RPI thermal capture cross section over-predicted the eigenvalues, $k_{\rm eff}$. In view of this conflicting situation, a careful examination and a least-squares fitting of the energy-dependent total cross sections of both Gd and ^{157}Gd in the energy region below 1 eV , showed that 2200 m/s capture cross section is 253332±930 b and the parameters of the s-wave resonance at 0.0314 eV are $\Gamma_n = 0.474 \pm 0.003$ meV and $\Gamma_\gamma = 107.2 \pm 1.9$ meV. These derived parameters of the 0.0314 eV resonance and the thermal capture cross section give a consistent picture with other measurements in EXFOR and show that it is unnecessary to invoke a large thermal capture background, as was done in JENDL-4.0 [9] to justify the embracing of the Leinweber *et al.* [155] parameters of the 0.0314 eV resonance. The capture resonance integral of the ENDF/B-VII.1 evaluation is 758.5 b.

To summarize this section, the 2200 m/s cross sections and resonance integrals of ENDF/B-VII.1 and ENDF/B-VII.0 are collected in Table XXI to highlight the changes made in these quantities. The following points have been achieved:

- Except for ^{95}Mo, the major significant discrepancies of the reactivity-worth results of [13] are removed in the ENDF/B-VII.1 evaluations.
- The ^{62}Ni capture cross section was reevaluated so that the computed ENDF/B-VII.1 30-keV Maxwellian capture cross section agreed with direct measurements.
- The thermal capture cross sections of ^{90}Zr and ^{91}Zr are reevaluated on account of a new measurement and those of ^{113}Cd and ^{157}Gd modified to reflect recent differential and integral measurements.

F. Actinides

1. ^{232}Th

The ^{232}Th ENDF/B-VII.0 evaluation was adopted from the results derived within an IAEA Coordinated Research Project in 2005 [157, 158]. No changes have been made for ENDF/B-VII.1 as compared to ENDF/B-VII.0. Nevertheless, below we make some observations on the assessment of our thorium evaluation.

The most precise fast neutron benchmark involving thorium is the THOR assembly, which is described in the ICSBEP compilation as PU-MET-FAST-008 [113]. It is a plutonium sphere in a cylindrical thorium reflector. It is quoted with an experimental uncertainty of 60 pcm due to the uncertainty in the critical mass. We believe that the uncertainty quoted for this benchmark is underestimated. The criticality of this benchmark is under predicted by about 200 pcm with ENDF/B-VII.0 thorium data. Substitution of ENDF/B-VII.0 ^{232}Th data with JENDL-4.0, in which the fission cross section from 1.2 to 5 MeV is higher by about 8 %, improves the criticality prediction, but not the reaction rate ratios, which were also measured for this benchmark. Additionally, the Comet assembly of a U-sphere with Th reflector (HEU-MET-FAST-085 case

TABLE XXI: Comparisons of the ENDF/B-VII.1 and ENDF/B-VII.0 for the thermal capture cross sections and capture resonance integrals for the materials considered in this section.

Nucleus	σ_γ(b) ENDF/B-VII.1	σ_γ (b) ENDF/B-VII.0	I_γ (b) ENDF/B-VII.1	I_γ (b) ENDF/B-VII.0
^{92}Mo	0.080	0.02075	0.864	0.0968
^{95}Mo	13.1	13.57	104.4	11O.28
^{99}Tc	20.0	22.80	322.4	361.7
^{103}Rh	142.0	144.91	967.5	1034.30
^{109}Ag	90.23	91.08	1466	1473.00
^{133}Cs	29.0	29.0	366.	420.49
^{143}Nd	325.15	325.15	130.2	130.17
^{145}Nd	42.00	49.83	220.	245.04
^{147}Sm	56.98	56.98	774.57	774.57
^{149}Sm	40138.7	40138.7	3434.	3434.
^{152}Sm	209.2	209.02	2977.	2977.
^{153}Eu	358.	312.	1422.8	1415.8
^{155}Gd	60886.6	60886.6	1540.14	1540.14
^{58}Co	1855	172	6519	221
^{62}Ni	14.90	14.41	7.26	6.01
^{90}Zr	0.01	0.078	0.133	0.19
^{91}Zr	1.22	0.832	6.01	5.88
^{113}Cd	19858.0	20610.0	383.25	392.9
^{157}Gd	253332.0	254200.0	758.6	753.3

5) does not show the same trend in k_{eff}, although the Comet benchmark uncertainty is higher. Plots of criticality benchmarks in ICSBEP relevant to ^{232}Th data can be found in a companion paper by Kahler *et al.* in this edition [8].

Since the observed discrepancies are in contradiction with one another, and the under prediction of reactivity is not excessive, we have chosen to carry over the ENDF/B-VII.0 evaluation unchanged for ENDF/B-VII.1. It might be that, in the future, conclusions from the IAEA coordinated research project on prompt fission neutron spectra (PFNS) [159, 160] could lead to an impact on the thorium evaluation as well as on the other major actinides.

2. ^{237}Np

The ^{237}Np evaluation has been updated for the $(n, 2n)$ and $(n, 3n)$ channels using a recent evaluation by Maslov *et al* [161] for these reactions. Fig. 47 compares the ENDF/B-VII.1 evaluation to both the previous ENDF/B-VII.0 evaluation and the available experimental data for the ground state and the isomer+ground state. As can be seen, the new (n,2n) evaluation (solid black) corrects unphysical behavior near threshold of the previous ENDF/B-VII.0 evaluation (black dashed). Additionally, the new evaluation reproduces well experimental data for both the total (n,2n) (black circles) and production of $^{236(short)}$Np (1^-) (blue circles).

Updates to the ^{237}Np evaluation also include new resonance parameters fitted to the thermal (n,γ) cross section of Mughabghab, $\sigma_\gamma^0 = 175.9 \pm 2.9$ b.

Integral reaction rate measurements of ^{237}Np(n, γ) in a critical assembly can be used to assess the cross section, see Fig. 48. These Los Alamos data have not been previously reported; they indicate that the ENDF/B-VII.1 capture cross section appears to be accurate.

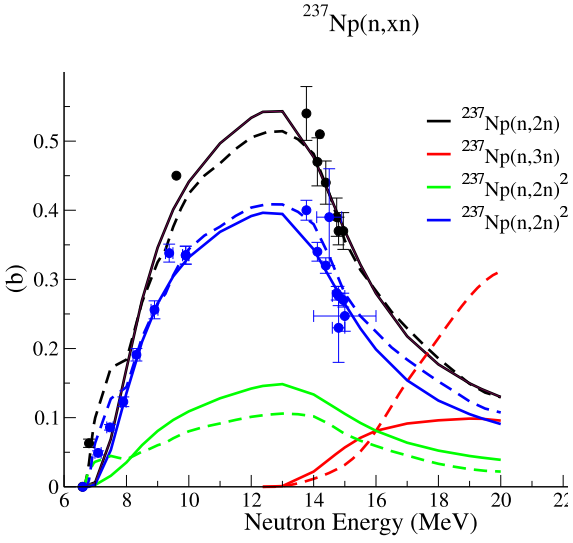

FIG. 47: The ^{237}Np$(n, 2n)$ cross section (black). [2] The $(n, 2n)$ cross section to the short-lived 1^- state (blue) and to the long-lived 6^- state (green) compared with data. The $(n, 3n)$ cross section is shown in red. The solid lines, taken from Maslov, are for ENDF/B-VII.1, while the dashed lines are for ENDF/B-VII.0.

3. ^{233}U

The previous total inelastic cross section in ENDF/B-VII.0 had an unusual shape below 1 MeV, which is very different from JENDL-4 and other evaluations. From a

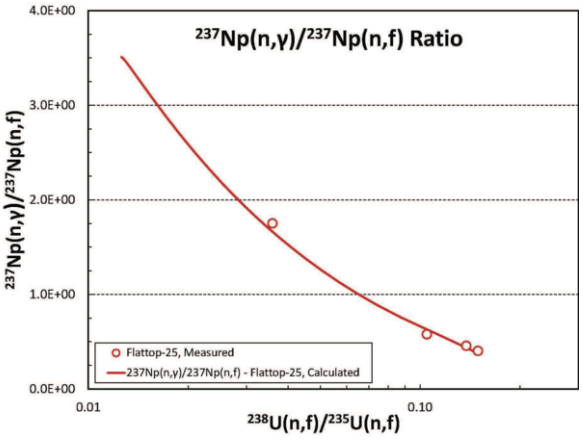

FIG. 48: ^{237}Np(n,γ) comparison of experimental radiochemical data with an MCNP simulation using ENDF/B-VII.1 data. The measured data, from Efurd (1986) [162], were in Flattop-25 at locations 11, 6, 4, 1 cm from the center, where the measured neptunium capture to neptunium fission (237c/238f) ratios - as reassessed by MacInnes - were 1.75, 0.578. 0.457. and 0.403 ($\pm$ 4%) (with Ir-193m/192 indices of 0.257. 0.871, 1.104, 1.271), respectively.

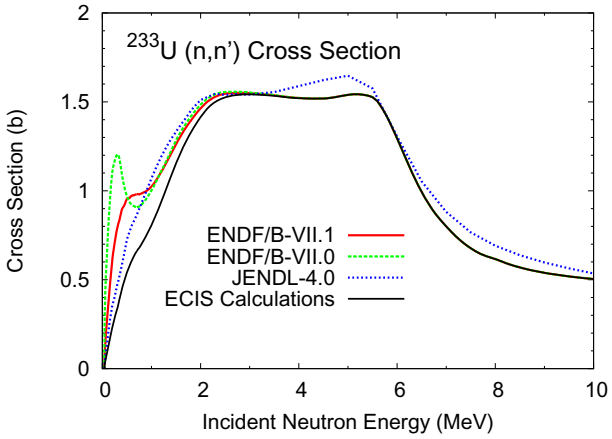

FIG. 49: The revised ENDF/B-VII.1 total inelastic cross section ^{233}U (n,n') is compared to ENDF/B-VII.0 and JENDL-4.0 evaluations, as well as ECIS calculations.

physical point of view, the shape of the ^{233}U inelastic cross section is expected to be similar to the ^{235}U inelastic cross section, both being fissile odd-neutron nuclei. Indeed, evaluated inelastic cross sections for ^{235}U were very similar in JENDL-4 and ENDF/B-VII.0, which was not the case for the ^{233}U cross section. This anomaly was identified at an IAEA meeting in late 2010 [163].

The n+^{233}U ENDF/B-VII.1 evaluation is a modification of the ENDF/B-VII.0 evaluation to correct the cross sections and angular distributions of the ground-state rotational band of ^{233}U. The correction was required because the compound-nucleus components for these states in the ENDF/B-VII.0 evaluation did not take proper account of fission competition. This error resulted in the inelastic cross sections of the ground-state rotational band, particularly the first two excited states, being overestimated below 1 MeV. As a result the integrated (n,n′) cross section exhibited an anomalous peak near 200 keV (see ENDF/B-VII.0 curve in Fig. 49), largely due to excessive cross sections in the first two states of ^{233}U.

To correct this problem, the compound nucleus cross sections for the ground-state rotational band (MT2,51,52,53,55,58, and 65) were first re-calculated and combined with the direct components from ECIS calculations. However, it was apparent that the corrected cross sections for the first two excited states disagreed with the experimental data of Haouat *et al* [164]. That is, the corrected cross sections fell below Haouat's data, as can be seen in Fig. 50 (see ECIS calculations curve).

It was surmised that the deformed optical model potential used in the evaluation might not be adequate at incident energies below approximately 1.0-1.5 MeV. To correct this problem, the compound nucleus contributions to these states were scaled by a single factor to produce better agreement with the Haouat *et al.* experiment [164]. The difference in the inelastic cross sections was then absorbed into the elastic cross section, keeping the total cross section fixed. With this method, corrections were made to the elastic and first two inelastic level cross sections and angular distributions. The data for the remaining ground-state rotational band levels were adjusted using the corrected ECIS calculations of the compound nucleus contributions.

The results of these corrections are illustrated by the curves labeled "ENDF/B-VII.1" in Figs. 49 and 50. The large peak in the (n,n′) cross section near 200 keV in the previous ENDF/B-VII.0 evaluation is now reduced to a shoulder in the cross section (Fig. 49). The level cross sections for the first and second excited states now agree well with Haouat's data [164] (Fig. 50). Clearly, these changes only affect the (n,n′) data below 1.5 MeV, and the rest of the evaluation is virtually unchanged.

4. ^{235}U

At present we have not made changes for the ^{235}U evaluation, other than reverting to ENDF/B-VI.8 delayed neutron parameters for the reasons discussed in Section VI G, and adding covariances. The previous prompt fission neutron spectrum from Madland has been carried over to ENDF/B-VII.1 but with a finer outgoing neutron energy representation. The important recent mass spectrometry measurements of capture by Wallner and collaborators, by broad neutron sources peaked at 25 keV and 426 keV, are consistent with (but slightly lower than) the ENDF/B-VII.1 ^{235}U(n,γ) capture evaluation. Ongoing work on ^{235}U that will be made available in future ENDF releases is summarized in Section XI. This includes considerations, raised by our JENDL colleagues,

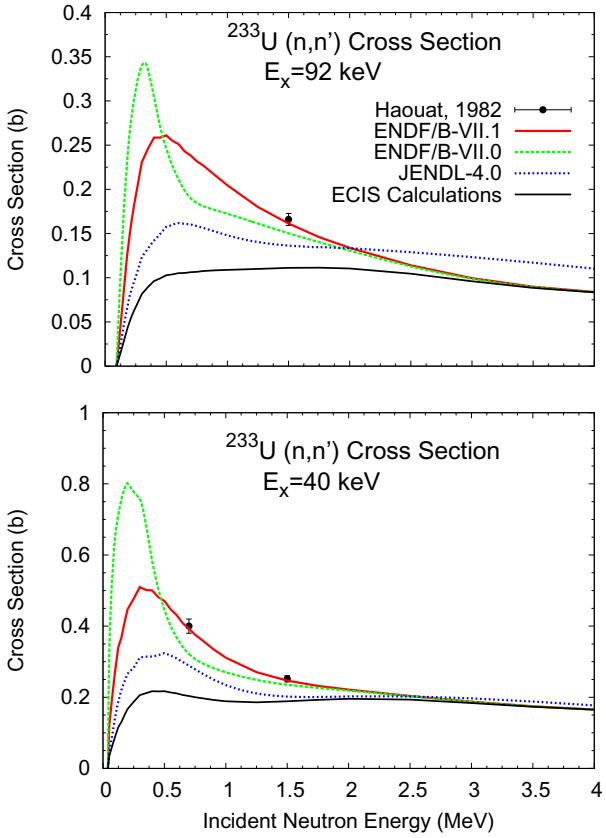

FIG. 50: ^{233}U (n,n′) cross sections to the 40 keV and 92 keV inelastic states. As discussed in the text, the ECIS coupled channels calculations were unable to reproduce the measured data by Haouat and were therefore modified for the evaluated file.

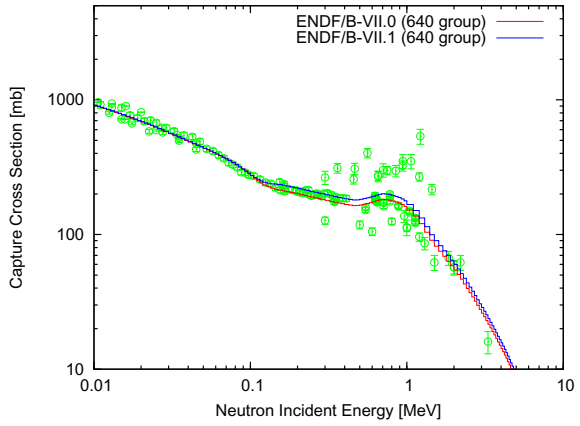

FIG. 51: Evaluated ^{236}U(n,γ) used for ENDF/B-VII.1, compared with ENDF/B-VII.0 and experimental data from the LANSCE/DANCE detector.

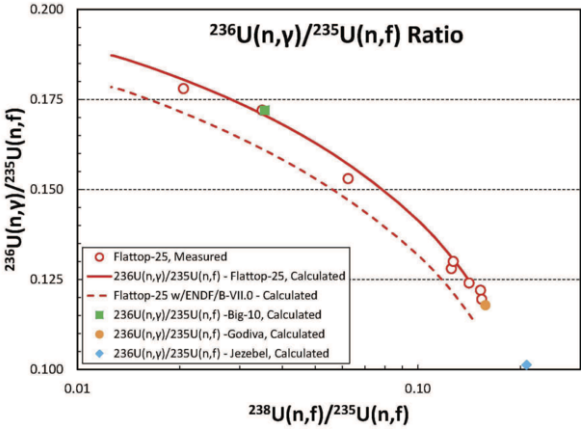

FIG. 52: ^{236}U(n,γ) comparison of experimental radiochemical data with an MCNP simulation using ENDF/B-VII.1 and ENDF/B-VII.0 data. The spectral index, a measure of the hardness of the neutron spectrum, is given on the x-axis.

that the capture cross section should perhaps be lowered by as much as 25%. Covariance uncertainty data were assessed by LANL and ORNL for the fast and resonance regions and included in the VII.1 evaluations, as described in companion papers by Talou *et al.* and Leal *et al.* in this edition.

5. ^{236}U

We have made two modifications to the ^{236}U evaluation: in the energy region near 100 keV the fission cross section has been modified slightly to provide a smoother match to the unresolved resonance region; and radiative capture has been increased by about 10% for the energy region above 100 keV.

The capture modification was motivated mainly by MCNP simulations of ^{236}U(n,γ) in fast critical assemblies that previously underpredicted the measured LANL data by about 10%, as we documented in Ref. [1, 3]. The higher capture cross section is still consistent with the measured cross section data in this region, which have significant uncertainties, see Fig. 51, but leads to improved MCNP predictions of the Los Alamos critical assembly capture reaction rate data as shown in Fig. 52. In this figure the x-axis is a measure of the hardness of the neutron spectrum in the assembly (*e.g.* locations at outer tamper regions of Flattop being on the left hand side; locations at the center of Flattop being on the right hand side), and we tabulated the data in Ref. [3].

6. ^{237}U

The ENDF/B-VII.0 evaluation for ^{237}U had various limitations, originating largely from the fact that very little measured data exist for this unstable nucleus and nuclear reaction modeling has a limited predictive power for reactions that involve fission. Indeed, model cal-

culations presently have an improved predictive power once they involve some calibration to measured data on nearby uranium isotopes (for example calculation of fission on ^{237}U needs fission barriers for ^{238,237,236}U compound systems, which can be inferred by fission modeling on ^{238}U, where second-chance fission involves barriers for the same ^{238}U compound nucleus that can be assessed from measured data). This is the case for analyses with our GNASH code, where we model reactions on the whole uranium chain in one consistent set of calculations, as well as for more fundamental studies such as that of Goriely *et al.* [165, 166] using Hartree-Fock-Bogoliubov theory with some calibration. The main limitations of the ENDF/B-VII.0 evaluation were: (1) Its crude low energy resonance representation that did not connect smoothly to the higher energy region above 100 keV; and (2) some arguments that the fission cross section in the keV – few MeV region should be modified. The first issue is addressed for ENDF/B-VII.1 by us smoothly matching our evaluation onto the JENDL-3.3 resolved and unresolved resonance evaluation below 100 keV (we modified the unresolved resonance representation slightly to facilitate this). The second issue, on fission, is discussed below.

Measured data for fission in the keV-MeV region are widely discrepant. This includes inferred values from surrogate reaction data by researchers from Livermore (Younes, Burke) using Livermore and Los Alamos measurements; the McNally, LANL underground nuclear explosion data (which possibly involve contamination from some ^{237}Np in growth as suggested by Wilhelmy); and Los Alamos critical assembly fission rate measurements by Barr *et al.* reported in Ref. [3]. Because of our higher confidence in the Barr data, which involve broad neutron sources within the Flattop critical assembly, we have adjusted GNASH fission modeling parameters to better match these measurements, which involve a higher slope between 0.01 and 4 MeV. The evaluation is also consistent with the fission systematics of Behrens [167].

The various measurements and the evaluations are shown in Figs. 53, 54, 55, and the calculated and measured fission rates in Flattop that motivated this change are shown in Fig. 56. We note that our present evaluation in the 0.1-4 MeV region, which was completed a few years ago, is in fairly good agreement with the recently published HFB calculation by Goriely and coworkers [166], as well as with Eric Lynn's calculations.

We doubt this will be the final word on fission for ^{237}U! After all, the various estimates of this cross section in the literature and in evaluated data files vary significantly. Our present evaluation was motivated by the aforementioned considerations, but new data in the future will hopefully clarify the situation. A measurement is presently being carried out at Los Alamos' lead slowing down spectrometer at LANSCE, using a small sample being made at Oak Ridge (from double capture on ^{235}U), although this will be limited to neutron energies below about 1 keV where the neutron fluence is high.

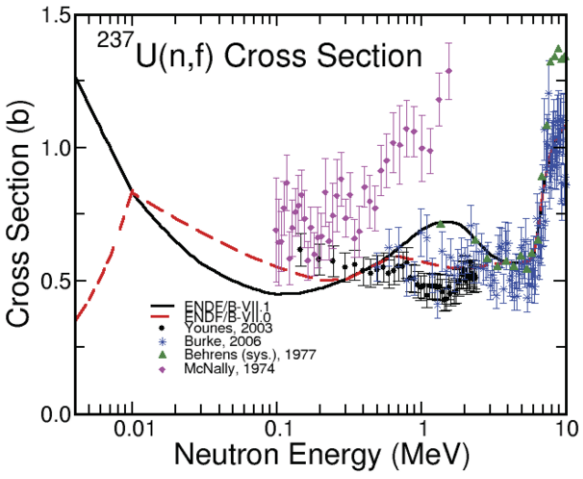

FIG. 53: Evaluated ^{237}U fission cross section for ENDF/B-VII.1 compared with data, and with ENDF/B-VII.0 (as in previous figure, except log-log).

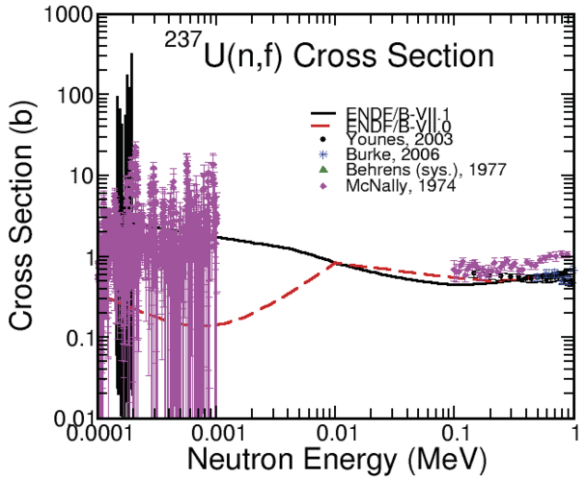

FIG. 54: Evaluated ^{237}U fission cross section for ENDF/B-VII.1 compared with data, and with ENDF/B-VII.0 (as in previous figure except lin-lin).

7. ^{238}U

At present we are not making substantive changes for the ^{238}U evaluation, other than reverting to ENDF/B-VI.8 delayed neutron parameters for the reasons discussed in Sec. VI G, and adding covariances. The previous prompt fission neutron spectrum from Madland has been carried over to ENDF/B-VII.1 but with a finer outgoing neutron energy representation.

Although the $(n, 2n)$ and (n, γ) cross sections have not changed for VII.1, is it still useful to observe the integral performance of reaction rate calculations of these quantities against LANL critical assembly reaction rate data for VII.0. These results are shown in Figs. 57, 58, and are similar to those we showed in Refs. [1, 3]. In these

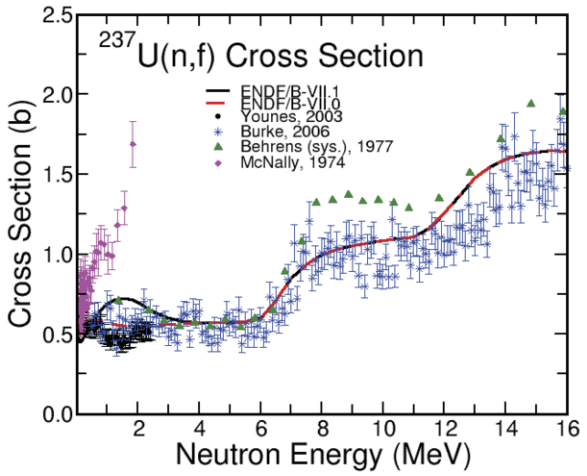

FIG. 55: Evaluated ^{237}U fission cross section for ENDF/B-VII.1 compared with data, and with ENDF/B-VII.0.

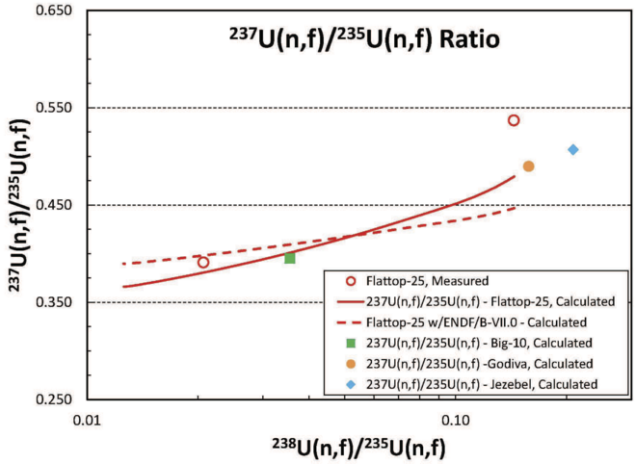

FIG. 56: MCNP calculated ^{237}U fission reaction rate (in ratio to the well known ^{235}U fission rate) compared with measurements, for samples placed in the Flattop-25 fast critical assembly at LANL. Two measurements were made by Barr, one in the (hot) center, and one in the (softer) tamper region.

figures the x-axis is a measure of the hardness of the neutron spectrum in the assembly (*e.g.*, locations at outer tamper regions of Flattop, and Bigten, being on the left hand side; locations at the center of Flattop, and Jezebel, being on the right hand side), and we tabulated the data in Ref. [3].

The recent accelerator mass spectrometry measurements on capture by Wallner and collaborators, using broad neutron sources peaked at 25 keV and 426 keV, have provided some additional confirmation of the ENDF/B-VII.0 standards ^{238}U(n,γ) capture evaluation and are described in Secs. VII and X D. Ongoing work on ^{238}U that will be made available in future ENDF releases is summarized in Sec. XI. Covariance uncertainty data were assessed by LANL and ORNL for the fast and

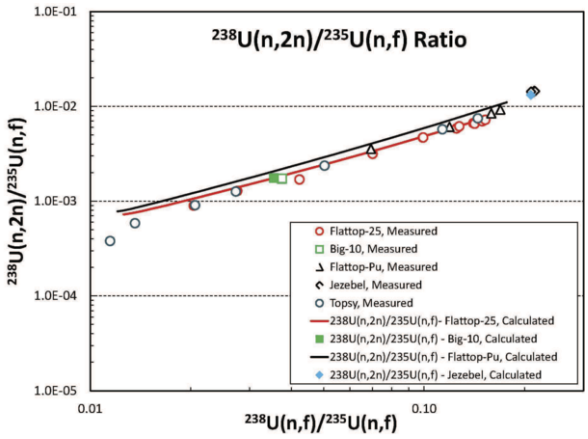

FIG. 57: The ratio of the ^{238}U(n,2n) reaction rate to the ^{235}U fission rate is plotted against the ratio of the ^{238}U fission rate to the ^{235}U fission rate (spectral index) for different positions (with central positions to the right and positions in the reflector to the left).

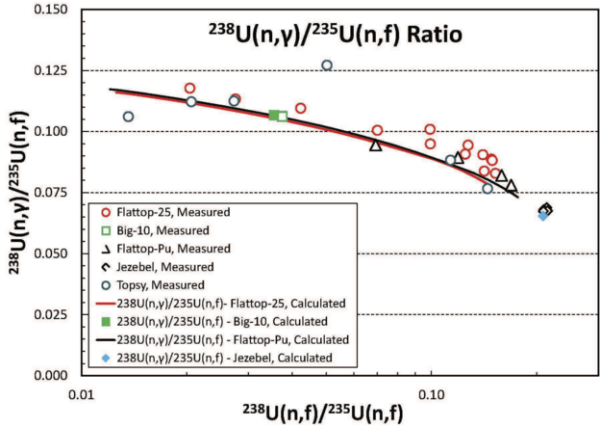

FIG. 58: The integral ^{238}U neutron capture rate (divided by the ^{235}U fission rate) as a function of spectral index for different critical assembly locations.

resonance regions and included in the VII.1 evaluations, as described in companion papers by Talou *et al.* [26] and Leal *et al.* [27].

8. ^{239}U

^{239}Pu is created through the neutron radiative capture reaction on ^{238}U followed by β decays of ^{239}U through ^{239}Np to ^{239}Pu. Given ^{239}U's short half life (23.45 min.), it is no surprise that this nucleus is somewhat under studied. Indeed, ENDF/B-VII.0 was the first ENDF-series library to contain an evaluation of ^{239}U [1, 3]. Fortunately, in the years since ENDF/B-VII.0 was released our knowledge of ^{239}U has advanced: Younes and Britt have reanalyzed legacy (t,pf) and (^{3}He,xf) surrogate data

[168, 169] and new surrogate reaction experiments using the (^{18}O,^{16}O) two-neutron transfer reaction were performed by Burke et al. [170]. In all three cases, the surrogate reactions create the same compound nucleus (^{240}U) that one would find in the ^{239}U(n,f) reaction. In addition, issues have arisen with the unusual shape of the low energy cross sections (resonance region and below). We have made a new evaluation of ^{239}U which incorporates these data and an entirely new resonance region evaluation.

The original ENDF/B-VII.0 ^{239}U evaluation was based on several works:

- The original Younes and Britt surrogate analysis [168] and the 1977 systematics by Behrens [167]. The surrogate analysis of Ref. [168] matches nicely on to Behrens' (n,f) cross section systematics in the 2.5-5 MeV region so Young et al. extrapolated Behrens' scale factor up to 30 MeV [3].
- All high energy cross section data are based on GNASH calculations which were tuned to reproduce Behrens (n,f) systematics.
- The fission neutron spectrum is the Watt spectrum from the ENDF/B-VII.0 ^{237}U evaluation.
- The prompt $\bar{\nu}$ is taken from Manero and Konshin's systematics [171].
- The resonances are taken from the ENDF/B-VII.0 ^{237}U evaluation.

In performing our new evaluation, we changed the resonance region and all of the cross section data. Below we detail our changes.

Our new (n,f) cross section evaluation combines the reanalyses of Younes and Britt [168, 169] with the new surrogate reaction experiment performed by Burke et al. [170]. Both sets were treated as "real (n,f)" data and then fitted with a linear spline. The resulting curve is shown in Fig. 59. From the upper end of the fit region (20 MeV) to 30 MeV, we scale the ENDF/B-VII.0 evaluation using the ratio of the original evaluation to our new fit. To perform our fit, we required an estimate of uncertainties of Younes and Britt's data. Younes and Britt used legacy (t,pf) and (^{3}He,xf) data to extract fission probabilities and extended these with GNASH calculations to establish the first chance fission cross section. We assigned a 10% uncertainty to this first chance fission cross section. Next, Younes and Britt extrapolated to second and third chance fission using estimates of pre-equilibrium neutron emission from GNASH. As the extrapolated first chance fission underpins the second and third chance fission, we assign 20% and 25% uncertainties to second and third chance fission, respectively. Given the simplicity of these uncertainty estimates we have not included them in the evaluation.

As we have changed the fission cross section, we must correct the remaining high-energy cross sections so that

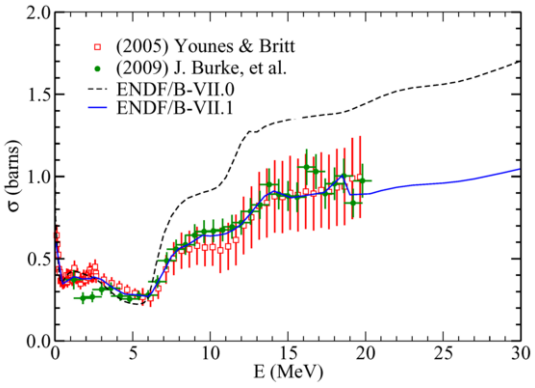

FIG. 59: Comparison of the new ENDF/B-VII.1 ^{239}U evaluation with the ENDF/B-VII.0 evaluation and surrogate data from Ref. [168, 169, 170] in the high energy region for the (n,f) channel.

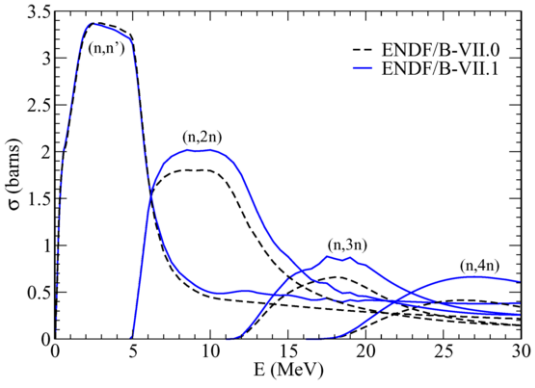

FIG. 60: Comparison of the new ENDF/B-VII.1 ^{239}U evaluation with the ENDF/B-VII.0 evaluation in the high energy region for the (n,n'), (n,2n), (n,3n) and (n,4n) channels.

all of the cross sections add up to the reaction cross section, $\sigma_{\rm rxn}$. To do this, we assume that we can work in the Weisskopf-Ewing limit and that the contribution from the compound elastic is negligible. With these assumptions, the correction is a simple rescaling:

$$\sigma_{\rm new} = \sigma_{\rm old} \frac{\sigma_{\rm rxn} - \sigma_{\rm new\ (n,f)}}{\sigma_{\rm rxn} - \sigma_{\rm old\ (n,f)}}. \quad (3)$$

The final cross-sections are shown in Fig. 60.

The resonance region in the previous ENDF/B-VII.0 evaluation has several deficiencies:

- The cross sections have an unusual shape (see Fig. 61) and are uniformly high: the Westcott factor is 4, which is unusually high (the ^{239}U Westcott factor in the CENDL-3.1 library is 1) [172]. The Westcott factor is a measure of the deviation of the low energy cross section from the usual $1/v$ like shape.
- The thermal cross sections did not match systematics from Ref. [35].

TABLE XXII: ^{239}U+n thermal cross sections and resonance integrals computed from the resonance region of the new ENDF/B-VII.1 evaluation.

Channel	Thermal σ (barns)	Thermal σ (Ref. [35]) (barns)	Resonance Integral (barns)
(n,tot)	47.48		697.6
(n,el)	10.91		175.1
(n,γ)	22.33	22 ± 5	311.51
(n,f)	14.24	14 ± 3	208.3

- Because the resonance region was taken from the ^{237}U evaluation, both the J^{Π} and mean level spacing D_0 are incorrect for ^{239}U.

To correct these problems, we generated a new "picket fence" resolved resonance. The location of each resonance was set by

$$E_n = E_{\rm therm} + (n + \frac{1}{2})D_0(E_{n-1}),$$
$$\text{where } n = [-2, -1, 0, 1, 2, ...], \quad (4)$$

with $E_0 = E_{\rm therm} + D_0/2$ and an average s-wave level spacing $D_0 = 2.5$ eV. We assume the level spacing decreases with energy following a simple constant temperature level density ansatz with temperature $T = 0.45$ MeV. Both D_0 and T are chosen to correspond roughly to the systematics given in RIPL-3 [85]. The widths of the resonances were tuned to match the average capture and fission widths of [35] while the average elastic width remained close to the value from the ^{237}U evaluation. We comment that the average gamma width required for this matching is somewhat high (53 meV) indicating that p-wave resonances are probably required. At the upper end of the resolved resonance region, we generated an interpolating unresolved resonance region using the average widths from the resolved resonance region at the low end, but matching onto the high energy cross sections at the upper end. As these unresolved resonances were created solely to match the resolved resonances onto the high energy region, the cross section probability tables one can generate from the unresolved resonance parameters may not be useful. The thermal cross section and resonance integrals are given in Table XXII and plots of the resonance region are given in Fig. 61.

9. ^{238}Pu

A new evaluation was performed for neutron-induced reactions on ^{238}Pu in the fast neutron region. The evaluation is based on model calculations, as well as analysis of experimental data. The ECIS94 code [87] was used to perform coupled-channels optical model calculations, and obtain total, shape and reaction cross sections, as well as all discrete elastic and inelastic cross sections and angular distributions. Neutron transmission coefficients used for statistical Hauser-Feshbach calculations were also inferred from the coupled-channels results. The optical model potential developed recently by Soukhovitskii *et al.* for even-even plutonium isotopes [173] was used in this work.

The GNASH [174] and COMNUC [175] codes, which implement the Hauser-Feshbach equations, width fluctuation corrections as well as pre-equilibrium components, were used to compute (n, xn) reaction cross sections. The COH code [60] was used for computing the neutron radiative capture cross section.

The GLUCS statistical analysis code [176] was used to analyze experimental data sets, and in particular, infer the fission cross section as well as prompt fission neutron multiplicity.

The JENDL-4.0 evaluation [177] was also used to complement the present work in certain areas.

In the following, we have compared the new ENDF/B-VII.1 evaluation to other evaluations, ENDF/B-VII.0, JENDL-4.0 and JEFF-3.1. The ENDF/B-VII.0 evaluation is more than 30 years old, carried from ENDF/B-V. The JEFF-3.1 evaluation was mostly taken from JENDL-3.2, and the unresolved resonance parameters were taken from BROND-2.2. The JENDL-4.0 is the most recent evaluation from JAEA, including modern coupled-channels calculations, a new set of resolved resonance parameters, and covariance data.

Total, Elastic, Non-Elastic and (n, xn) Reaction Cross-Sections

Below 60 keV, the resonance parameters evaluated in JENDL-4.0 were adopted [177]. The shape and magnitude of the cross sections below 60 keV however are consistent with the Soukhovitskii optical model calculations, and only a very small adjustment was required for joining the cross sections at 60 keV. From 60 keV up to 30 MeV, the total cross section results were obtained entirely from the coupled-channels calculations using the Soukhovitskii potential [173].

Our evaluated n+^{238}Pu total cross section is compared in Fig. 62 to the ENDF/B-VII.0, the JEFF-3.1.1, and the JENDL-4.0 evaluations between 0 and 20 MeV. Our results are in very close agreement with the JENDL-4.0 data. In Fig. 63 we compare our results with the same evaluations and the experimental data of T.E. Young *et al.* [178] in the resonance range.

Again, good consistency with the JENDL-4.0 evaluation above 60 keV is apparent. Below 60 keV we adopted the JENDL-4.0 resonance parameters, so the two evaluations are identical.

The non-elastic cross-section is inferred by summing the inelastic, (n,xn), fission and capture cross sections. The non-elastic cross section is compared to other evaluations in Fig. 64.

The elastic cross section, which is the sum of shape and compound nucleus components, is obtained by subtracting the non-elastic cross section from the total cross-section, and is shown in Fig. 65, together with the ENDF/B-VII.0, the JEFF-3.1.1, and the JENDL-4.0 evaluations.

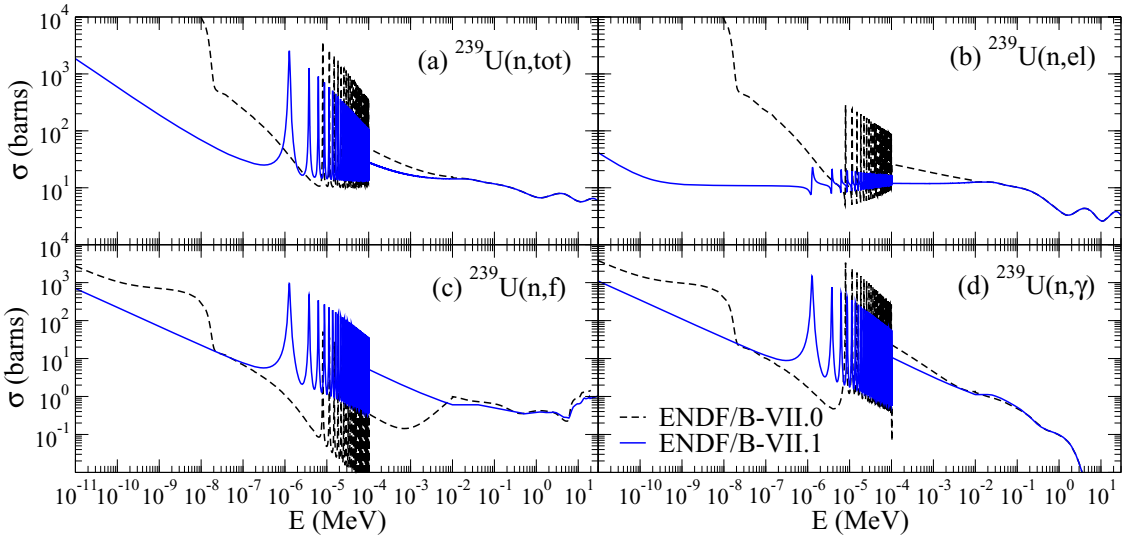

FIG. 61: Comparison of the new ENDF/B-VII.1 ^{239}U evaluation with the ENDF/B-VII.0 evaluation in the resonance region for the (n,tot), (n,el), (n,f) and (n,γ) channels.

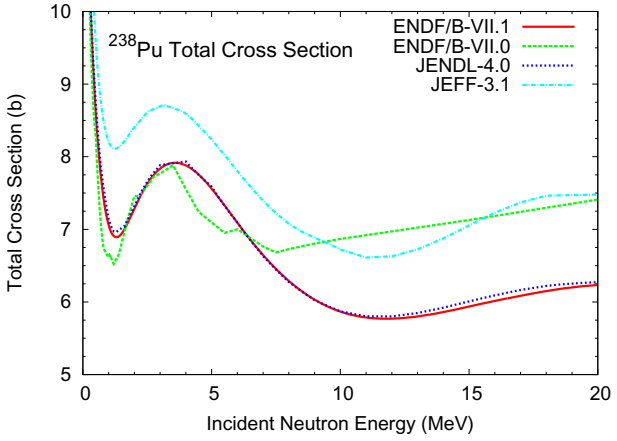

FIG. 62: Total cross section for the neutron-induced reaction on ^{238}Pu.

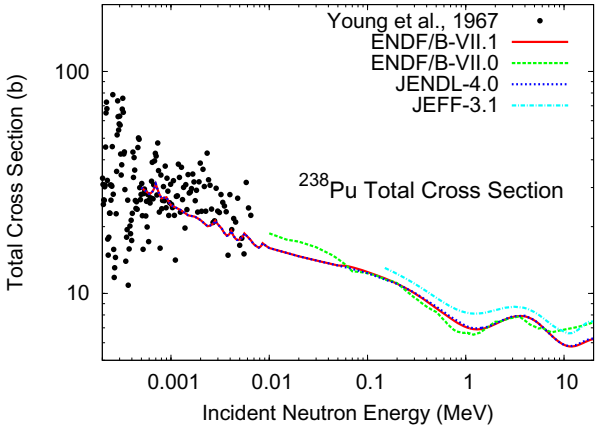

FIG. 63: Same as in Fig. 62 but for incident neutron energies extending down to 1 keV, and compared to experimental data by Young *et al.* [178]. Good agreement with JENDL-4.0 is observed.

The total inelastic cross section is simply the sum of all discrete inelastic cross sections, including the continuum. Our evaluation is compared to the other evaluations in Fig. 66. It is seen to differ significantly from ENDF/B-VII.0 and JEFF-3.1.1 but it is reasonably similar to JENDL-4.0. These differences are due to the inclusion of the pre-equilibrium neutron contribution in recent evaluations, which tend to increase the tail of the (n,n') cross section at the expense of the (n,2n) cross section.

The (n,xn) cross sections and energy-angle distributions result from our GNASH [174] calculations. The (n,2n) cross section is shown in Fig. 67. It is significantly lower than the previous ENDF/B-VI evaluation, as well as JEFF-3.1. Again, this large difference can be explained by the contribution of pre-equilibrium neutrons, neglected in older evaluations. The ENDF/B-VII.1 result is closer to JENDL-4.0, yet lower by a factor of 2 near 14 MeV. This channel strongly depends on level density parameters, whose associated uncertainties are too large to make reliable predictions without constraints from direct cross section measurements.

The (n,3n) cross section is illustrated in Fig. 68. Again, it is substantially lower than the ENDF/B-VII.0 and JEFF-3.1.1 evaluations but is very close to the JENDL-4.0 evaluation.

Discrete Inelastic Level Cross Sections

As mentioned above, optical model coupled-channel calculations were performed using the ECIS96 code [87] and the optical potential derived by Soukhovitskii [173].

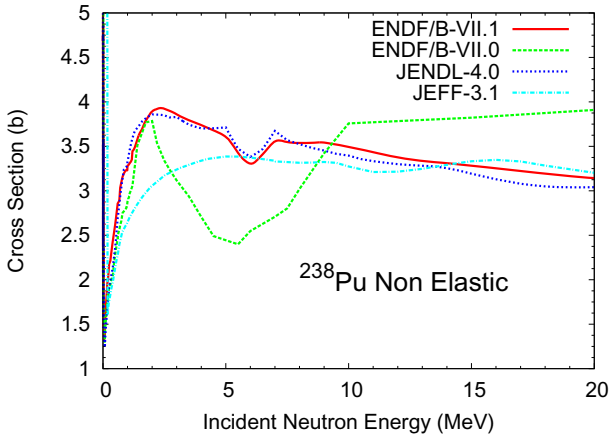

FIG. 64: Non-elastic cross section for n+^{238}Pu. Both ENDF/B-VII.1 and JENDL-4.0 evaluations show a pronounced dip near 5 MeV, due in part to a minimum in the fission cross section.

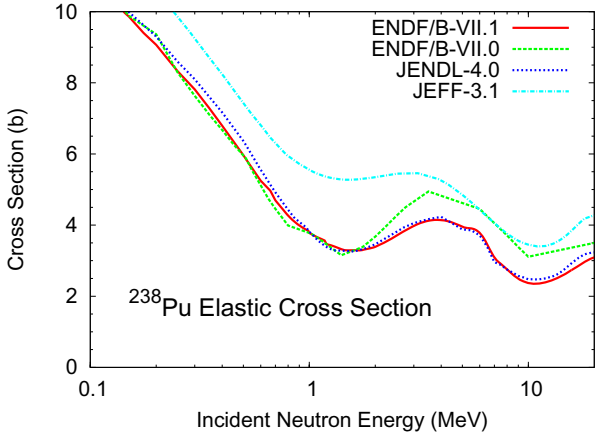

FIG. 65: Elastic cross section for n+^{238}Pu.

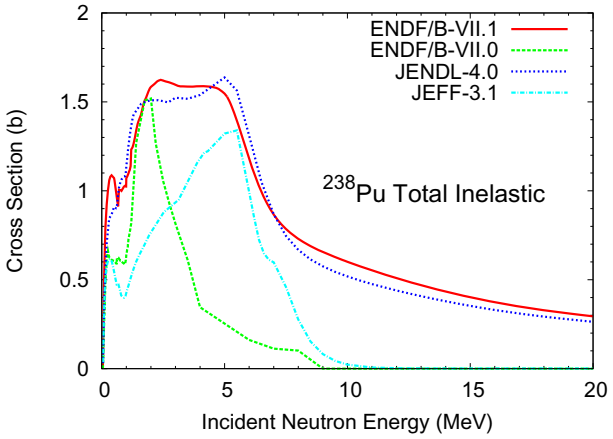

FIG. 66: Total inelastic cross section for n+^{238}Pu. The ENDF/B-VII.0 and JEFF-3.1 results drop quickly to zero as they neglect the contribution from pre-equilibrium and direct neutrons, which extend the tail of the total inelastic cross section at the expense of the (n,2n) cross section.

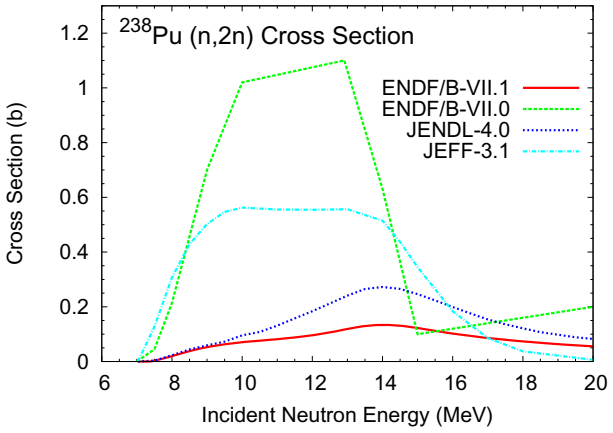

FIG. 67: The calculated ^{238}Pu(n,2n) cross section is compared to other major evaluations. No experimental data exist for this reaction.

The ground-state and four lowest excited states that are part of the ground-state rotational band were coupled. Overall, twenty-one states were included in the optical model calculations. The deformation parameters were taken from Soukhovitskii for ^{240}Pu: β_2=0.208, β_4=0.074 and β_6=-0.0071. Those values are close to those reported by Möller *et al.* [179], and similar for both ^{238}Pu and ^{240}Pu. The cross section for the first excited state is compared to other evaluations in Fig. 69.

The compound nucleus cross sections for the first 15 discrete inelastic states were taken from the coupled-channel calculations. Above those, collective 2^+ and 3^- states were assumed and were taken from ^{238}U (n,n') reactions from the ENDF/B-VII.0 evaluation. Those data, in turn, are based on DWBA/vibrational model calculations performed with the ECIS code, assuming a set of 2^+ or 3^- vibrational states. Deformation parameters were determined by matching the 14-MeV Baba measurements [180] of neutron emission spectra at various angles. The calculations were used to extrapolate the 14-MeV cross sections to lower and higher energies, and to obtain the angular distributions for each assumed state. The spins, parities, and deformation parameters used in the calculations are the same as used in our ^{240}Pu evaluation (see below and Ref. [181]). These results affect the evaluation in the excitation energy range E_x=1.17-3.91 MeV. Characteristics of those assumed vibrational states are shown in Table XXIII.

The inelastic continuum neutron cross section is based on the GNASH Hauser-Feshbach statistical/pre-equilibrium calculations, described above. The evaluated cross section is shown in Fig. 70 with the other evaluations. Note that the continuum threshold lies at 1.17 MeV, so discrete states with excitation energies above

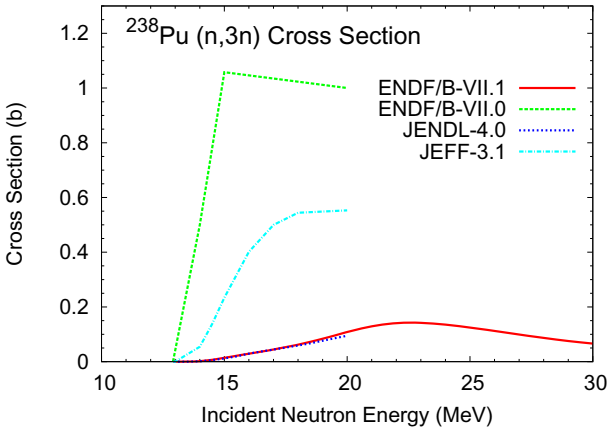

FIG. 68: The calculated ^{238}Pu(n,3n) cross section, which extends up to 30 MeV, is compared to other major evaluations.

TABLE XXIII: Characteristics of the ^{238}Pu 2^+ and 3^- inelastic vibrational states assumed above 1.17 MeV excitation energy.

Energy (MeV)	Spin	Parity	β
1.170	3.0	-1	3.8087E-02
1.250	2.0	+1	3.0175E-02
1.440	3.0	-1	5.6001E-02
1.590	3.0	-1	3.8111E-02
1.750	3.0	-1	3.9460E-02
1.850	3.0	-1	3.5265E-02
1.950	3.0	-1	4.0750E-02
2.150	3.0	-1	4.7400E-02
2.300	3.0	-1	5.3002E-02
2.390	2.0	+1	8.8154E-03
2.490	2.0	+1	2.5122E-02
2.940	2.0	+1	2.7150E-02
3.189	2.0	+1	2.5287E-02
3.388	2.0	+1	2.5070E-02
3.538	2.0	+1	1.5390E-02
3.637	2.0	+1	1.6125E-02
3.737	2.0	+1	1.6472E-02
3.837	2.0	+1	1.4293E-02
3.909	2.0	+1	1.5091E-02

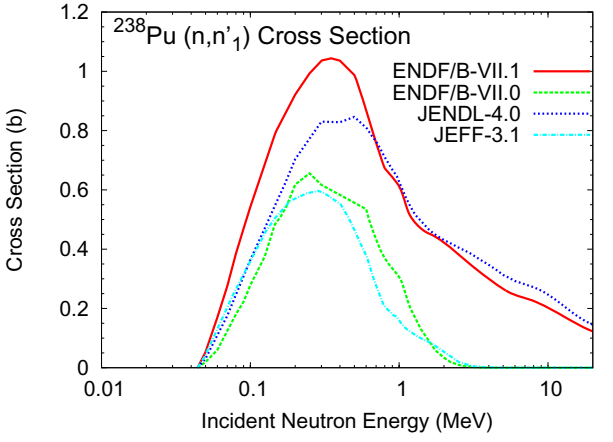

FIG. 69: The calculated ^{238}Pu cross section for the first excited state of the ground-state rotational band is compared to other major evaluations.

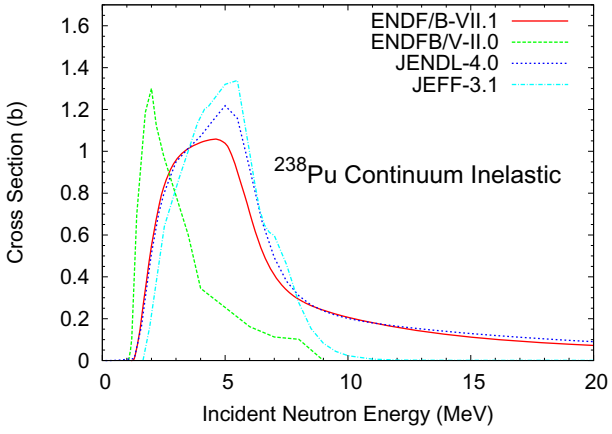

FIG. 70: The ^{238}Pu continuum inelastic cross section calculated from threshold to 20 MeV. The ENDF/B-VII.1 result actually extends up to 30 MeV.

1.17 MeV overlap the continuum region.

Neutron Elastic Scattering Angular Distributions
The elastic scattering angular distributions are based on the ECIS coupled-channel calculations for the ground-state rotational band, and the Soukhovitskii potential. The ground-state rotational band direct and compound nucleus angular distributions also were taken from the ECIS96 calculations. For higher excited levels, the compound nucleus angular distributions were obtained from ECIS96 calculations with the Sukovitskii optical model potential, as before. Finally, for the assumed collective 2^+ and 3^- states, the angular distributions were obtained from vibrational model calculations for the n+^{238}U reactions using the ECIS96 code [87], as described above.

Fission Cross Sections

At energies below 60 keV, the fission cross section is determined from the resonance parameters, which are taken from the JENDL-4.0 evaluation [177]. The values calculated from the resonance parameters agree well with the results of a GLUCS covariance analysis of the experimental data from 20 keV − 30 MeV, in the energy region where the data overlap.

From 60 keV − 30 MeV, the (n,f) cross section is based on a smooth curve through the GLUCS covariance analysis results. The covariance analysis results are influenced strongly by the extensive measurements of Silbert *et al.* [182], Budtz-Jørgensen *et al.* [183], Ermagambetov and Smirenkin [184], and others. The complete list of experimental data on fission cross sections used in this work is discussed in another paper of this issue.

The result of the GLUCS covariance analysis of experimental data sets is shown in Fig. 71 along with all (undifferentiated) experimental data points, and the ENDF/B-

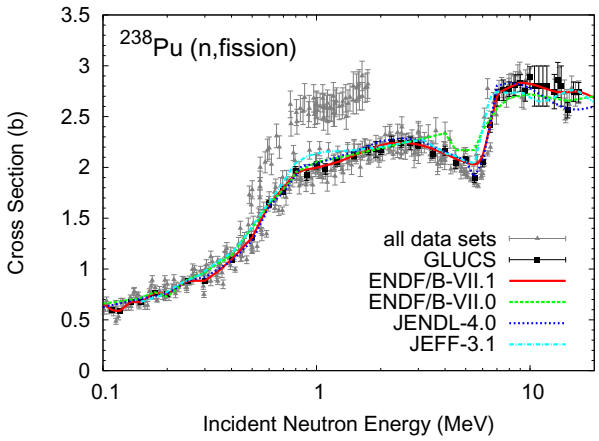

FIG. 71: The result of a GLUCS covariance analysis of all experimental data sets on the neutron-induced fission cross section for ^{238}Pu is shown (solid squares) along with the experimental data points. The ENDF/B-VII.1 evaluation (red solid curve) follows the GLUCS results, except at the dip near 5 MeV. Results from ENDF/B-VII.0, JENDL-4.0 and JEFF-3.1.1 are also shown for comparison.

VII.0, JEFF-3.1.1, and JENDL-4.0 evaluations. The ENDF/B-VII.1 evaluation follows exactly the GLUCS results except at the dip observed near 5 MeV, which is due to a few data sets pulling the least-square result down locally. We have smoothed-out the GLUCS result to obtain a smoother result for the elastic cross section (see Fig. 65). Nonetheless, a small dip still occurs in the nonelastic cross section (see Fig. 64).

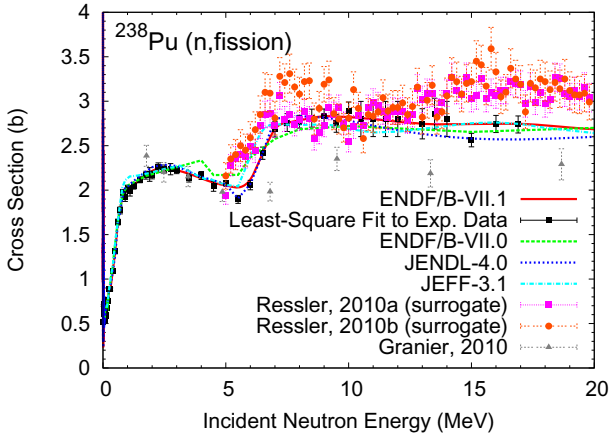

FIG. 72: The ^{238}Pu (n,fission) cross-section evaluations are compared to results from surrogate data by Ressler *et al.* [185] and recent preliminary data by Granier *et al.* [186].

Fig. 72 compares the evaluated fission cross-sections with experimental data obtained from LLNL surrogate measurements by Ressler *et al.* [185] and preliminary results from Granier *et al.* [186]. The surrogate data were obtained by studying the inelastic α-induced fission of ^{239}Pu, and are in relatively good agreement with the evaluations up to 10 MeV. At higher energies, the surrogate data lie higher than previous measurements and all evaluations. On the contrary, the new data by Granier *et al.* lie below all the evaluated results above 7 MeV incident neutron energy. Those data were not taken into account in the ENDF/B-VII.1 evaluation above 6 MeV.

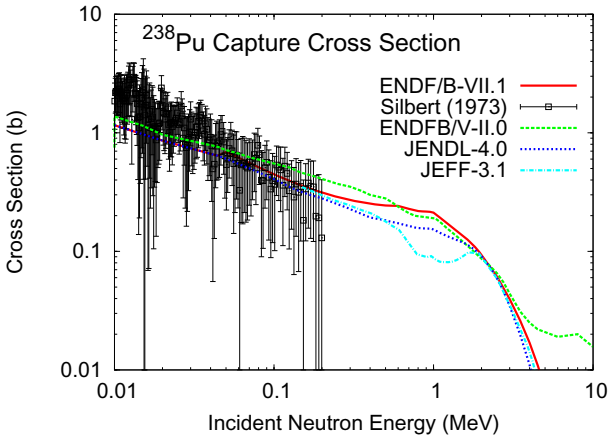

FIG. 73: The calculated radiative capture of n+^{238}Pu is compared to the experimental data of Silbert and Berreth [187], and with the ENDF/B-VII.0, JEFF-3.1, and JENDL-4.0 evaluations.

Neutron Radiative Capture Cross Section

Below 60 keV, the radiative capture cross section is based on the JENDL-4.0 resonance analysis. Above 60 keV, the COH code [60] was used, implementing the standard gamma-ray strength function formalism. The result is compared to the experimental data of Silbert and Berreth [187] in Fig. 73, together with the ENDF/B-VII.0, JEFF-3.1, and JENDL-4.0 evaluations.

Average PFNS and Multiplicity

The average prompt fission neutron spectrum (PFNS) and multiplicity (PFNM) were evaluated using Los Alamos (Madland-Nix) model calculations [188]. The systematics developed by Tudora and Vladuca for the model input parameters [189] were used as prior parameters in our analysis. Very little experimental data exist on the neutron multiplicity– only two values are reported in the EXFOR database at thermal energy, and none on the experimental spectrum, except for one value on the average neutron outgoing energy.

The spectrum was evaluated for 21 incident energies from thermal up to 20 MeV, on the same incident energy grid as for ^{239}Pu. This is to be compared with the ENDF/B-VII.0 file for ^{238}Pu, which contains only one spectrum, i.e., a Maxwellian at temperature 1.33 MeV, for all incident energies.

The calculated PFNS for thermal neutrons is shown in Fig. 74 as a ratio to a Maxwellian at temperature T=1.33

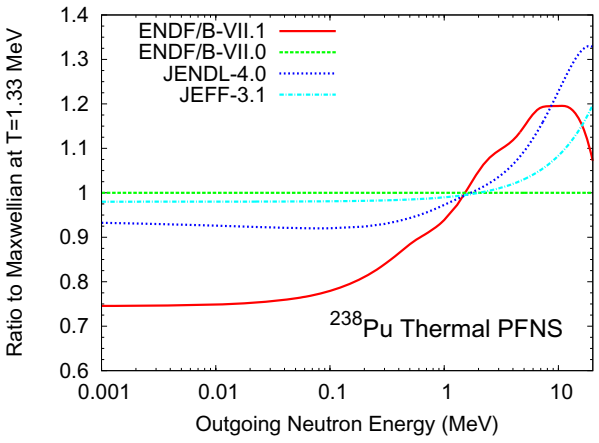

FIG. 74: The calculated prompt fission neutron spectrum of ^{238}Pu for thermal neutrons is plotted as a ratio to a Maxwellian at temperature T=1.33 MeV (= ENDF/B-VII.0). The results from ENDF/B-VII.0, JENDL-4.0, and JEFF-3.1 evaluations are shown for comparison.

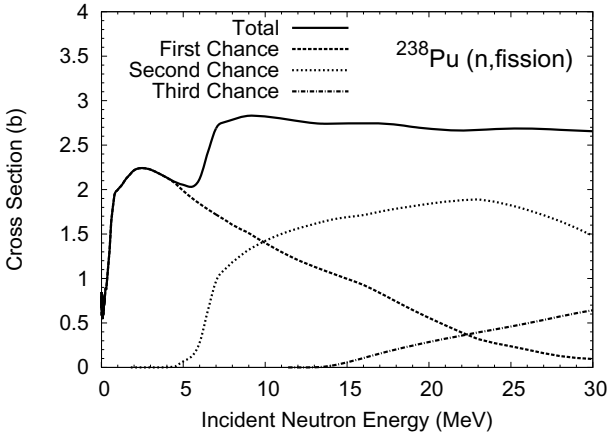

FIG. 75: The ENDF/B-VII.1 multi-chance fission probabilities for the n+^{238}Pu were calculated with the GNASH code.

MeV, together with ENDF/B-VII.0, JENDL-4.0 and JEFF-3.1 evaluations. Since ENDF/B-VII.0 is exactly described as a Maxwellian at T=1.33 MeV, it appears as a constant ratio of unity. Besides ENDF/B-VII.0, other evaluations rely on very similar models, based on the Madland-Nix model [188], to compute PFNS. Only changes in model parameters are to account for the observed differences. Since there is no experimental measurement of the n+^{238}Pu PFNS, it is difficult to state which one is closer to the truth than the others. In this specific case, the spread in the different evaluations can be used as an estimator of PFNS uncertainties.

At higher energies, multi-chance fission occurs, and has to be taken into account in the evaluation process. As the ENDF/B-VII.0 evaluation represent all PFNS from thermal to 20 MeV as a single Maxwellian at a given temperature, it is lacking the important multi-chance fission component. The ENDF/B-VII.1 evaluation corrects this defect by including multi-chance fission probabilities calculated with the GNASH code, as shown in Fig. 75. Note that while the multi-chance fission probabilities were in fact calculated in ENDF/B-VII.0, they were not used for evaluating the prompt fission neutron spectra at higher energies. Also, the ENDF/B-VII.0 multi-chance fission probabilities look dubious, as the first-chance fission probability flattens out past the neutron separation energy, as opposed to decreasing while the second-chance fission increases. The same observation can be made for higher-order fission probabilities.

The PFNS calculated for 20.0 MeV incident neutron energies is shown in Fig. 76, and compared with other evaluations. The ENDF/B-VII.1 result is in fair agreement with JENDL-4.0 and JEFF-3.1, and deviates significantly from the older ENDF/B-VII.0 evaluation.

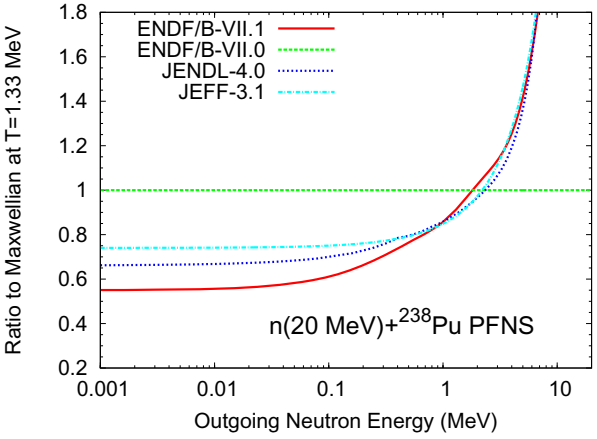

FIG. 76: Same as in Fig. 74 but for 20 MeV incident neutrons.

The average prompt fission neutron multiplicity was also evaluated using the Madland-Nix model. Experimental data on PFNM exist for thermal neutrons only: Jaffey and Lerner [190] and Kroshkin and Zamjatnin [191]. Our calculated result is shown in Fig. 77, in comparison with other evaluations. Again, since no experimental exist for this quantity beyond the thermal value, it is difficult to make a good case for one particular result. Additional work based on systematics over suites of isotopes is needed to better constrain those unmeasured quantities. However, since our evaluation uses the model parameter systematics established by Tudora [189], which encompasses many actinides, the ENDF/B-VII.1 result should be reasonable.

10. ^{239}Pu

At present we are not making substantive changes for the ^{239}Pu evaluation, other than reverting to ENDF/B-VI.8 delayed neutron parameters for the reasons discussed in Sec. VI G, and adding covariances. The previ-

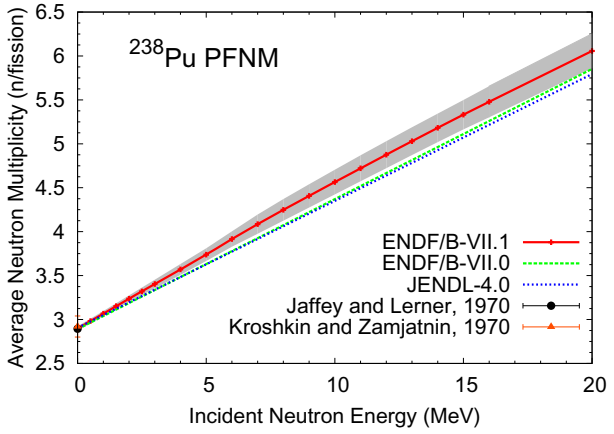

FIG. 77: The average prompt fission neutron multiplicity for n+^{238}Pu was calculated using the Madland-Nix model, and model parameters were slightly adjusted to reproduce the experimental thermal point. Uncertainties were also estimated assuming some prior uncertainties for the model parameters.

ous prompt fission neutron spectrum from Madland has been carried over to ENDF/B-VII.1 but with a finer outgoing neutron energy representation. Ongoing work on ^{239}Pu that will be made available in future ENDF releases is summarized in Sec. XI. This includes ongoing work on the prompt fission neutron spectrum, and on neutron inelastic scattering. Covariance uncertainty data were assessed by LANL and ORNL for the fast and resonance regions and included in the VII.1 evaluations, as described in companion papers by Talou *et al.* and Leal *et al.* in this edition.

11. ^{240}Pu

The evaluation of neutron-induced reactions on ^{240}Pu follows the exact same methodology used for ^{238}Pu. The ECIS, COH, GNASH, COMNUC, GLUCS, PFNS codes were also used here.

Coupled-channel calculations were performed with the ECIS96 code [87] using a slightly modified version of the Soukhovitskii potential [173]. It was used to compute all discrete elastic and inelastic cross sections and angular distributions, as well as the neutron transmission coefficients used in the statistical Hauser-Feshbach calculations. The modification applied to the original Soukhovitskii potential, which consisted in decreasing the λ parameter in the imaginary surface derivative potential W_d from 0.01759 to 0.010, led to a better agreement with experimental data near 10 MeV.

The JENDL Actinoid evaluation [177] was also used to complement the present work in various places.

Total, Elastic, Non-Elastic and (n, xn) Reaction Cross-Sections

Between 0 and 40 keV incident neutron energies, the total cross section was obtained from the JENDL Actinoid evaluation [177], but it was renormalized slightly to match the covariance analysis of experimental data above 40 keV. The shape of the cross sections below 40 keV follows the Sukovitskii optical model calculation closely.

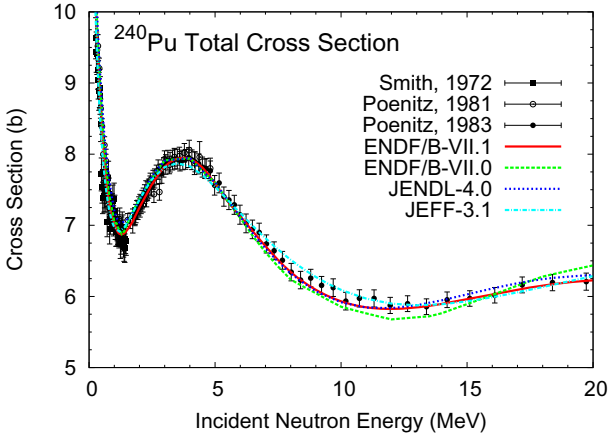

FIG. 78: Total cross section for the neutron-induced reaction on Pu-240. Experimental data are from Smith *et al.* [194], and Poenitz *et al.* [192, 193].

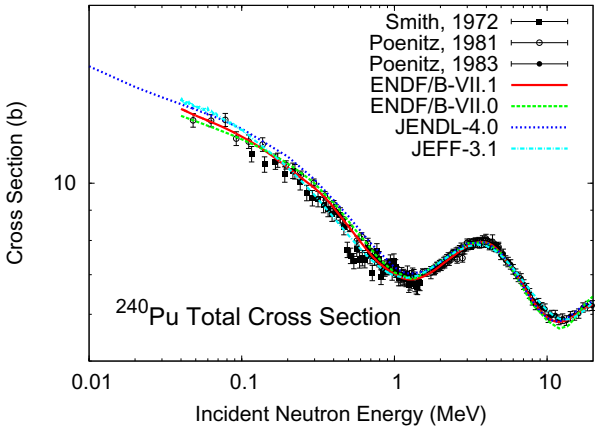

FIG. 79: Same as in Fig. 78 but in log-scale.

The evaluation of the neutron total cross section in the MeV region resulted from a covariance analysis with the GLUCS code [176] of the experimental data. Experimental data used were those of Poenitz, Whalen and Smith [192], Poenitz and Whalen [193], and Smith, Whalen and Lambropoulos [194]. We used the optical model results from our modified version of the Sukovitskii potential [173] as the prior in the GLUCS analysis, and the analysis results are very close to the optical model values at all energies. The evaluated total cross section is a smooth curve through the covariance analysis results, and above 8 MeV is identical to the optical model calculation.

See Figs. 78,79

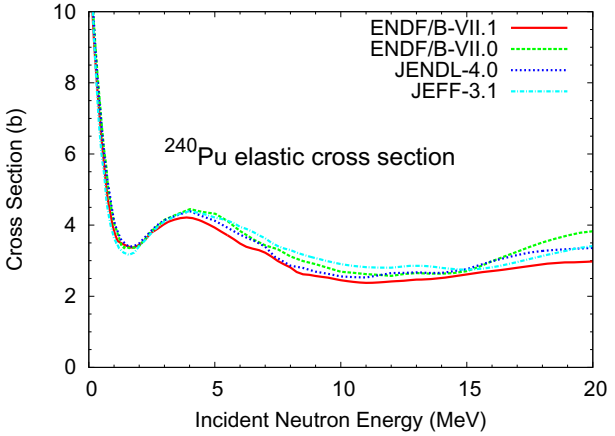

FIG. 80: The ^{240}Pu elastic cross section is compared to other evaluations.

The elastic cross section was obtained by subtracting the non-elastic cross section from the total cross section. It is consistent with the modified Soukhovitskii optical results. The non-elastic cross section is the sum of the total inelastic (n,n'), (n,2n), (n,3n), (n,4n), (n,f) and (n,γ) cross sections. The elastic cross section is shown in Fig. 80

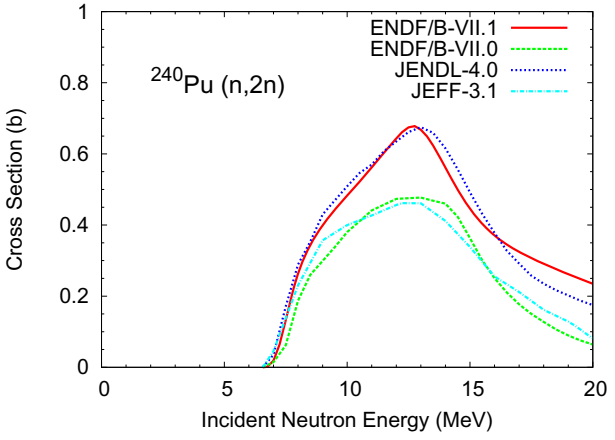

FIG. 81: The ENDF/B-VII.1 ^{240}Pu (n,2n) cross section is compared to other evaluations.

The (n,xn) cross sections (and energy-angle distributions) were obtained from our GNASH calculations. The (n,2n) cross section is shown in Fig. 81 in comparison with other evaluations. The ENDF/B-VII.1 result is somewhat higher near 14 MeV than the earlier ENDF/B-VII.0, JEFF-3.1, and JENDL-3.3 evaluations but is lower than the JENDL-4.0 evaluation [177]. Overall, however, the ENDF/B-VII.1 (n,2n) cross section is reasonably consistent with the JENDL-4.0 evaluation.

Discrete Inelastic Level Cross Sections

The ground-state rotational band direct and compound nucleus cross sections were taken from ECIS96 calculations with our modified version of the Soukhovitskii optical model potential. For higher excited states, the compound nucleus cross sections were taken from the ECIS96 coupled-channel calculations. Finally, as for ^{238}Pu, cross sections for the grouped collective 2^+ and 3^- states were assumed to be the same as for ^{238}U (n,n') reactions and were taken from the ENDF/B-VII.0 ^{238}U evaluation. Those data, in turn, are based on DWBA/vibrational model calculations performed with the ECIS code (see above for ^{238}Pu for more details).

The inelastic continuum neutron cross section is based on the GNASH Hauser-Feshbach statistical/pre-equilibrium calculations, as described above. The total inelastic cross section is shown in Fig. 82 in comparison to other evaluations.

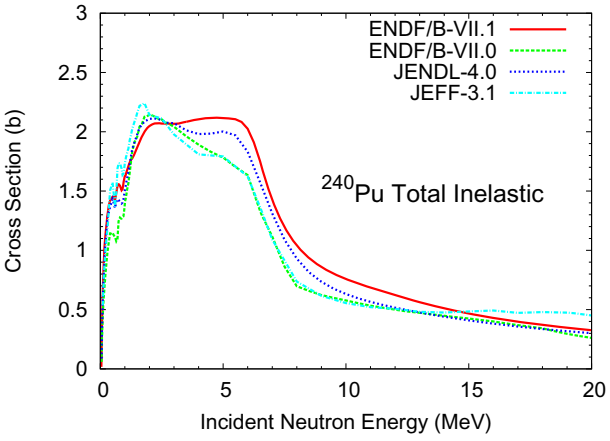

FIG. 82: The ENDF/B-VII.1 ^{240}Pu total inelastic cross section is compared to other evaluations.

Neutron Elastic Scattering Angular Distributions

Coupled-channels calculations were used to calculate the elastic scattering angular distributions for the ground-state rotational band, as well as the compound nucleus angular distributions for the higher excited states. For the assumed collective 2^+ and 3^- states, the angular distributions were obtained from vibrational model calculations for the n+^{238}U reactions, as described above.

Fission Cross Sections

From 0 to 550 keV, the fission cross section was taken from the JENDL Actinoid evaluation [177]. These data agree well with the results of a GLUCS covariance analysis of the experimental data from 60 keV to 30 MeV, where they overlap (see Figs. 83,84).

From 550 keV to 30 MeV, the neutron-induced fission cross section is based on a smooth curve through the GLUCS covariance analysis results. These results are influenced strongly by the extensive measurements of Sta-

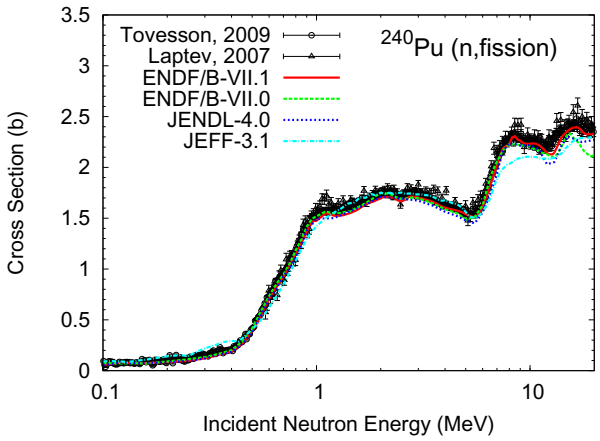

FIG. 83: The ENDF/B-VII.1 neutron-induced fission cross section of ^{240}Pu was obtained from a least-square analysis of the experimental data with the GLUCS code. It is shown here with the two most recent data sets by Tovesson *et al.* [195] and Laptev *et al.* [196], and other recent evaluations.

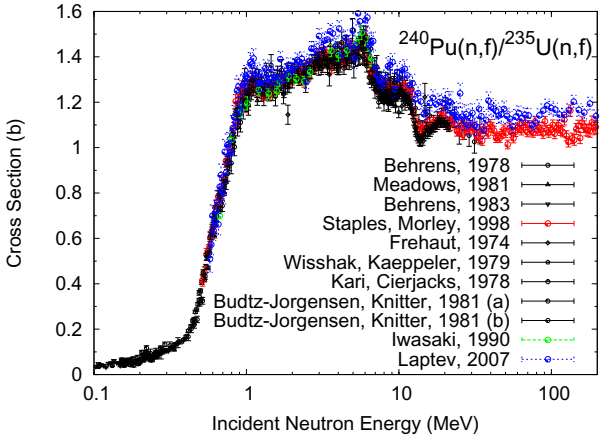

FIG. 84: Experimental data on the ratio of neutron-induced fission cross sections of ^{240}Pu to ^{235}U.

ples and Morley [197]. At some energies in this range, the present evaluation differs appreciably from the ENDF/B-VII.0, JEFF-3.1, JENDL-3.3, and JENDL Actinoid evaluations. The GNASH analysis closely follows the evaluation at most energies.

At higher energies, the multi-chance fission cross sections are obtained by scaling the GNASH calculations by the ratio of the new evaluated total fission cross section to the GNASH total fission cross section. The multi-chance fission cross sections are shown in Fig. 85.

Neutron Radiative Capture Cross Section

From 0 to 30 keV, the radiative capture cross section is taken from the JENDL Actinoid evaluation [177], which is consistent near 30 keV with our GLUCS covariance analysis between 20 and 300 keV. From 30 to 400 keV, our evaluation is based on a smooth curve through

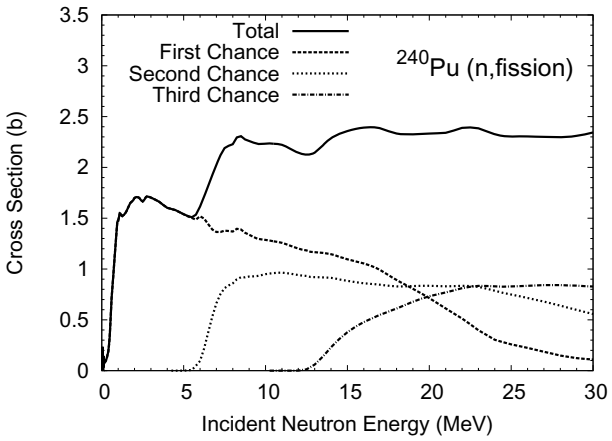

FIG. 85: Multi-chance fission components calculated for the total neutron-induced fission cross section of ^{240}Pu.

the result of our covariance analysis of the available experimental data. The 0.4 to 2 MeV energy range is treated as a smooth transition of the data below 0.4 MeV to the ENDF/B-VII.0 evaluation at 2.0 MeV. And from 2 to 30 MeV, the evaluation is taken from the ENDF/B-VII.0 evaluation to 20 MeV and smoothly extrapolated to 30 MeV.

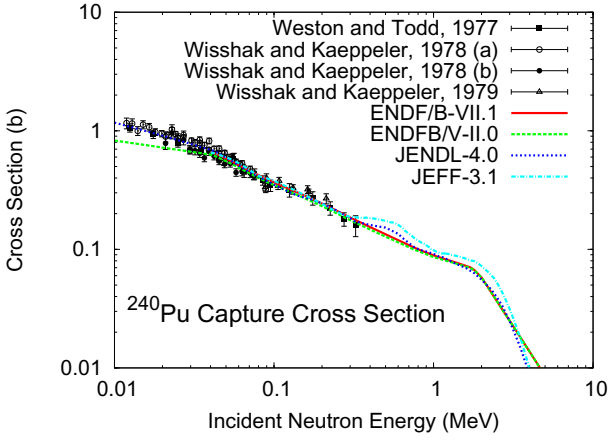

FIG. 86: Capture cross section for the neutron-induced reaction on ^{240}Pu. Experimental data are from Weston and Todd [198], and from Wisshak and Käppeler [199, 200].

Average PFNS and Multiplicity

The average prompt neutron multiplicity $\overline{\nu}$ as a function of incident neutron energy is evaluated from a covariance analysis of existing experimental data. The ENDF/B-VII.1 evaluation is shown in Figs. 87 and 88 compared with experimental data and other evaluations.

The Madland-Nix model [188] was used to evaluate the prompt fission neutron spectrum (PFNS) for incident neutron energies from thermal up to 20 MeV. As no direct experimental measurement of the n+^{240}Pu PFNS

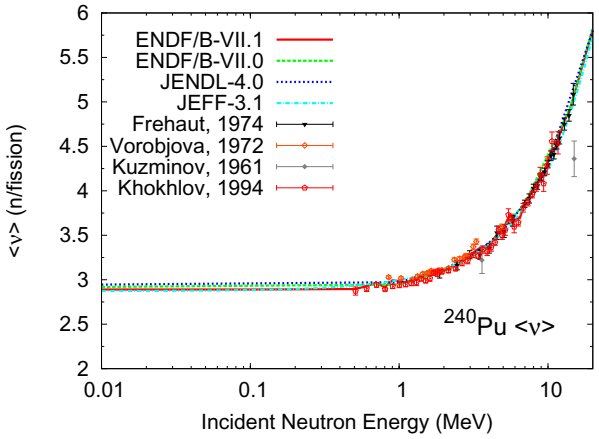

FIG. 87: The ENDF/B-VII.1 average prompt fission neutron multiplicity as a function of incident neutron energy was obtained from a covariance analysis of experimental data. It is compared to other evaluations as well as to experimental data sets from Fréhaut *et al.* [201], Vorob'jova *et al.* [202], Kuzminov [203], and Khokhlov *et al.* [204].

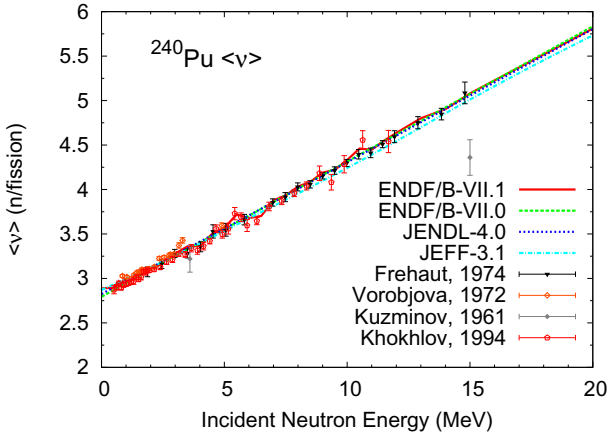

FIG. 88: Same as Fig. 87 but on a linear scale.

exist, only $\overline{\nu}(E_{inc})$ data were used to constrain the model parameters.

Table XXIV summarizes the values of the Madland-Nix model parameters used in this work. At high energies, i.e., above about 6 MeV, multi-chance fission probabilities calculated with GNASH (see Fig. 85) are used.

The PFNS obtained with those model parameters is shown in Fig. 89 as a ratio to a Maxwellian at temperature T=1.346 MeV, which is identical to the ENDF/B-VII.0 spectrum. All newer evaluations show similar trends, although the JENDL-4.0 is higher than ENDF/B-VII.1 and JEFF-3.1 in the low-outgoing energy range. The lack of experimental data makes it difficult to discuss the merits of each evaluation.

TABLE XXIV: Parameters used in the Madland-Nix model to compute the prompt fission neutron spectra for n+^{240}Pu. $\langle TKE\rangle$ stands for the average total kinetic energy, $\langle E_r\rangle$ is the average energy release, $\langle a\rangle$ the average level density parameter, $\langle B_n\rangle$ the average neutron binding energy, $\langle S_n\rangle$ the average neutron separation energy, and $\langle E_\gamma\rangle$ the average total γ-ray energy.

	First Chance	Second Chance	Third Chance
Parent nucleus	Pu-241	Pu-240	Pu-239
Light Fragment	Zr-101	Zr-100	Zr-100
$\langle TKE\rangle$ (MeV)	178.2	177.0	175.5
$\langle E_r\rangle$ (MeV)	198.0	197.5	197.0
$C = A/\langle a\rangle$	10.5	10.0	9.5
$\langle B_n\rangle$	5.241	6.534	5.646
$\langle S_n\rangle$	5.202	5.110	5.217
$\langle E_\gamma\rangle$	6.77	6.74	6.71

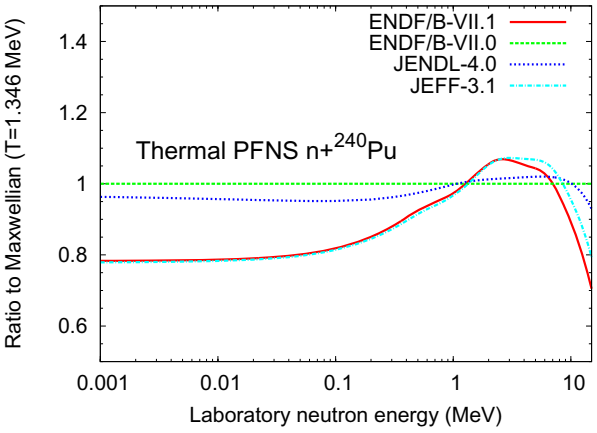

FIG. 89: Ratio of the average prompt fission neutron spectrum for thermal neutrons incident on ^{240}Pu to a Maxwellian at temperature T=1.346 MeV (= ENDF/B-VII.0).

12. ^{242}*Pu*

The MCNP5 analysis of Palmiotti and Hiruta [205] for the PROFIL1 and PROFIL2 irradiations at the CEA PHENIX fast reactor showed 12 % and 11.4 % discrepancies, respectively between measured and computed capture reaction rates for Pu-242 when the JENDL-4.0 data were adopted. Additionally in view of the fact that the ENDF/B-VII.0 evaluation was carried out in the 1970's, this warranted a new evaluation for the thermal, resonance, and URR regions, as well as the fast capture regions of ^{242}Pu. A detailed analysis and careful examination of measured and evaluated JENDL-4.0 capture cross sections in the thermal, resonance, URR and fast regions revealed that the major source of this discrepancy can be attributed to fast neutron capture in the energy region, 45 - 800 keV. This conclusion is supported by the integral capture measurement of Druzhinin *et al.* [206]. When the reported ^{242}Pu integral capture cross section for the fast spectrum, as specified in [206], is properly normalized to the ^{197}Au integral capture cross section,

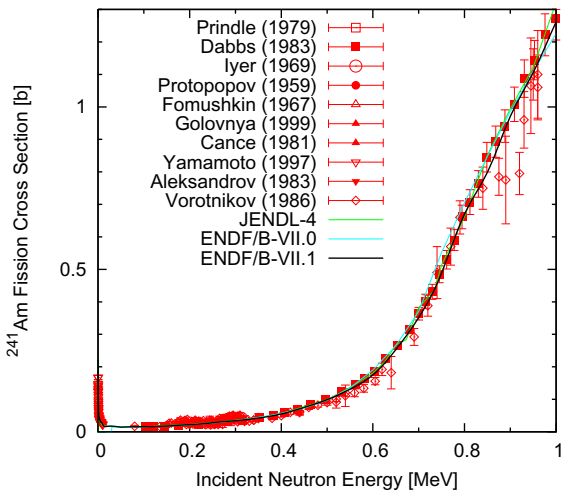

FIG. 90: Evaluated ^{241}Am(n, f) used for ENDF/B-VII.1, compared with ENDF/B-VII.0 and experimental data.

the result shows that the JENDL-4.0 capture cross section in the fast energy region has to be reduced by 20%. In addition, we note that, based on recent thermal capture cross section measurements of Marie *et al.* [207], as well as earlier pile neutron cross section measurements of Butler *et al.* [208], corrected for the presently evaluated capture resonance integral,I_γ=1123 b, a 2200 m/s capture cross section of 21.28 ± 0.77 b is derived.

13. ^{241}*Am*

Our ^{241}Am evaluation for ENDF/B-VII.1 builds on the ENDF/B-VII.0 work, and makes some modest changes for fission and capture. We performed a new SOK code statistical analysis of measured data to obtain a new evaluated fission cross section down to 150 eV. The subthreshold fission cross sections are now given in File 3. Our results are shown in Fig. 90 compared to experimental data. Integral americium fission rate calculations with MCNP are compared against fast critical assembly measurements in Fig. 93, and are seen to be comparable in quality to the previous evaluation compared to data [1].

We modified the ^{241}Am capture cross slightly for VII.1. The evaluation is compared with data in Fig. 91, including comparisons with the recent measurement from the DANCE detector at Los Alamos' LANSCE facility [209]. We have also not changed the split between capture to the ^{242}Am isomer and ground state in VII.1 compared to VII.0, so the g/tot ratio is unchanged. The evaluation is shown in Fig. 92, and is seen to agree well with the data, including the recently published Tommasi CEA measurement [210] (Profil data from the Phenix fast reactor) at 100 keV (g/tot=0.85). Note also that the LANL data that we presented in our VII.0 documentation were plotted at the wrong energy: it is a value of 0.815 at an average energy causing capture of about 500 keV as

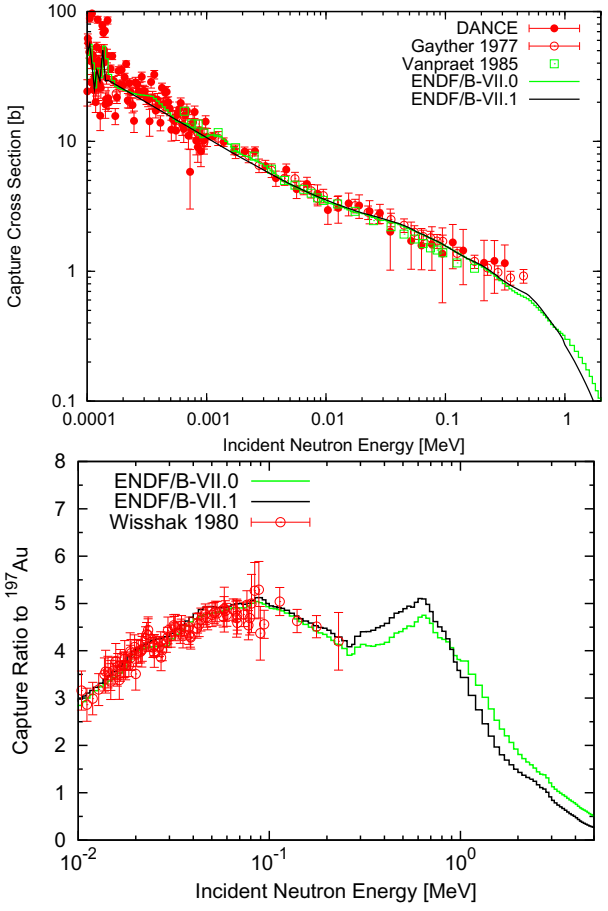

FIG. 91: Evaluated ^{241}Am(n, γ) used for ENDF/B-VII.1, compared with ENDF/B-VII.0 and experimental data.

shown in the figure here (and also a value of 0.867 at an average energy of 1 keV).

In the integral validation testing of our previous ENDF/B-VII.0 capture evaluation we showed that MCNP predictions of ^{241}Am capture creating ^{242}Cm agreed well with measurements in different locations in fast critical assemblies. Such reaction rate comparisons test both the evaluated capture cross section as well as the m/g branching ratio we adopted [1] (in addition, of course, to the fidelity with which we model the broad neutron spectrum at the irradiated sample's location). Figure 93 shows this comparison for VII.1, and again agreement is rather good.

In the resolved resonance region, the ENDF/B-VII.0 resonance parameters (same as ENDF/B-VI) were replaced by the JENDL-4 resonance parameters [9]. The energies of resolved resonances are almost identical to the values in ENDF/B-VI, but spins and widths show some differences. In the unresolved resonance range, we adopted an LSSF=1 option, which means the diluted cross sections are given in File 3, and the unresolved resonance parameters are used only for self-shielding calculations.

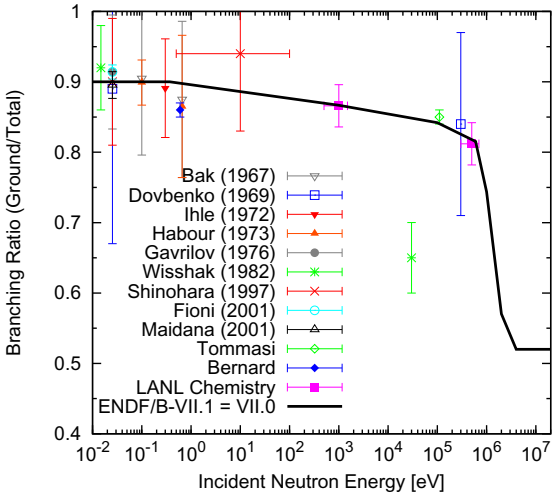

FIG. 92: Evaluated ratio for ^{241}Am neutron capture, g/(g+m)= g/tot in ^{242}Am.

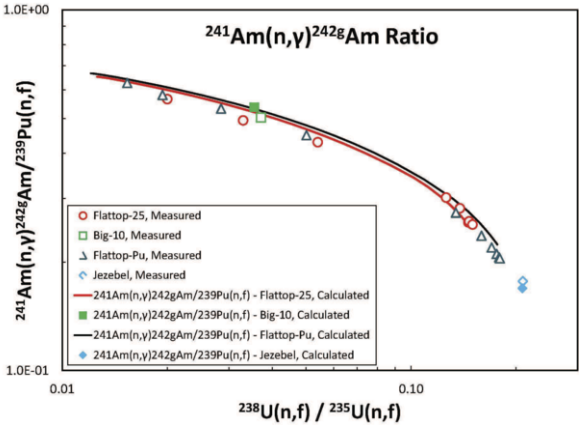

FIG. 93: The integral ^{241}Am neutron capture rate (divided by the ^{239}Pu fission rate) as a function of spectral index for different critical assembly locations. In this case the measurements, which detect the ^{242}Cm are divided by 0.827 to account for the fraction of ^{242g}Am that beta decays to ^{242}Cm.

A final word is warranted on the predictive success of model calculations for the $(n, 2n)$ reaction. We are not changing this cross section for ENDF/B-VII.1, but remind readers that we developed an evaluation of the ^{241}Am(n,2n) excitation function in 2006 where we relied on our GNASH model calculations for this reaction, having undertaken some calibration to measurements at the one energy that was measured reliably at the time, 14.1 MeV, where we had activation data from both Lougheed (LLNL) and Gancarz (LANL) [1, 211]. Following this calculational prediction of the whole excitation function, measurements were made by a collaboration of experimentalists from North Carolina (Tonchev *et al.* TUNL), LANL and LLNL [212], and these new data confirmed the GNASH predictions. Since then, additional measurements have been recently published by

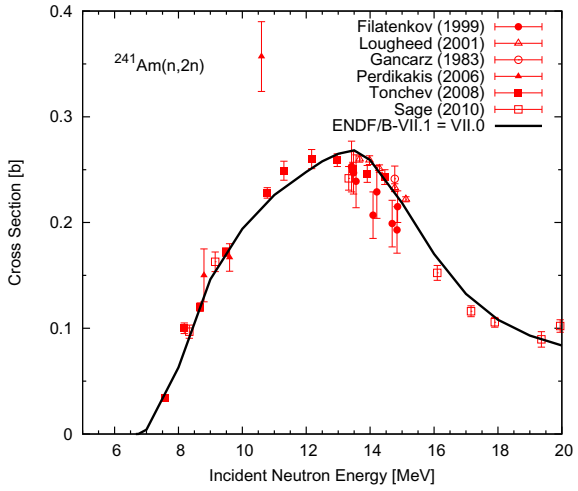

FIG. 94: Evaluated ^{241}Am$(n, 2n)$ in ENDF/B-VII.1 (unchanged from VII.0), compared with experimental data.

Sage, Plompen and collaborators [213] and these also validate the predictions (including both the rise of the excitation function, but also the "tail" in the 14-19 MeV region which is sensitive to preequilibrium neutron emission processes), see Fig. 94. Additional aspects of this work can be found in Ref. [214].

14. ^{243}*Am*

Motivated by the analysis of Palmiotti and Hiruta [205], where a 16.6 % discrepancy was observed between measured and computed capture reaction rates for ^{243}Am when the ENDF/B.VII.0 was adopted, a new evaluation for the thermal, resonance, and URR regions has been carried out for ENDF/B-VII.1. A detailed analysis and examination (by SM) of measured and evaluated capture cross sections in these regions revealed that the source of this discrepancy is traced to the 2200 m/s capture cross section, 74.8 b, adopted by Weston and Todd [215] in their capture cross section measurements. Based on recent thermal capture cross section measurements by Marie *et al.* [207], thermal reactor reactor cross section measurements by Ohta *et al.* [216], as well as an earlier pile neutron cross section measurements of Butler et al. [208] (corrected in the present evaluation for the capture resonance integral), an evaluated 2200 m/s capture cross section of 80.4 ±2.1 b is derived for ENDF/B.VII.1.

A least-squares fit to the renormalized capture data of [215] in the energy region 0.25 keV - 40 keV was then carried out to determine the s- and p-wave radiative widths for the URR region; the resulting values are 39.1 ± 0.6 meV and 68.8 ± 4.3 meV, respectively. The former value is in excellent agreement with the Atlas value 39 ± 1 meV obtained from the resolved resonances; we note that there are no previous determinations for the latter value. With these parameters, along with s- and p-wave neu-

tron strength functions 0.98 and 2.6, respectively, as well as an average s-wave average level spacing of 0.66 eV, the capture cross section in the URR region was generated. In the energy region from 30 keV to 40 keV, the present calculated capture cross section shows that it is 15.5 % larger than that of the ENDF/B.VII.0. This value is in good agreement with the VII.0 discrepancy found by Palmiotti and Hiruta [205].

On this basis, the model calculations of Talou *et al.* [211] for the capture cross section of ENDF/B.VII.0 above neutron energy corresponding to the first inelastic threshold, i.e. 43 keV, is normalized by the factor 1.155.

A comparison of the ENDF/B-VII.1 (solid red line) and ENDF/B-VII.0 (dotted red line) capture cross section evaluations and measurements is made in Fig. 95. The blue and green data points represent the normalized data of Weston and Todd [215], while the black data points correspond to the Wisshak and Kappeler [217] measurements in the energy region from 34 keV to 226 keV. We note that the latter data [217] were renormalized to the ^{197}Au capture cross section standard of ENDF/B-VII.1. Although the VII.1 evaluation is seen to lie above the Wisshak and Käppeler data, we think this is reasonable because: (1) we have been unable to obtain reasonable average capture resonance parameters from their data; and (2) Weston and Todd noted that the Wisshak and Kappeler data are low compared to their measurements, see their Fig. 4 and the discussion in Ref. [215].

The changes here for ENDF/B-VII.1 lead to a thermal capture cross section of 80.4b (previously 75.1b), and a capture resonance integral of 2050.7b (previously 1815.5b). They largely resolve the ^{243}Am capture reaction rate discrepancy previously obtained by Palmiotti using ENDF/B-VII.0, as shown in Kahler's paper [8].

We have also revised the $(n, 2n)$ reaction, based on arguments given by Maslov [161] on the similar spin structure of residual nuclei in $(n, 2n)$ reactions on ^{243}Am and ^{237}Np. This led to a decrease in the isomer cross section by about a factor of 3, and a corresponding decrease in the total $(n, 2n)$ cross section. The excitation function to the ground state is unchanged (and it agrees with the 1983 Los Alamos measurement by Gancarz, 153 mb ($\pm$5%) at 14.77 MeV as reported in Ref. [211]). See Fig. 96.

LANL has critical assembly measurements of ^{243}Am(n,γ) in the Flattop-25 critical assembly (Efurd, 1986) [162]. These measurements are shown in Fig. 97 in ratio to the measured ^{241}Am(n,γ)^{242g}Am cross section at the same locations, and since ^{241}Am(n,γ) is well understood to about 5% or better (see Fig. 92) these ratio data provide a valuable test of the ^{243}Am capture cross section. Profil data are also shown in the figure. It is evident that the calculated reaction rate agrees rather well with the data (although the data have very large uncertainties), providing some support for Mughabghab's increase in the capture cross section for VII.1

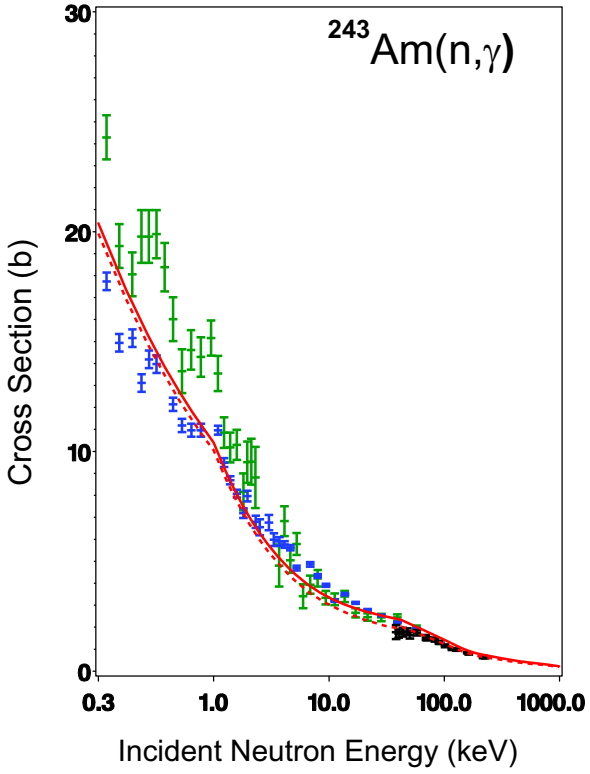

FIG. 95: Comparison of the ENDF/B-VII.1 capture data for ^{243}Am with the experimental data of Weston and Todd [215](green and blue data points) and Wisshak and Kappeler [217] data in the energy region 34-226 keV (black data points).

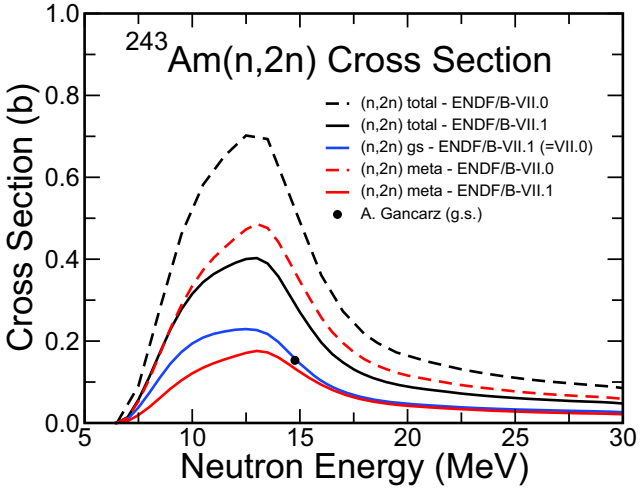

FIG. 96: Comparison of the ENDF/B-VII.1 $(n, 2n)$ cross section on ^{243}Am with ENDF/B-VII.0 and with the experimental data of Gancarz (LANL) for the ground state. The evaluated cross section to the ground state is unchanged but the isomer cross section is reduced, based in part on feedback from Maslov.

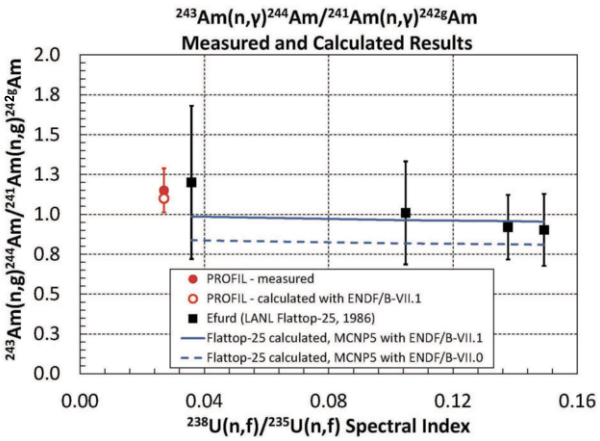

FIG. 97: Measured reaction rate ratios for ^{243}Am(n,γ)/^{241}Am(n,γ)^{242g}Am compared to LANL radiochemistry critical assembly data [162] and to PROFIL reactor data. The LANL measurements are in Flattop-25, located at 1,4, 6 and 11 cm from the center, where ratio values were measured to be 0.90, 0.92, 1.0, and 1.2 with uncertainties of about 25%.

15. Minor Actinides from JENDL-4.0

In 2008, the Japan Atomic Energy Agency released the JENDL Actinoid File 2008 (JENDL/AC-2008), a new library consisting of new and revised evaluations for both major and minor actinides [177, 218]. This library was amended and improved and forms the core of the JENDL-4.0 library [9, 10, 219, 220]. These evaluations are of good quality and are a valuable source for the minor actinides. D. Brown has reviewed these evaluations and made a series of recommendations for LLNL's internal Evaluated Nuclear Data Library and for the ENDF/B-VII.1 library [221] based on comparison of the evaluated cross sections and available experimental data. Many of these evaluations were adopted by the CSEWG committee, see Table III.

G. Delayed Neutrons from ENDF/B-VI.8

The 6-group delayed neutron data parameters for the actinides ^{233}U, ^{234}U, ^{235}U, ^{236}U, ^{237}U, ^{238}U, ^{237}Np, and ^{239}Pu are reverted back to those found in ENDF/B-VI, as discussed by Kiedrowski [222]. Significant differences, on the order of a factor of two to four, have been observed in the decay constants for the shorter-lived delayed precursor groups between ENDF/B-VII.0 and other published values (*e.g.*, Keepin, ENDF/B-VI).

To illustrate these differences, a test is run using MCNP5-1.60 on a centrally-located, pulsed 14.1 MeV neutron source in a subcritical version (sphere radius decreased by 10%) of the Godiva (heu-met-fast-001) benchmark. The time-resolved leakage current from the sphere, displayed in Fig. 98, is obtained, and a statistically significant difference in the shape of the delayed portion of the spectrum is observed between ENDF/B-VII.0 data and ENDF/B-VI. While this does not prove whether one is superior to the other, the difference is observable and is consistent with the difference in the data.

This confirms feedback that has been received from Dr. Yedvab on time-dependent problems where delayed neutrons are of a particular significance. Analysis shows that ENDF/B-VII.0 leads to a 15% difference from rod-drop experimental results and shows that the Keepin's data are most appropriate for their application (Ref. [223]). Further, C. Wemple at Studsvik Scandpower provides the following analysis for nuclear reactor applications:

"Comparing the delayed neutron data for ^{235}U from ENDF/B-VI.8 (same data for all VI releases), ENDF/B-VII.0, and JENDL-4.0, we see that there are some pretty dramatic differences in the groups 5 and 6 lifetimes and some less dramatic, but still significant, differences in the precursor yields. Our testing with both ENDF/B-VII.0 and the new JENDL-4.0 show similar problems — the Group 6 data negatively affect our rod-worth predictions to an alarming degree. The effects obtained using the JENDL-4.0 data were not as bad as the ENDF/B-VII.0, but still give unacceptable results because of the large change in the Group 6 precursor yields...Pending the outcome of such a review, the most likely course that will be adopted for applications of delayed neutron data is use of the ENDF/B-VI.8 data; this makes the reversion to the VI.8 lifetimes and precursor yield fractions in ENDF a bit more palatable as a temporary, palliative solution."

Unfortunately, the exact reasons for the differences are not entirely known and little published information exists. Based on unfavorable feedback noted earlier, there is evidence to suggest that the ENDF/B-VII.0 delayed data are not as reflective of physical reality as the earlier ENDF/B-VI.8 delayed data.

To verify the changes, the average decay constant of the shortest (sixth) delayed precursor λ_6 is calculated for Godiva (heu-met-fast-001) and Jezebel-240 (pu-met-fast-002) to cover a variety of actinides. For Godiva, the average decay constants calculated by MCNP5-1.60 for ENDF/B-VI and ENDF/B-VII.1 match exactly within four significant digits having a value of 2.858 s^{-1}; the ENDF/B-VII.0 data yields 8.678 s^{-1}. For Jezebel-240, the average decay constants calculated by MCNP5-1.60 for ENDF/B-VI and ENDF/B-VII.1 match exactly within three significant digits having a value of 2.79 s^{-1}; the ENDF/B-VII.0 data yields 6.48 s^{-1}. Further confirmation that the decay times are consistent is seen from the time-resolved leakage current in Fig. 98, where qualitatively the shape of the calculations with ENDF/B-VI and ENDF/B-VII.1 match, whereas ENDF/B-VII.0 is qualitatively different.

Table XXV (courtesy of C. Wemple) gives both precursor decay constants and yields from ENDF/B-VI (also ENDF/B-VII.1 because of reversion), ENDF/B-VII.0, and JENDL-4.0 (derived from Keepin's data) for ^{235}U.

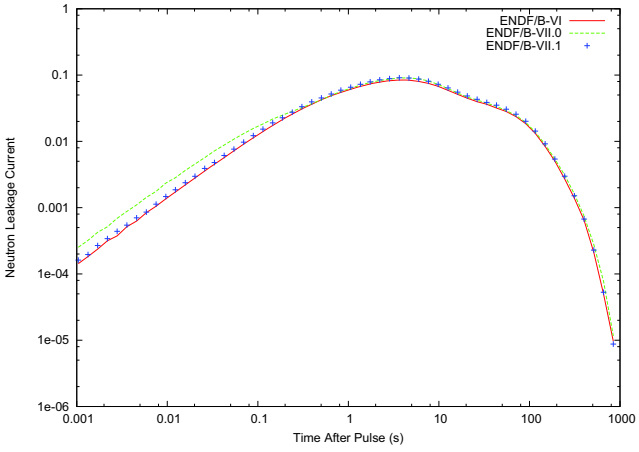

FIG. 98: Time resolved leakage delayed neutron current for Godiva, calculated with MCNP, compared with measured data.

Comparisons on this table are made with respect to ENDF/B-VI or ENDF/B-VII.1. Generally speaking, there is better agreement between ENDF/B-VII.1 and JENDL-4.0 for the decay constants, whereas the precursor yields are more indeterminate; most notable are the fifth and sixth precursor yields that merit further investigation. Testing on the Godiva critical benchmark shows that the average emission energy of all three data sets to be in good agreement.

While a detailed analysis on delayed neutron precursors should be performed, present resources are such that the most favorable short-term solution is to revert to the ENDF/B-VI 6-group delayed data since they appear to better agree with other published values and are more widely accepted as matching experiment. Other recommendations have been made for reversion to Keepin's data, as they seem to most agree with experiment for their applications. More analysis will need to be performed to decide if this set is more appropriate in the future.

H. Components of Energy Release Due to Fission (MT=458)

One of the most important basic parameters required for nuclear reactor design and safety analysis is the amount of energy released in a fission event. Knowledge of this quantity and its distribution among the various components resulting from a fission event is required for the determination of the power level of a reactor during normal operation and the decay heat generation during transients [224].

The working definitions for the components of energy release due to fission are based on the work of Sher and Beck done during the late 1970s and early 1980s. This work was sponsored by EPRI (Electric Power Research Institute) and directed primarily towards light-water thermal reactor calculations. Definitions for each component are generally based on Sher and Beck 1981 [224], as adopted by the ENDF102, ENDF-5 and later format specifications.

The ENDF102 format manual defines nine components of fission energy released. The kinetic energy (KE) of the fission fragment post prompt neutron emission ($E_{\rm FR}$), the KE of the prompt fission neutrons ($E_{\rm NP}$), the KE of the delayed fission neutrons ($E_{\rm ND}$), the total energy (TE) released by prompt gamma ray emission ($E_{\rm GP}$), the TE released by delayed gamma ray emission ($E_{\rm GD}$), the TE released by delayed beta emission ($E_{\rm B}$), the TE released by neutrino emission ($E_{\rm NU}$), the sum of these components ($E_{\rm T}$) and the sum excluding neutrino emission ($E_{\rm R}$). The incident energy of the neutron causing fission is generally written as E_n. By ENDF102 definition, the $E_{\rm R}$ value is the pseudo-Q-value to be used for the File 3 fission reaction sections. Sher and Beck also defined the total energy released by delayed emission ($E_{\rm D}$) and the total prompt energy release per fission ($E_{\rm P}$). The quantity $E_{\rm D}$ is defined as $E_{\rm B}+E_{\rm GD}+E_{\rm NU}$ but does not include $E_{\rm ND}$. In keeping with recent usage [1, 225], $E_{\rm P}$ is defined herein to be $E_{\rm FR}+E_{\rm NP}+E_{\rm GP}$ whereas $E_{\rm FR}+E_{\rm NP}+E_{\rm GP}-E_n$, the original definition [224], is better defined as the prompt Q-value.

Sher and Beck used experimental data to evaluate these quantities for the isotopes ^{232}Th, ^{233,235,238}U, and ^{239,241}Pu. Beck also used systematics to estimate the values for ^{230}Th, ^{233}Pa, ^{234,236}U, ^{237}Np, ^{237,238,240,242,244}Pu, ^{241,242m,243}Am, and ^{241,242,243,244,248}Cm. Updates through 1983 were included in the final ENDF/B-V.2 library and subsequently carried over to later ENDF/B libraries (see Table XXVI). These data form the basis for all of the fission energy release data in ENDF/B except ^{235,238}U and ^{239}Pu in ENDF/B-VII.0 [1] and ENDF/B-VII.1, and the minor actinide updates for ENDF/B-VII.1 as described herein.

The work of Sher and Beck was focused on accurate values for thermal (or threshold for fissile actinides) incident neutron energy. While the ENDF102 manual attributes the energy dependence assumed for these values to their work, no mention of the energy dependence is given in Ref. [224]. The source of the energy dependence described for these components in ENDF102 manual is currently a mystery. Starting with the ENDF-5 format, energy dependence for all of the fission energy release components has been recommended as shown by the linear fits in Eqs. (5)-(11). The energy dependence of $E_{\rm R}$ and $E_{\rm T}$ can be constructed using the appropriate summations. The value $E_{\rm ND}$ should be dependent on incident energy with $\overline{\nu}_{\rm D}(E_n)$ but is assumed to be constant and equal to $\overline{\nu}_{\rm D}$(thermal) $\times$ $\overline{E}_{\rm D}$.

ENDF102 defines the incident energy dependence of the components of the fission energy release for those data

TABLE XXV: Delayed neutron emission decay constants λ_i's (top) and precursor yields (bottom) for ^{235}U. ENDF/B-VII.1 has reverted to using the ENDF/B-VI.8 delayed neutron data.

Group	1	2	3	4	5	6
ENDF/B-VI.8	1.3336E-02	3.2379E-02	1.2078E-01	3.0278E-01	8.4949E-01	2.8530E+00
ENDF/B-VII.0	1.2491E-02	3.1824E-02	1.0938E-01	3.1699E-01	1.3540E+00	8.6364E+00
% diff from VI.8	-6.34%	-1.71%	-9.44%	4.69%	59.39%	202.71%
JENDL-4.0	1.2440E-02	3.0540E-02	1.1140E-01	3.0140E-01	1.1360E+00	3.0140E+00
% diff from VI.8	-6.72%	-5.68%	-7.77%	-0.46%	33.73%	5.64%
ENDF/B-VI.8	3.501E-02	1.807E-01	1.725E-01	3.868E-01	1.586E-01	6.643E-02
ENDF/B-VII.0	3.197E-02	1.664E-01	1.613E-01	4.596E-01	1.335E-01	4.720E-02
% diff from VI.8	-8.68%	-7.91%	-6.49%	18.82%	-15.83%	-28.95%
JENDL-4.0	3.300E-02	2.190E-01	1.960E-01	3.950E-01	1.150E-01	4.200E-02
% diff from VI.8	-5.74%	21.20%	13.62%	2.12%	-27.49%	-36.78%

TABLE XXVI: History of the fission energy release data in the previous ENDF/B libraries.

Nuclide	ENDF/B-V.0	ENDF/B-VI.8	ENDF/B-VII.0
^{230}Th	-	Sher1977[2]	Sher1977
^{232}Th	Sher1977	Sher1983[3]	Sher1983[a]
^{233}Pa	Sher1977	Sher1983	-
^{233}U	Sher1976[1]	Sher1983	Sher1983[a]
^{234}U	Sher1976	Sher1983	Sher1983
^{235}U	Sher1976[a]	Sher1983[a]	Madland[b]
^{236}U	Sher1976	Sher1983	Sher1983
^{238}U	Sher1976[a]	Sher1983	Madland[b]
^{240}U	-	-	[c]
^{237}Np	Sher1976	Sher1983	Sher1983
^{237}Pu	-	Sher1976	Sher1976
^{238}Pu	Sher1976	Sher1983	Sher1983
^{239}Pu	Sher1976	Sher1983[a]	Madland[b]
^{240}Pu	Sher1976[a]	Sher1983	Sher1983
^{241}Pu	Sher1976[a]	Sher1983[a]	Sher1983[a]
^{242}Pu	Sher1976	Sher1983	Sher1983
^{244}Pu	-	Sher1976	Sher1976
^{241}Am	Sher1976	Sher1983[a]	Sher1983[a]
^{242m}Am	Sher1976	Sher1976	-
^{243}Am	Sher1976	Sher1983	Sher1983
^{241}Cm	-	Sher1976	Sher1976
^{242}Cm	-	Sher1976	Sher1976
^{243}Cm	Sher1976	-	-
^{244}Cm	Sher1976	Sher1983	-
^{248}Cm	-	Sher1976	Sher1976

[1]R. Sher, S. Fiarman, and C. Beck, Private Communication to CSEWG (1976).
[2]R. Sher, S. Fiarman, and C. Beck, Private Communication to CSEWG (1977).
[3]R. Sher and C. Beck, Private Communication to CSEWG (1983).
[a]Best guess as evaluation fails to cite source.
[b]Includes Madland [225] $E_{\rm FR}(0)$ and $E_{\rm GP}(0)$ values.
[c]Data are replicate of ENDF/B-V.2 ^{238}U data.

given only at $E(0)$ as

$$E_{\rm FR}(E_n) = E_{\rm FR}(0) \ , \quad (5)$$

$$E_{\rm NP}(E_n) = E_{\rm NP}(0) + 1.307E_n - 8.07\times10^6[\overline{\nu}_{\rm P}(E_n) - \overline{\nu}_{\rm P}(0)] \ , \quad (6)$$

$$E_{\rm ND}(E_n) = E_{\rm ND}(0) \ , \quad (7)$$

$$E_{\rm GP}(E_n) = E_{\rm GP}(0) \ , \quad (8)$$

$$E_{\rm GD}(E_n) = E_{\rm GD}(0) - 0.075E_n \ , \quad (9)$$

$$E_{\rm B}(E_n) = E_{\rm B}(0) - 0.075E_n \ , \quad (10)$$

$$E_{\rm NU}(E_n) = E_{\rm NU}(0) - 0.1E_n \ . \quad (11)$$

Madland revisited the topic of prompt fission energy release focusing on the incident neutron energy dependence in 2006. He concluded that first or second order polynomials,

$$E_{\rm COMP}(E_n) = c_0 + c_1E_n + c_2E_n^2 \ , \quad (12)$$

were adequate to fit the energy dependence though concern was expressed for the validity of the fits at higher energies. Fits to the available experimental data for ^{235,238}U and ^{239}Pu for the components $E_{\rm FR}$, $E_{\rm NP}$ and $E_{\rm GP}$ were also provided [225]. Interested readers are referred to the original work for a description of the fitting process. No estimates or updates of the delayed components were undertaken by Madland. While the residuals from the fitting process are given, no estimate of the systematic uncertainties were provided. As the ENDF102 format did not allow for the polynomial energy dependent description at that time, ENDF/B-VII.0 was not able to

adopt these values in full. However, ENDF/B-VII.0 did adopt the thermal $E_{\rm FR}$ and $E_{\rm GP}$ values from Madland's work for ^{235,238}U and ^{239}Pu.

The relative changes from the previous Sher values were less than 0.13% for $E_{\rm FR}$ and 6%, -2%, and 15% for $E_{\rm GP}$ for ^{235,238}U and ^{239}Pu, respectively. Madland's estimates of $E_{\rm NP}$ were not adopted for ENDF/B-VII.0. The $E_{\rm NP}$ values were taken instead from the average of the evaluated thermal spectrum in the file in order to maintain self-consistency.

After the release of ENDF/B-VII.0, the ENDF102 ENDF-6 format was updated to allow for a polynomial dependence for the fission energy release [22]. For ENDF/B-VII.1, the full Madland fits for ^{235,238}U and ^{239}Pu for the components $E_{\rm FR}$, $E_{\rm NP}$ and $E_{\rm GP}$ have been adopted. A comparison of these values between ENDF/B-VII.0 and ENDF/B-VII.1 is shown in Table XXVII. While the differences for the total prompt energy release are small, there are significant differences for the partial components for energies above thermal.

The work of Madland was extended by Vogt to create evaluated data for all the actinides in ENDF/B-VII.1 [226, 227, 228]. The kinetic energy released to the fission fragments is calculated using a Coulomb approximation for the zero-energy point with a linear slope based on the atomic number and the average slopes based on Madland's uranium and plutonium values. The energy released by prompt and delayed neutron emission, $E_{\rm NP}$ and $E_{\rm ND}$, is fitted directly to the evaluated data (i.e. $\overline{\nu}_{\rm PR}\overline{E}_{\rm PR}$ as a function of incident energy) for self-consistency. The energy release for prompt gamma emission at thermal incident energy is computed directly from the evaluation, if available, and given a "generic" positive, linear slope based on the average of the data in the ENDL2008 [229] library. The general energy dependence given in ENDF102 for $E_{\rm GD}$, $E_{\rm B}$, and $E_{\rm NU}$ are kept unchanged with zero-point values based on averages suggested by Ref. [224]. The Vogt2010 data are adopted for 50 actinides as described below.

Table XXVIII summarizes the source of each fission energy release data set in the ENDF/B-VII.1 library. A number of minor actinide evaluations were adopted from JENDL-4.0 [219]. Where present, the fission energy release data from these files was kept. It is unfortunate, but five actinides were overlooked in this process and still do not have data.

The uncertainties for ^{235,238}U and ^{239}Pu have been compared to those found on the JEFF-3.1 evaluations. For ^{235,238}U, the values are identical to the ENDF/B-VII.0 values. For ^{239}Pu uncertainties for $E_{\rm FR}$ and $E_{\rm GP}$ ENDF/B-VII.1 adopts the JEFF-3.1 [11] uncertainties for $E_{\rm FR}$ and $E_{\rm GP}$ of 0.4 and 0.47 MeV, respectively, in place of the ENDF/B-VII.0 values of 0.1 and 0.22 MeV. The issue of uncertainties regarding these data needs to be revisited particularly in light of the inclusion of the energy dependence. The uncertainties assigned to zero-energy point values are based on well-known thermal measurements. It is believed that simple extrapolation to higher energies based on these uncertainties will fail to take into account greater uncertainty in the values at higher energies.

VII. NEUTRON CROSS SECTION STANDARDS

There were no changes made to the standards for the ENDF/B-VII.1 library since this library is not a new version, but instead is an update of ENDF/B-VII.0. Future updates will be made in future releases of the library.

The ENDF/B-VII.0 standards evaluation [7] was directly adopted from an extensive international cooperative effort by the CSEWG from the United States, the WPEC of the NEANSC, and the IAEA responding to a need for improved neutron standard cross sections. As a follow-on to that effort, an IAEA Data Development Project, "Maintenance of the Neutron Cross Section Standards" was recently initiated [230, 231] to provide a mechanism for allowing new experimental data and improvements in evaluation procedure to be used in future evaluations of the neutron standards. In the past very long periods sometimes occurred between evaluations of the standards. Through the use of this project, such long periods need not occur. This project will help to ensure that we are prepared for the next evaluations of the neutron cross section standards. Historically the standards evaluation activity has included high accuracy data other than the cross section standards, *e.g.*, the thermal constants and the ^{252}Cf spontaneous fission neutron spectrum. It was decided that this project should have a broader range of activities than just the cross section standards and thus encompass standards related activities.

So in addition to the standard cross section work, included are improvements in the gold cross section at energies below where it is considered a standard; work on certain cross sections which are not as well known as the cross section standards but could be very useful as reference cross sections relative to which certain types of cross section measurements can be made, such as prompt gamma-ray production cross sections for fast neutron-induced reactions; and updates on the ^{252}Cf spontaneous fission neutron spectrum and the ^{235}U thermal neutron fission spectrum.

Some of the results of this work are given below.

- **Traditional neutron cross section standards work**
  Since the completion of the recent cross section standards evaluation, many measurements related to the standards evaluation have been made or are underway. Work has been done related to the H(n,p), ^{3}He(n,p), ^{6}Li(n,t), ^{10}B(n,α), C(n,n), ^{197}Au(n,γ), ^{235}U(n,f), ^{238}U(n,γ), ^{238}U(n,f), and ^{239}Pu(n,f) cross sections. The standards database has been updated to include final results from these experiments. Many of the measurements are in fairly good agreement with the evaluations. There

TABLE XXVII: Energy release values in units of MeV for $E_{\rm FR}$, $E_{\rm NP}$, $E_{\rm GP}$ and $E_{\rm P}$ for ENDF/B-VII.0 versus ENDF/B-VII.1. The VII.0 values are taken from Madland [225] where they are referred to as "energy deposition".

Nuclide	Incident Energy E_n	$E_{\rm FR}(E_n)$ (Fission Fragments)		$E_{\rm NP}(E_n)$ (Prompt Neutrons)		$E_{\rm GP}(E_n)$ (Prompt Gammas)		$E_{\rm P}(E_n)$ (Total Prompt)	
		VII.0	VII.1	VII.0	VII.1	VII.0	VII.1	VII.0	VII.1
^{235}U	0.0253 eV	169.130	169.130	4.916	4.838	6.600	6.600	180.65	180.57
	1.0 MeV	169.130	168.864	5.455	5.138	6.600	6.678	181.19	180.68
	14.0 MeV	169.130	165.406	7.409	9.044	6.600	7.688	183.14	182.14
^{238}U	0.0253 eV	169.800	169.800	4.804	4.558	6.680	6.680	181.28	181.04
	1.0 MeV	169.800	169.481	5.536	4.865	6.680	6.804	182.02	181.15
	14.0 MeV	169.800	166.102	7.180	8.856	6.680	8.415	183.66	183.37
^{239}Pu	0.0253 eV	175.550	175.550	6.070	6.128	6.741	6.741	188.36	188.42
	1.0 MeV	175.550	175.093	6.278	6.471	6.741	6.856	188.57	188.42
	14.0 MeV	175.550	169.158	7.744	10.927	6.741	8.039	190.03	188.12

TABLE XXVIII: Summary of the fission energy release data in the ENDF/B-VII.1.

ENDF/B-VII.0:
^{232}Th, ^{233,234,236,240}U, ^{237}Np, ^{240,241}Pu, ^{241,243}Am
Madland2006:
^{235,238}U, ^{239}Pu
Vogt2010:
^{225,226,227}Ac, ^{228,230,231,233,234}Th ^{229,230,231,232,233}Pa, ^{230,231,237,239,241}U ^{234,235,236,239}Np, ^{236,237,238,243,244,246}Pu ^{240,242,242m,244,244m}Am, ^{240,241,247,249,250}Cm ^{245,246,247,248,249,250}Bk, ^{246,248,250,252,253,254}Cf
JENDL-4.0:
^{227,229}Th, ^{232}U, ^{238}Np, ^{242}Pu ^{242,243,244,245,246,248}Cm, ^{249,251}Cf, ^{254}Es, ^{255}Bk
Missing:
^{251,252,253,254m,255}Es

are still concerns with the H(n,p), ^{3}He(n,p) and the fission cross sections. Also a study of the uncertainties obtained in the international standards evaluation was done. This work was done as a result of concerns that had been expressed that the uncertainties obtained from that evaluation are too small. Extensive use of correlations was employed for that evaluation. The present investigation concluded that the uncertainties are reasonable [7]. Taking correlations into account suggests that uncertainties (variances) will be reasonable when calculated over a broad spectrum for a practical system.

Improved smoothing of the capture evaluations was obtained using a physical model calculation as a pseudo-experimental data set in the fitting program. The covariance matrix that was used had large correlation components for neighboring points to help smooth the cross section and nearly free shape normalization. The results maintain the inelastic scattering structure and minimize structure caused by statistical effects.

- **The gold capture cross section at energies below where it is considered a standard**

  Values were obtained below the standards energy region for the international standards evaluation of the gold capture cross section. These data were determined accurately but are not considered standards since there is significant structure at these lower energies. A standard should have a smooth energy dependence. The value near 25 keV from an astrophysics-Maxwellian evaluation is approximately 6% to 8% lower than the result from the standards evaluation. This astrophysics evaluation was based on the results of measurements by Ratynski and Kappeler [232] of the ^{197}Au(n,γ) cross section averaged over a Maxwellian-like experimentally simulated spectrum with temperature near 25 keV and measurements by Macklin [233, 234]. In an attempt to clarify this inconsistency, capture measurements have been performed at the n_TOF [235] and GELINA facilities [236, 237]. The results of these experiments are consistent with that obtained from the standards evaluation.

  Also another experiment [238] has recently been completed in which the ^{238}U(n,γ) cross section (in addition to the ^{235}U(n,γ) cross section) has been measured relative to the gold capture standard, see Subsection X D. Data were obtained at thermal, 426 keV and with a simulated-Maxwellian spectrum (kT about 25 keV). For this experiment neutron activation with subsequent accelerator mass spectrometry was used to determine the uranium capture events. This technique represents a novel approach independent of previous TOF measurements, because any interference with the fission channel is excluded. The results for the ^{238}U(n,γ) cross section are in agreement with the standards evaluation, using the values from the gold standards evaluation for the conversion from the cross section ratio. The ^{238}U(n,γ) cross section relative to gold capture can be used to improve both of those cross sections in the program used to evaluate the neutron cross section standards.

  Very recent results by Krasa *et al.* [239] obtained

for a simulated ∼25 keV Maxwellian spectrum averaged ^{197}Au(n,γ) cross section confirm values obtained by Ratynski and Kaeppeler, for measurements done under the same conditions as those used by Ratynski and Kaeppeler. But Krasa *et al.* also made measurements under experimental conditions that better simulate the ∼25 keV Maxwellian neutron spectrum. For those measurements, the averaged ^{197}Au(n,γ) cross section is in close agreement with the results obtained from the standards evaluation. The apparent inconsistency may be due to the different angular acceptances in the two measurements. These data are preliminary but a detailed publication on this work [240] is being prepared.

It is clear that more work needs to be done to understand the differences obtained in the various investigations concerning the gold capture cross section near 25 keV. In the framework of EUFRAT2010 complementary measurements and calculations are planned to further validate the simulated spectrum for kT=25 keV as well as the spectrum averaged cross sections of gold. The project aims also at the verification of systematic uncertainties by varying the parameters of the neutron production target and of the experimental setup.

- **Prompt gamma-ray production reference cross sections**
  The project is investigating possible reference cross sections relative to which gamma-ray production cross sections could be measured. This would simplify making measurements of such cross sections. Many cross sections are under consideration. There are several criteria, the most important are whether the cross section is large, smooth, well-known and can be used with small background corrections. The cross sections under initial consideration were those for the Fe(n,n'γ) 847-keV and Cr(n,n'γ) 1434-keV γ rays. However, natural abundance titanium with two gamma lines, 984 keV from the ^{48}Ti(n,2n) and 160 keV from the ^{47}Ti(n,n') reaction, appears to be the most appropriate candidate due to good physical properties, large cross section, small (n,p)-beta-decay feeding, and usually low presence in experimental apparatus. Accurate measurements of these cross sections are needed.

- **Reference fission spectra**
  The ^{252}Cf spontaneous fission neutron spectrum is used for fluence determinations. A concern is that the uncertainties for the latest evaluation are large for both the lowest and highest energy neutrons. A review of the existing experimental data indicates that a new evaluation is not justified. However, since some new experiments [241, 242] have been done measuring the ^{235}U thermal neutron fission spectrum relative to the ^{252}Cf spontaneous fission neutron spectrum, a combined evaluation of both spectra is underway using all appropriate experiments. This should provide reduced uncertainties for both spectra, however it is expected that the improvement will be greater for the ^{235}U thermal neutron fission spectrum. An IAEA Coordinated Research Project (CRP) was recently initiated to provide new evaluations of prompt fission neutron spectra (PFNS) of major actinides including covariance matrices. The work of this CRP will be utilized in the present studies of fission neutron spectra.

VIII. FISSION PRODUCT YIELD SUBLIBRARY

For ENDF/B-VII.1 a new fission product yield (FPY) evaluation for n+^{239}Pu was developed by Chadwick *et al.* [14, 15], updating the previous evaluation for ENDF/B-VI by England and Rider [243]. The evaluation was not changed for incident neutrons at thermal energies as we find that the original evaluation is reliable here; but significant changes were made for incident neutrons with energies corresponding to fission spectrum, and 14 MeV neutrons. The fission spectrum n + ^{239}Pu evaluation work is described in detail in a previous issue of *Nuclear Data Sheets* [15, 244], whilst the 14 MeV LANL experimental work is discussed in this issue by MacInnes *et al.* [245].

Below we summarize aspects of our recently-published [15] 0.5–2.0 MeV fission spectrum neutron work incorporated in VII.1. We also describe the basis for the 14-MeV FPY changes for VII.1 [245]. We have not had time yet to update the ^{235}U and ^{238}U FPY evaluations to account for the same energy-dependence issues as for plutonium.

A. Fission Spectrum n+^{239}Pu FPY

The work of Ref. [15] added additional fidelity to the FPY representations in the fast range (fission spectrum neutron energies) by providing new data at 2 MeV average-neutron incident energy as well as at the traditional 0.5 MeV, enabling users to determine FPY at other intermediate average neutron energies by linearly interpolating between the 0.5 and 2.0 MeV data. This level of detail cannot be ignored if one needs a high accuracy (1–2% accuracy, in some cases) FPY determinations in this energy range. Such FPY accuracy requirements exist in applications that use the measured fission products to determine the number of fissions that have occurred in a plutonium sample, for example, ^{147}Nd, a nuclide of central importance for the US National Laboratories.

Prior to this recent work, it was thought that the mass spectrometry measurements of Maeck *et al.* [246, 247], which are generally thought to be of high accuracy, were in contradiction to the Los Alamos LANL-ILRR (Interlaboratory Reaction Rate) radiochemical measurements for ^{147}Nd [244]. This presented a puzzle since for other

FPs these two independent measurements agree remarkably well, as noted in Refs. [15, 244]. The energy dependence proposed by Chadwick *et al.* [14, 15] removes this apparent contradiction, and shows that the A=147 trend identified is in line with general systematics for the energy dependence of all FPs, in which the valley and tail FPs increase with increasing neutron energy, and the peak FPs decrease with increasing neutron energy. For ^{147}Nd in particular, in the 0.2–2 MeV "fast" region Chadwick (ENDF/B-VII.1) [15] finds a plutonium FPY energy dependence of 4.6%-relative ± 1.0%-relative per-MeV, based on all the experimental data available, and a 3.7%-relative ± 1.1%-relative per-MeV for just the LANL radiochemical data. This compares favorably with Livermore's recent evaluation [248] of 3.2%-relative ± 1.2%-relative per-MeV, and Prussin *et al.* [249] analysis of just the isotope dilution mass spectrometry data of 4.0%-relative ± 1.2%-relative per-MeV (from an analysis of the Maeck and Lisman (^{147}Sm) data), and 2.4%-relative per-MeV from an interpolation of the A=146 and A=148 data. Lestone's paper in this edition of NDS [250] provides a physical basis for FPY energy dependencies. All these studies point to a small – few %-relative per MeV – positive energy dependence for the A=147 chain yield in the 0.2-2 MeV region. Although in Ref. [15] we noted that Lestone's model for A=147 was thought to give a smaller energy dependence FPY slope than the value we observed in the data, Lestone's new work [250] – using his same model – now suggests a slope of 3.5%-relative per MeV consistent with our ENDF/B-VII.1 results (the change was due to the realization that the model is based on a finite mass resolution of a few units, and an averaging is needed because the slope and the FPYs are both varying strongly in the A=147 region).

1. FPY at 0.5 MeV

We have continued the previous approach of England and Rider, used in ENDF/B-VI, of using the nominal neutron energy of 0.5 MeV to represent data in the fast region that have been "pooled"; that is, the 0.5 MeV evaluation really represents an average of many measured FPY data that have average incident energies that tend to range from about 0.2 to 2 MeV. The use of 0.5 MeV as the nominal energy to quote is a reasonable incident energy to identify this evaluation with because of the dominance of the Maeck *et al.* data in the evaluation (owing to the very small uncertainties that are often less than 1–2%-relative), which were measured in the Idaho EBR-II fast reactor at locations that corresponded to average neutron energies in the range 0.2–0.5 MeV.

For this evaluation, a new source of measured FPY data was incorporated into the ENDF/B-VII.1 work — the LANL-ILRR radiochemical measurements from the late 1970s, based on actinide samples placed in in Los Alamos' fast critical assemblies [244], which provide broad neutron sources with average energies ranging from about 0.2 to 2 MeV depending on the assembly and the location of the sample. Until recently these data were not widely available to evaluators, were not well documented in the open literature, and the measured radiochemical fission product data (K, Q, and R-factors) were not converted into the more widely used FPY form until the recent detailed publication of Selby *et al.* [244]. Although the new LANL-ILRR data generally agree extremely well with ENDF/B-VI and also with Maeck's data — to better than 1-2% for most FPs — a significant 4% discrepancy was noted with the previous ENDF/B-VI evaluation for ^{99}Mo. This is noteworthy because many laboratories, in addition to Los Alamos, have used ^{99}Mo as a reference FP to which other FP data are measured in ratio. Thus, changing the ^{99}Mo FPY can have the impact of changing other reported FPY that were determined in ratio to ^{99}Mo. As part of this work Chadwick *et al.* [15] undertook a *meta-analysis* that expanded the sparse data set of directly-measured ^{99}Mo FPY data to include inferred ^{99}Mo data from ratio experiments and this statistical analysis provided an independent confirmation on the accuracy of the LANL-ILRR ^{99}Mo FPY measurement. Our new ENDF/B-VII.1 0.5 MeV FPY evaluation incorporates this change for the FPs measured by LANL-ILRR, which amounts to an increase of 4% for ^{99}Mo, but changes of less than 1–2% for ^{95}Zr, ^{140}Ba, and ^{141,144}Ce.

Our work also noted that a number of previous evaluations for fission spectrum n+^{239}Pu FPY lie significantly below our new ENDF/B-VII.1 evaluation for FPs such as ^{99}Mo and ^{147}Nd: the ENDF/B-VI evaluation, but also Livermore's 1985 evaluation by Nethaway [16], and the JEFF and JENDL present evaluations, and we suggest that these other evaluations could be updated to account for our findings. Recent work at Livermore is in good agreement with our results [248]. Also, a group of scientists led by Prussin, of LBNL, has used an independent method that mainly focuses on the isotope dilution mass spectrometry measurements of Maeck and others, and has obtained results that are consistent with our findings [15, 249]. Our 0.5 MeV FPY results are given in Table XXIX.

2. FPY at 2.0 MeV

As noted earlier, we provide new ENDF/B-VII.1 data at 2.0 MeV average neutron incident energy to enable users to determine FPY at other energies between 0.5 and 2.0 MeV using linear interpolation. A linear dependence on average incident energy only approximates the true form (which will depend on the location of the FP; for example, FPs in the valley depend exponentially on the neutron energy), but is, we feel, a sufficiently accurate approximation for most applications in this limited neutron energy region.

Much emphasis was placed on the ^{147}Nd FPY energy dependence in Ref. [15], where various data sets (mass spectrometry, LANL-ILRR, *etc*) indicate a FPY that in-

creases by 3–5%-relative per MeV over this 0.5–2.0 MeV range. This FP has more data available than most owing to the comprehensive measurements made in Los Alamos' critical assemblies that range from incident energies in the 0.2 – 0.6 MeV region (Bigten, and the outer tamper regions of the Flattop assembly) up to 1.9 MeV at the center of Jezebel, a plutonium sphere.

Systematics were developed [15] for the energy dependence of other FPs. These were based on various sets of measurements in this neutron energy range: the Los Alamos LANL-ILRR radiochemical data (see the figures in the Appendix of Ref. [15]), the quasi-monoenergetic measurements by Gindler *et al.* [251]; and the energy dependence seen in mass spectrometry data between 0.2 and 1.3 MeV average neutron energies. Other data based on other nearby energy ranges (*e.g.* spontaneous ^{240}Pu fission versus thermal n+^{239}Pu fission), and other nearby fissioning systems (^{238}U) were also considered. Based on the ensemble of these data (which were in some cases in contradiction with one another, unfortunately) we developed a functional form that accounted for the observed trends in these measurements, and that preserved the integrated FPY distribution at 200%, to create a new 2.0 MeV FP cumulative yield evaluation for all FPs.

We emphasize that this evaluation is just a first step to more accurately representing FPYs for all FPs near 2 MeV average incident energy. It does include the expected physical behavior of the peak FPs decreasing, and the valley and wing FPs increasing, with increasing incident energy. But, as noted above, some of the measurements upon which this evaluation was based were discrepant with one another (especially in the valley region), and the assumption of symmetry in the functional form about the valley mid-point is only an approximation and it breaks down because of the energy-dependence of nubar [15]. For the VII.1 evaluation for the mass region A=141-145 we over-rode the 2.0 MeV FPY values based on the systematics formula (Eq. (16) of Ref. [15]) so as to specifically use the measurements from LANL-ILRR and mass spectrometry data studies by Prussin that indicate a negative energy-dependence between A=141 and 145.

The energy dependence for neutrons on ^{239}Pu with energies from 0.5 to 2 MeV (%-change relative per MeV) of various data sets, as well as our ENDF/B-VII.1 evaluation, are shown in Fig. 99 for the A=134 – 150 mass region. Prior to this work, ENDF did not account for any energy dependence in this energy region and therefore essentially a slope of zero was assumed. As seen in Fig. 99, VII.1 more faithfully represents the measurements. Our 2 MeV FPY results are given in Table XXIX.

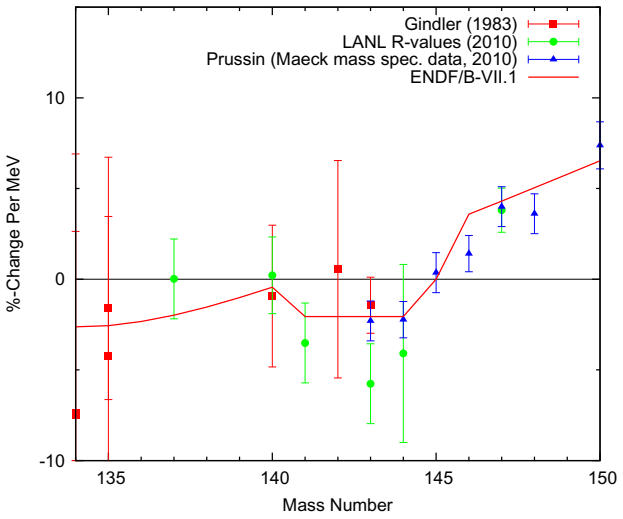

FIG. 99: The 0.5-2.0 MeV energy dependence (%-change relative per MeV) of various data sets for ^{239}Pu, as well as our ENDF/B-VII.1 evaluation for the A=134 – 150 mass region. ENDF/B-VII.0 would be at 0, since no energy dependence was considered in ENDF/B-VII.0.

B. 14 MeV n+^{239}Pu FPY

Some recent studies [245, 252] have led us to conclude that the 14-MeV ENDF/B-VI data for plutonium, referred to as "239H" data by England and Rider, need to be revised especially for important dosimetry FPs near the peaks. In contrast, we do not think such a deficiency exists for the ENDF/B-VI ^{235}U or ^{238}U 14-MeV data. As is discussed below, this has led us to reevaluate the 14 MeV FPYs for ^{239}Pu in the present work.

The 14 MeV plutonium FP data deficiency was first identified by Los Alamos radiochemists Michael MacInnes and Don Barr in the late 1990s. The reason for the likely-deficiency in the existing evaluated data is easy to understand. England and Rider's ENDF/B-VI evaluation was heavily influenced by Los Alamos measurements reported by Ford and Norris [253]. Although the historic Los Alamos 14-MeV experiments, performed in 1956 and 1971, were carefully done, the reported FPY results at the time were biased low because the 14-MeV ^{239}Pu fission cross section that was used at the time of these experiments was erroneously high. It is now known that in the 1950s the ^{239}Pu 14 MeV fission cross section assessed at the time was too high by about 20% (2.91b in 1956 versus the 2.41b evaluated today!). Because these experiments monitored the number of fissions that occurred by using a neutron flux multiplied by a fission cross section, the 1950s-1970s experiments inferred a number of fission events that was too high, and therefore FPYs that were too low. MacInnes, Barr *et al.* updated the originally reported radiochemical FP data (so called K factors, Q-values, and R-values) to reflect this modern understanding [245, 252].

Our evaluation procedure for ENDF/B-VII.1 was to begin by comparing the ENDF/B-VII.0 evaluation for the 14 MeV A-chain yields with measured data. There are few absolute FPY measurements: 2 LANL measurements from 1956 and 1971 described in a companion paper in this edition [245], and Nethaway's 1971 measurement

TABLE XXIX: New ENDF/B-VII.1 ^{239}Pu FPY chain yields evaluations for 0.5 and 2.0 MeV average neutron energies, and for 14 MeV neutrons. For A =141 – 145, the 2.0-MeV FPY data were modified from the values obtained using the systematics energy dependence in Eq. (16) in Ref. [15] to better match the LANL experimental data shown in the appendix in Ref. [15]. The 0.5 MeV FPYs are almost identical to ENDF/B-VI for all FPs except for ^{99}Mo, ^{147}Nd, ^{95}Zr, ^{140}Ba and ^{144}Ce. Very small differences compared to Ref. [15] reflect the requirement to normalize the chain yields to 200 %.

Mass	FPY (0.5 MeV) (%)	FPY (2 MeV) (%)	FPY (14 MeV) (%)	Mass	FPY (0.5 MeV) (%)	FPY (2 MeV) (%)	FPY (14 MeV) (%)
66	8.66350E-7	1.30232E-6	6.23000E-5	120	5.55841E-2	7.01613E-2	1.24800E+0
67	2.86454E-6	4.24037E-6	9.82000E-5	121	6.29680E-2	7.84120E-2	1.44468E+0
68	8.40399E-6	1.22514E-5	2.17000E-4	122	6.97721E-2	8.52198E-2	1.46070E+0
69	3.11407E-5	4.47101E-5	3.71000E-4	123	7.66630E-2	9.14124E-2	1.72950E+0
70	8.67348E-5	1.22654E-4	6.70000E-4	124	1.20544E-1	1.39857E-1	1.88218E+0
71	2.02614E-4	2.82233E-4	1.19600E-3	125	1.77508E-1	2.00032E-1	1.95490E+0
72	5.19011E-4	7.12199E-4	2.18000E-3	126	2.66279E-1	2.91389E-1	2.54790E+0
73	7.04658E-4	9.52649E-4	3.75900E-3	127	4.99912E-1	5.31909E-1	2.20420E+0
74	1.73270E-3	2.30809E-3	5.88000E-3	128	8.77329E-1	9.09964E-1	2.50227E+0
75	2.54316E-3	3.33833E-3	1.02300E-2	129	1.44831E+0	1.46950E+0	2.80608E+0
76	5.79895E-3	7.50211E-3	1.64180E-2	130	2.44943E+0	2.44119E+0	3.31213E+0
77	1.26679E-2	1.61538E-2	2.37000E-2	131	3.87105E+0	3.80613E+0	3.60793E+0
78	2.28854E-2	2.87690E-2	4.15000E-2	132	5.31940E+0	5.18181E+0	4.21067E+0
79	6.06555E-2	7.51791E-2	8.62000E-2	133	6.95789E+0	6.74152E+0	5.10243E+0
80	9.23361E-2	1.12857E-1	1.57400E-1	134	7.36892E+0	7.12581E+0	5.20837E+0
81	1.41600E-1	1.70695E-1	2.72000E-1	135	7.54023E+0	7.29819E+0	5.21217E+0
82	2.18434E-1	2.59752E-1	3.49800E-1	136	7.05034E+0	6.84629E+0	5.21080E+0
83	3.14987E-1	3.69567E-1	4.73500E-1	137	6.57770E+0	6.42001E+0	5.12594E+0
84	4.97769E-1	5.76335E-1	6.02045E-1	138	6.11497E+0	6.00754E+0	4.90796E+0
85	6.03042E-1	6.89180E-1	8.01713E-1	139	5.60091E+0	5.54477E+0	4.60488E+0
86	7.87965E-1	8.89046E-1	1.00140E+0	140	5.30000E+0	5.29170E+0	4.20369E+0
87	1.04139E+0	1.16028E+0	1.20116E+0	141	5.13736E+0	5.00849E+0	4.16621E+0
88	1.32719E+0	1.46056E+0	1.50419E+0	142	4.74537E+0	4.62633E+0	3.73138E+0
89	1.72206E+0	1.87234E+0	1.70381E+0	143	4.33374E+0	4.22503E+0	3.29499E+0
90	2.04461E+0	2.19689E+0	1.92189E+0	144	3.69000E+0	3.59743E+0	2.99296E+0
91	2.51176E+0	2.66785E+0	2.23730E+0	145	2.99847E+0	3.01366E+0	2.65509E+0
92	3.03196E+0	3.18435E+0	2.62171E+0	146	2.45537E+0	2.60796E+0	2.30576E+0
93	3.81845E+0	3.96677E+0	3.00237E+0	147	2.01000E+0	2.14882E+0	1.92218E+0
94	4.22513E+0	4.34306E+0	3.48870E+0	148	1.65829E+0	1.80300E+0	1.50212E+0
95	4.76000E+0	4.84328E+0	4.39478E+0	149	1.23876E+0	1.36325E+0	1.20150E+0
96	4.84709E+0	4.88415E+0	4.37410E+0	150	9.94979E-1	1.10857E+0	9.93760E-1
97	5.28721E+0	5.27893E+0	4.87316E+0	151	7.83447E-1	8.83949E-1	8.41060E-1
98	5.62234E+0	5.56598E+0	4.86400E+0	152	6.25510E-1	7.14857E-1	6.41035E-1
99	6.23000E+0	6.08970E+0	5.66942E+0	153	4.25038E-1	4.92125E-1	5.76214E-1
100	6.53190E+0	6.37531E+0	5.12130E+0	154	2.66743E-1	3.12963E-1	4.20964E-1
101	6.65721E+0	6.46453E+0	4.99700E+0	155	2.08424E-1	2.47848E-1	3.10796E-1
102	6.71908E+0	6.50340E+0	5.00493E+0	156	1.54460E-1	1.86198E-1	2.56436E-1
103	6.81606E+0	6.59119E+0	5.87685E+0	157	1.05935E-1	1.29478E-1	1.50380E-1
104	6.57220E+0	6.36783E+0	4.58894E+0	158	6.55332E-2	8.12248E-2	9.32061E-2
105	5.35091E+0	5.21250E+0	4.27480E+0	159	3.84737E-2	4.83649E-2	6.00775E-2
106	4.35720E+0	4.28413E+0	3.57730E+0	160	1.60205E-2	2.04290E-2	4.00478E-2
107	3.21497E+0	3.20417E+0	2.86220E+0	161	8.63256E-3	1.11680E-2	2.27435E-2
108	1.99896E+0	2.02820E+0	2.39820E+0	162	6.12932E-3	8.04577E-3	9.00000E-3
109	1.03431E+0	1.07279E+0	2.47640E+0	163	3.14102E-3	4.18409E-3	3.20000E-3
110	6.46101E-1	6.87455E-1	1.74430E+0	164	1.78959E-3	2.41940E-3	1.84000E-3
111	3.56339E-1	3.89941E-1	1.92386E+0	165	8.95294E-4	1.22854E-3	7.00000E-4
112	1.88568E-1	2.12496E-1	1.86484E+0	166	6.33793E-4	8.82845E-4	5.00000E-4
113	1.27419E-1	1.47833E-1	1.29520E+0	167	2.66492E-4	3.76855E-4	2.70000E-4
114	9.40858E-2	1.12187E-1	1.25660E+0	168	7.64544E-5	1.09769E-4	1.38000E-4
115	8.12542E-2	9.92441E-2	1.52257E+0	169	2.57509E-5	3.75397E-5	6.63000E-5
116	6.02432E-2	7.50189E-2	1.15719E+0	170	7.64544E-6	1.13175E-5	4.80000E-5
117	6.97382E-2	8.80275E-2	1.15140E+0	171	2.57509E-6	3.87097E-6	3.67000E-5
118	5.97502E-2	7.59480E-2	1.26530E+0	172	7.64544E-7	1.16716E-6	1.84000E-5
119	5.49124E-2	6.97987E-2	1.25180E+0				
				Total	200	200	200

[254], and Laurec's measurement from the late 1970s that was recently documented [21]. Other measurements such as Nethaway's work from 1983/1984, and Bonyushkin's measurements, are *relative* and so of less direct use. The two LANL measurements, and that of LLNL (Nethaway 1971), are all very consistent, but Laurec's CEA data are generally lower for plutonium for reasons we do not understand. For ENDF/B-VII.1 we perturbed the previous ENDF/B-VII.0 evaluation to better reproduce the LANL and LLNL data, putting more weight on them than on Laurec's data.

One complication did arise with this approach: In order to preserve the integral of 200%, some FPYs for FPs adjacent to those measured by LANL & LLNL/Nethaway (1971) were evaluated to be significantly lower, resulting in some spikes and discontinuities in the FPY evaluation that are not well grounded physically. Ultimately this was because the evaluator (Chadwick) placed a higher premium on matching the LANL and Nethaway (1971) plutonium FPY data than on requiring a smooth FPY distribution. Indeed, in the early 1970s Nethaway noted this same issue and at that time took a different approach [255]: he concluded that he and Prindle must have made an unidentified 9% normalization error on the 14 MeV

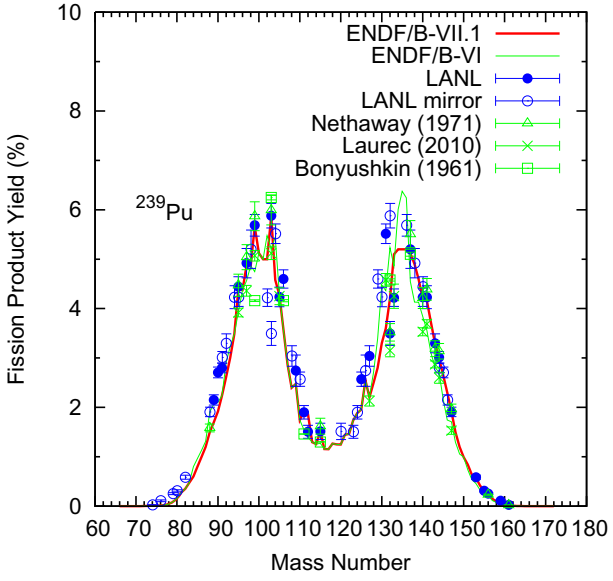

FIG. 100: 14 MeV ^{239}Pu A-chain yield in ENDF/B-VII.1 compared to ENDF/B-VII.0 and to measured data.

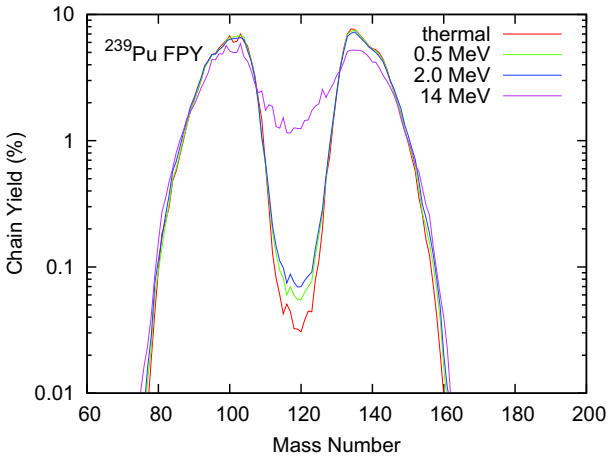

FIG. 101: A-Chain yields for n+^{239}Pu in ENDF/B-VII.1. Thermal yields are unchanged from ENDF/B-VI.

neutron fluence assessment, and then he renormalized his plutonium 14 MeV FPYs down by this amount [16, 255], enabling him to put a smooth FPY doubled-hump distribution through these data and match 200% for the integral. The new ENDF/B-VII.1 approach by Chadwick instead reproduces the absolute scale of the LANL and LLNL/Nethaway (1971) ^{239}Pu FPYs reported herein, because three US experiments agreed in this absolute scale (LANL 1956, LANL 1971, and Nethaway 1971); nevertheless we still conclude that there remain significant uncertainties in the absolute magnitude of the 14 MeV plutonium FPY, and future measurements most likely will be needed to more confidently assess the 14 MeV plutonium FPYs [256]. Our 14 MeV ENDF/B-VII.1 A-chain FPY results for ^{239}Pu are given in Table XXIX and shown in Fig. 100.

We have not changed the ^{235,238}U 14 MeV FPYs in ENDF/B-VII.1 since the recently published LANL and CEA data [21, 245] are in fair agreement with the existing evaluation.

C. Individual, Cumulative, and Chain Yields

The evaluation of both the independent and cumulative yields of fission products is accomplished in way that ensures consistency with our evaluated chain yield in Table XXIX, using the following procedure. We start with the previous independent yields in the ENDF/B-VII.0=VI FPY library, and calculate the cumulative yields from them by tracing the decay chain of each isotope toward the stable nucleus with the decay constants and half-lives taken from CINDER2008 (which therefore uses updated decay data compared to England and Rider's original calculation). The next step is to calculate sensitivities of individual independent yield to each chain yield, and the initial (prior) independent yields are adjusted with the KALMAN code by comparing the calculated and newly evaluated chain yields. This led to a new set of individual, and cumulative FPYs for VII.1 that are consistent with the new VII.1 chain yields. Figure 101 shows the new VII.1 chain yields for neutrons on plutonium for thermal, fast (0.5 and 2.0) and 14 MeV.

IX. DECAY DATA SUBLIBRARY

The new ENDF/B-VII.1 decay data sublibrary represents a considerable improvement over the previous ENDF/B-VII.0 as briefly described below.

A. Improvements in ENDF/B-VII.1

The new sublibrary contains data for 3,817 materials, where each material corresponds to a long-lived level, ground state or isomer. We note that ENDF/B-VII.0 contained 3,838 materials, including some with poorly known data which were dropped in ENDF/B-VII.1.

The sublibrary is based on decay data in the Evaluated Nuclear Structure Data File (ENSDF) [258], translated into the ENDF-6 format. The data in ENSDF is continuously being updated and re-evaluated, with a given mass chain revisited, on average, every 7 years. Thus, a significant amount of the data incorporated in ENDF/B-VII.0 has been re-evaluated in ENDF/B-VII.1. For those nuclei where no decay radiation has been measured or the known decay scheme is incomplete, basic information was taken from the latest version of the Nuclear Wallet Cards (2011).

In addition to the incorporation of new and updated

data from ENSDF, the new ENDF/B-VII.1 contains a number of modifications, additions and error resolutions, compared with ENDF/B-VII.0. These include a more thorough treatment of the atomic radiation, improved Q value information, recent theoretical calculations of the continuous spectrum from beta-delayed neutron emitters, and new TAGS (Total Absorption Gamma-ray Spectroscopy) data.

Atomic radiation, X-rays and Auger electrons, are produced from the filling of atomic vacancies created in electron capture and electron conversion. A detailed description of these processes is important for nuclides for which the main decay mode is electron capture. It is also relevant in heavy deformed nuclei where gamma-ray transitions are strongly converted, as well as in the deformed actinides where the gamma-ray transition energy is smaller than the K binding energy. In ENDF/B-VII.0, the atomic data included fluorescence yields, energies and intensities taken from the 8^{th} edition of the Table of Isotopes [259].

In the new ENDF/B-VII.1, the atomic data from the Evaluated Atomic Data Library [260] developed by LLNL was used, in a similar way to the calculations described by Stepanek [261]. All the K-L, K-M and K-N as well as the Lα, Lβ and Lγ X-rays are included. In addition, the KLL, KLX, KXY, LLX, LMM, LMX, LXY, MMX, and MXY average Auger electrons are also listed. The electron conversion to atomic sub-shells was calculated with the code BRICC [262].

An essential component of any decay process is the total energy available for the decay (Q value). The previous ENDF/B-VII.0 makes use of the 2003 Audi mass evaluation [263]. Since then, with the advent of multiple Penning traps around the world, numerous masses of both neutron and proton rich nuclei have been measured with very high precision. These are incorporated into the 2009 and 2011 updates of the mass evaluation and have been used in creating the ENDF/B-VII.1 decay sublibrary. Changes in the overall Q value for a decay impact the values of energy for electromagnetic radiation, light particles, and heavy particles.

In some neutron rich nuclei, beta-decay followed by neutron emission is an energetically favored decay mode. The resulting neutron spectrum is very difficult to measure experimentally and data are available for only a select few cases. As this decay mode has particular relevance for energy applications, ENDF/B-VII.1 includes new theoretical calculations using the Cascading Gamma Multiplicity (CGM) model of continuous gamma, beta, and neutron spectra [264]. The calculations were performed for beta-delayed neutron emitters which comprise the thermal neutron fission fragment yield of ^{235}U and ^{239}Pu. The previous ENDF/B-VII.0 modeled the neutron spectrum using Gross theory whereas in the present calculations, a micro-macroscopic (QRPA) theory of the beta-decay strength function is coupled with a statistical modeling of the levels and continuum in the daughter nucleus. Depending on the known available data, different types of files were generated. For those nuclei where the complete neutron spectrum is known, the neutron data from ENDF/B-VI.8 was combined with the beta-decay data in ENSDF, as in ^{136}I. In cases where only a portion of the neutron spectrum is measured, the neutron data from ENDF/B-VI.8 were merged with the CGM calculations to provide a complete neutron spectrum up to the available Q value. For those nuclei where no neutron data are available, but detailed gamma and beta radiation have been determined, the information from ENSDF was combined with the neutron spectrum from the CGM calculations. Finally, for those nuclei where no measurements have been performed, the theoretical calculations provided the gamma, beta, and neutron spectra. The values of Pn (delayed neutron emission probability) were taken from ENSDF when experimentally known; otherwise, the values from the CGM calculations were used. Lifetimes were also taken from ENSDF when experimentally known, otherwise the systematic values provided by Pfeiffer *et al.* [265], were adopted.

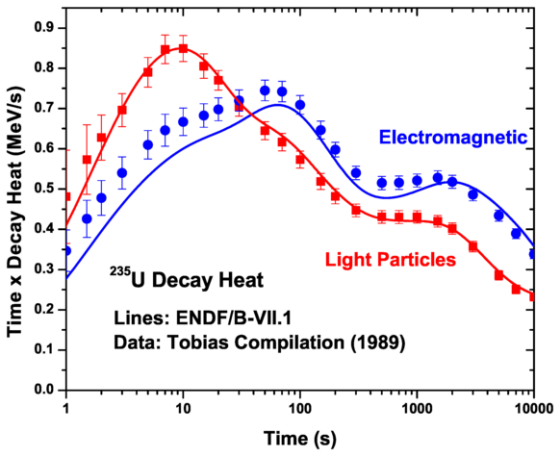

FIG. 102: Decay heat multiplied by time for a single fission event for ^{235}U(n,f) at neutron thermal energy. Shown are the electromagnetic (blue) and light particle (red) components of the decay heat. ENDF/B-VII.1 values are compared with experimental data [267].

Total Absorption Gamma-ray Spectrometry (TAGS) is sensitive to the total beta-decay population of all nuclear levels, rather than to individual, discrete gamma-rays. Particularly in cases where the Q value is quite large, discrete gamma rays can be missed, and the TAGS method is preferred for an accurate measurement of the total beta-decay strength. The values of energy of electromagnetic radiation and energy of light particles from the recently published TAGS data for ^{105}Mo, ^{104,105,106,107}Tc [266], were included in ENDF/B-VII.1.

Finally, the new ENDF/B-VII.1 decay data sublibrary

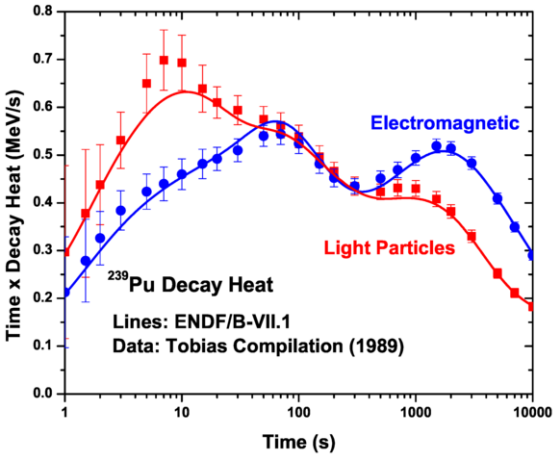

FIG. 103: Decay heat multiplied by time for a single fission event for ^{239}Pu(n,f) at neutron thermal energy. Shown are the electromagnetic (blue) and light particle (red) components of the decay heat. ENDF/B-VII.1 values are compared with experimental data [267].

TABLE XXX: The number of benchmarks per main ICSBEP category for compound and metal systems with thermal, intermediate, fast and mixed neutron spectra.

	COMP				MET			
	therm	inter	fast	mixed	therm	inter	fast	mixed
LEU	385				23			
IEU	5	4	1				17	
HEU	134	6		8	49	5	139	5
MIX	39		5				31	
PU	0	1		30		1	98	6
^{233}U	8						10	
Total	571	11	6	38	72	6	295	11

TABLE XXXI: The number of benchmarks per main ICSBEP category for solution and miscellaneous systems with thermal, intermediate, fast and mixed neutron spectra.

	SOL				MISC			
	therm	inter	fast	mixed	therm	inter	fast	mixed
LEU	67							
IEU	13							
HEU	339							
MIX	53				46		10	
PU	368							
^{233}U	59							
Total	899				46		10	

includes fixes to errors, such as the positron intensity, which was left as zero in ENDF/B-VII.0.

B. Decay Heat

The above improvements, in particular inclusion of TAGS data has improved the calculation of decay heat for ^{235}U(n,f) as well as for ^{239}Pu(n,f). As shown in Figs. 102, 103 values computed from ENDF/B-VII.1 are in good agreement with experimental data by Tobias [267]. We note that prior TAGS data in ENDF/B-VII.0 was slightly modified according to the new Audi mass evaluation, resulting in some changes to values of energy of electromagnetic radiation and energy of light particles.

X. INTEGRAL DATA TESTING SUMMARY

A. Criticality Testing

As for ENDF/B-VII.0 [1, 6], our data validation testing for VII.1 is comprised of two main efforts: that from the US CSEWG validation committee as described by Kahler in the companion article in this issue [8] (and summarized below), and that performed by S. van der Marck (vdM) of NRG, Petten, as described below. There is value in having two independent validation studies to provide cross-checks on the respective methods and results. The summary below provides a brief high-level perspective (vdM plans to publish a more detailed follow-on description of this work), whilst the Kahler publication gives more detail and more interpretation, but for a smaller set (still large!) of criticality calculations, as well as providing comparisons with PROFIL fast reactor transmutation (reaction rate) data.

As was done for ENDF/B-VII.0 in 2006, the new data have been tested by performing calculations for a very large number of criticality safety benchmark cases, taken from the International Handbook of Evaluated Criticality Safety Benchmark Experiments. Among the benchmark cases are ones for a variety of fuel types (leu, ieu, heu, pu, mix, u233); for many different physical forms of the fissile component (compound, metal, solution, miscellaneous); and for many types of neutron spectra (thermal, intermediate, fast, mixed). The number of calculated cases in each category is summarized in Tables XXX–XXXI.

All the nuclear data evaluations in the vdM validation work were processed by NJOY-99.364, and the criticality safety simulations were done using MCNP-4C3. The average results for all these calculations are summarized in Tables XXXII–XXXIII, for each main International Criticality Safety Benchmark Evaluation Project (ICSBEP) main category separately, for the beta4 version of VII.1. In these tables the results for ENDF/B-VII.0 are also listed, for easy comparison (the values for ENDF/B-VII.0 are different from those in Ref. [1], because many benchmark cases (Figs. 104,105,106,107) have been added since). It has been a humbling experience for us to observe the overall C/E-1 and standard deviation changes between VII.1 and VII.0: for all the work invested in VII.1, these overall metrics do not show a clear improvement! Nevertheless, Figs. 104,105,106,107 do show more

clearly the improvements for cases discussed in more detail below.

Based on the set of simulated criticality safety benchmark cases, several observations can be made.

- Overall the results for the majority of benchmark cases are similar to those obtained with ENDF/B-VII.0. This implies that the good performance of ENDF/B-VII.0 has been preserved for ENDF/B-VII.1, including for the LEU-COMP-THERM category. This is as expected, given that the evaluations for the major actinides have not been changed (as far as the cross sections are concerned).

- The new W evaluations lead to improvements in calculated $k_{\rm eff}$ values for several benchmark series: for ieu-met-fast-014, heu-met-fast-067, pu-met-fast-005 and u233-met-fast-004 the lower values are closer to the benchmark values.

- The new ^{9}Be evaluation also has a noticeable impact. The results for benchmarks series heu-met-fast-005, heu-met-fast-059, heu-met-fast-066, heu-met-fast-069, and u233-met-fast-005 are higher with ENDF/B-VII.1 than with ENDF/B-VII.0, with the VII.1 values being closer to the benchmark value. But heu-met-fast-041, heu-met-fast-058, and mmf-7 get worse compared to VII.0. See also Kahler's paper [8], and Fig. 108.

- The new capture cross section for $^{\rm nat}$C has a significant impact on the results for leu-comp-therm-060 (a Russian RBMK type benchmark). Compared to results based on ENDF/B-VII.0, the results are about 1000 pcm lower, and thus in much better agreement with the benchmark values. This was a consequence of the modification to the carbon capture cross section for VII.1.

- The new Mn and Cr evaluations lead to improved performance in the ZPR assemblies (not shown in the figures here, but described by Kahler [8]).

- The new Ti evaluations lead to improved performance, especially for HMF-79 (also described by Kahler [8]).

- The new Zr evaluations lead to improved performance (also described by Kahler [8]).

- The new Cd evaluation leads to improved performance (described by Kahler [8]).

- Gd in VII.1 performs very similarly to VII.0. This reflects the fact that Mughabghab's evaluation attempted to reconcile a variety of measurements, including some new data, but the final VII.1 evaluation has a thermal capture cross section similar to that in VII.0. (in fact an earlier version in the pre-VII.1 beta3 file was rejected because of poor performance in our simulations).

- The beta4 version of the VII.1 library, shown here in the figures, included a proposed update for ^{19}F that was later removed for the final ENDF/B-VII.1 library. Hence the footnotes shown in Tables XXXII, XXXIII.

Although the vdM simulations shown here were done with MCNP-4C3, and those done by Kahler were using MCNP5, we have also used the new LANL code MCNP6 [268] for this large suite of ICSBEP benchmarks. MCNP6 merges MCNP5 and MCNPX and represents the code that will be evolved for future MCNP capability upgrades. The results from these MCNP6 calculations have not yet been analyzed in detail, but overall the results are in line with the MCNP-4C3 results shown in this paper: 94% are within 2 standard deviations.

Another set of benchmark results can be described that illustrate the progress made for VII.1. Los Alamos maintains a suite of 119 critical assembly benchmarks that span the various neutron spectra types and nuclear material types for testing MCNP, as has been described by Mosteller. Using MCNP5 we can calculate the standard deviation in k-eff for various versions of ENDF. For VI.8 it was 0.60 %, and for VII.0 it was 0.48%. For VII.1 we calculate a standard deviation of 0.41%, reflecting modest overall improvement.

B. Delayed Neutron Testing, $\beta_{\rm eff}$

The delayed neutron data have been changed with respect to ENDF/B-VII.0, and it is therefore worthwhile to test these data against measurements of effective delayed neutron fraction $\beta_{\rm eff}$ in critical configurations. Unlike the situation for $k_{\rm eff}$, only a handful of measurements of $\beta_{\rm eff}$ have been reported in open literature with sufficiently detailed information. In Ref. [6] more than twenty measurements are listed, including several measurements of α, which is closely related to $\beta_{\rm eff}$ through the prompt neutron generation life time. Here we restrict ourselves to measurements of $\beta_{\rm eff}$ only, and then only the ones that are deemed most suitable for nuclear data testing. The same approach was used for testing ENDF/B-VII.0 in 2006 [1, 6]. We avoid the term 'benchmark' for these cases, because a good benchmark description, comparable to those given in the ICSBEP Handbook [113], is not available.

We have chosen two thermal spectrum cores (TCA and IPEN/MB-01), and five fast spectrum ones (Masurca and FCA). The same choice was made for testing ENDF/B-VII.0, and brief descriptions of these systems can be found in Ref. [1]. Note that for a thermal spectrum, only the ^{235}U delayed neutron data are tested by these calculations, whereas for a fast spectrum ^{235,238}U and ^{239}Pu data are tested. Also, one should bear in mind that the tests performed here are only sensitive to the total delayed neutron yields. The delayed neutron yields per group are not tested, nor are the values for the decay constant per group. The tests described here therefore

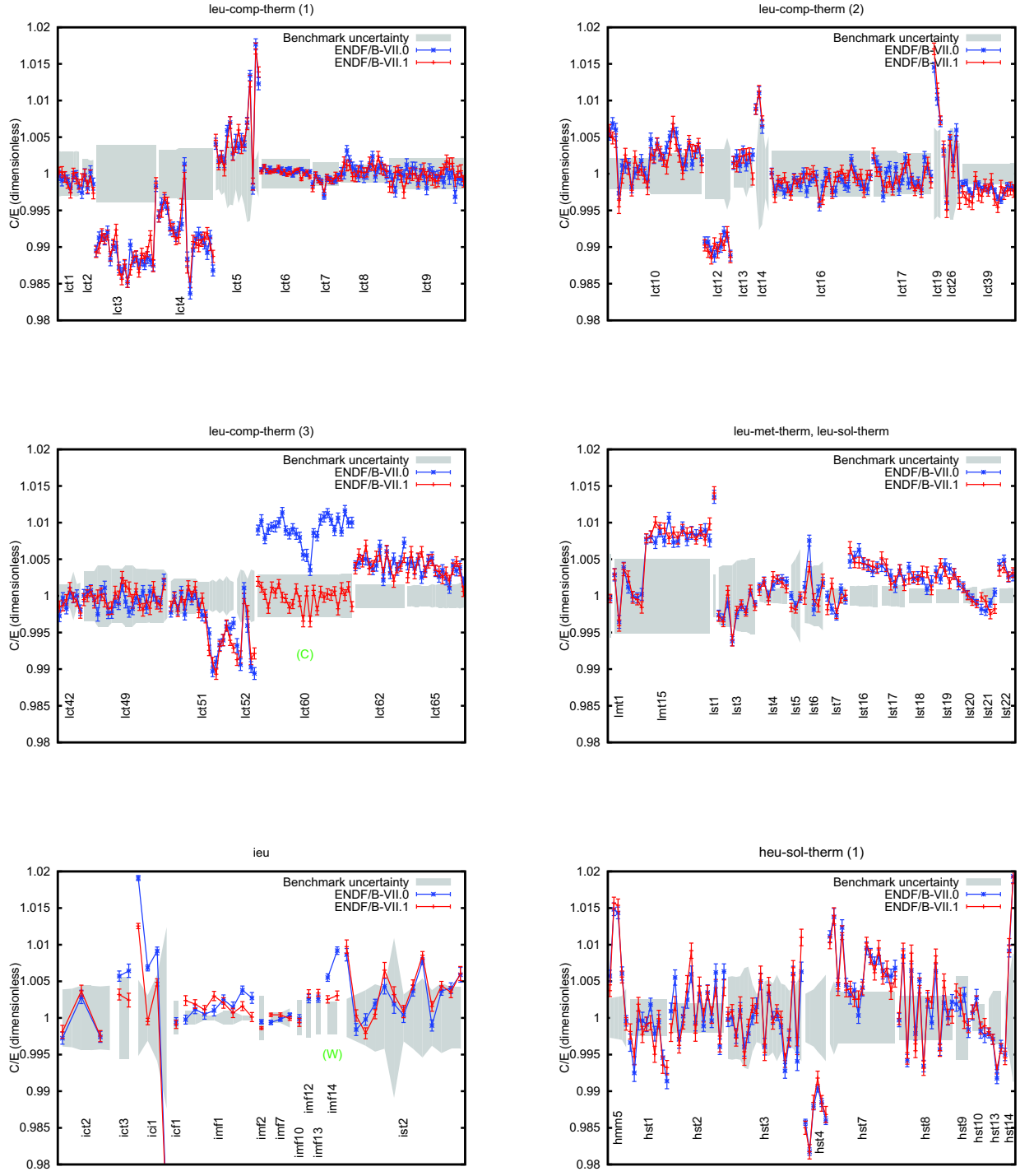

FIG. 104: Various vdM figures showing validation testing using MCNP simulations of ICSBEP benchmarks, comparing ENDF/B-VII.1 and VII.0. (Calculation/Experiment -1) values are given, together with the experimental uncertainty (gray band). For cases where a significant change occurs between VII.1 and VII.0, the element responsible for the change is shown in green in parentheses.

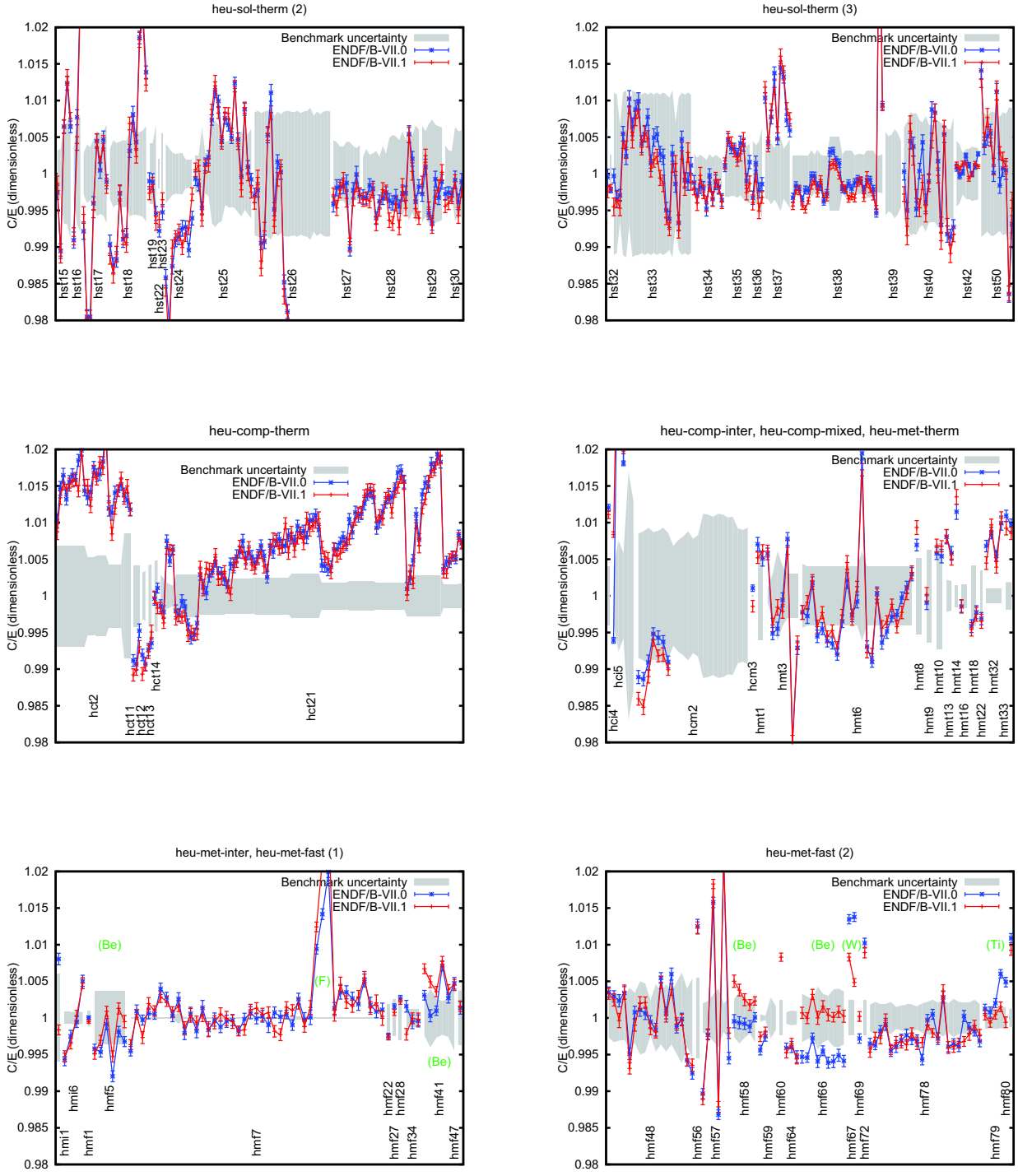

FIG. 105: Various vdM figures - continued - showing validation testing using MCNP simulations of ICSBEP benchmarks, comparing ENDF/B-VII.1 and VII.0. (Calculation/Experiment -1) values are given, together with the experimental uncertainty (gray band). For cases where a significant change occurs between VII.1 and VII.0, the element responsible for the change is shown in green in parentheses.

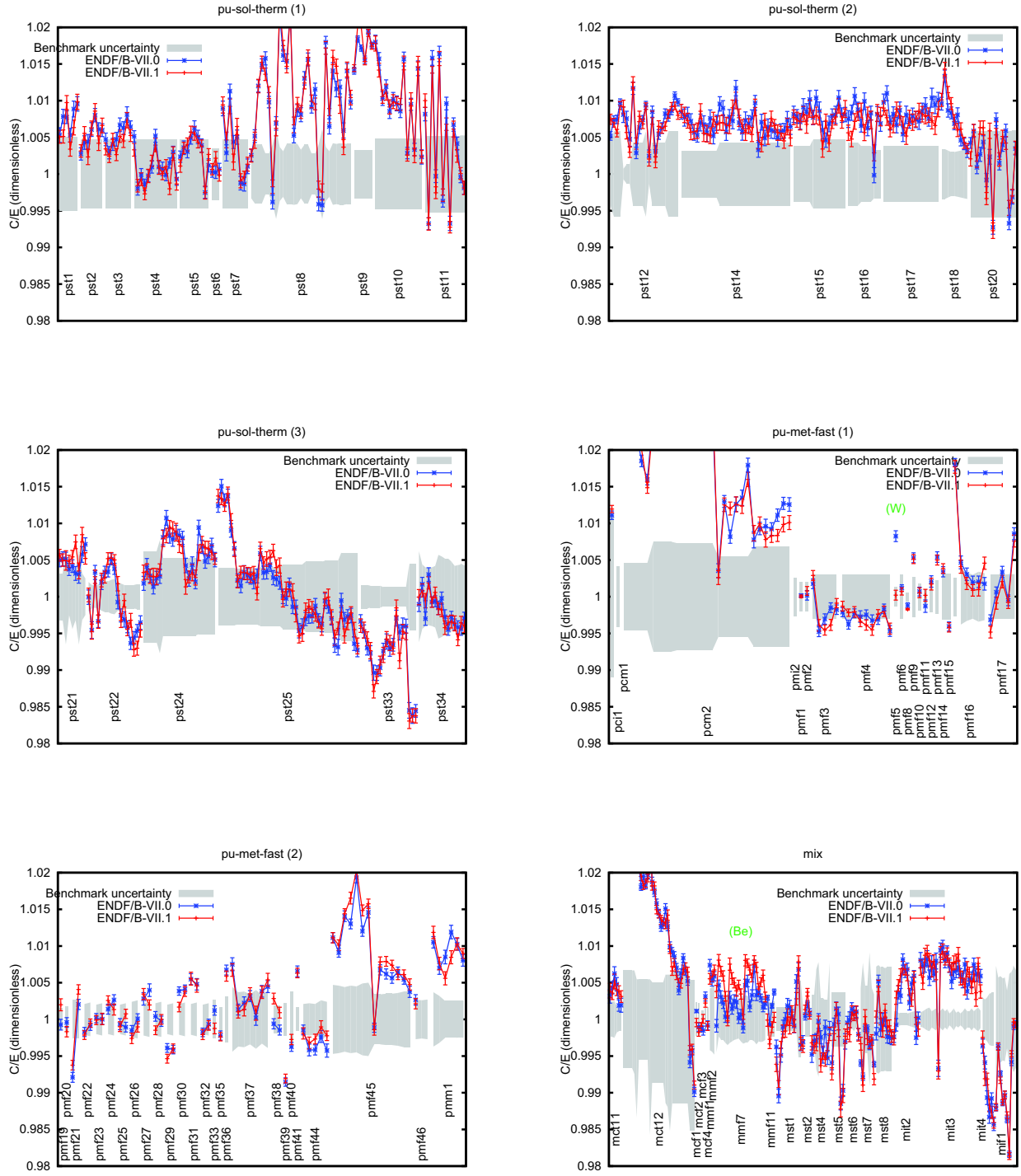

FIG. 106: Various vdM figures - continued - showing validation testing using MCNP simulations of ICSBEP benchmarks, comparing ENDF/B-VII.1 and VII.0. (Calculation/Experiment -1) values are given, together with the experimental uncertainty (gray band). For cases where a significant change occurs between VII.1 and VII.0, the element responsible for the change is shown in green in parentheses.

TABLE XXXII: The average value of $C/E-1$ in pcm (100 pcm=0.1%) for ENDF/B-VII.1 per main ICSBEP category for compound and metal systems Shown in *italics* are the values for the ENDF/B-VII.0 library.

	COMP				MET			
	therm	inter	fast	mixed	therm	inter	fast	mixed
LEU	-86±472 *-18±539*				572±425 *554±397*			
IEU	99±263 *194±395*	-264±1507 *211±1724*	-87 *-49*				141±141 *188±246*	
HEU	732±701 *766±691*	2095±5075 *1617±3941*		-924±414 *-708±378*	80±660 *48±689*	-106±345 *88±500*	39±432[a] *5±505* [b]	791±656 *812±557*
MIX	401±1640 *427±1609*		-17±135 *12±176*				426±309 *258±224*	
PU		1195 *1111*		1945±921 *1961±872*		3763 *4626*	173±532 *168±512*	880±197 *937±167*
^{233}U	1±154 *147±181*						-241±174 *-84±367*	

[a]Value would be 84±532 if ^{19}F bearing assemblies HMF7-32,33,34 were included.
[b]Value would be 36±545 if ^{19}F bearing assemblies HMF7-32,33,34 were included.

TABLE XXXIII: The average value of $C/E-1$ in pcm (100 pcm=0.1%) for ENDF/B-VII.1 per main ICSBEP category for solution and miscellaneous systems Shown in *italics* are the values for the ENDF/B-VII.0 library.

	SOL				MISC			
	therm	inter	fast	mixed	therm	inter	fast	mixed
LEU	138±291 *150±293*							
IEU	367±331 *304±308*							
HEU	-29±716[a] *4±699*[b]							
MIX	-213±368 *-182±356*				354±613 *342±619*		-831±557 *-842±548*	
PU	442±608 *451±610*							
^{233}U	504±753 *525±748*							

[a]Value would be 56±957 if ^{19}F bearing assembly HST-039 were included.
[b]Value would be 56±791 if ^{19}F bearing assemblies HST-39 were included.

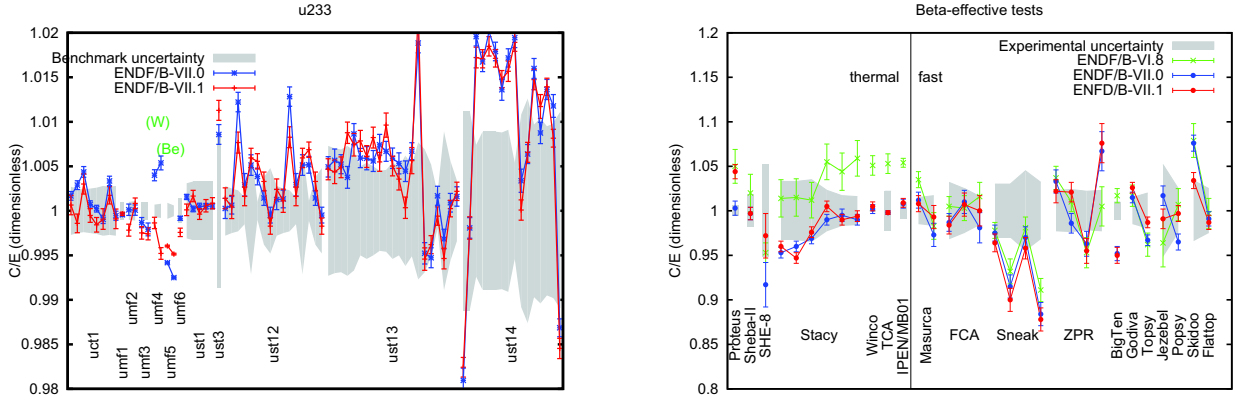

FIG. 107: Various vdM figures - continued - showing validation testing using MCNP simulations of ICSBEP benchmarks, comparing ENDF/B-VII.1 and VII.0. (Calculation/Experiment -1) values are given, together with the experimental uncertainty (gray band). For cases where a significant change occurs between VII.1 and VII.0, the element responsible for the change is shown in green in parentheses.

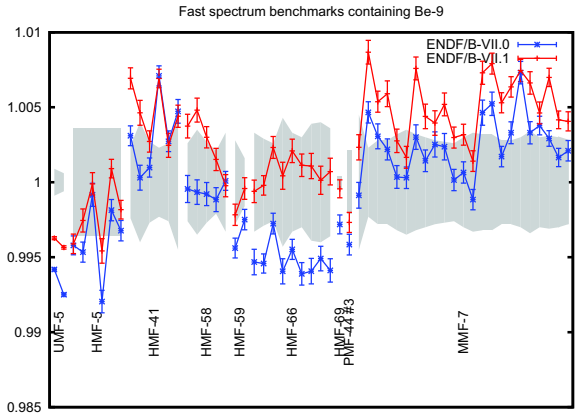

FIG. 108: Criticality testing for assemblies sensitive to beryllium in the fast neutron energy range.

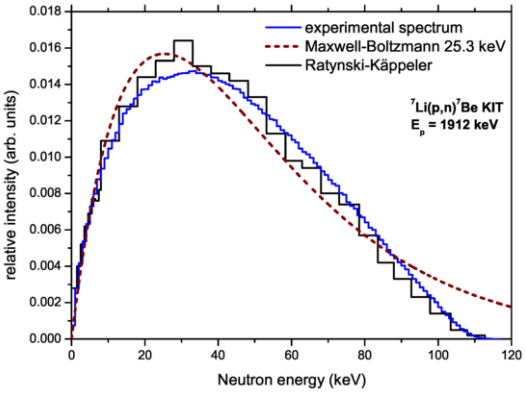

FIG. 109: Experimental energy distribution (blue line) which approximates a Maxwell-Boltzmann distribution for kT = 25 keV (dashed line). For comparison the Ratynski-Käppeler spectrum (obtained from a measurement [232]) used for nuclear astrophysics studies is plotted as histogram.

do not address the problem described in Section VI.G.

The calculation of $\beta_{\rm eff}$ for these systems was done using a version of MCNP-4C3 with an extra option added to it as described in Ref. [269]. This method was used earlier to test delayed neutron data from ENDF/B-VII.0 [6], JEFF-3.1 and JENDL-3.3 [270]. The results based on ENDF/B-VII.1 are given in Table XXXIV, as well as the results based on these other libraries. The results for the effective delayed neutron fraction are similar to those obtained with ENDF/VII.0. See the right-hand picture in Fig. 107. Kahler's paper [8] shows additional comparisons of $\beta_{\rm eff}$ and Rossi-α which are favorable.

C. Calculated Critical Masses

The calculated critical masses of actinides provides a convenient way to assess some of the changes that have been introduced in moving to ENDF/B-VII.1 from ENDF/B-VII.0, especially changes to the cross sections in the fast energy region. Results, shown in Table XXXV, confirm essentially no changes for ^{233,234,235,236,238}U, ^{237}Np, ^{239,241,242}Pu, ^{241,242,243}Am, and generally significant changes for the remainder of the actinides.

D. AMS ^{235,8}U(n,γ) at 25 and 426 keV

Here we describe integral validation of ENDF/B-VII.1=VII.0 ^{235}U(n,γ) and ^{238}U(n,γ) using accelerator mass spectrometry (AMS) measurements recently reported by Wallner [238]. Such measurements are valuable because this kind of measurement can determine capture cross sections accurately, and these two cross sections are of central importance in nuclear technologies.

The combination of neutron activation with subsequent accelerator mass spectrometry (AMS) measurement was used to determine ^{235}U and ^{238}U capture cross sections in the keV neutron energy range. AMS represents a technique with excellent sensitivity for the detection of long-lived radionuclides through ultra-low isotope ratio measurements with accuracies for actinides of the order of a few %. For such atom counting techniques interference from fission is completely excluded. AMS does not suffer from molecular isobaric interferences due to the use of tandem accelerators and it can also be used for separating specific atomic isobars.

Neutron activations of U_3O_8 pellets (provided by IRMM, Belgium) were performed within the European EFNUDAT program. At Karlsruhe Institute of Technology (KIT) keV neutrons were produced via the ^{7}Li$(p,n)^7$Be reaction by bombarding a Li target with protons [232] at appropriate energies: a neutron energy distribution peaking at 35 keV was produced (see Fig. 109) which closely resembles an energy distribution of a Maxwellian-Boltzmann type of 25 keV [232]. Such an irradiation setup at KIT with a Maxwell-Boltzmann distribution of $\approx$ 25 keV was also used for a series of neutron capture measurements in nuclear astrophysics. A second irradiation was performed with neutron energies centered around 426 keV and an energy spread of 150 keV FWHM (see Fig. 110). A proton beam intensity of $\approx$100 μA resulted in a fluence of 1.75×10^{15} (25 keV) and 4.34×10^{15} n cm^{-2} (426 keV), respectively. Au foils were used for the fluence determination.

The use of natural uranium samples allowed to measure simultaneously the ^{235}U(n,γ) and ^{238}U(n,γ) capture cross sections from the very same samples. The produced long-lived radionuclides, ^{236}U and the decay product of ^{239}U, ^{239}Pu, were counted by AMS at the Vienna Environmental Research Accelerator (VERA) [238]. The high sensitivity of AMS requires only very small samples of some 10 mg. However, the sample material is sputtered and consumed in the measurement and as such

TABLE XXXIV: C/E values for $\beta_{\rm eff}$ of several critical systems, using ENDF/B-VII.1 and other nuclear data libraries.

System	Experiment	C/E			
		ENDF/B-VII.1	ENDF/B-VII.0	JEFF-3.1	JENDL-3.3
TCA	771 ± 17	0.998 ± 0.002	0.998 ± 0.002	1.029 ± 0.002	0.987 ± 0.012
IPEN/MB-01	742 ± 7	1.009 ± 0.005	1.008 ± 0.005	1.040 ± 0.005	1.019 ± 0.005
Masurca R2	721 ± 11	1.011 ± 0.009	1.012 ± 0.009	1.011 ± 0.009	1.018 ± 0.010
Masurca ZONA2	349 ± 6	0.993 ± 0.013	0.973 ± 0.013	1.021 ± 0.013	0.994 ± 0.014
FCA XIX-1	742 ± 24	0.984 ± 0.010	0.987 ± 0.010	1.010 ± 0.010	0.985 ± 0.011
FCA XIX-2	364 ± 9	1.007 ± 0.013	1.010 ± 0.013	1.054 ± 0.013	1.022 ± 0.013
FCA XIX-3	251 ± 4	1.000 ± 0.017	0.981 ± 0.017	0.997 ± 0.016	0.996 ± 0.016

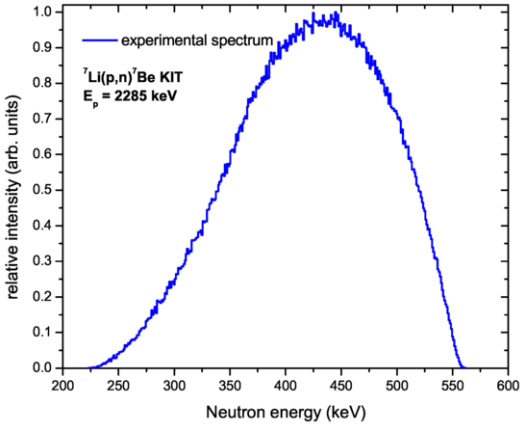

FIG. 110: Experimental energy distribution (blue line) for the second neutron irradiation around 426 keV.

AMS is a destructive technique. The measured isotope ratios, *e.g.* for ^{235}U(n,γ) the isotope ratio ^{236}U/^{235}U, gives directly the product of cross section times neutron fluence. A small fraction of the pellets was used for the AMS measurements of the ^{236}U /^{235}U isotope ratios without any pretreatment, i.e. for the direct measurement of ^{235}U(n,γ). The larger fraction of the samples was dissolved in nitric acid and a spike of ^{233}U (IRMM-058) and ^{242}Pu (IRMM-085) was added. ^{239}Pu together with ^{242}Pu was then separated from the U bulk material. Again ^{236}U was quantified for ^{235}U(n,γ) and for ^{238}U$(n,\gamma)^{239}$U, the decay product ^{239}Pu was measured relative to the well-known ^{242}Pu spike as isotope ratio ^{239}Pu/^{242}Pu. U and Pu oxide samples were produced as sputter targets and were measured by AMS in about 10 different beam times (for more details see [238]).

The cross-section values were directly calculated from the neutron fluence and the isotope ratio measurements obtained by AMS. An important aspect was the stability of the measured ^{236}U/^{235}U isotope ratio because the intrinsic ^{236}U content was comparable to the additional ^{236}U signal from the neutron activations. For ^{239}Pu, the natural concentration was negligible compared to the number of ^{239}Pu produced during the neutron activations.

For quantifying and minimizing systematic uncertainties several redundant data were available:

- for ^{235}U$(n,\gamma)^{236}$U, isotope ratios were generated relative to ^{235}U and ^{238}U (certified stoichiometry and isotope ratio ^{235}U/^{238}U; see IRMM, Report EUR 22924 EN, Belgium).
- two U samples were irradiated with thermal (cold) neutrons serving as additional reference samples [238]. Their measured thermal capture value was 102±3 and 101±3 b respectively. Therefore, all measured values for ^{235}U$(n,\gamma)^{236}$U were scaled by 2% in order to reproduce the thermal cross section value of 98.96 b. Final data are listed in Table XXXVI.
- in the case of ^{235}U$(n,\gamma)^{236}$U, AMS of ^{236}U was also performed relative to a ^{233}U spike which confirmed the measured thermal value within 3%.
- in the case of ^{238}U$(n,\gamma)^{239}$U, AMS of ^{239}Pu was performed relative to a ^{242}Pu spike.
- about 10 measurement series were performed to reduce systematic AMS uncertainties.

All data listed (see Table XXXVI) represent cross section values for the experimental neutron energy distribution and are not normalized; i.e. they represent experimental spectrum-averaged cross sections and not Maxwellian-averaged cross sections (MACS). The neutron energy distribution was calculated applying the program PINO [271] and sensitivity studies were performed to check for variations with slightly changed geometries. These experimental spectra were folded with the ENDF cross section values and those values were then compared with the experimental cross sections obtained via AMS. The final cross-section data rely on the ^{197}Au$(n,\gamma)^{198}$Au capture cross section value for the corresponding neutron energies. However, as the very same samples were used for both capture reactions, for ^{235}U and ^{238}U, their neutron fluence was the same, and the ratio of the reaction cross section is equivalent to the AMS ratios ^{239}Pu/^{238}U (=^{239}U/^{238}U) over ^{236}U/^{235}U, i.e. the neutron fluence cancels. Therefore, these isotope ratios will directly represent the ratio of the cross sections, independent of Au: (^{239}Pu/^{238}U) / (^{236}U/^{235}U) translates into the

TABLE XXXV: Critical masses in kg for four cross-section libraries, calculated using MCNP. *k_∞ is given when there is no critical mass.

Isotope	Density (g/cm3)	ENDF/B-VII.1 (kg)	ENDF/B-VII.0 (kg)	JENDL-4.0 (kg)	JEFF-3.1 (kg)
U-230	18.5209	11.2	-	11.2	-
U-231	18.5646	12.1	-	12.1	-
U-232	18.6822	6.14	6.90	6.14	3.65
U-233	18.7621	15.6	15.6	15.6	15.3
U-234	18.8431	128.0	128.0	111.6	127.4
U-235	18.9231	46.6	46.6	47.0	47.12
U-236	18.8853	0.710	0.712	0.662	0.710
U-237	18.9655	225.6	256.5	237.2	75.7
U-238	19.0457	0.306*	0.306*	0.307*	0.306*
Pu-236	19.3668	4.96	7.59	4.97	7.59
Pu-238	19.5312	8.44	10.0	8.91	8.36
Pu-239	19.6135	10.2	10.2	10.2	10.2
Pu-240	19.6957	39.9	38.0	41.9	33.8
Pu-241	19.7780	13.1	13.1	11.8	12.2
Pu-242	19.8602	88.9	88.8	75.9	63.5
Pu-244	20.0247	115.4	250.5	115.4	250.5
Pu-246	20.1893	0.803*	0.814*	0.802*	0.815*
Pu-247	19.4491	4.97	3.18	4.97	3.18
Pa-229	15.2025	37.4	-	37.4	-
Pa-230	15.2691	36.3	-	36.3	-
Pa-231	15.3355	0.925*	0.925*	0.956*	0.924*
Pa-232	15.4021	113.6	104.7	113.59	104.93
Pa-233	15.4686	0.221*	0.221*	0.226*	0.221*
Th-231	11.6764	0.762*	-	0.762*	0.762*
Th-232	11.7270	0.063*	0.061*	0.063*	0.063*
Th-234	11.8284	0.025*	0.033*	0.025*	0.025*
Th-237	11.4738	0.918*	3460	0.919*	0.919*
Th-238	11.5244	0.361*	0.130*	0.360	0.360
Th-239	11.5751	30840.	2832.	30840.	-
Np-234	20.2171	5.40	-	5.40	-
Np-235	20.3035	8.06	11.96	8.06	12.03
Np-236	20.3901	10.8	6.91	10.8	15.8
Np-237	20.4762	58.7	58.7	58.7	63.8
Np-238	20.5621	19.9	24.2	19.9	12.8
Np-239	20.6487	10.8	36.5	10.8	38.7
Am-240	13.6033	11.1	-	11.1	-
Am-241	13.6601	70.2	69.9	61.3	57.2
Am-242g	13.7171	10.9	10.9	12.4	13.7
Am-242m	13.7171	11.6	11.6	12.8	12.5
Am-243	13.4071	152.	152.	191.	224.
Am-244	13.4623	-	-	31.8	-
Cm-240	13.2961	11.1	-	11.1	23.6
Cm-241	13.3517	6.99	9.82	6.99	9.82
Cm-242	13.4071	14.5	376.	14.5	17.9
Cm-243	13.4631	5.95	11.9	5.95	6.97
Cm-244	13.5181	27.1	27.7	27.1	34.0
Cm-245	13.5731	11.8	12.7	11.8	12.6
Cm-246	13.6291	87.7	48.6	87.7	49.0
Cm-247	13.6841	7.47	8.25	7.47	7.07
Cm-248	13.7401	98.2	41.0	98.2	68.4
Cm-250	13.8501	1865.	23.5	1865.	23.6
Bk-245	14.7801	82.4	-	82.4	-
Bk-246	14.8406	7.77	-	7.79	-
Bk-247	14.9010	318	-	318	73.3
Bk-249m	15.0219	155.	188.	155.	211.
Bk-250m	15.0824	28.2	6.01	28.2	6.01
Cf-246	14.9271	4.62	-	4.62	-
Cf-248	15.0486	21.9	-	21.9	-
Cf-249	15.1094	6.02	7.2	6.02	5.8
Cf-250	15.1702	19.1	6.60	19.2	8.88
Cf-251	15.2301	12.5	5.49	12.5	5.47
Cf-252	15.2901	3.35	5.68	3.35	5.70
Cf-253	15.3510	42.3	-	42.3	-
Cf-254	15.4101	7.90	4.29	7.90	4.27
Es-251	8.7730	58.0	-	58.0	-
Es-252	8.8080	9.56	-	9.56	-
Es-253	8.8430	209.	-	209.	182.
Es-254	8.8781	13.00	9.89	13.00	9.89
Es-255	8.9131	2526.	11.3	2526.	11.3
Fm-255	7.2411	14.8	10.1	14.8	10.2

cross-section ratio $\sigma_{^{238}U(n,\gamma)}/\sigma_{^{235}U(n,\gamma)}$. For 25 keV ($\approx$ Maxwell-Boltzmann) an AMS ratio of 0.60±0.05 was obtained, in agreement with ENDF (0.60, see Tab. XXXVI) [238]. For 426 keV, the measured ratio was 0.65±0.05, compared to the ENDF value of 0.60. We note, though, that changing the Au cross section value for 25 keV to the value used for astrophysics-Maxwellian would also lower the U-5 and U-8 values for this energy by ≈ 6-8%, worsen-

TABLE XXXVI: AMS data for ^{235}U and ^{238}U(n,γ): All experimental data were compared to the spectrum-averaged data, i.e. spectrum folded with the ENDF/B-VII.1 (=VII.0) cross section values. The experimental cross sections were obtained from a neutron fluence calculated from ^{197}Au(n,γ) data from ENDF (see [238]).

Energy	^{235}U(n,γ)	ENDF/B-VII.0	Exp./ENDF/B-VII.0	^{238}U(n,γ)	ENDF/B-VII.0	Exp./ENDF/B-VII.0
25 keV	(0.646±0.040) b	0.679 b	0.95±0.06	(0.386±0.025) b	0.408 b	0.95±0.06
426 keV	(0.167±0.013) b	0.182 b	0.92±0.08	(0.108±0.004) b	0.109 b	0.99±0.04

ing the agreement between ENDF and the measurement. For 25 keV the AMS data have uncertainties of this difference (6%) and we note the Au capture cross section is not established as a standard below 200 keV. Nevertheless the ENDF Au capture data used here are consistent with the recent data from n_TOF for the ^{197}Au$(n,\gamma)^{198}$Au capture cross section in this energy range [235].

In summary, the new AMS measurements produce neutron capture data with uncertainties between 3 and 8% [238]. They provide in general somewhat lower values than ENDF/B-VII.0 (=VII.1), however, still within their 1-σ uncertainty: for the 25 keV energies, both ^{235}U(n,γ) and ^{238}U(n,γ) are 5% lower than ENDF; for the 426 keV broad neutron energy source we find the AMS data about 8% lower for ^{235}U(n,γ) and see an excellent agreement in the case of ^{238}U(n,γ) where the measurement has highest accuracy. (On the other hand, Palmiotti's reaction rate data testing shown in Kahler's paper [8], for a fast reactor spectrum, suggests an experimental ^{235}U(n,γ) value *higher* than ENDF/B-VII.1=VII.0).

E. Reaction Rates in Critical Assemblies

In our previous ENDF/B-VII.0 papers [1, 3] we described the use of LANL reaction-rate data for fission, capture, and $(n,2n)$ reactions, measured in fast critical assemblies, for integral testing of our ENDF cross sections and our MCNP simulation code. We have repeated some of these same comparisons throughout this paper, see Figs. 48,52,56,57,58,93.

In this section we first describe integral reaction rate validation testing for *fission*. After this we summarize observations from data testing on *capture* and *(n,2n)* reaction rates. We augment observations based on LANL radiochemical measurements in critical assemblies with those from Palmiotti, as described in Kahler's companion paper [8], based on the PROFIL measurements in the CEA PHENIX fast reactor. Both the PROFIL data and the LANL critical assembly data are dominated by fast neutrons in the keV-MeV region.

Summary of fission reaction rate testing:

For the reaction rates for fission at the center of various Los Alamos fast critical assemblies, we present our calculated results using ENDF/B-VII.1 data, in ratio to the ^{235}U fission rate. Such fission rate ratios are known as spectral indices, and when the numerator is for a threshold fissioner, such as ^{238}U or ^{237}Np, the ratio is a measure of the hardness of the neutron spectrum within the assembly. For example, the U238f/U235f spectral index is higher at the center of Jezebel (0.21) than at the center of Godiva (0.16), reflecting a hotter neutron spectrum in a plutonium assembly compared to a HEU assembly. Table XXXVII compares our calculated spectral indices with measured data. The measurements are typically made using either fission chambers that detect the recoiling fission fragments, or with activation methods that count fission products using radiochemical methods (the former method being more precise).

Comparison between calculation and measurement provides a test of the cross sections and of the critical assembly neutron spectrum (and its energy dependence) as calculated by MCNP. It is evident from Table XXXVII that the calculated values agree with measurement very well, often within the (small) experimental uncertainties quoted. The results for VII.1 are almost identical to those for VII.0, except for the assemblies involving ^{233}U where the VII.1 calculated spectral indices better agree with data. But in some assemblies the U238f/U235f spectral indices are calculated 2-4% low. Since these cross sections in the fast range are thought to be accurate to about 1% or better, this discrepancy is hard to understand. A possible explanation is that it reflects deficiencies in the calculated neutron spectrum in the assembly, the calculated spectrum being possibly too soft - and since ^{238}U has a fission threshold of about 1 MeV, such a deficiency would lead to an under predicted spectral index. This would point to future work needed to improve the cross sections that influence the assembly neutron spectrum, such as the inelastic scattering cross sections or the prompt fission spectrum energy dependence. And indeed, recent work on adjusted libraries by Ishikawa and by Palmiotti have studied such modifications to plutonium inelastic cross sections and to the PFNS to better reproduce these spectral index data.

Additional fission reaction rate comparisons are made in Kahler's companion paper [8], showing results from Barr *et al.* (LANL) measured at two locations in the Flattop-25 critical assembly (also, see Table XXXVII), from the Russian fast reactor benchmark FUND-IPPE-RR-MULT-RRR-01, and from the CEA COSMOS experiment. The center location of the Flattop-25 assembly has a neutron spectrum hardness (238f/235f=0.149) similar to the Russian fast reactor value (238f/235f=0.165), but COSMOS has a softer spectrum (238f/235f=0.042). In some cases we see consistency between the feedback from fission-rate vali-

TABLE XXXVII: Comparison of calculated spectra indices for ENDF/B-VII.1 with measured values in the center of various Los Alamos critical assemblies. U238f/U235f refers to the ^{238}U fission rate divided by the ^{235}U fission rate, *etc.* Because ^{238}U and ^{237}Np are threshold fissioners, the spectral indices for these isotopes (in ratio to ^{235}U) measure the hardness of the neutron spectrum in the assembly Exp-A refers to experimental data as documented in the CSEWG Fast Reactor Benchmark Compilation, BNL 19302 (June 1973); Exp-B refers to the same measurements, but as reanalyzed by G. Hansen, one of the lead experimentalists, and transmitted to R. MacFarlane in 1984. The C/E ratios are based on the Hansen values where available.

Assembly	Quantity	U238f/U235f	Np237f/U235f	U233f/U235f	Pu239f/U235f
Godiva	Calc	0.1579	0.8301	1.5687	1.3823
(HMF001)	Exp-B	0.1643 ±0.0018	0.8516±0.012		1.4152 ± 0.014
	Exp-A	0.1642 ±0.0018	0.837 ±0.013	1.59±0.03	1.402±0.025
	Calc/Exp	C/E=0.9610	C/E=0.9747	C/E=0.9866	C/E=0.9768
Jezebel	Calc	0.2085	0.9708	1.5561	1.4242
(PMF001)	Exp-B	0.2133 ±0.0023	0.9835 ±0.014		1.4609 ± 0.013
	Exp-A	0.2137 ±0.0023	0.962 ±0.016	1.578 ±0.027	1.448 ±0.029
	Calc/Exp	C/E=0.9775	C/E=0.9871	C/E=0.9861	C/E=0.9749
Jezebel-23	Calc	0.2111	0.9970		
(UMF001)	Exp-B	0.2131 ±0.0026	0.9970 ±0.015		
	Exp-A	0.2131 ±0.0023	0.977 ±0.016		
	Calc/Exp	C/E=0.9906	C/E=1.000		
Flattop-25	Calc	0.1438	0.7693	1.5674	1.3586
(HMF028)	Exp-B	0.1492 ±0.0016	0.7804 ±0.01	1.608 ±0.003	1.3847 ±0.012
	Exp-A	0.149 ±0.002	0.76 ±0.01	1.60 ±0.003	1.37 ±0.02
	Calc/Exp	C/E=0.9638	C/E=0.9858	C/E=0.9748	C/E=0.9812
Flattop-Pu	Calc	0.1767	0.8521		
(PMF006)	Exp-B	0.1799 ±0.002	0.8561 ±0.012		
	Exp-A	0.180 ±0.003	0.84 ±0.01		
	Calc/Exp	C/E=0.9822	C/E=0.9953		
Flattop-23	Calc	0.1882	0.9128		
(UMF006)	Exp-B	0.1916 ±0.0021	0.9103 ±0.013		
	Exp-A	0.191 ±0.003	0.89 ±0.01		
	Calc/Exp	C/E=0.9823	C/E=1.0027		

TABLE XXXVIII: MCNP calculations for ENDF/B-VII.1 of various $(n,2n)$ and (n,γ) reaction rates in ratio to the ^{239}Pu fission rate, at the center of Jezebel and of Flattop-Pu. The only measurements available (Barr, 1971) are for the ^{241}Am capture rate creating the ground state of ^{242}Am, which then decays to curium with a branching ratio of 0.827 (this factor is included into the tabulated calculated values below). Data at other positions in Flattop-Pu are compared with calculations in Fig. 93.

Assembly	Quantity	^{239}Pu$(n,2n)$/ ^{239}Pu(n,f)	^{239}Pu(n,γ)/ ^{239}Pu(n,f)	^{241}Am$(n,2n)$/ ^{239}Pu(n,f)	^{241}Am$(n,\gamma)^{242}$Cm/ ^{239}Pu(n,f)
Jezebel	Calc	0.0021	0.033	0.0007	0.1418
	Exp				0.1486
Flattop-Pu	Calc	0.00184	0.044	0.0006	0.1849
	Exp				0.1847

dation testing from these two sets of experiments (*e.g.* they point to the accuracy of the ^{237}Np, ^{233,235,238}U, and ^{239}Pu fission evaluations, and they suggest ^{236}U fission is evaluated low). However, for other cases these experiments tend to provide discrepant feedback as is the case for ^{238}Pu, $^{240-242}$Pu and ^{241}Am fission rates. Additional comparisons have been made by Capote *et al.* [123] of averaged fission cross sections within reference neutron spectra - both the ^{235}U thermal spectrum from VII.0=VII.1, and the ^{252}Cf spectrum as evaluated by Mannhart for the IAEA's IRDF-2002 dosimetry evaluated file. For ^{235,238}U, ^{237}Np, and ^{239}Pu fission in ENDF/B-VII.1 the reported agreement with the measurements is excellent, better than 1-2%.

Summary of (n,γ) and (n,2n) reaction rate testing:

In Table XXXVIII we provide some other calculated reaction rates in ratio to the ^{239}Pu fission rate, at the center of Jezebel (a sphere of plutonium) and of Flattop-Pu (a smaller plutonium sphere made critical by a ^{238}U reflector shell. Rates are given for $(n,2n)$ reactions and for (n,γ) reactions. Most of these values are unmeasured, except for the ^{241}Am capture rate to the ^{242}Am ground state that is then measured as curium following its beta decay. The agreement between calculation and experiment here is fairly good (given that capture cross sections are known less well than fission cross sections) - 5% for Jezebel and less than 1% for Flattop-Pu; comparisons at other locations in critical assemblies with softer neutron spectra can be seen in Fig. 93. We provide calculated values for the other rates in XXXVIII as predictions, in the hope that future measurements can be made in fast critical assemblies to test our cross sections.

The integral feedback on actinide reaction rates in ENDF/B-VII.1 (compared to VII.0) can be summarized in the **fast** neutron range, based on comparisons of simulations to the LANL radiochemical (RC) critical assembly data in Figs. 48,52,56,57,58,93, the PROFIL data (from PHENIX, a fast reactor with a spectral index 238f/235f=0.027) [8] , and Wallner AMS data as follows:

- ^{235}U(n,γ) may be a few percent low according to PROFIL, but the Wallner 426 keV broad neutron source AMS spectrometry data (*i.e.* which are for similar neutron energies) suggests it may be high instead. Thus we may have contradictory feedback.
- ^{236}U(n,γ) VII.1 is improved v. VII.0 according to LANL RC data, see Fig. 52.
- ^{237}U(n,f) VII.1 is improved v. VII.0 according to LANL RC data, see Fig. 56.
- ^{238}U(n,γ) VII.1=VII.0 is fairly accurate according to LANL RC (Fig. 58), PROFIL, and Wallner AMS data.
- ^{237}Np(n,γ) VII.1 is perhaps 6% low according to PROFIL data, but VII.1 appears to be accurate when comparing to LANL RC data, see Fig. 48.
- ^{238}Pu(n,γ) VII.1 is improved v. VII.0 according to PROFIL, but still perhaps 10% or more too high.
- ^{239}Pu(n,γ) VII.1=VII.0 is perhaps 8–9% too low according to PROFIL. This is important and needs further study.
- ^{239}Pu$(n,2n)$ VII.1=VII.0 may need to rise more quickly from threshold according to PROFIL. See additional considerations in Ref. [257].
- ^{240}Pu(n,γ) VII.1 (and VII.0) are perhaps 4–5% too low according to PROFIL.
- ^{241}Pu(n,γ) VII.1 (and VII.0) are perhaps 5% too low according to PROFIL.
- ^{242}Pu(n,γ) VII.1 is improved according to PROFIL, whereas VII.0 was 12 % high.
- ^{241}Am(n,γ) VII.1 is accurate according to LANL RC (Fig. 93) and PROFIL data.
- ^{243}Am(n,γ) VII.1 is improved according to PROFIL and LANL RC data (Fig. 97), whereas VII.0 was 17 % low.

The PROFIL experiments also gave feedback on capture cross sections on fission products in a fast neutron spectrum. This feedback is summarized in Kahler's paper [8].

F. 14 MeV Neutron Transmission

In a previous paper [6] Steven van der Marck presented extensive data testing results that show comparisons of MCNP simulation predictions that use our ENDF/B-VII.0 cross sections and measured data, for neutron transmission (shielding) benchmarks. Also, our

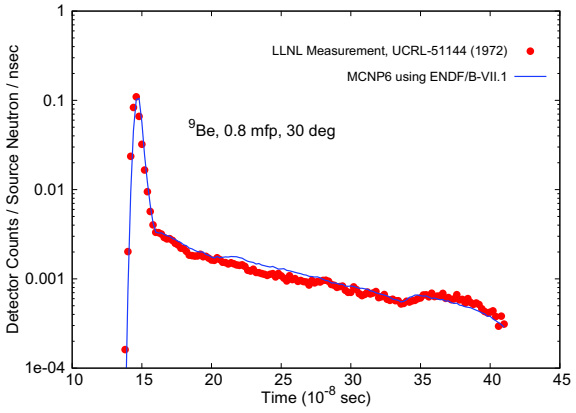

FIG. 111: Simulation of 14 MeV neutron transmission through 15 cm Be, at 30 degrees [6].

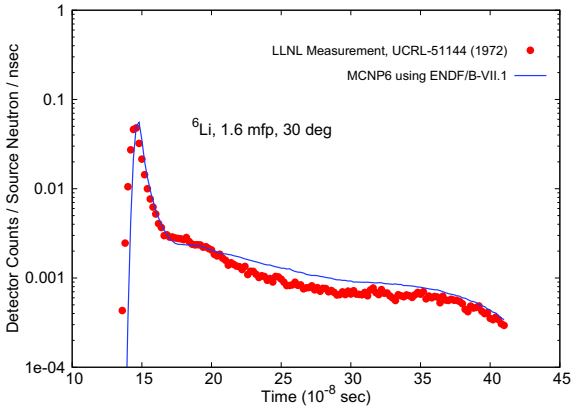

FIG. 112: Simulation of 14 MeV neutron transmission through 1.6 mfp ^{6}Li at 30 degrees [6].

ENDF/B-VII.0 paper [1] provided some illustrative comparisons for a few cases, with particular focus on Livermore's pulsed sphere measurements. Here, we give illustrative examples for these same cases – ^{235,238}U, ^{239}Pu, ^{6}Li and ^{9}Be). We show ^{6}Li and ^{9}Be because these evaluations have changed from VII.0 to VII.1, though no changes are observable in the figures shown here because the changes were all focused at lower energies.

Numerous high-energy pulsed-sphere experiments have been performed in which small, medium, and large spheres of 32 different materials were pulsed with a burst of high-energy (14 MeV) neutrons at Lawrence Livermore National Laboratory's ICT (Insulated Core Transformer) accelerator facility. Measured time-dependent neutron fluxes at collimated detectors located at a distance of 7 - 10 meters provide a benchmark by which various neu-

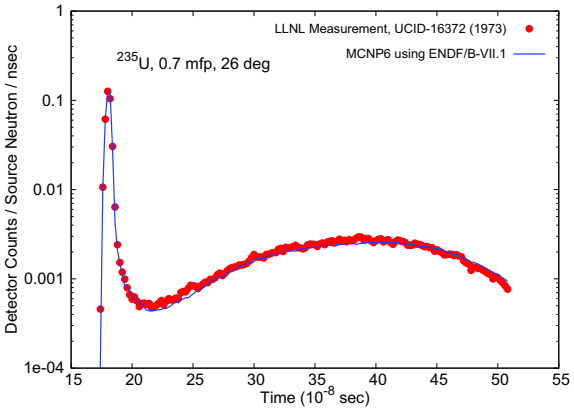

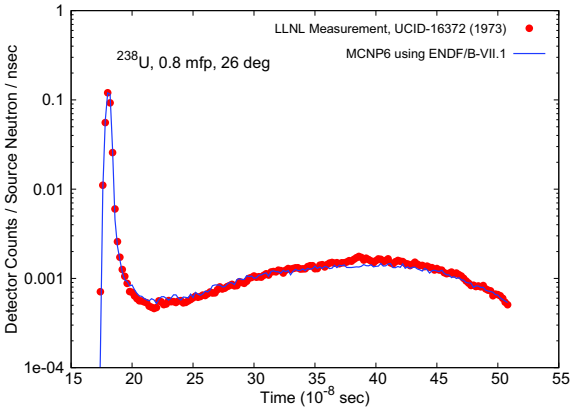

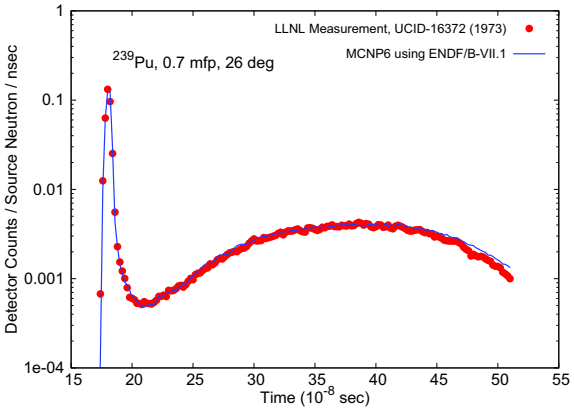

FIG. 113: Comparison of MCNP simulated results of 14 MeV neutron transmission in Livermore's pulsed spheres, using ENDF/B-VII.1 data for the 0.7 mfp spheres of ^{235}U, ^{238}U, and ^{239}Pu. The experiment used a NE-213 detector biased at 1.6 MeV and located 9.455 m along the 26 degree flightpath. Results using ENDF/B-VII.0 are indistinguishable.

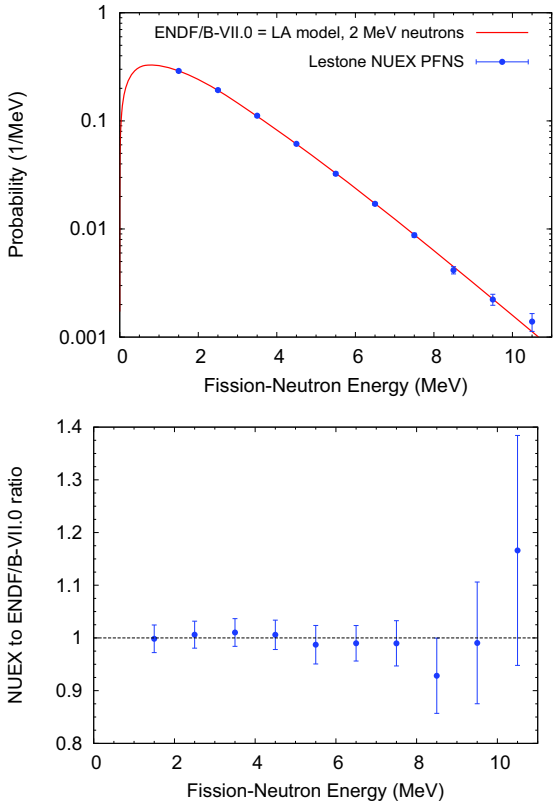

FIG. 114: Comparison of measured 2 MeV n + ^{239}Pu prompt fission neutron spectrum (PFNS) from a NUEX underground nuclear explosion experiment, with ENDF/B-VII.1=VII.0 (Madland's Los Alamos model analysis). The NUEX data are relative; they have been normalized to the ENDF/B-VII.1 value at 1.5 MeV. The upper panel shows the spectra; the lower panel shows the ratio to ENDF.

tron transport codes and cross-section libraries may be evaluated. Fig. 111 and Fig. 112 show results for 14 MeV neutron transmission on Be and on ^{6}Li. Results for ^{235}U, ^{238}U and ^{239}Pu can be seen in Fig. 113.

In these figures the peak on the left hand side corresponds to the transmission of the 14 MeV source neutrons; the broad peak further right (lower energies) corresponds to the neutrons created through compound nucleus and fission mechanisms. The reasonably good agreement in the region to the right of the 14 MeV peak in the minimum region ($E_n \approx 8$ - 12 MeV) associated with preequilibrium and inelastic scattering processes is directly related to the cross section improvements in the fundamental ENDF/B-VII.0 data (carried over to ENDF/B-VII.1 for ^{235,8}U and ^{239}Pu) [3]. In these figures we show only VII.1 results because they are indistinguishable from VII.0 results. See Ref. [1] for more details.

More comprehensive benchmarking against the larger set of 14 MeV transmission and shielding experimental data [6] will have to wait for a future publication.

TABLE XXXIX: Prompt fission-neutron energy spectrum (PFNS) for 2 MeV neutron induced fission of ^{239}Pu from a Los Alamos NUEX underground nuclear test experiment (referred to here as LANL-NUEX-1); these relative emission probabilities are given (normalized to unity at the lowest outgoing energy, 1.5 MeV), as well as scaled by 0.2892. The corresponding ENDF/B-VII.1=VII.0 values from Madland's Los Alamos model are given for comparison, as is the ratio of the NUEX to ENDF/B-VII.1 data. All uncertainties given are 1 σ.

Neutron energy (MeV)	NUEX Relative emission (dimensionless)	NUEX Probability (1/MeV)	ENDF/B-VII.1 (1/MeV)	Ratio NUEX ÷ENDF/B-VII.1 (dimensionless)
1.5	1.000 ± 0.026	0.2892 ± 0.0076	0.2897	0.998 ± 0.026
2.5	0.666 ± 0.017	0.1926 ± 0.0049	0.1914	1.006 ± 0.026
3.5	0.386 ± 0.010	0.1116 ± 0.0029	0.1105	1.010 ± 0.026
4.5	0.212 ± 0.006	0.0613 ± 0.0017	0.0609	1.006 ± 0.028
5.5	0.112 ± 0.004	0.0324 ± 0.0012	0.0328	0.987 ± 0.035
6.5	0.059 ± 0.002	0.01706± 0.00058	0.0172	0.990 ± 0.034
7.5	0.0303 ± 0.0013	0.00876 ± 0.00038	0.00885	0.990 ± 0.042
8.5	0.0144 ± 0.0011	0.00416 ± 0.00032	0.00448	0.930 ± 0.071
9.5	0.0077 ± 0.0009	0.00223 ± 0.00026	0.00225	0.990 ± 0.116
10.5	0.0048 ± 0.0009	0.00139 ± 0.00026	0.00119	1.239 ± 0.232

G. PFNS from Underground Experiment

Los Alamos has released data from a prompt fission neutron spectrum (PFNS) measurement for 2 MeV neutrons on ^{239}Pu, obtained from an underground nuclear explosion experiment (Lestone [272]) prior to the end of testing. These fundamental physical data should be of interest to the nuclear science and technology community in various applications, including nuclear energy research. The value of these data lies in the experiment's very high neutron fluence, enabling the spectra to be determined with statistical uncertainties that are much smaller than can be obtained in laboratory experiments. In this section we present these data and use them to assess the accuracy of the ENDF/B-VII.1=VII.0 PFNS data that come from Madland's Los Alamos Model.

The neutron experiment (NUEX) was a common diagnostic on nuclear tests conducted at the Nevada Test Site (NTS). In these experiments neutrons from a device pass up a collimated line of sight, and in the case of a Faraday cup NUEX, the neutrons pass through a thin CH_2 foil. Some of these neutrons interact with the nuclei in the foil, generating light charged particles (predominately protons) which are collected in a Faraday cup. The time dependence of the Faraday cup current is a measure of the energy spectrum of the neutrons that leak from the device. A key feature of the NUEX experiment is that the line of sight collimators are configured with a field of view that allows neutrons from the fission source region to pass to the CH_2 foil, while obscuring neutrons that scatter in the surrounding materials. With good device models and accurate neutron-transport codes, the leakage spectrum can be converted into a prompt fast-neutron-induced fission-neutron energy spectrum (PFNS) from 1 to 11 MeV.

This has been done for one of our underground experiments where the NUEX data were of a particularly high quality. The fission-neutrons in the device were produced by fission events induced by neutrons over a broad range of energies. We list the inferred 2 MeV n + ^{239}Pu prompt fission-neutron spectrum (PFNS) in Table XXXIX for outgoing neutron energies from 1.5 to 10.5 MeV, in 1-MeV steps. The listed values represent a shape measurement of the fission-neutron emission probability at the quoted outgoing neutron energies and are not the integrals over 1-MeV wide bins. The quoted relative emission probabilities are all relative to the probability of emitting 1.5 MeV neutrons. The relative emission probabilities are scaled by 0.2892 to obtained a match to the absolute emission probabilities per MeV for the Los Alamos fission model ^{239}Pu (2 MeV n,f) neutron spectrum. We are here most interested in the shape of the PFNS and the (relatively small) uncertainties presented in Table XXXIX are associated with the uncertainties of the shape measurement. Nevertheless, we have been able to assess the absolute magnitude of this spectrum and we obtain values essentially the same as those in the table, column 3. The systematic error in the absolute emission probabilities is 8 % – which is a 100% correlated sytemmatical uncertainty over the emission energy range.

The measured data and ENDF/B-VII.1 are compared in Fig. 114. The measured uncertainties are seen to be small, and significantly smaller than have been obtained in most PFNS laboratory experiments. It is evident that the agreement between the NUEX PFNS data and ENDF/B-VII.1 is remarkably good, and this provides a validation of the Madland model above about 1.5 MeV outgoing energy. (But more work is needed to understand this validation as it appears to be discrepant with the dosimetry activation testing described in Sec. X A for LANL's Jezebel and for IPPE/Russia's fast Pu reactor as described in Kahler's companion paper) [8]. In an underground nuclear explosion experiment the neutron fluence is so large that most of the background signals that affect standard laboratory experiments do not apply. When extracting the PFNS from LANL-NUEX-1 the only backgrounds of importance are associated with how 14 MeV neutrons down scatter in the device and complexities associated with how these neutrons interact with the NUEX detector. For neutron energies less than

7 MeV these backgrounds are small compared to the signals from the 2 MeV incident fission neutrons. However, backgrounds from these 14 MeV neutrons (and their uncertainties) increase significantly with increasing neutron energy above 7 MeV and limit meaningful PFNS extraction to outgoing energies less than 11 MeV (and this is why the data in Fig. 114 show increasing uncertainties above 8 MeV).

The measured data have not been extracted at lower emission energies below 1.5 MeV so the data here do not provide a validation of the low emission energy ENDF data below 1.5 MeV. Thus, they do not provide sufficient information to resolve questions raised by Maslov regarding whether there might be additional PFNS neutrons emitted below 1 MeV as compared to VII.1.

Future work is planned to extract similar data from other historic NTS events: this will be important for determining whether indeed the results presented here are repeatable. Such studies will also help assess if any additional (unidentified, to date) sources of systematic error exist in these measurements. Finally, we acknowledge the difficulty that the broader community faces when such data are presented, since details of the experiment and analysis method cannot be described in the open literature. We are, however, making this detailed analysis [272] available to colleagues at Livermore for peer review.

H. Integral Quantities in ENDF/B-VII.1

The low-energy neutron cross section values are often influenced by the contributions from resolved and unresolved resonance regions. To estimate these contributions across the whole ENDF/B-VII.1 library's range of materials and provide additional insights on the data quality for nuclear reactor and astrophysics applications, we have selected thermal and Maxwellian-averaged cross sections, resonance integrals and Westcott factors [35, 273] for study. ENDF/B-VII.0 [1] and ENDF/B-VII.1 evaluated neutron cross sections were Doppler broadened using the code PREPRO [274] with the precision of 0.1%. These reconstructed and linearized data were used to calculate selected quantities using the definite integration method [172, 275].

Thermal cross sections for neutron capture and fission are shown in Figs. 115, 116 and Table XL. Using visual inspection we notice the deviations for light and medium nuclei and minor actinides evaluations. These differences, in the low- and medium-Z region, are attributed to the lack or insufficient experimental data for ^{10}B, ^{17}O, ^{43}Ca, ^{86}Kr, ^{110}Pd, and the recent re-evaluation of ^{90}Zr. In the actinide region, deviations are due to new evaluations from the JENDL-4.0 [9]. Resonance integrals for neutron capture and fission were calculated for 0.5 eV - 20 MeV incident neutron energy range and shown in Fig. 117, 118. Several data outliers in this case could be traced to the lack of measurements and incomplete overlap of experimental and theoretical data for ^{17}O, ^{103}Ru, ^{166m}Ho

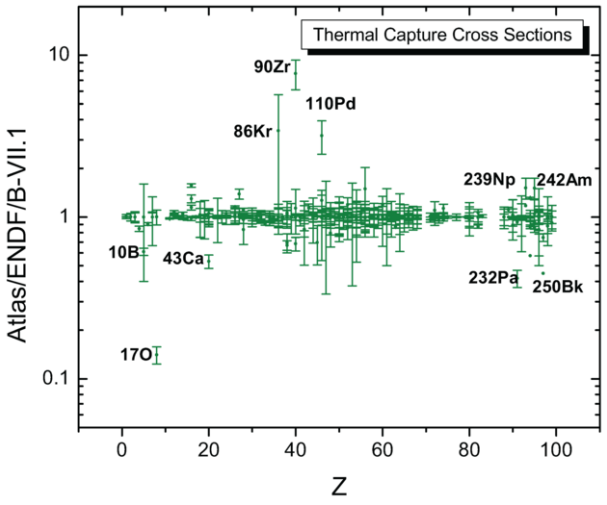

FIG. 115: Ratio of Atlas of Neutron Resonances [35] and ENDF/B-VII.1 thermal neutron capture cross sections.

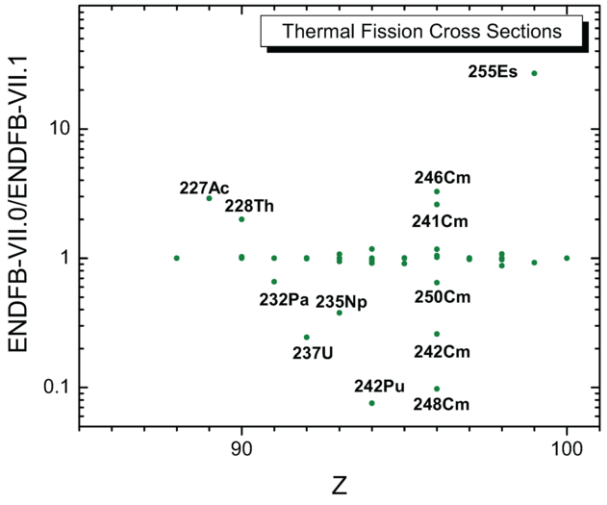

FIG. 116: Ratio of ENDF/B-VII.0 and ENDF/B-VII.1 thermal neutron fission cross sections. Where discrepancies are evident, VII.1 values are thought to be more accurate.

and ^{46}Ca, ^{135}Cs, ^{204}Hg, respectively. However, there are neutron capture cross section deficiencies in the keV region of energies for ^{30}Si and ^{208}Pb evaluations. In the ^{30}Si case, the evaluators used the higher value to tune the evaluation, while the IUPAC (International Union of Pure and Applied Chemistry) constants for NAA (Neutron-Activation Analysis) support the lower value. The same trend is observed for the MACS data in Fig.119. The data in JENDL-4.0 and JEFF-3.1 libraries are the same or worse.

Maxwellian-averaged cross sections (MACS) play an important role in power reactor developments and *s*-process nucleosynthesis calculations [276]. The slow-neutron capture is mostly responsible for element formation in stars from ^{56}Fe to ^{209}Bi.

TABLE XL: Thermal neutron fission and capture cross sections of actinoid nuclides from Atlas of Neutron Resonances [35] and ENDF/B-VII.1, ENDF/B-VII.0 [1], JENDL-4.0 [9] libraries ([a] No resonance parameters measured).

Material	Fission				Capture			
	Atlas (barns)	VII.1 (barns)	VII.0 (barns)	JENDL-4.0 (barns)	Atlas (barns)	VII.1 (barns)	VII.0 (barns)	JENDL-4.0 (barns)
^{227}Th[a]	2.020E+2±1.300E+1	2.021E+2	2.021E+2	2.021E+2		4.052E+2	1.536E+3	4.052E+2
^{228}Th	<0.3	1.501E-1	3.001E-1	1.501E-1	1.230E+2±1.500E+1	1.229E+2	1.199E+2	1.229E+2
^{229}Th	3.080E+1±1.500E+0	3.092E+1	3.165E+1	3.092E+1	6.280E+1±6.000E+0	7.056E+1	6.339E+1	7.056E+1
^{230}Th		9.494E-3		9.494E-3	2.290E+1±3.000E-1	2.341E+1	2.309E+1	2.341E+1
^{231}Th[a]		4.001E+1		4.001E+1		1.631E+3		1.631E+3
^{232}Th	5.200E-5±4.000E-5			5.371E-5	7.350E+0±3.000E-2	7.338E+0	7.338E+0	7.338E+0
^{233}Th	1.500E+1±2.000E+0	1.501E+1	1.501E+1	1.501E+1	1.330E+3±5.000E+1	1.291E+3	1.451E+3	1.291E+3
^{234}Th[a]	<0.01	5.002E-3		5.002E-3	1.800E+0±5.000E-1	1.801E+0	1.751E+0	1.801E+0
^{229}Pa[a]		1.000E+0		1.000E+0		3.999E+2		3.999E+2
^{230}Pa[a]	1.500E+3±2.500E+2	1.500E+3		1.500E+3		3.801E+2		3.801E+2
^{231}Pa	2.000E-2±1.000E-3	2.087E-2	2.087E-2	2.365E-2	2.006E+2±2.300E+0	2.007E+2	2.007E+2	2.017E+2
^{232}Pa	1.502E+3±2.800E+1	1.487+3	9.781E+2	1.487E+3	2.460E+2±3.000E+1	5.890E+2	6.514E+2	5.890E+2
^{233}Pa	<0.1			2.502E-6	3.950E+1±1.200E+0	4.252E+1	4.252E+1	3.942E+1
^{230}U[a]	2.500E+1±1.000E+1	2.501E+1		2.501E+1		2.001E+2		2.001E+2
^{231}U[a]	4.000E+2±3.000E+2	2.501+2		2.501E+2		2.001E+1		2.001E+1
^{232}U	7.680E+1±4.800E+0	7.652E+1	7.676E+1	7.652E+1	7.490E+1±1.600E+0	7.539E+1	7.520E+1	7.539E+1
^{233}U	5.291E+2±1.200E+0	5.313E+2	5.313E+2	5.313E+2	4.550E+1±7.000E-1	4.526E+1	4.526E+1	4.526E+1
^{234}U	6.700E-2±1.400E-2	6.702E-2	6.710E-2	6.702E-2	9.980E+1±1.300E+0	1.003E+2	1.009E+2	1.003E+2
^{235}U	5.826E+2±1.100E+0	5.851E+2	5.851E+2	5.851E+2	9.880E+1±8.000E-1	9.869E+1	9.871E+1	9.871E+1
^{236}U	6.600E-2±1.300E-2	4.711E-2	4.711E-2	2.594E-4	5.090E+0±1.000E-1	5.134E+0	5.134E+0	5.123E+0
^{237}U	<0.35	1.702E+0	4.165E-1	1.702E+0	4.430E+2±1.670E+2	4.523E+2	4.755E+2	4.523E+2
^{238}U	3.000E-6	1.680E-5	1.680E-5	1.680E-5	2.680E+0±1.900E-2	2.683E+0	2.683E+0	2.683E+0
^{239}U[a]	1.400E+1±3.000E+0	1.425E+1	1.411E+1		2.200E+1±5.000E+0	2.233E+1	2.057E+1	
^{240}U[a]		1.079E-3	1.079E-3			1.917E+1	1.917E+1	
^{241}U[a]		4.165E-1	4.165E-1			4.761E+2	4.761E+2	
^{234}Np[a]	9.000E+2±3.000E+2	2.001E+3		2.001E+3		1.101E+2		1.101E+2
^{235}Np[a]		5.302E+1	2.000E+1	5.302E+1	1.500E+2±2.000E+0	1.551E+2	1.501E+2	1.551E+2
^{236}Np	3.007E+3±9.000E+1	2.808E+3	3.011E+3	2.808E+3	1.420E+2	1.213E+2	1.259E+2	1.213E+2
^{237}Np	2.000E-2±1.000E-3	2.037E-2	2.037E-2	2.019E-2	1.759E+2±2.900E+0	1.754E+2	1.617E+2	1.781E+2
^{238}Np	2.088E+3±3.000E+1	2.202E+3	2.071E+3	2.202E+3		4.795E+2	4.503E+2	4.795E+2
^{239}Np[a]		2.801E-2		2.801E-2	6.800E+1±1.000E+1	4.501E+1	7.703E+1	4.501E+1
^{236}Pu	1.700E+2±3.500E+1	1.400E+2	1.649E+2	1.400E+2	1.590E+1	2.756E+1	3.123E+1	2.756E+1
^{237}Pu[a]	2.455E+3±2.950E+2	2.296E+3	2.103E+3	2.296E+3		2.001E+2	5.407E+2	2.001E+2
^{238}Pu	1.790E+1±4.000E-1	1.777E+1	1.701E+1	1.777E+1	5.400E+2±7.000E+0	4.129E+2	5.609E+2	4.129E+2
^{239}Pu	7.481E+2±2.000E+0	7.479E+2	7.479E+2	7.474E+2	2.693E+2±2.900E+0	2.707E+2	2.707E+2	2.715E+2
^{240}Pu	5.600E-2±3.000E-2	6.405E-2	6.405E-2	3.620E-2	2.895E+2±1.400E+0	2.876E+2	2.876E+2	2.893E+2
^{241}Pu	1.011E+3±6.200E+0	1.012E+3	1.012E+3	1.012E+3	3.621E+2±5.100E+0	3.630E+2	3.631E+2	3.631E+2
^{242}Pu	<0.2	1.382E-2	1.043E-3	2.436E-3	1.850E+1±5.000E-1	2.127E+1	1.917E+1	1.988E+1
^{243}Pu	1.960E+2±1.600E+1	1.814E+2	1.814E+2		8.700E+1±1.000E+1	8.813E+1	8.813E+1	
^{244}Pu		1.715E-3		1.715E-3	1.700E+0±1.000E-1	1.710E+0	1.831E+0	1.710E+0
^{246}Pu		3.201E-3		3.201E-3		8.003E+1	8.000E+2	8.003E+1
^{240}Am[a]		1.500E+3		1.500E+3		2.801E+2		2.801E+2
^{241}Am	3.200E+0±9.000E-2	3.122E+0	3.139E+0	3.122E+0	5.870E+2±1.200E+1	6.843E+2	6.188E+2	6.843E+2
^{242}Am	2.100E+3±2.000E+2	2.095E+3	2.095E+3	2.421E+3	3.300E+2±5.000E+1	2.190E+2	2.190E+2	3.303E+2
^{242m}Am	6.200E+3±2.000E+2	6.400E+3	6.400E+3	6.401E+3	1.290E+3±3.000E+2	1.231E+3	1.231E+3	1.141E+3
^{243}Am	1.983E-1±4.300E-3	8.134E-2	7.393E-2	8.158E-2	7.510E+1±1.800E+0	8.042E+1	7.511E+1	7.926E+1
^{244}Am[a]	2.300E+3±3.000E+2	2.301E+3	2.301E+3	2.301E+3		6.002E+2	6.002E+2	1.000E+3
^{244m}Am[a]	1.600E+3±3.000E+2	1.601E+3	1.601E+3	1.601E+3		4.001E+2	4.001E+2	6.002E+2
^{240}Cm[a]		3.001E+1		3.001E+1		5.001E+1		5.001E+1
^{241}Cm[a]		1.000E+3	2.601E+3	1.000E+3		2.000E+2	2.504E+2	2.000E+2
^{242}Cm	<5	4.665E+0	3.020E+0	4.665E+0	1.600E+1±5.000E+0	1.913E+1	1.687E+1	1.913E+1
^{243}Cm	6.170E+2±2.000E+1	5.874E+2	6.135E+2	5.874E+2	1.300E+2±1.000E+1	1.314E+2	1.305E+2	1.314E+2
^{244}Cm	1.040E+0±2.000E-1	1.022E+0	1.038E+0	1.022E+0	1.520E+1±1.200E+0	1.524E+1	1.511E+1	1.524E+1
^{245}Cm	2.144E+3±5.800E+1	2.054E+3	2.141E+3	2.054E+3	3.690E+2±1.700E+1	3.470E+2	3.589E+2	3.470E+2
^{246}Cm	1.400E-1±5.000E-2	4.401E-2	1.442E-1		1.220E+0±1.600E-1	1.179E+0	1.312E+0	
^{247}Cm	8.190E+1±4.400E+0	9.474E+1	1.113E+2	9.474E+1	5.700E+1±1.000E+1	5.993E+1	5.693E+1	5.993E+1
^{248}Cm	3.700E-1±5.000E-2	3.366E-1	8.737E-2	3.366E-1	2.630E+0±2.600E-1	2.872E+0	2.445E+0	2.872E+0
^{249}Cm[a]		1.000E+1	1.026E+1	1.000E+1	1.600E+0±8.000E-1	1.601E+0	1.751E+0	1.601E+0
^{250}Cm[a]		2.137E-2	2.089E-3	2.137E-2		8.133E+1	8.536E+1	8.133E+1
^{245}Bk[a]		2.902E+0		2.902E+0	7.460E+2±4.000E+1	1.000E+3		1.000E+3
^{246}Bk[a]		1.801E+3		1.801E+3		7.001E+2		7.001E+2
^{247}Bk[a]		3.702E+0		3.702E+0		1.000E+3		1.000E+3
^{248}Bk[a]		2.001E+3		2.001E+3		8.601E+2		8.601E+2
^{249}Bk		3.970E+0	3.994E+0	3.970E+0		7.110E+2	7.456E+2	7.110E+2
^{250}Bk[a]	9.600E+2±1.500E+2	9.805E+2	9.589E+2	9.805E+2	3.500E+2	7.805E+2	3.533E+2	7.805E+2
^{246}Cf[a]		1.401E+3		1.401E+3		1.701E+3		1.701E+3
^{248}Cf[a]		7.002E+2		7.002E+2		1.700E+3		1.700E+3
^{249}Cf	1.642E+3±3.300E+1	1.673E+3	1.634E+3	1.673E+3	4.970E+2±2.100E+1	5.065E+2	4.966E+2	5.065E+2
^{250}Cf		1.120E+2		1.120E+2	2.034E+3±2.000E+2	2.018E+3	1.612E+3	2.018E+3
^{251}Cf	4.895E+3±2.500E+2	4.939E+3	5.323E+3	4.939E+3	2.850E+3±1.500E+2	2.864E+3	2.863E+3	2.864E+3

TABLE XL: Thermal neutron fission and capture cross sections of actinoid nuclides from Atlas of Neutron Resonances [35] and ENDF/B-VII.1, ENDF/B-VII.0 [1], JENDL-4.0 [9] libraries ([a] No resonance parameters measured).

Material	Fission				Capture			
	Atlas (barns)	VII.1 (barns)	VII.0 (barns)	JENDL-4.0 (barns)	Atlas (barns)	VII.1 (barns)	VII.0 (barns)	JENDL-4.0 (barns)
^{252}Cf	3.200E+1±4.000E+0	3.303E+1	3.218E+1	3.303E+1	2.040E+1±1.500E+0	2.071E+1	2.050E+1	2.071E+1
^{253}Cf	1.300E+3±2.400E+2	1.301E+3	1.136E+3	1.301E+3	1.760E+1±1.800E+0	2.000E+1	3.414E+2	2.000E+1
^{254}Cf[a]		2.001E+0	2.001E+0	2.001E+0	4.500E+0±1.500E+0	4.502E+0	4.502E+0	4.502E+0
^{251}Es[a]		4.303E+1		4.303E+1	1.840E+2±1.500E+1	2.001E+2		2.001E+2
^{252}Es[a]		2.001E+3		2.001E+3		2.001E+2		2.001E+2
^{253}Es		2.502E+0		2.502E+0		1.839E+2	2.012E+2	1.839E+2
^{254}Es[a]	1.970E+3±2.000E+2	2.129E+3	1.967E+3	2.129E+3	2.830E+1±2.500E+0	2.831E+1	2.818E+1	2.831E+1
^{254m}Es	1.826E+3±8.000E+1	2.001E+3		2.001E+3		2.501E+2		2.501E+2
^{255}Es[a]		5.004E-1	1.344E+1	5.004E-1	5.500E+1±1.000E+1	5.500E+1	5.502E+1	5.500E+1
^{255}Fm[a]		3.362E+3	3.361E+3	3.362E+3		2.701E+2	2.601E+1	2.701E+2

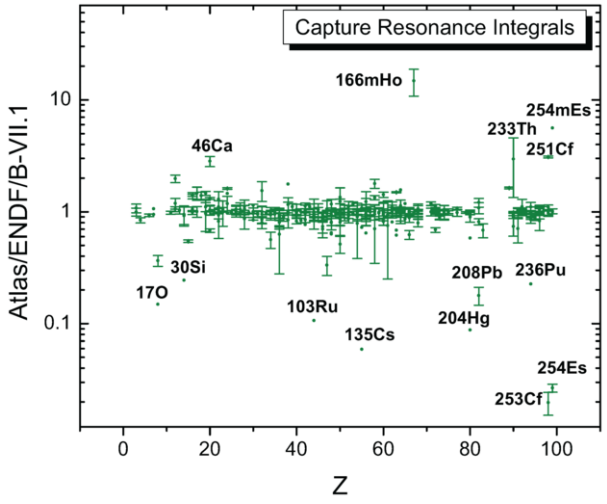

FIG. 117: Ratio of Atlas of Neutron Resonances [35] and ENDF/B-VII.1 neutron capture resonance integrals.

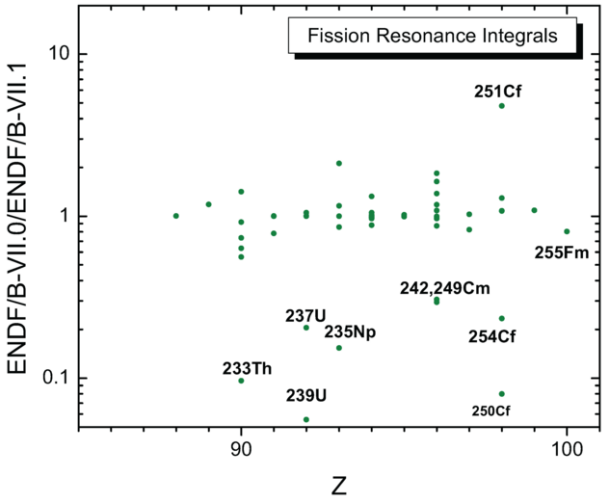

FIG. 118: Ratio of ENDF/B-VII.0 and ENDF/B-VII.1 neutron fission resonance integrals. Where discrepancies are evident, VII.1 values are thought to be more accurate.

A detailed analysis of the Fig. 119 and Table XLI (App. A) data demonstrates the nuclear astrophysics potential of ENDF libraries as a complementary source of evaluated cross sections and reaction rates [273]. There are noticeable differences between KADoNiS [36] and ENDF/B-VII.1 libraries for light and medium nuclei. The ^{1}H deviation is due to differences between center of mass and lab system cross section values, and therefore this is not a discrepancy. The ^{3}He VII.1 value is higher than KADoNiS; it comes from an R-matrix evaluation, see Fig. 4. For ^{28,30}Si, ^{31}P, ^{64}Ni and ^{196}Hg the KADoNiS values are based on a single recent measurement. Due to lack of experimental data theoretical values were adopted for ^{38}Ar, ^{82}Se, ^{115m}Cd, ^{141}Ce, ^{143}Pr and ^{148m,149}Pm. Discrepancies for ^{46,48}Ca and ^{33,36}Si occur in part because of their small isotopic abundances and in consequence the lack of measured data [59]. Figs. 119 and 117 provide an additional proof that ^{31}P and ^{46}Ca data in ENDF/B-VII.1 are not very realistic compare to available benchmarks.

Fig. 120 shows the ratio of capture Westcott factors, and indicates large deviations for ^{239}U and ^{176}Lu between VII.1 and VII.0. These deviations reflect the changes in the ENDF/B-VII.1 library where Westcott factors evolved from 3.997 to 0.989 and from 1.002 to 1.711 for ^{239}U and ^{176}Lu, respectively. The last number agrees well with the recommended value of 1.75 [35]. Smaller deviations as in ^{123}Xe are due to adoption of new evaluations in ENDF/B-VII.1 library and lack of experimental data for this material.

XI. ONGOING WORK

Here we outline some of the major current areas of research in the CSEWG community. These efforts – both experimental and theoretical – are not yet mature enough to impact the new ENDF/B-VII.1 evaluation, but they

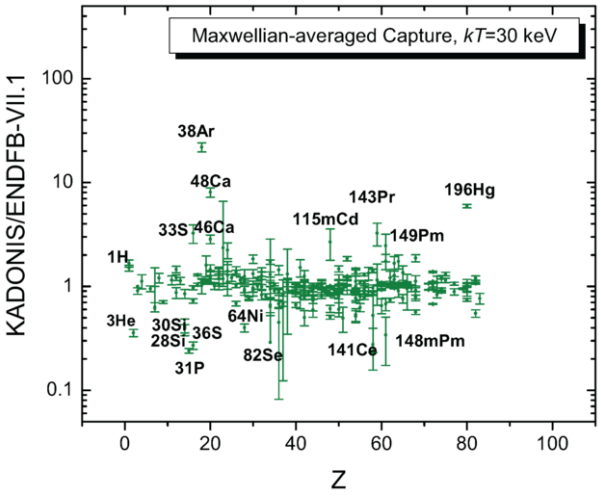

FIG. 119: Ratio of Karlsruhe Astrophysical Database of Nucleosynthesis in Stars (KADoNiS) [36] and ENDF/B-VII.1 Maxwellian-averaged capture cross sections at kT=30 keV.

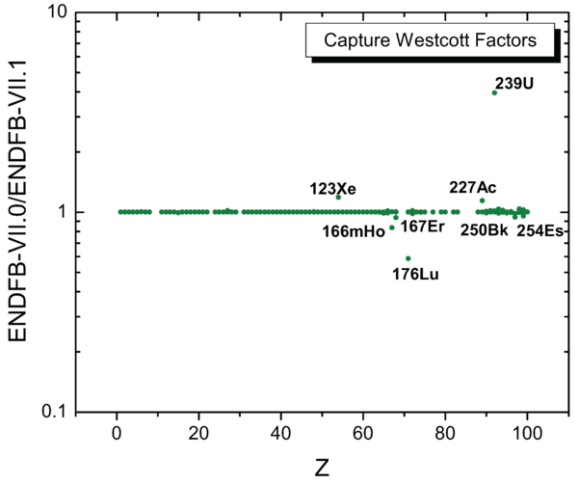

FIG. 120: Ratio of thermal neutron capture Westcott factors between ENDF/B-VII.0 and ENDF/B-VII.1 libraries.

may be able to impact the next ENDF release in a few years time.

A. Major Actinides

Presently there are extensive research programs underway to improve our understanding of neutron reactions on ^{239}Pu and ^{235,238}U. Potential modifications to fission, capture, inelastic *etc.*, actinide evaluated data will require extensive collaborative work by the nuclear cross section evaluators and the integral data testers to ultimately create a new ENDF library that maintains (and hopefully even improves upon) the present good performance in a wide range of criticality benchmark validation tests. We anticipate that this will be a major challenge requiring significant resources. It will be important to do, though, because our goal should always be to predict criticality accurately "for the right reasons". It is possible that some of the research directions in uncertainty quantification (UQ) and calibration, for example the potentially game-changing work of Koning and Rochman [277], will facilitate this goal.

1. *Prompt fission neutron spectra (PFNS)*

Our understanding of PFNS is still surprisingly poor. The current ensemble of measured PFNS data are widely discrepant. The Madland-Nix approach used in ENDF/B-VII.0 applies certain well-motivated, but relatively simple, model assumptions and calibrates the model to a best fit to the measured PFNS and nubar data. Other databases such as JEFF and JENDL tend to rely on extensions to the Madland-Nix model, but ultimately the results obtained are often close to Madland's estimates in ENDF/B-VII.0. But there is an interesting possibility that all these evaluated libraries could have significant systematic errors associated with them. Maslov, and Kornilov, in particular have suggested that the PFNS for all major actinides, and for essentially all incident energies, should have more neutrons below 1 MeV (*e.g.* an increase of 10–15% at 0.1 MeV outgoing energy), and fewer neutrons above 6-10 MeV and above outgoing energies [161]. Some LANL integral $(n, 2n)$ reaction rate critical assembly data, with MCNP simulations, tend to support this conjecture that there should be 20-30% fewer PFNS neutrons above 10 MeV for ^{239}Pu and ^{235}U [5] for fast incident neutrons, and similar results are seen in the dosimetry testing shown in Kahler's companion paper [8] for the fast plutonium Russian/IPPE reactor. Maslov's argument is motivated by some measurements that indicate an excess of neutrons below 1 MeV, for example those of Starostov for thermal neutrons on ^{235}U. But a counter argument is that such measurements are notoriously difficult and could be an artifact due to multiple scattered neutrons. Ignatyuk has reminded us that for many decades the lab experimental data on thermal ^{235}U fission points to an average neutron energy of about 1.99 MeV [241], yet integral transport simulations of the thermal criticality data point to values closer to 2.03 MeV (the value in ENDF/B-VII.0=ENDF/B-VII.1, JENDL-4.0, JEFF3.1, IPPE, *etc*) to match the k-eff criticality experiment data (though of course there could be other compensating errors). But we do note that Capote's [123] dosimetry cross section testing of the ENDF/B-VII.0=VII.1 thermal ^{235}U PFNS appears to support the PFNS high energy tail in ENDF at thermal.

To address these concerns the community has a number of measurement efforts underway. The IAEA is presently supporting a CRP on this topic, involving both experiments and modeling. A collaboration in the US is field-

ing new detectors at LANSCE by LANL, LLNL, and the CEA, involving a number of advances in the technology: an improved parallel plate avalanche counter (PPAC) fission chamber being designed at Livermore [278]; usage of various detectors that include liquid scintillators, lithium glass, and organic detectors. Much work is needed to reduce systematic uncertainties arising from questions such as neutron multiple scattering, room return, detector efficiencies. In addition, models that go beyond the Madland-Nix approach are being developed, notably ones that use Monte Carlo sequential decay formulations and are able to be matched against a wide variety of fission data such as P(ν), ν(A), and TKE distributions [279, 280, 281]. And whilst we have noted some data suggesting that the current ENDF/B-VII PFNS might be deficient in various ways, the recently-released PFNS data from Los Alamos by Lestone does support Madland's VII.0=VII.1 PFNS evaluation for plutonium for the fast-neutron ($< E_{inc} >= 2$ MeV) induced region, for outgoing energies between 1.5 and 10 MeV, as described in Sec. X G. But these plutonium PFNS data from Lestone do not rule out the ideas proposed by Maslov that there should be more PFNS neutrons below 1 MeV. An additional observation can be made from Figure 57 that shows $(n, 2n)$ activations in both ^{235}U (center regions of Flattop-25) and ^{239}Pu (center region of Flattop-Pu): the simulation of the measured data shows a bigger difference for $(n, 2n)$ activations in ^{235}U and ^{239}Pu than is observed in the critical assembly data (the difference between the red and the black points). Since both simulations use the same $(n, 2n)$ cross section data, this would suggest that either the 0.5-1.5 MeV incident energy VII.1 ^{239}Pu fission spectrum is too hard, or the VII.1 ^{235}U fission spectrum is too soft. Striving for new PFNS evaluations for the actinides that are consistent with all these types of data remains a challenge for a future ENDF/B-VIII.

2. *Precise fission cross sections*

The US National Laboratories are also developing a capability to measure total fission cross sections to high accuracy using a time projection chamber (TPC) at LANSCE. The detector is being developed collaboratively by groups at Livermore, Los Alamos, and Idaho, with university partners too, and is expected to lead to new results after 2015. The goal of this collaboration is to be able to measure fission to 1 % accuracy or better, with systematic errors that differ from traditional fission chamber technologies. This level of uncertainty is still higher than the current standards evaluation [7] in ENDF/B-VII, which, for example, assesses uncertainties at both 1 MeV and at 14 MeV neutron energy of 0.6 % for ^{235}U (and 0.7 % for ^{239}Pu). The principal motivation, though, for such an experiment is that the TPC community of researchers tends to believe that the aforementioned standards uncertainty assessments are too small. The lead author of this paper (MBC) thinks the value of the TPC measurements is more likely to be a "confirmatory experiment" to the existing standards assessment. Such a confirmatory experimental effort is worthwhile because of the central importance of accurately understanding fission for all nuclear applications, and because the systematic uncertainties associated with the TPC measurements are generally different from those of traditional fission chamber methods. And if future TPC results contradict our present understanding, as embodied in the standards [7], much new experimental work would then be needed to resolve such a contradiction.

3. *Neutron capture for ^{235}U and ^{239}Pu*

In the keV - MeV range, radiative neutron capture cross sections for ^{235}U and ^{239}Pu are poorly known: the covariance evaluation in ENDF/B-VII.1 has capture uncertainties of the order of 15% for each of these nuclei. These reactions are so important that should new assessments, based on new measured data, lead to significant changes in these evaluated cross sections, there will be significant implications for nuclear applications, for example in our criticality calculations. Our Japanese colleagues have suggested that the ^{235}U capture cross section in ENDF/B-VII.1 (=ENDF/B-VII.0) is 25% or more too high near 1 keV, from feedback from integral reactor experiments. The community is studying this important topic using a NEA/WPEC subgroup of scientists from Japan, Europe, Russia and the US. In the US, we are hoping that a DANCE detector measurement at LANSCE by M. Jandel will be able to resolve this question through a measurement at the 5-10% accuracy level. In fact the present ENDF/B-VII evaluation has a "bump" near 1 keV (that came from an Oak Ridge ORELA and SAMMY analysis), whereas CoH code Hauser-Feshbach model calculations do not show such a bump in the capture cross section shape; a measurement of the *shape* of the capture cross section, which could be obtained before accurate absolute measurements are obtained, would help resolve this question. High-energy resolution transmission measurements of ^{235}U capture and fission cross sections made at RPI are also being analyzed and will cover the energy range from thermal to 10 keV [282].

B. Other Work

New capture measurements on ^{157}Gd were done at LANL [283] and additional capture measurements of ^{155,156,157,158,160}Gd isotopes were done at RPI [284]. New resonance parameters were obtained and will extend the unresolved resonance region of ^{155,157}Gd to 1 keV. Capture cross section of ^{94,95}Mo were also obtained at LANL [285] and high energy resolutions transmission measurements of ^{95,96,98,100}Mo were performed at RPI [286]. These measurements will result in extensions of the unresolved resonance region of some of the isotopes (^{95}Mo for

example) to higher energy and will also provide accurate data on the total cross section in the unresolved resonance region. In addition transmission measurements of the Mo isotopes in the energy range from 0.5 to 20 MeV were done in a 250 m flight path at RPI and will supplement previous elemental Mo transmission data [287]. Measurements of resonance parameters of several isotopes is ongoing at ORNL; this includes ^{182,183,184,186}W, and ^{63,65}Cu [287].

TUNL is working on measurements using a mono energetic neutron beam, and several recent results [287] include ^{69}Ga(n,2n)^{68}Ga, ^{69}Ga(n,p)^{69m}Zn, ^{71}Ga(n,p)^{17m}Zn, and ^{75}As(n,2n)^{74}As, ^{75}As(n,p)^{75}Ge and ^{75}As(n,α)^{72}Ga. These new data may influence new evaluations.

Continued improvement in standard measurements will also impact future release of ENDF. Work in progress includes all the standards.

Future evaluation work will also be needed for iron. The present evaluations differ significantly, especially inelastic scattering in the threshold region. Because of these ambiguities we have assigned generous uncertainties to the iron inelastic in VII.1=COMMARA-2.0. Future work on this will benefit from international collaborative efforts, and indeed there are focused collaborations on inelastic scattering in general that have started.

XII. CONCLUSIONS

This paper has described how the ENDF/B-VII.1 library represents a major advance over the previous ENDF/B-VII.0 library and reflects work done in the CSEWG community over the last 5 years.

As is documented in detail in the companion paper by Kahler *et al.* [8], the good integral nuclear criticality performance that was demonstrated in ENDF/B-VII.0 [1, 6] is preserved, and improved upon in various ways: (1) the criticality of many systems involving the elements Be, Ti, Mn, Cr, Zr, Cd, and W show notable improvement; (2) Although the major actinides ^{235,238}U and ^{239}Pu have not been changed (apart from delayed neutrons and covariances, and FPYs for Pu), some of the criticality testing for the minor actinides is improved. (3) The work by Mughabghab on thermal properties of many fission products (Mo, Tc, Rh, Ag, Cs, Nd, Sm, Eu) should lead to improved integral performance in reactors. (4) β_{eff} and Rossi-α testing are generally favorable.

In addition to integral simulations of criticality, we have described integral simulations of reaction rates – *i.e.* rates for fission, capture, *etc.*, measured within broad neutron sources created by critical assemblies or reactors. This included validation testing for: capture reactions – ^{236,238}U(n,γ), $^{238-242}$Pu(n,γ), ^{241,243}Am(n,γ); fission reactions – ^{235,237,238}U(n,f), $^{238-242}$Pu(n,f), ^{241,243}Am(n,f). A number of improvements are described, but future progress is still needed. We also describe accelerator mass spectrometry measurements of capture reactions on ^{235,238}U from broad neutron sources at 25 keV, and 426 keV, that provide some validation of the VII.1 data.

Evolving the ENDF database is clearly an ongoing and iterative effort, and we recognize that much future work is still needed. The covariance uncertainty data that are presented here, whilst a notable accomplishment, are just a first step and will need to be refined in the coming years as more resources are devoted to this, as our understanding of these uncertainties improves, and as the user community becomes more experienced with usage of uncertainties in their analyses, and provides feedback to us.

One area of great concern is the lack of reliable uncertainty information for experimental data. The prospects of extracting such information from earlier experiments is relatively dim, so the focus needs to be on ensuring that reasonable estimates of uncertainties are provided by investigators in future experimental work. In this regard, it should be an important goal for the CSEWG community to educate experimenters on the techniques they can employ to estimate and report uncertainties. However, work in this area is still in a relatively early state, both as it concerns the estimation of underlying uncertainties and in employing them in statistically rigorous evaluation procedures. As mentioned earlier, in ENDF/B-VII.1 this community has made a major effort to provide a considerable quantity of uncertainty data as well as improved central values. During the next several years considerable effort will be expended in achieving advancements in both areas.

Acknowledgments

We acknowledge with gratitude the use of JENDL-4.0 evaluations for minor actinides developed by our Japanese colleagues O. Iwamoto, K. Shibata, T. Nakagawa, and G. Chiba, *et al.*

We would like to note with gratitude the extensive contributions of our experimental colleagues for discussions, and data, that have impacted the VII.1 library, especially R.C. Haight, F. Tovesson, M. Jandel, J. Ullmann, M. Devlin, T.A. Bredeweg, A. Couture, R.S. Rundberg, D.J. Vieira, J.B. Wilhelmy, C.Y. Wu, J.A. Becker, A. Tonchev, S. Wender, R. Nelson, and A.J.M. Plompen.

We thank S. Prussin for the discussions on plutonium fission product yields, especially his insightful analysis of isotope-dilution mass spectrometry reactor data that we quote. We also thank D. Barr, C. Burns and C. Wilkerson for useful input on radiochemistry issues.

We acknowledge help from our IAEA and WPEC colleagues R. Forrest, M. Kellett, N. Otsuka, V. Simakov, V. Zerkin, A. Koning, E. Bauge, C. Nordborg, R. Jacqmin, O. Bouland, E. Dupont, R. Mills, and A.J.M. Plompen.

We would like to note with gratitude enlightening discussions with A. Ignatyuk and V. Maslov. We thank A. Koning, D. Rochman, M. Salvatores, and M. Ishikawa for

insightful discussions on covariances.

We owe a special thanks to C. Wemple and Y. Yedvab for feedback on 6-group delayed neutron parameter problems in VII.1, and C. Dean for feedback on deficiencies in the VII.0 fission product capture cross section that led to improvements of the library.

We also thank W. Haxton for alerting us to some of the light nucleus capture deficiencies in VII.0 that we have now (partly) resolved, for astrophysical applications.

Finally, we would like to note with gratitude the extensive contributions of our colleagues who played an important role in the VII.0 library, upon which VII.1 is built: N.M. Greene, S.C. Frankle, D.G. Madland, P. Moller, R.D. Mosteller, P.R. Page, H. Trellue, W.B. Wilson, C.L. Dunford, D. Rochman, C.R. Lubitz, T.H. Trumbull, J.P. Weimann, D.E. Cullen, D.P. Heinrichs, D.P. McNabb, R.C. Block, J.B. Briggs, E.T. Cheng, H.C. Huria, M.L. Zerkle, K.S. Kozier, A. Courcelle, and R.Q. Wright.

We would like to express our appreciation for continuing support to several sponsors. In particular to T. Hallman and T. Barnes, DOE-SC, Office of Nuclear Physics (US Nuclear Data Program), R. Meisner, J. Pruet, and R. Hanrahan, DOE-NNSA (Advanced Simulation and Computing and Science Campaigns Programs), J. McKamey, J. Felty, DOE-NNSA (Nuclear Criticality Safety Program).

Work at Los Alamos National Laboratory was carried out under the auspices of the National Nuclear Security Agency of the U.S. Department of Energy under Contract No. DE-AC52-06NA25396. Work at Brookhaven National Laboratory was sponsored by the Office of Nuclear Physics, Office of Science of the U.S. Department of Energy under Contract No. DE-AC02-98CH10886 with Brookhaven Science Associates, LLC. Work at Lawrence Livermore National Laboratory was performed under Contract DE-AC52-07NA27344 and Oak Ridge National Laboratory under contract DE-AC05-00OR22725. Work supported at INL by the U.S. Department of Energy, Office of Nuclear Energy, under DOE Idaho Operations Office Contract DE-AC07-05ID14517.

[1] M. B. Chadwick, P. Obložinský, M. Herman, N. M. Greene, R. D. McKnight, D. L. Smith, P. G. Young, R. E. MacFarlane, G. M. Hale, S. C. Frankle, A. C. Kahler, T. Kawano, R. C. Little, D. G. Madland, P. Moller, R. D. Mosteller, P. R. Page, P. Talou, H. Trellue, M. C. White, W. B. Wilson, R. Arcilla, C. L. Dunford, S. F. Mughabghab, B. Pritychenko, D. Rochman, A. A. Sonzogni, C. R. Lubitz, T. H. Trumbull, J. P. Weinman, D. A. Br, D. E. Cullen, D. P. Heinrichs, D. P. McNabb, H. Derrien, M. E. Dunn, N. M. Larson, L. C. Leal, A. D. Carlson, R. C. Block, J. B. Briggs, E. T. Cheng, H. C. Huria, M. L. Zerkle, K. S. Kozier, A. Courcelle, V. Pronyaev, and S. C. van der Marck, "ENDF/B-VII.0: Next Generation Evaluated Nuclear Data Library for Nuclear Science and Technology," Nuclear Data Sheets **107**, 2931 (2006).

[2] R. E. MacFarlane, S. Kahler, "Methods for Processing ENDF/B-VII with NJOY," Nuclear Data Sheets **111**, 2739 (2010).

[3] P. G. Young, M. B. Chadwick, R. E. MacFarlane, P. Talou, T. Kawano, D. G. Madland, and W. B. Wilson, "Evaluation of Neutron Reactions for ENDF/B-VII: $^{232-241}$U and ^{239}Pu," Nuclear Data Sheets **108**, 2589 (2007).

[4] M. B. Chadwick, T. Kawano, P. Talou, E. Bauge, S. Hilaire, P. Dossantos-Uzarralde, P. Garrett, J. A. Becker, and R.O. Nelson, "Yttrium ENDF/B-VII Data from Theory and LANSCE/GEANIE Measurements and Covariances Estimated using Bayesian and Monte-Carlo Methods," Nuclear Data Sheets **108**, 2742 (2007).

[5] M. B. Chadwick, S. Frankle, H. Trellue, P. Talou, T. Kawano, P. G. Young, R. E. MacFarlane, and C. W. Wilkerson, "Evaluated Iridium, Yttrium, and Thulium Cross Sections and Integral Validation Against Critical Assembly and Bethe Sphere Measurements," Nuclear Data Sheets **108**, 2716 (2007).

[6] S. C. van der Marck, "Benchmarking ENDF/B-VII.0," Nuclear Data Sheets **107**, 3061 (2006).

[7] A. D. Carlson, V. G. Pronyaev, D. L. Smith, N. M. Larson, Z.-P. Chen, G. M. Hale, F. J. Hambsch, E. V. Gai, S.-Y. Oh, S. A. Badikov, T. Kawano, H. M. Hofmann, H. Vonach, and S. Tagesen,"International Evaluation of Neutron Cross Section Standards," Nuclear Data Sheets **110**, 3215 (2009).

[8] A. Kahler, R.E. MacFarlane, R.D. Mosteller, B.C. Kiedrowski, S.C. Frankle, M.B. Chadwick, R.D. McKnight, R.M. Lell, G. Palmiotti, H. Hiruta, M. Herman, R. Arcilla, S.F. Mughabghab, J.C. Sublet, A. Trkov, T.H. Trumbull, and M. Dunn, "ENDF/B-VII.1 Neutron Cross Section Data Testing with Critical Assembly Benchmarks and Reactor Experiments," Nuclear Data Sheets **112**, 2997 (2011).

[9] K. Shibata, O. Iwamoto, T. Nakagawa, N. Iwamoto, A. Ichihara, S. Kunieda, S. Chiba, K. Furutaka, N. Otuka, T. Ohsawa, T. Murata, H. Matsunobu, A. Zukeran, S. Kamada, and J. Katakura, "JENDL-4.0: A New Library for Nuclear Science and Engineering," J. Nucl. Sci. Technol. **48**, 1 (2011).

[10] G. Chiba, K. Okumura, K. Sugino, Y. Nagaya, K. Yokoyama, T. Kugo, M. Ishikawa and S. Okajima, "JENDL-4.0 Benchmarking for Fission Reactor Applications," J. Nucl. Sci. Technol., 48(2), 172 (2011).

[11] A.J. Koning *et al.*, "Status of the JEFF nuclear data library," J. Korean Phys. Soc. **59**, No. 2, 1057 (2011).

[12] A. Ignatyuk, (2009) [private communication]; A.A. Alekseev, A.A. Bergman, A.I. Berlev, E.A. Koptelov, B.F. Samylin, A.M. Trufanov, B.I. Fursov and V.S. Shorin, "^{242m}Am and ^{245}Cm neutron fission cross sections," Atomic Energy **106**, 133 (2009).

[13] C.D. Dean, P.J. Smith, and R.J. Perry, "Validation of important fission product evaluations through CERES integral benchmarks," Proceedings of the In-

ternational Conference on Nuclear Data for Science and Technology" April 22-27, 2007, Nice, France, editors O.Bersillon, F.Gunsing, E.Bauge, R.Jacqmin, and S.Leray, EDP Sciences, **2**, 829 (2007).

[14] M. B. Chadwick, "Evaluation of Fission Product Yields from Fission Spectrum n+^{239}Pu Including a Meta Analysis of Benchmark Data," Los Alamos Technical Report, LA-UR-09-4446 (2009); M. B. Chadwick, Proc. 4th Int. Workshop on Nuclear Fission and Fission Product Spectroscopy, CEA, Cadarache, France, May 13–16, 2009, AIP Conf. Proc. **1175**, 71 (2009).

[15] M. B. Chadwick, T. Kawano, D. W. Barr, M. R. Mac Innes, A. C. Kahler, T. Graves, H. Selby, C. J. Burns, W. C. Inkret, A. L. Keksis, J. P. Lestone, A. J. Sierk, and P. Talou, "Fission Product Yields from Fission Spectrum n+^{239}Pu for ENDF/B-VII.1," Nuclear Data Sheets **111**, 2923 (2010).

[16] D. R. Nethaway, "PROPHET Fission Yields," Nuclear Chemistry Division Memorandum LJW-45-85-189, Lawrence Livermore National Laboratory (1985).

[17] R. W. Mills, "Fission Product Yield Evaluation," Thesis, University of Birmingham, Uinited Kingdom (1995).

[18] M. F. James, R. W. Mills, and D. W. Weaver, "UKFY2 Part 1: Methods and Outline," AEAT report, AEA-TRS-1015 (1991).

[19] M. F. James, R. W. Mills, and D. W. Weaver, "UKFY2 Part 2: Tables of Measured Data," AEAT report, AEA-TRS-1018 (1991).

[20] M. F. James, R. W. Mills, and D. W. Weaver, "UKFY2 Part 3: Tables of Discrepant Data," AEAT report, AEA-TRS-1019 (1991).

[21] J. Laurec, A. Adam and T. de Bruyne, E. Bauge, T. Granier, J. Aupiais, O. Bersillon, G. Le Petit, N. Authier, P. Casoli, "Fission Product Yields of ^{233}U, ^{235}U, ^{238}U, and ^{239}Pu in Fields of Thermal Neutrons, Fission Neutrons, and 14.7 MeV Neutrons," Nuclear Data Sheets **111**, 2965 (2010).

[22] M. Herman (editor), "ENDF-6 Formats Manual: Data Formats and Procedures for the Evaluated Nuclear Data File ENDF/B-VI and ENDF/B-VII," Tech. Rep. BNL-NCS-44945-05-Rev, Document ENDF-102, Brookhaven National Laboratory, June 2010.

[23] X-5 Monte Carlo Team, "MCNP - A General N-Particle Transport Code," Version 5 - Volume I: Overview and Theory, Los Alamos National Laboratory Report LA-UR-03-1987, (April, 2003).

[24] B. Pritychenko, A.A. Sonzogni, D.F. Winchell, V.V. Zerkin, R. Arcilla, T.W. Burrows, C.L. Dunford, M.W. Herman, V. McLane, P. Obložinský, Y. Sanborn, J.K. Tuli, "Nuclear Reaction and Structure Data Services of the National Nuclear Data Center," Ann. Nucl. Energy **33**, 390 (2006).

[25] D. Smith, "Evaluated Nuclear Data Covariance: From ENDF/B-VII.0 to ENDF/B-VII.1 ", Nuclear Data Sheets **112**, 3037 (2011).

[26] P. Talou *et al.*, "Quantification of Uncertainties for Evaluated Neutron-Induced Reactions on Actinides in the Fast Energy Range," Nuclear Data Sheets **112**, 3075 (2011).

[27] L. Leal *et al.*, "ORNL Resolved Resonance Covariance Generation in ENDF/B-VII.1," Nuclear Data Sheets, submitted.

[28] S. Hoblit *et al.*, "Neutron Cross Section Covariances for Structural Materials and Fission Products," Nuclear Data Sheets **112**, 3075 (2011).

[29] A. Trkov *et al.*, "Covariances of evaluated nuclear cross-section data for ^{232}Th, ^{180,182,183,184,186}W and ^{55}Mn", Nuclear Data Sheets **112**, 3098 (2011).

[30] M. Salvatores *et al.*, "Uncertainty and Target Accuracy Assessment for Innovative Systems Using Recent Covariance Data Evaluations," Report NEA/WPEC-26 (NEA, Paris 2008).

[31] R.C. Little, T. Kawano, G.D. Hale *et al.*, "Low-fidelity Covariance Project," Nuclear Data Sheets **109**, 2828 (2008). Available from www.nndc.bnl.gov/lowfi.

[32] P. Obložinský *et al.*, P. Talou *et al.*, "Neutron Cross Section Covariance Library AFCI-1.2," Brookhaven National Laboratory Report BNL-90897-2009, Brookhaven National Laboratory & Los Alamos National Laboratory, September 2009.

[33] M. Herman *et al.*, P. Talou *et al.*, "Neutron Cross Section Covariance Library AFCI-2.0," Brookhaven National Laboratory Report BNL-94830-2011, Brookhaven National Laboratory & Los Alamos National Laboratory, under preparation.

[34] B. Pritychenko, A.A. Sonzogni, "Sigma: Web Retrieval Interface for Nuclear Reaction Data," Nuclear Data Sheets **109**, 2822 (2008).

[35] S.F. Mughabghab, Atlas of Neutron Resonances, Resonance Parameters and Neutron Cross Sections Z = 1-100, Elsevier, Amsterdam (2006).

[36] I. Dillmann, M. Heil, F. Käppeler *et al.*, "KADoNiS - The Karlsruhe Astro Phys. Database of Nucleosynthesis in Stars," AIP Conf. Proc. **819**, 123 (2006); Data downloaded from ⟨http://www.kadonis.org⟩ on April 14, 2011.

[37] F. Fröhner, "On Uncertainty Evaluation and Fluctuations in the Resolved and Unresolved Resonance Regions", Proc. Nucl. Data Conf. 1994 **2**, 597 (1994), Gatlinburg, May 9-13, 1994.

[38] H. Derrien *et al.*, "Neutron Resonance Parameters and Covariance Matrix of ^{239}Pu", Oak Ridge National Laboratory Report ORNL/TM-2008/123, September 2008.

[39] N. Jarmie *et al.*, "Elastic Scattering of tritons by He-4," Los Alamos Report LA-8492 (1980); R.A. Hardekopf *et al.*, "^{4}He(t,t)^{4}He elastic scattering: analyzing powers and differential cross sections," Los Alamos report LA-6188 (1977).

[40] R.L. Macklin, R.W. Ingle, and J. Halperin, "^{6}Li(n,α)^{3}H cross section from 70 to 3000 keV from the 235U(n,fission) calibration of athin glass scintillator," Nuclear Science and Engineering **71**, 205 (1979).

[41] M. Drosg, D.M. Drake, and J. Masarik, "Calibration of a Li-Glass Detector for Neutron Energies Above 50 keV by the 1H(t,n)3He Reaction," Nuclear Instruments and Methods **B 94**, 319 (1994).

[42] M. Devlin, T.N. Taddeucci, G.M. Hale, R.C. Haight, and J.M. O'Donnell, "Differential Cross Section Measurements for the 6Li(n,t)a Reaction in the few MeV Region," Proc. 13th Intl. Symp. on Capture Gamma-Ray Spectroscopy and Related Topics, Cologne, Germany, 25-29 August 2008, p.215.

[43] H.-H. Knitter, C. Butz-Jorgensen, D.L. Smith, and D. Marletta, "Angular Distribution Measurements for the Reaction 6Li(n, t)4He," Nuclear Science and Engineering **83**, 229 (1983).

[44] J.C. Overley, R.M. Sealock, and D.H. Ehlers, "^{6}Li(n,t)^{4}He Differential Cross Sections between 0.1 and

1.8 MeV," NUCLEAR PHYSICS **A221**, 573 (1974).
[45] H. Condé, T. Andersson, L. Nilsson, and C. Nordborg, "Studies of the ^{6}Li(n,t)^{4}He Reaction," Proc. Int. Conf. on Nucl. Data for Science and Technology, Antwerp, Belgium, 6-10 September 1982, p. 447.
[46] C.M. Bartle, "Total Cross Sections for the ^{6}Li(n, a)^{3}H Reaction between 2 and 10 MeV," NUCLEAR PHYSICS **A330**, 1 (1979).
[47] Y. Danon *et al.*, "Beryllium and Graphite High-Accuracy Total Cross-Section Measurements in the Energy Range from 24 to 900 keV," NUCLEAR SCIENCE AND ENGINEERING **161**, 321 (2009).
[48] L. C. Leal and H. Derrien, "R-Matrix Evaluation of ^{19}F Neutron Cross Section up to 1 MeV," TRANSACTION OF THE AMERICAN NUCLEAR SOCIETY 494 (2003), San Diego California.
[49] R. O. Sayer, K. H. Guber, L. C. Leal, N. M. Larson, and T. Rauscher, "R-Matrix Evaluation of Cl Neutron Cross Section up to 1.2 MeV," Oak Ridge National Laboratory Report ORNL/TM-2003/50, March, 2003. See also R. O. Sayer, K. H. Guber, L. C. Leal, N. M. Larson, and T. Rauscher, "R-matrix analysis of Cl neutron cross sections up to 1.2 MeV", PHYS. REV. **C73**, 044603 (2006).
[50] K. H. Guber, L. C. Leal, R. O. Sayer, P. E. Koehler, T. E. Valentine, H. Derrien, and J. A. Harvey, "Neutron cross section measurements at ORELA for improved nuclear data and their application," RAD. PROTECTION DOSIMETRY **116**, 579 (2005); K. H. Guber, L. C. Leal, R. O. Sayer, P. E. Koehler, T. E. Valentine, H. Derrien, and J. A. Harvey, " New neutron cross-section measurements at ORELA and their application in nuclear criticality calculations," NUCL. INST. METH. PHYS. RES. **B241**, 218 (2005).
[51] W. M. Good, J. A. Harvey, and N. W. Hill, "Neutron Total Cross Sections in the KeV Energy Range," Oak Ridge National Laboratory Report ORNL-4937, 198 (1973); J. A. Harvey, [private communication].
[52] S. Cierjacks, P. Forti, D. Kopsch, L. Kropp, J. Nebe, and H. Unseld, "High Resolution Total Neutron Cross Sections for Na, Cl, K, V, Mn and Co between 0.5 and 30 MeV", Kemforschungszentrum Karlsruhe KFK-1000, 2. Supplement, EUR-3963e (1969).
[53] U. N. Singh, H. I. Liou, G. Hacken, M. Slagowitz, F. Rahn, J. Rainwater, W. Makofske, and J. Garg, "Neutron Resonance Spectroscopy: Chlorine," PHYS. REV. **C10**, 2138 (1974).
[54] E. G. Joki, L. G. Miller, and J. E. Evans, "Total Neutron Cross Sections of Na, K and Rb in the 0.03- to 10-eV region," Phillips Petroleum Report IDO-16276, (1955).
[55] D. C. Stupegia, M. Schmidt, C. R. Keedy, and A. A. Madson, "Neutron capture between 5 keV and 3 MeV", J. NUCL. ENERG. **22**, 267 (1968).
[56] K. Shibata, T. Kawano, T. Nakagawa, O. Iwamoto, J. Katakura, T. Fukahori, S. Chiba, A. Hasegawa, T. Murata, H. Matsunobu, T. Ohsawa, Y. Nakajima, T. Yoshida, A. Zukeran, M. Kawai, M. Baba, M. Ishikawa, T. Asami, T. Watanabe, Y. Watanabe, M. Igashira, N. Yamamuro, H. Kitazawa, N. Yamano, H. Takano, "Japanese Evaluated Nuclear Data Library Version 3 Revision-3: JENDL-3.3," J. NUCL. SCI. TECHNOL., **39**, 1125 (2002).
[57] D. Dashdorj, T. Kawano, P. E. Garrett, J. A. Becker, U. Agvaanluvsan, L. A. Bernstein, M. B. Chadwick, M. Devlin, N. Fotiades, G. E. Mitchell, R. O. Nelson, and W. Younes, "Effect of preequilibrium spin distribution on ^{48}Ti+n cross sections," PHYS. REV. **C 75**, 054612 (2007).
[58] L. Leal, K. Guber, G. Arbanas, D. Wiarda, and P. Koehler, "Resonance Evaluation of ^{48}Ti Including Covariance for Criticality Safety Applications," International Conference on Nuclear Criticality, September 19-22, 2011, Edinburgh, Scotland.
[59] International Network of Nuclear Reaction Data Centres (NRDC), "Compilation of experimental nuclear reaction data (EXFOR/CSISRS)", (Available from *h*ttp://www-nds.iaea.org/exfor/, http://www.nndc.bnl.gov/exfor/).
[60] T. Kawano, "Optical and Hauser-Feshbach Statistical Model Code, CoH ver. 3.1 (Ariel)," [unpublished] (2010).
[61] A. Langsdorf *et al.*, Argonne National Laboratory Report ANL-5569 (Rev.) (1961).
[62] E.Barnard, J. Devilliers, D. Reitmann, P. Moldauer, A.Smith, J.Whalen, "Neutron Scattering from Titanium; Compound and Direct Effects," Argonne National Laboratory Report ANL/NDM-3 (1973); NUCL. PHYS. **A229**, 189 (1974).
[63] P. Guenther, D. Havel, A. Smith, and J. Whalen, "Titanium I: Fast Neutron Cross Section Measurements," Argonne National Laboratory Report ANL/NDM-31 (1977).
[64] A. B. Smith, D. L. Smith, P. T. Guenther, J. W. Meadows, R. D. Lawson, R. J. Howerton, T. Djemil, and B. J. Micklich, "Neutronic Evaluated Nuclear-Data File for Vanadium ," Argonne National Laboratory Report ANL/NDM-105 (1988).
[65] A. B. Smith, P. T. Guenther, R. D. Lawson, "Fast-Neutron Elastic Scattering from Elemental Vanadium," Argonne National Laboratory Report ANL/NDM-106 (1988).
[66] D. L. Smith, J. W. Meadows, I. C. Gomes, "Cross-sections for hydrogen production from vanadium in a fusion neutron environment," FUSION ENG. DES. **47**, 61 (1999).
[67] D. Rochman, M. Herman, P. Obložinský, "New evaluation of ^{51}V(n, np + pn) and ^{51}V(n, t) cross sections for the ENDF/B-VII library," FUSION ENG. DES. **81**, 2109 (2006).
[68] N.D. Dudey, R.R. Heinrich, A.A. Madson,"Fast neutron capture by vanadium and titanium," J. NUCL. ENERGY **23**, 443 (1969).
[69] H.S. Sahota, V.K. Mittal, N.P. Sidhu, "Neutron capture cross-sections by comparative γ-activation," ANN. NUCL. EENERGY **13**, 287 (1986).
[70] K. Shibata, "Calculation of Neutron-Induced Reaction Cross Section of Manganese-55", J. NUCL. SCI. & TECH. (JAPAN) **26**, 955 (1989).
[71] K.I. Zolotarev, "Evaluation of cross-section data from threshold to 40-60 MeV for specific neutron reactions important for neutron dosimetry applications," *Technical report INDC(NDS)-0546*, IAEA, Vienna, Austria (2009).
[72] K.H. Guber, P.E. Koehler, D. Wiarda, J.A. Harvey, T.E. Valentine, R.O. Sayer, L.L. Leal, N.M. Larson, T.S. Bigelow, C. Ausmus, D.R. Brashear, R.B. Overton, J.A. White, V.M. Cauley, "New neutron cross section measurements from ORELA and new resonance parameter evaluations," Proc.Intern.Conf.Nuclear Data

for Science and Technology, Nice, France, April 22-27, 2007, O.Bersillon, F.Gunsing, E.Bauge, R.Jacqmin, and S.Leray, Eds., EDP Sciences, 403 (2008).

[73] G. Aerts *et al.*, "GELINA measurements (unpublished)", (2006) [private communication].

[74] J. B. Garg, R. L. Macklin, and J. Halperin, "Neutron capture cross section of manganese", PHYS. REV. **C18**, 2079 (1978).

[75] L. Perrot, A. Billebaud, R. Brissot, A. Giorni, D. Heuer, J.-M. Loiseaux, O. Meplan, and J.-B. Viano, "Precise Validation of Database (n,γ) Cross Sections Using a Lead-Slowing-Down Spectrometer and Simulation from 0.1 eV to 30 keV: Methodology and Data for a Few Elements", NUCL. SC. & ENG. **144**, 142 (2003).

[76] H. Derrien, L. C. Leal, N. M. Larson, K. Guber, D. Wiarda, and G. Arbanas, "Neutron resonance parameters of ^{55}Mn from Reich-Moore analysis of recent experimental neutron transmission and capture cross sections," International Conference on the Physics of Reactors "Nuclear Power: A Sustainable Resource" Casino-Kursaal Conference Center, Interlaken, Switzerland, September 14-19, 2008.

[77] R.E. Coté, L.M. Bollinger, and G.E. Thomas, "Total Neutron Cross Section of Manganese", PHYS. REV. **134**, B1047-B1051 (1964).

[78] L.J. Rainwater, W.W. Havens, C.S. Wu, J.R. Dunning, "Slow neutron velocity spectrometer studies. I. Cd, Ag, Sb, Ir, Mn", PHYS. REV. **71**, 65 (1947).

[79] F. Widder, "Neutron capture cross section measurements in the energy region from 0.01 to 10 electron volts", EIDG. INST. REAKTORFORSCH. WUERENLINGEN REPORTS No.217, Switzerland (1975).

[80] V.P. Kolotov and F. De Corte, "An electronic database with compilation of k_0 and related data for NAA", J. RADIOAN. NUCL. CHEM. **257**, 501 (2003). (Available from *http://old.iupac.org/projects/2001/2001-075-1-500.html*).

[81] J. Harvey *et al.*, "ORELA measurements", EXFOR number 13770 (1980).

[82] M. Herman, R. Capote, B.V. Carlson, *et al.*, "EMPIRE, Nuclear Reaction Code System for Data Evaluation," NUCLEAR DATA SHEETS **108**, 2655 (2007).

[83] D.W. Muir, "Global Assessment of Nuclear Data Requirements – the GANDR Project ", (Available from *http://www-nds.iaea.org/gandr/*); D. W. Muir, A. Mengoni, and I. Kodeli, "Integration International Standards Evaluation into a Global Data Assessment," NUCL. DATA SHEETS **109**, 2874 (2008).

[84] D. Wiarda, S. Goluoglu, M. E. Dunn, N. M. Greene, and L. M. Petrie, "AMPX-6: A Modular Code System for Processing ENDF/B Evaluations," to be published as an ORNL/TM Report.

[85] R. Capote, M. Herman, P. Obložinský *et al.*, "RIPL - Reference Input Parameter library for Calculation of Nuclear Reaction and Nuclear Data Evaluation," NUCLEAR DATA SHEETS **110**, 3107 (2009).

[86] T. Belgya, O. Bersillon, R. Capote, T. Fukahori, Zhigang Ge, S. Goriely, M. Herman, A.V. Ignatyuk, S. Kailas, A. Koning, V. Plujko and P. Young, "Handbook for calculations of nuclear reaction data, Reference Input Parameter Library-2", *Tech. Rep. IAEA-TECDOC-1506* , International Atomic Energy Agency, Vienna, Austria (2006) (Available from *http://www-nds.iaea.org/RIPL-2/*).

[87] J. Raynal, "Optical model and coupled-channel calculations in nuclear physics", in: Computing as a language of physics, ICTP International Seminar Course, Trieste, Italy, 1971, International Atomic Energy Agency, Vienna, Austria, 281 (1972); "ECIS96", in: Proc. OECD/NEA Specialists Meeting on Nucleon-Nucleus Optical Model to 200 MeV, Bruyères-le-Châtel, France, 1997, 159–166 (Available from *http://www.nea.fr/html/science/om200/*).

[88] W. Hauser and H. Feshbach, "The Inelastic Scattering of Neutrons", PHYS. REV. **87**, 366 (1952).

[89] H. M. Hofmann, J. Richert, J. W. Tepel, and H. A. Weidenmüller, "Direct reactions and Hauser-Feshbach theory", ANN. PHYS. **90**, 403 (1975).

[90] A.I. Lashuk, A.I. Gonchar, and I.P. Sadokhin, "Gamma-quanta production cross-sections at inelastic scattering of the neutrons on the nuclei of reactor construction materials", *Vop. At.Nauki i Tekhn.,Ser.Yadernye Konstanty*, Issue.1, p.26 (1994). EXFOR number 41186001.

[91] L. Leal, H. Derrien, K. Guber, G. Arbanas, and D. Wiarda, "Evaluation of the Chromium Resonance Parameters Including Resonance Parameter Covariance," J. KOREAN PHYS. SOC. **59**, 1644 (2011).

[92] N. M. Larson, "Updated Users' Guide for SAMMY: Multilevel R-Matrix Fits to Neutron Data Using Bayes Equations," ORNL/TM-9179/R7, 2007.

[93] D. Wiarda and M. E. Dunn, "PUFF-IV: A Code for Processing ENDF Uncertainty Data into Multigroup Covariance Matrices," Oak Ridge National Laboratory Report ORNL/TM-2006/147, UT-Battelle, LLC, October 2006.

[94] H. Derrien, L. C. Leal, K. H. Guber, D. Wiarda, and G. Arbanas, "Re-evaluation of ^{58}Ni and ^{60}Ni resonance parameters in the neutron energy range thermal to 800 keV," Wonder 2009 - 2nd International Workshop on Nuclear Data Evaluation for Reactor Applications, Cadarache, France, 2009.

[95] M.J. Trbovich, D.P. Barry, R.E. Slovacek *et al.*, "Hafnium Resonance Parameter Analysis using Neutron Capture and Transmission Experiments", PROCEEDINGS OF INT. CONF. ON NUCLEAR DATA FOR SCIENCE AND TECHNOLOGY, Santa Fe, September 26 - October 1, 2004, **AIP 769**, 949 (2005).

[96] S.F. Mughabghab, NEUTRON CROSS SECTIONS, Vol.1, Part B, Academic Press, New York (1984).

[97] E.D. Arthur and C.A. Philis, "New Calculations of Neutron-Induced Cross Sections on Tungsten Isotopes", *Technical report LA-8630-PR*, Los Alamos National Laboratory, NM, USA (1980).

[98] E.D. Arthur, P.G. Young, A.B. Smith, C.A. Philis, Dec. 1980, "Evaluated nuclear data files of neutron induced reactions on tungsten isotopes", Documentation of the Tungsten Evaluation for ENDF/B-V (MAT=1475,1476,1477,1478 MF=1 MT=451).

[99] J. Frehaut, A. Bertin, R. Bois, and J. Jary, "Status of (n,2n) cross section measurements at Bruyères-le-Châtel" in Proc. Symp. on Neutron Cross Sections from 10-50 MeV, Upton, Long Island, U.S.A., May 12-14, 1980, Brookhaven Technical report BNL/NCS-51245, 399 (l980).

[100] M.B. Chadwick, P.G. Young, S. Chiba, S. Frankle, G.M. Hale, H.G. Hughes, A. Koning, R.C. Little, R.E. MacFarlane, R.E. Prael, and L.S. Waters, "Cross-section evaluations to 150 MeV for accelerator-driven systems

and implementation in MCNPX", *Nucl. Sc. & Eng.* **131**, 293 (1999).

[101] CSEWG-Collaboration, "Evaluated Nuclear Data File ENDF/B-VI.8" released in October 2001 (Available from *http://www.nndc.bnl.gov/endf*).

[102] I. Kodeli, "Reflection on the present status of Tungsten cross sections based on the analysis of FNG and FNS Benchmark Experiments", *Technical report EFFDOC-1002*, OECD/NEA, Paris (2007).

[103] I. Kodeli and A. Trkov, "Validation of the IRDF-2002 Dosimetry Library", Nucl. Instr. Meth. in Phys. Res. **A577**, 664 (2007).

[104] W.P. Abfalterer, F.B. Bateman, F.S. Dietrich, R.W. Finlay, R.C. Haight and G.L. Morgan, "Measurement of neutron total cross sections up to 560 MeV", Phys. Rev. **C63**, 044608 (2001).

[105] F.S. Dietrich, J.D. Anderson, R.W. Bauer, S.M. Grimes, R.W. Finlay, W.P. Abfalterer, F.B. Bateman, R.C. Haight, G.L. Morgan, E. Bauge, J.P. Delaroche, and P. Romain, "Importance of isovector effects in reproducing total cross section differences", Phys. Rev. **C67**, 044606 (2003).

[106] R. Capote, A. Trkov, I. Kodeli, E. Soukhovitskii, L.C. Leal, M. Herman, and D.W. Muir, "Evaluation of tungsten isotopes in the fast neutron range including cross section covariance estimation", Proceedings of the International Conference on Nuclear Data for Science and Technology, April 22-27, 2007, Nice, France, editors O.Bersillon, F.Gunsing, E.Bauge, R.Jacqmin, and S.Leray, EDP Sciences, 689 (2008).

[107] A. Trkov, R. Capote, I. Kodeli and L. Leal, "Evaluation of Tungsten Nuclear Reaction Data with Covariances", Nucl. Data Sheets **109**, 2905 (2008); (evaluated data files and comments at *http://www-nds.iaea.org/wolfram/*).

[108] O. Bersillon, L.R. Greenwood, P.J. Griffin, *et al.*, "International Reactor Dosimetry File 2002 (IRDF-2002)", *Technical Reports Series* No. 452, International Atomic Energy Agency, Vienna, Austria (2006). (Available from *http://www-pub.iaea.org/MTCD/publications/*).

[109] R. Capote, E.Sh. Soukhovitskii, J.M. Quesada, and S. Chiba, "Isospin dependent dispersive coupled channel optical model potential for tungsten isotopes", presented at 11th International Conference On Nuclear Reaction Mechanisms, Varenna, Italy, June 12-16 ,2006 (unpublished).

[110] R. Capote, M. Sin and A. Trkov, "Modelling of nuclear data in the fast neutron region", in NEMEA-3 Proceedings of the 3rd Workshop on Neutron Measurements, Evaluations and Applications, October 25-28, 2006 Borovets, Bulgaria, editor A.J. Plompen, *EUR report 22794 EN*, ISBN 978-92-79-06158-5, European Communities, 13 (2007).

[111] P.T. Guenther, A.B. Smith, and J.F. Whalen, "Fast-neutron total and scattering cross sections of ^{182}W, ^{184}W, and ^{186}W", Phys. Rev. **C26**, 2433 (1982).

[112] P. Batistoni, M. Angelone, L. Petrizzi, and M. Pillon, "Neutronics Benchmark Experiment on Tungsten", J. Nucl. Materials **329–333**, Part 1, 683 (2004).

[113] "ICSBEP 2006", International Handbook of Evaluated Criticality Safety Benchmark Experiments, *Technical Report NEA/NSC/DOC(95)03*, NEA Nuclear Science Committee, Nuclear Energy Agency, Organization for Economic Co-operation and Development.

[114] C. Lampoudis, K. Guber, S. Kopecky, P. Schillebeeckx and P. Siegler, " Neutron Total and Capture Cross Section of Tungsten Isotopes," J. Korean Physical Society **59**, 2, 1860 (2011).

[115] S. Kunieda, R.C. Haight, T. Kawano, M.B. Chadwick, T. Fukahori, and Y. Watanabe, "Measurement and Model Analysis of $(n, x\alpha)$ Cross Sections for Cr, Fe, ^{59}Co and ^{58,59}Ni from Threshold Energy to 150 MeV", Los Alamos National Laboratory report, in preparation (2011).

[116] K. Shibata G. Chiba, A. Ichihara, S. Kunieda, "Evaluation of Neutron Nuclear Data on Arsenic-75 for JENDL-4," J. Nucl. Sci. Technol. **47**, 40 (2010).

[117] F. Bazan, "(n, 2n) Cross-Section Measurements of Krypton and Xenon Isotopes," LLNL Internal Report UCRL-53929 162 (1989).

[118] A.J. Koning, S. Hilaire and M.C. Duijvestijn, "TALYS-1.0",*Proceedings of the International Conference on Nuclear Data for Science and Technology - ND2007*, April 22-27, 2007, Nice, France (2008).

[119] A.J. Koning and J.P. Delaroche, "Local and Global Nucleon Optical Model from 1 keV to 200 MeV," Nucl. Phys. **A 713**, 231 (2003).

[120] D.A. Brown *et al.*, "2009 Release of the Evaluated Nuclear Data Library (ENDL2009)," LLNL Internal Report LLNL-TR-452511 (2009).

[121] T. Kawano, H. Matsunobu, T. Murata, A. Zukeran, Y. Nakajima, M. Kawai, O. Iwamoto, K. Shibata, T. Nakagawa, T. Ohsawa, M. Baba, and T. Yoshida, "Simultaneous Evaluation of Fission Cross Sections of Uranium and Plutonium Isotopes for JENDL-3.3," J. Nucl. Sci. Technol. **37**, 327 (2000).

[122] K.I. Zolotarev, "Evaluation of cross-section data from threshold to 40 MeV for some neutron reactions important for fusion dosimetry applications," International Atomic Energy Agency Report INDC(NDS)-0584, November 2010.

[123] R. Capote, K.L. Zolotarev, V.G. Pronyaev, A. Trkov, "Updating and extending the IFDR-2002 Dosimetry Library," to be published in the proceedings of the International Symposium on Reactor Dosimetry (ISDR-14), May 2011, Bretton Woods, USA.

[124] E.D. Arthur, and C. Philis, "Applied nuclear data research and development: July 1-September 30, 1980," Los Alamos National Laboratory Report LA-8630-PR (1980).

[125] B.P. Bayhurst, J.S. Gilmore, R.J. Prestwood, J.B. Wilhelmy, N. Jarmie, B.H. Erkkila, and R.A. Hardekopf, "Cross sections for (n,xn) reactions between 7.5 and 28 MeV," Phys. Rev. **C 12**, 451 (1975).

[126] S.F. Mughabghab and C.L. Dunford, "Nuclear level density and the effective nucleon mass," Phy. Rev. Lett. **81**, 4083 (1998).

[127] S.F. Mughabghab,"What do s- and p-wave neutron average radiative widths reveal?" International Conference on Nuclear Data for Science and Technology April 27 - May 1, 2010, Jeju Island, Korea, J. Korean Phys. Soc. 59,821 (2011).

[128] S. F. Mughabghab, "Spin-orbit splitting of the 3p neutron single particle state:non-statistical effects in neutron radiative capture," Brookhaven National Laboratory Report BNL-80311-2008-JA (2008).

[129] S. Oh, J. Chang and S. F. Mughabghab, "Neutron cross section evaluations of fission products below the fast en-

ergy region," Brookhaven National Laboratory Report BNL-NCS-67469 (2000).
[130] L. Koester, K. Knopf, and W. Waschkowski, "Interaction of slow neutrons with the isotopes of molybdenum," Z. Phys. **A 326**, 227 (1987).
[131] K. Furutaka, H. Harada, S. Nakaruma, T. Katoh, T. Fujii, H. Yamana, and S. Raman, "Cross Section of thermal neutron capture reaction by ^{99}Tc," J. Nucl. Radiochem. Sciences **6**, 283 (2005).
[132] L. Molnar, T. Belgya, Zs. Revay, and S.M. Qaim, "Partial and total thermal neutron capture cross section for non destructive assay and transmutation monitoring of ^{99}Tc," Radiochim Acta **90**, 479 (2002).
[133] S.F. Mughabghab, M. Divadeenam, and N. Holden, Neutron Cross Sections, Vol. **1**, Part A, Academic Press, New York (1981).
[134] F. Gunsing, A. Lepretre, C. Mounier, C. Raepsaet,A. Brusegan, and E. Macavero, "Neutron resonance spectroscopy of ^{99} Tc from 3 eV to 150 keV," Phys. Rev. **C 61**, 054608 (2000).
[135] S. Lee, S. Yamamoto, K. Kobayashi, G. Kim, and J. Chang, "Neutron capture cross Section measurement of Rhodium in the energy region from 0.003 eV to 80 keV by linac time-of flight method," Nucl. Sci. Eng. **144**, 94 (2003).
[136] A. Brusegan, E. Berthoumieux, A. Borella *et al.*, "Neutron capture and transmission measurements on ^{103}Rh down to thermal energies," Proceedings of Int. Conf. on Nuclear Data for Science and Technology, Santa Fe, September 26 - October 1, 2004, AIP 769, 953 (2005).
[137] F. De Corte and S. Van Lierde, "Evaluation of (n,γ) cross sections from k_0-factors for radionuclides with a short half-life and/or a complex activation-decay scheme," J. Radioanalitical nucl. Chem. **248**, 103 (2001).
[138] Y. Nakajima, M. Ohkubo, M. Sujimoto, M. Mizumoto, and Y. Kawarasaki, "Neutron Resonances of ^{133}Cs," Ann. Nuc. Energy **17**, 569 (1990).
[139] R.E. Heft, "A consistent set of nuclear-parameter values for absolute instrumental neutron activation analysis," Computers in Activation Analysis and Gamma-Ray Spectroscopy, Mayagues, Puerto Rico, 30 April - 4 May, 495 (1978).
[140] M.J. Cabell and W. Wilkens, "Mass spectrometric measurements of the neutron capture Cross sections of ^{142}Nd, ^{143}Nd, ^{144}Nd, and ^{145}Nd for reactor and Maxwellian neutrons," J. Inorg. Chem. **30**, 897 (1967).
[141] D.B. Barry, M.J. Trbovich, Y. Danon *et al.*, "Neutron transmission and capture measurements and resonance analysis of neodymium from 1 to 500 eV," Nuc. Sci Eng. **153**, 8 (2006).
[142] J.A. Harvey, J. Halperin, N.W. Hill, R.L.Macklin, and S. Raman, "Parameters 0f the 203.4 eV resonance in ^{59}Ni," DOE/NDC-12/U, 231, April 1978.
[143] A.M. Alpizar-Vicente, T.A. Bredeweg, E.I. Esch *et al.*, "Neutron capture cross section of ^{62}Ni at s-process energies," Phys. Rev. **C 77**, 015806 (2008)
[144] C. Domingo-Pardo, I. Dillman T. Faestermann *et al.*, "s-Process nucleosynthesis in massive stars: new results on ^{60}Fe, ^{62}Ni and ^{64}Ni," Proc. Capture Gamma-ray Spectroscopy and Related topics **AIP 978**, 230 (2009).
[145] C. Lubitz, [private communication].
[146] M.A.Lone, "Thermal-neutron capture cross section measurements," Proc. Neutron Capture Gamma-Ray Spectroscopy and Related Topics 383 (1981), 7-11 September 1981 Grenoble, France.
[147] S. Nakamura, H. Harada, S. Raman, and P. Koehler, "Thermal neutron capture cross sections of zirconium-91 and zirconium-93 by prompt γ-ray spectroscopy," J. Nuc. Sci Tech. **44**, 21 (2007).
[148] S. F. Mughabghab, "Uncertainty treatment in the unresolved energy region" Report to CSWEG meeting, Santa Fe, November 2010, available from *http://www.nndc.bnl.gov/proceedings/2010csewgusndp/Tuesday/CSEWG/Mugabgab_SIGTOTAL.pdf*.
[149] E.Sh. Soukhovitskij, G.B. Morogovskij, S. Chiba, O. Iwamoto and T. Fukahori, "Physics and Numerical Methods of OPTMAN: A Coupled-channels Method Based on Soft-rotator Model for a Description of Collective Nuclear Structure and Excitations," JAERI-Data/Code 2004-002 (March 2004).
[150] M. Herman, P. Obložinský, C.M. Mattoon, M. Pigni, S. Hoblit, S.F. Mughabghab, A. Sonzogni, P. Talou, M.B. Chadwick, G.M. Hale, A.C. Kahler, T. Kawano, R.C. Little, P.G. Young, "COMMARA-2.0 Neutron Cross Section Covariance Library," BNL- 94830-2011 (2011).
[151] R.D. Mosteller, R.E. Macfarlane, S. F. Mughabghab, and S.S. Kim, "Development and testing of a revised ENDF/B-VII capture cross section for ^{113}Cd, Proceedings of PHYSOR-2008, contribution 088 (2008).
[152] Y. Danon, R.C. Block, N. Francis, M. Lubert, F. Saglime, R. Bahran, D.P. Barry N.J. Drindak, J.G. Hoole, and G. Leinweber, "Cross Section Measurements and Analysis at Rensselaer," Report to CSWEG meeting, November 2007 (unpublished).
[153] S. Kopecky, I. Ivanov, M. Moxon, P. Schillebeecks, P. Siegler, and I. Sirakov, "The total cross section and resonance parameters for the 0.178 eV resonance of ^{113}Cd," Nuc. Inst. Meth. **B 267**, 2345 (2009).
[154] H. Rauch, M. Zawisky, Ch.Stellmch, and P. Geltenbort, "Giant absorption cross section of ultracold neutrons in gadolinium," Phys. Rev. Lett. **83**, 4955 (1999).
[155] G. Leinweber, D. P. Barry, M. J. Trbovich, J. A. Burke, N.J. Drindak, H. D. Knox, and R. V. Ballad, "Neutron capture and total cross section measurements and resonance parameters of gadolinium", Nucl. Sci. Eng. **154**, 261 (2006).
[156] G. Perret, M.F. Murphy, F. Jatuff, J-Ch. Sublet, O.Bouland, and R. Chawla, "Impact of new Gadolinium cross sections on reaction rate distributions in 10X10 BWR assemblies," Nucl. Sci. Eng. **163**, 17 (2009).
[157] M. Sin, R. Capote, A. Ventura, M. Herman and P. Obložinský, "Fission of light actinides: ^{232}Th(n,f) and ^{231}Pa(n,f) reactions", Phys. Rev. **C74**, 014608 (2006).
[158] R. Capote, L. Leal, Liu Ping, Liu Tingjin, P. Schillebeeckx, M. Sin, I. Sirakov, and A. Trkov, "Evaluated Nuclear Data for Nuclides within the Thorium-Uranium Fuel Cycle", *Technical report STI/PUB/1435*, ISBN 978–92–0–101010–0, International Atomic Energy Agency, Vienna, Austria (2010). (Available from *http://www-nds.iaea.org/reports-new/tecdocs/*).
[159] R. Capote Noy, V. Maslov, E. Bauge, T. Ohsawa, A. Vorobyev, M.B. Chadwick, and S. Oberstedt "Summary Report of the Consultants' Meeting on Prompt Fission Neutron Spectra of Major Ac-

tinides", Vienna, Austria 24-27 November 2008, *Report INDC(NDS)–282*, International Atomic Energy Agency, Vienna, Austria (2008). (Available from *http://www-nds.iaea.org/reports-new/indc-reports/ indc-nds/indc-nds-0541.pdf*).

[160] R. Capote Noy, "Summary Report of the First Research Coordination Meeting on Prompt Fission Neutron Spectra of Major Actinides", IAEA Headquarters Vienna, Austria, 6-9 April 2010, *Report INDC(NDS)–282*, International Atomic Energy Agency, Vienna, Austria (2010) (Available from *http://www-nds.iaea.org/reports-new/indc-reports/indc-nds/indc-nds-0571.pdf*).

[161] N.A. Tetereva, V.G. Pronyaev, T. Granier, and F.J, Hampsch, "Advanced evaluation of ^{237}Np and ^{243}Am neutron data", J. Korean Physical Society **59**, 867-870 (2011).

[162] D.W. Efurd,"3037-Flattop Irradiations of ^{241}Am, ^{243}Am, ^{237}Np, and Ir," Los Alamos National Laboratory memo INC11-86-541 (1986).

[163] R. Capote Noy, "Summary Report of the Consultants' Meeting on Review Benchmarking of Nuclear Data for the Th/U Fuel Cycle", Vienna, Austria 20-22 December 2010, *Report INDC(NDS)–0586*, International Atomic Energy Agency, Vienna, Austria (2008). (Available from *http://www-nds.iaea.org/publications/indc/indc-nds-0586.pdf*).

[164] G. Haouat, J. Lachkar, Ch. Lagrange, J. Jary, J. Sigaud, and Y. Patin, "Neutron Scattering Cross Sections for ^{232}Th, ^{233}U, ^{235}U, ^{238}U, ^{239}Pu, and ^{242}Pu between 0.6 and 3.4 MeV," Nucl. Sci. Eng. **81**, 491 (1982).

[165] S. Goriely, S. Hilaire, A.J. Koning, and R. Capote, "Towards improved evaluation of neutron-induced fission cross section," J. Kor. Phys. Soc. **59**, 979 (2011).

[166] S. Goriely, S. Hilaire, A.J. Koning, and R. Capote, "Towards improved evaluation of neutron-induced cross sections on actinides", Phys. Rev. **C83**, 034601 (2011).

[167] J. W. Behrens, "Systematics of Neutron-Induced-Fission Cross Sections in the MeV Range," Phys. Rev. Lett. **39**, 68 (1977); "Systematics of neutron-induced fission cross sections over the energy range 0.1 through 15 MeV, and at 0.0253 eV," LLNL Internal Report UCIS-17509-2 (1977).

[168] W. Younes and H. C. Britt, "Simulated neutron-induced fission cross sections for various Pu, U, and Th isotopes," Phys. Rev. C **68**, 034610 (2003).

[169] W. Younes and H. C. Britt, "Estimates of the 237,239U(n,f) Cross Sections for 0.1 < En(MeV) <= 20," LLNL Internal Report UCRL-TR-212600 (2005).

[170] J.T.Burke *et al.*, LLNL Internal Report LLNL-TR-460634-DRAFT (2009), to be submitted to Phys. Rev. C.

[171] F. Manero and V. A. Konshin, "Status of the energy dependent nu-values for the heavy isotopes (Z¿90) from thermal to 15 MeV and nu-values for spontaneous fission," At. En. Rev. **10**, 637 (1972).

[172] B. Pritychenko, "Nuclear Data Resources for Capture gamma-Ray Spectroscopy and Related Topics," Proc. 14^{th} Int. Symp. Capt. Gamma-Ray Spectr. Rel. Topics, August 28 - September 2 2011, University of Guelph, Guelph, Ontario, Canada.

[173] E. Soukhovitskii, S. Chiba, J.-Y. Lee, O. Iwamoto, T. Fukahori, "Global coupled-channel optical potential for nucleon-actinide interaction from 1 keV to 200 MeV," Journal Phys. G: Nucl. Part. Phys. **30**, 905 (2004).

[174] P. G. Young, E.D. Arthur, and M. B. Chadwick, *"Comprehensive Nuclear Model Calculations: Theory and Use of the GNASH Code,"* Proc. Workshop on Nuclear Reaction Data and Nuclear Reactors, ICTP, Trieste, Italy, 15 April - 17 May 1996, Ed: A. Gandini and G. Reffo, World Scientific Publ. Co., Singapore, p.227-404 (1998).

[175] C. L. Dunford, "A Unified Model for Analysis of Compound Nucleus Reactions," AI-AEC-12931 (1970).

[176] D. M. Hetrick and C. Y. FU, *"GLUCS: A Generalized Least-Squares Program for Updating Cross-Section Evaluations with Correlated Data Sets,"* Oak Ridge National Laboratory Report ORNL/TM-7341 (ENDF-303) (1980).

[177] O. Iwamoto, T. Nakagawa, N. Otuka, S. Chiba, K. Okumura, G. Chiba, T. Ohsawa, K. Furutaka, "JENDL Actinoid File 2008," J. Nucl. Sci. Technol. **46**, 510 (2009).

[178] T. E. Young, F. B. Simpson, J. R. Berreth, and M.S. Coops, "Neutron Total and Absorption Cross Sections of Pu-238," Nucl. Sci. Eng. **30**, 355 (1967).

[179] P. Möller, J. R. Nix, W. D. Myers, and W. J. Swiatecki, "Nuclear Ground-State Masses and Deformations," Atomic Data Nucl. Data Tables **59** 185 (1995).

[180] M. Baba, H. Wakabayashi, N. Itoh, K. Maeda, and N. Hirakawa, "Measurements of Prompt Fission Neutron Spectra and Double-differential Neutron Inelastic-scattering Cross Sections for ^{238}U and ^{232}Th," IAEA Int. Nucl. Data report INDC(JPN)-129 (1989).

[181] P. Talou, P. G. Young, T. Kawano, A. C. Kahler, and M. B. Chadwick, "Technical Report on n+^{240}Pu Evaluation and Uncertainty Quantification," Los Alamos National Laboratory Report LA-UR 09-08071 (2009).

[182] M. G. Silbert, A. Moat, and T. E. Young, "Fission cross section of plutonium-238," Nucl. Sci. Eng. **52**, 176 (1973).

[183] C. Budtz-Jørgensen, H.H. Knitter, D.L. Smith, H. Bax and R. Vogt, "Fission Cross Section of ^{238}Pu," Proc. Int. Conf. on Nuclear Data for Science and Technology, K.H. Böckhoff, Ed., Antwerp, Sep. 6-10, 1982, D. Reidel Publishing Company, 206 (1982).

[184] S. B. Ermagambetov and G. N. Smirenkin, "Cross-section of Pu-238 fission by fast neutrons," At. Energ. **25**, 527 (1968).

[185] J.J. Ressler, J.T. Burke, J.E. Escher, C.T. Angell, M.S. Basunia, C.W. Bausang, L.A. Bernstein, D.L. Bleuel, B.L. Goldblum, J. Gostic, R. Hatarik, R.A. Henderson, J. Munson, E.B. Norman, L.W. Phair, T. Ross, N.D. Scielzo, M. Wiedeking, "Surrogate Measurement of the ^{238}Pu (n,f) Cross Section", LLNL Technical Report LLNL-TR-457798 (2010).

[186] T. Granier, R. Nelson, P. Romain, M. Devlin, and N. Fotiades, "New Measurement of the ^{238}Pu (n,f) Cross-Section", Proceedings of the Fourth International Workshop on Nuclear Fission and Fission-Product Spectroscopy, Cadarache, France, 13-16 May 2009, Eds. A.Chatillon, H.Faust, G.Fioni, D.Goutte, H.Goutte, **AIP CP1175**, 227 (2009).

[187] M. G. Silbert and J. R. Berreth, "Neutron Capture Cross Section of Plutonium-238: Determination of Resonance Parameters," Nucl. Sci. Eng. **52**, 187 (1973).

[188] D. G. Madland and J. R. Nix, "New Calculation of Prompt Fission Neutron Spectra and Average Prompt Neutron Multiplicities," Nucl. Sci. Eng. **81**, 213

(1982).
[189] A. Tudora, "Systematic Behaviour of the Average Parameters Required for the Los Alamos Model of Prompt Neutron Emission," Annals of Nuclear Energy **36**, 72 (2009).
[190] A. H. Jaffey and J. L. Lerner, "Measurement of prompt neutron fission yield (imagep) in thermal neutron fission of ^{232}U, ^{238}Pu, ^{241}Pu, ^{241}Am, ^{242m}Am, ^{243}Cm, ^{245}Cm and in spontaneous fission of ^{244}Cm," Nucl. Phys. **A145**, 1 (1970).
[191] N. I. Kroshkin and J. S. Zamjatnin, "Measurement of energy spectrum and average number of prompt fission neutrons," Atomic Energy **29**, 790 (1970).
[192] W. P. Poenitz, J. F. Whalen, and A.B. Smith, "Total Neutron Cross Sections of Heavy Nuclei," Nucl. Sci. Eng. **78**, 333 (1981).
[193] W. P. Poenitz and J. F. Whalen, "Neutron Total Cross Section Measurements in the Energy Region from 47 keV to 20 MeV," Argonne National Laboratory Report ANL/NDM/80 (1983).
[194] A. B. Smith, J. F. Whalen, and P. Lambropoulos, " Fast Neutron Total and Scattering Cross Sections of Plutonium-240," Nucl. Sci. Eng. **47**, 19 (1972).
[195] F. Tovesson, T. S. Hill, M. Mocko, J. D. Baker, and C. A. Mcgrath, "Neutron Induced Fission of ^{240}Pu and ^{242}Pu from 1eV to 200 MeV," Phys .Rev. **C 79**, 014613 (2009).
[196] A. B. Laptev, A. Yu. Donets, A. V. Fomichev, A. A. Fomichev, R. C. Haight, O. A. Shcherbakov, S. M. Soloviev, Yu. V. Tuboltsev, and A. S. Vorobyev, "Neutron Induced Fission Cross Sections of ^{240}Pu and ^{243}Am in the Energy Range 1−200 MeV," Nucl. Phys. **A734**, E45 (2004).
[197] P. Staples and K. Morley, "Neutron-Induced Fission Cross-Section Ratios for ^{239}Pu, ^{240}Pu, ^{242}Pu, and ^{244}Pu Relative to ^{235}U from 0.5 to 400 MeV," Nucl. Sci. Eng. **129**, 149 (1998).
[198] L. W. Weston and J. H. Todd, "Neutron Capture Cross Section of Plutonium-240," Nucl. Sci. Eng. **63**, 143 (1977).
[199] K. Wisshak and F. Käppeler, "Neutron Capture Cross-Section Ratios of Pu-240, Pu-242,U-238 and Au-197 in the Energy Range from 10 to 90 keV," Nucl. Sci. Eng. **66**, 363 (1978).
[200] K. Wisshak and F. Käppeler, "A Measurement of the Subthreshold Neutron Fission Cross-Section of Pu-240 in the Energy Range from 10 to 250 keV," Nucl. Sci. Eng. **69**, 39 (1979).
[201] J. Fréhaut, G. Mosinski, R. Bois, and M. Soleilhac, "Measurement of the Average Number, NU-Bar, of the Prompt Neutrons Emitted in the Pu-240 and Pu-241 Fission Induced by Neutrons of Energy Between 1.5 and 15 MeV," CEA Technical Report CEA-R-4626, 7411 (1974).
[202] V. G. Vorobjova, N. P. Djachenko, N. P. Kolosov, B. D. Kuzminov, A.I. Sergachjov, and ,V. M. Surin, "Yields and Kinetic Energies of Fragments from Fission of the Pu-241 Nuclei Induced by Fast Neutrons," Yadernaya Fizika **19 (6)**, 1276 (1974).
[203] B. D. Kuzminov, "Average Number of Prompt Neutrons in Pu240 Fission by 3.6- And 15-MeV Neutrons," Nejtronfiz **246** (1961).
[204] Yu. A. Khokhlov, I. A. Ivanin, V. I. Inkov, Yu. I. Vinogradov, L. D. Danilin, and B. N. Polynov, "Measurements results of average neutron multiplicity from neutron induced fission of actinides in 0.5-10 MeV energy range," Proc. of the Int. Conf. Nuclear Data for Science and Technology, Gatlinburg, Tennessee, USA, May 9-13, **I**, 272 (1994).
[205] G. Palmiotti and H. Hiruta, "Data testing at INEL using irradiation experiments," Mini CSWEG Meeting June 22, 2011, Montauk, NY, unpublished.
[206] A.A. Druzhinin, V.K. Grigor'ev, A.A. Lbov *et al.*, "Fast neutron capture Cross sections", Atomnaya Energiya **42**, 314 (1977).
[207] F. Marie, A. Letourneau, G. Fioni *et al.*, "Thermal neutron capture cross section measurements of ^{243}Am and ^{242}Pu using the new mini-INCA α- and γ- spectroscopy station," Nucl. Inst. Meth. **A 556**, (2006).
[208] J. P. Butler, M. Loundsbury, and J. S. Merritt, "The neutron capture cross section of ^{238}Pu ^{238}Pu and ^{243}Am in the thermal and epicadmium regions," Can. J. Phys. **35**, 147 (1957).
[209] M. Jandel, T.A. Bredeweg, E.M. Bond, M.B. Chadwick, R.R. Clement, A. Couture, J.M. O'Donnell, R.C. Haight, T. Kawano, R. Reifarth,, R.S. Rundberg, J.L. Ullmann, D.J. Vieira, J.B. Wilhelmy, J.M. Wouters, U. Agvaanluvsan, W.E. Parker, C.Y. Wu, J.A. Becker, "Neutron capture cross section of ^{241}Am," Phys. Rev. **C 78**, 034609 (2008).
[210] J. Tommasi, G. Noguere, "Analysis of the PROFIL and PROFIL-2 sample irradiation experiments in Phenix for JEFF-3.1 nuclear data validation", Nucl. Sci. Eng. **160**, 232-241 (2008).
[211] P. Talou, T. Kawano, M.B. Chadwick, and R. E. MacFarlane, "Improved evaluations of neutron-induced reactions on americium isotopes", Nuc. Sci. Eng. 155, 84, (2007).
[212] A, Tonchev, *et al.*, "Measurement of the ^{241}Am$(n, 2n)$ reaction cross section from 7.6 MeV to 14.5 MeV", Phys. Rev. **C 77**, 054610 (2008).
[213] C. Sage, V. Semkova, O. Bouland, P. Dessagne, A. Fernandez, F. Gunsing, C. Nastren, G. Noguere, H. Ottmar, A.J.M. Plompen, P. Romain, G. Rudolf, J. Somers, and F. Wastin, "High resolution measurements of the ^{241}Am$(n, 2n)$ reaction cross section, Phys. Rev. **C81**, 064604 (2010).
[214] M.B. Chadwick, NEDPC (2008).
[215] L. W. Weston and J. H. Todd, "Neutron capture cross section of ^{243}Am," Nucl. Sci. Eng. **91**, 444 (1985).
[216] M. Ohta, S. Nakaruma, H. Harada, T. Fujii, and H. Yamana, "Measurement of the effective capture cross section of Americium-243 for thermal neutrons," J. Nucl. Sci. Tech. **43**, 144 (2006).
[217] K. Wisshak and F. Kappeler, "Neutron capture and fission cross sections of americium-243 in the energy range from 5 to 250 keV," Report KFK 3506 (1983); Nucl. Sci. Eng. **85**, 251 (1983).
[218] O. Iwamoto, T. Nakagawa, N. Otuka, S. Chiba, K. Okumura, and G. Chiba, "JENDL Actinoid File 2008 and Plan of Covariance Evaluation," Nuclear Data Sheets **109**, 2885 (2008).
[219] K. Shibata, O. Iwamoto, T. Nakagawa, N. Iwamoto, A. Ichihara, S. Kunieda, S. Chiba, N. Otuka, and J. Katakura, "JENDL-4.0: A New Library for Innovative Nuclear Energy Systems," J. Korean Phys. Soc. **59**, 1046 (2011).
[220] O. Iwamoto, T. Nakagawa, N. Otuka, and S. Chiba,

"Covariance Evaluation for Actinide Nuclear Data in JENDL-4," J. Korean Phys. Soc. **59**, 1224 (2011).
[221] D. A. Brown, "Review of JENDL Actinoid File 2008," Lawrence Livermore National Laboratory Internal Report LLNL-TM-419387 (2009).
[222] B.C. Kiedrowski,"Theory, Interface, Verification, Validation, and Performance of the Adjoint-Weighted Point Reactor Kinetics Parameter Calculations in MCN", Tech. Rep., Los Alamos National Laboratory, LA-UR-10-01700 (2010).
[223] Y. Yedvab, I. Reiss, et. al., "Determination of Delayed Neutrons Source in the Frequency Domain Based on inpile Oscillation Measurements", Proc. PHYSOR 2006, Vancouver, Canada, Sept. 10-14 (2006).
[224] R. Sher and C. Beck, "Fission Energy Release for 16 Fissioning Nuclides," EPRI-NP-1771, Stanford University (1981).
[225] D. Madland, "Total Prompt Energy Release in the Neutron-Induced Fission of ^{235}U, ^{238}U and ^{239}Pu," Nucl. Phys. **A 772**, 113 (2006).
[226] R. Vogt, B. Beck, D. A. Brown, F. Daffin and J. Hedstrom, "Implementation of Energy-Dependent Q Values for Fission," UCRL-TR-234617, Lawrence Livermore National Laboratory (2007).
[227] R. Vogt, "Generalized Energy-Dependent Fission Q Values," LLNL-TR-407620, Lawrence Livermore National Laboratory (2008).
[228] R. Vogt, "Generalized Energy-Dependent Q Values for Fission," J. Korean Phys. Soc. **59**, 899 (2011).
[229] D. A. Brown, M.-A. Descalle, R. Hoffman, K. Kelley, P. Navratil, J. Pruet, N. Summers, I. Thompson, R. Vogt, "Release of the 2008 Evaluated Nuclear Data Library (ENDL2008)," LLNL-TR-413190, Lawrence Livermore National Laboratory (2009).
[230] V. Pronyaev, A. Carlson, R. Capote Noy, and A. Wallner, "Summary Report from the Consultants' Meeting on International Cross-Section Standards:Extending and Updating, 13 - 15 October 2010, Vienna," *Report INDC(NDS)–0583*, International Atomic Energy Agency, Vienna, Austria (2011). (Available from *http://www-nds.iaea.org/publications/indc/indc-nds-0583.pdf*).
[231] V. Pronyaev, A. Carlson, R. Capote Noy, and A. Wallner, "Summary Report from the Consultants' Meeting on International Neutron Cross-Section Standards: Measurements and Evaluation Techniques, 13 - 15 October 2008, Vienna," *Report INDC(NDS)–0540*, International Atomic Energy Agency, Vienna, Austria (2008). (Available from *http://www-nds.iaea.org/publications/indc/indc-nds-0540.pdf*).
[232] W. Ratynski and F. Käppeler, "Neutron capture cross section of ^{197}Au: A standard for stellar nucleosynthesis," Phys. Rev. **C37**, 595 (1988).
[233] R.L. Macklin, J. Halperin and R.R. Winters, "Gold neutron-capture cross section from 3 to 550 keV," Phys. Rev. **C11**, 1270 (1975).
[234] R.L. Macklin, "Gold neutron capture cross section from 100 TO 2000 keV," private communication to S.F. Mughabghab, 1982; see also EXFOR 12720.
[235] C. Lederer *et al.* (n_TOF Collaboration), "197Au(n,gamma) cross section in the unresolved resonance region", Phys. Rev. **C83**, 034608 (2011).
[236] A. Borella *et al.*, "Determination of the ^{232}Th(n,γ) Cross Section from 4 to 140 keV at GELINA", Nucl. Sci. Eng. **152**, 1 (2006).
[237] C. Lampoudis, IRMM, Private Communication (2011).
[238] A. Wallner, T. Belgya, M. Bichler, K. Buczak, I. Dillmann, F. Käppeler, A. Mengoni, F. Quinto, P. Steier, L. Szentmiklosi, "Neutron-capture studies of ^{235}U and ^{238}U via AMS," J. Korean Phys. Soc. **59**, 1410 (2011).
[239] A. Krasa, A. Plompen, G. Georginis, G. Feinberg, M. Friedman, A. Shor , Y. Eisen , D. Berkovits , M. Paul, "^{197}Au(n,γ) cross-section in Maxwellian-like neutron spectrum," paper presented at the Workshop on Activation Data, 1-3 June 2011, Prague, Czech Republic (http://www.ccfe.ac.uk/easy2011/Prague-2011/eaf2011-08-krasa.pdf).
[240] G. Feinberg *et al.* "Quasi-stellar neutrons from the 7Li(p,n) reaction with an energy-broadened proton beam", publication in preparation (2011).
[241] N.V. Kornilov *et al.* "The ^{235}U(n,f) prompt fission neutron spectrum ay 100^{o}K input neutron energy", Nucl. Sci. Eng. **165**, 117 (2010).
[242] A. Vorobyev *et al.* "EFNUDAT Workshop: Measurements and Models of Nuclear Reactions", Eur. Phys. J Web of Conferences **8**, 03004, Paris (2010).
[243] T. R. England and B. F. Rider, "Evaluation and Compilation of Fission Product Yields," ENDF-349, LA-UR-94-3106, Los Alamos National Laboratory (1994); Available from `http://t2.lanl.gov/publications/yields/apxA.txt`.
[244] H. D. Selby, M. R. Mac Innes, D. W. Barr, A. L. Keksis, R. A Meade, C. J. Burns, M. B. Chadwick, and T. C. Wallstrom, "Fission Product Data Measured at Los Alamos for Fission Spectrum and Thermal Neutrons on ^{239}Pu, ^{235}U, ^{238}U," Nuclear Data Sheets **111**, 2891 (2010).
[245] M. MacInnes, M.B. Chadwick, and T. Kawano, "Fission Product Yields for 14 MeV Neutrons on ^{235}U, ^{238}U and ^{239}Pu," Nuclear Data Sheets **112**, 3135 (2011).
[246] W. J. Maeck, "Fast Reactor Fission Yields for ^{239}Pu and ^{241}Pu," Allied Chemical Corporation, Idaho Chemical Programs Rept., ICP-1050-II (1977).
[247] W. J. Maeck, "The correlation of ^{239}Pu thermal and fast reactor fission yields with neutron energy," Allied Chemical Corporation — Idaho Chemical Programs Report, ENICO-1030 (1981).
[248] I.J. Thompson, Y.M.X.M. Dardenne, J.M. Keneally, A. Roberton, L.E. Ahle, C.A. Hagmann, R.A. Henderson, D. Vogt, C.Y. Wu, and W. Younes, "Evaluations of Fission Chain Yields for ^{239}Pu from Fission-Spectrum Neutrons", Livermore report LLNL-JRNL-463744 (2011), submitted to Nucl. Sci. Eng. (2011).
[249] H. C. Britt, J. M. Dairiki, R. W. Lougheed, D. P. McNabb, and S. Prussin, "Review of the Status of Cumulative Fission Yields from ^{239}Pu(n,f) of Interest to Nuclear Forensics," Lawrence Livermore Laboratory Report, LLNL-TR-458777 (2010).
[250] J.P. Lestone, "Energy dependence of Pu fission product yield," Nuclear Data Sheets **112**, 3120 (2011).
[251] J. E. Gindler, L. E. Glendenin, D. J. Henderson, and J.W. Meadows, "Mass distributions in monoenergetic-neutron-induced fission of ^{239}Pu," Phys. Rev. **C 27**, 2058 (1983).
[252] J. A. Schecker, M. R. Mac Innes, D. W. Barr, and W. C. T. Inkret, "A Re-evaluation of LANL's Historic Radiochemistry Constants," LA-UR-05-3760, Los Alamos National Laboratory (2005).

[253] G. P. Ford and A. E. Norris, "A Compilation of Yields from Neutron-Induced Fission of ^{232}Th, ^{235}U, ^{236}U, ^{237}Np, ^{238}U and ^{239}Pu Measured Radiochemically at Los Alamos," LA-6129, Los Alamos National Laboratory (1976).

[254] D. L. Nethaway to M. MacInnes, Private communication, "Fission Product Yields at 14 MeV", Lawrence Livermore National Laboratory, October 12, (1971).

[255] D. L. Nethaway and A. L. Prindle, "Evaluation of fission yields for ^{239}Pu plus 14 MeV neutrons", Lawrence Livermore National Laboratory Chemistry Department Technical Note No. 72-48, September 21 (1972). See also Note No. 72-51 for ^{235,238}U, October 25 (1972).

[256] J.A. Becker, D.J. Vieira, R.S. Rundberg, J.B. Wilhelmy, R. Macri, C. Hagmann, M.A. Stoyer, A. Tonchev, "Modernizing the fission basis", Lawrence Livermore National Laboratory report LLNL-PROP-246546 (2010).

[257] J.A. Becker, M.B. Chadwick, and J. Ferguson, "The ^{239}Pu(n,2n) Story (U)," Defense Research Review **14.1**, 19 (2006).

[258] T.W. Burrows, "The evaluated nuclear structure data file: Philosophy, content, and uses" Nucl. Instr. and Meth. **A 286** 595, (1990); J.K. Tuli, "Evaluated nuclear structure data file," Nucl. Instr. and Meth. **A 369** 506, (1996); (Available from www.nndc.bnl.gov/ensdf).

[259] "Table of Isotopes," 8th edition, R.B. Firestone, V. Shirley, C.M. Baglin, S.Y.F. Chu and J. Zipkin. John Wiley & Sons (1996).

[260] D.E. Cullen *et al.*, "Tables and graphs of photon interaction cross-sections from 10-eV to 100-GeV derived from the LLNL evaluated photon data library (EPDL). Part A: Z = 1 to 50," Lawrence Livermore National Laboratory Report, UCRL-50400, Vol. 30, (1991).

[261] J. Stepanek, "Methods to determine the fluorescence and Auger spectra due to decay of radionuclides or due to a single atomic-subshell ionization and comparisons with experiments," Medical Physics, **27**, 1544 (2000).

[262] T. Kibedi, T.W. Burrows, M.B. Trzhaskovskaya, P.M. Davidson, C.W. Nestor, Jr., "Evaluation of theoretical conversion coefficients using BrIcc," Nucl. Instr. and Meth. **A 589**, 202 (2008).

[263] G. Audi, A.H. Wapstra, C. Thibault, "The AME2003 atomic mass Evaluation (II). Tables, graphs, and references," Nuclear Physics **A729**, 337 (2003).

[264] T. Kawano, P. Moller, W.B. Wilson, "Calculation of delayed-neutron energy spectra in a quasiparticle random-phase approximation-Hauser-Feshbach model," Physical Review **C 78**, 054601 (2008).

[265] B. Pfeiffer, K. Kratz, P. Moller, "Status of delayed-Neutron Precursor Data: Half-Lives and Neutron Emission Probabilities," Prog. Nucl. Energy **41**, 39 (2002).

[266] A.Algora, D.Jordan, J.L.Tain, B.Rubio, J.Agramunt, A.B.Perez-Cerdan, F.Molina, L.Caballero, E.Nacher, A.Krasznahorkay, M.D.Hunyadi, J.Gulyas, A.Vitez, M.Csatlos, L.Csige, J.Aysto, H.Penttila, I.D.Moore, T.Eronen, A.Jokinen, A.Nieminen, J.Hakala, P.Karvonen, A.Kankainen, A.Saastamoinen, J.Rissanen, T.Kessler, C.Weber, J.Ronkainen, S.Rahaman, V.Elomaa, S.Rinta-Antila, U.Hager, T.Sonoda, K.Burkard, W.Huller, L.Batist, W.Gelletly, A.L.Nichols, T.Yoshida, A.A.Sonzogni, K.Perajarvi, "Reactor Decay Heat in ^{239}Pu: Solving the γ Discrepancy in the 4-3000-s Cooling Period," Phys.Rev.Lett. **105**, 202501 (2010).

[267] A. Tobias, "Derivation of Decay Heat Benchmarks for U-235 and Pu-239 by a Least. Squares Fit to Measured Data," Central Electricity Generating Board, CEGB Report No. RD/B/6210/R89 (1989).

[268] T. Goorley, "Initial MCNP6 Release Overview," submitted to Nuclear Technology (2011).

[269] R. Klein Meulekamp and S.C. van der Marck, "Calculating the effective delayed neutron fraction by Monte Carlo", Nucl. Sci. Eng. **152** (2006) 142-148.

[270] S.C. van der Marck, R. Klein Meulekamp, A. Hogenbirk, and A.J. Koning, "Benchmark results for delayed neutron data", Proc. ND2004, Santa Fe, USA (2004) 531.

[271] R. Reifarth, M. Heil, F. Käppeler, and R. Plag, "PINO-a tool for simulating neutron spectra resulting from the ^{7}Li(p,n) reaction," Nuclear Instruments and Methods in Physics Research **A 608**, 139 (2009).

[272] J.P. Lestone, "Preliminary Release of a Plutonium Prompt-Fission Neutron Energy Spectrum (PFNS) from the Analysis of NTS NUEX Data", Los Alamos National Laboratory report LA-UR-03167 (2011).

[273] B. Pritychenko, S.F. Mughabghab, and A.A. Sonzogni, "Calculations of Maxwellian-averaged cross sections and astrophysical reaction rates using the ENDF/B-VII.0, JEFF-3.1, JENDL-3.3, and ENDF/B-VI.8 evaluated nuclear reaction data libraries", Atomic Data and Nuclear Data Tables **96**, 645 (2010).

[274] D.E. Cullen, "The ENDF/B Pre-processing codes (PREPRO-2010)," Available online from *http://www-nds.iaea.org/ndspub/endf/prepro/*.

[275] B. Pritychenko, "Complete calculation of evaluated Maxwellian-averaged cross sections and their uncertainties for s-process nucleosynthesis", Proc. Nuclei in Cosmos, PoS(NIC-XI)197, Heidelberg, Germany, July 19-23 (2010).

[276] Z.Y. Bao, H. Beer, F. Käppeler *et al.*, "Neutron Cross Sections for Nucleosynthesis Studies", Atomic Data and Nuclear Data Tables **76**, 70 (2000).

[277] A.J. Koning, D. Rochman, "How to Randomly Evaluate Nuclear Data: A New Data Adjustment Method Applied to ^{239}Pu," Nucl. Sci. Eng. **169**, 68 (2011).

[278] C.-Y. Wu, R. Henderson, J. Gostic, R.C. Haight, and H.Y. Lee, "Low-Mass Fission Detector for the Fission Neutron Spectrum Measurement," Lawrence Livermore National Laboratory Internal Report LLNL-TR-461044 (2010).

[279] P. Talou, B. Becker, T. Kawano, and M.B. Chadwick, "Advanced Monte Carlo modeling of prompt fission neutrons for thermal and fast neutron-induced fission reactions on 239Pu ," Phys. Rev. **C 83**, 064612 (2011).

[280] J. Randrup and R. Vogt, "Calculation of fission observables through event-by-event simulation," Phys. Rev. **C 80**, 024601 (2009)

[281] S. Lemaire, P. Talou, T. Kawano, M.B. Chadwick, D.G. Madland, "Monte Carlo approach to sequential neutron emission from fission fragments", Phys. Rev. **C 72**, 024601 (2005).

[282] D. Williams, R. Bahran, E. Blaine, B. McDermott, M. Rapp, Y. Danon, D. Barry, G. Leinweber, R. Block, J. Hoole, "A new method for the measurement of the neutron capture and fission cross sections of ^{235}U", Submitted Proceedings of the Tenth International Topical Meeting on Nuclear Applications of Accelerators (Ac-

cApp 2011), Knoxville, TN, 2011.
[283] A. Chyzh, "Neutron Capture Measurements on ^{157}Gd and ^{89}Y at DANCE," PhD dissertation, North Carolina State University (2009).
[284] Yeong-Rok Kang, Tae-TK Ro, Taofeng Wang, Sung-shul Yang, Manwoo Lee, Guinyun Kim, Jong-Hwan Lee, Robert Block, Devin Barry and Yaron Danon, "Neutron Capture Measurements and Parameters of Gadolinium", International Conference on Nuclear Data for Science and Technology (ND2010), Korea, 26-30 April, 2010
[285] Baramsai Bayarbadrakh, "Neutron capture reactions on gadolinium isotopes," PhD dissertation, North Carolina State University (2010).
[286] R. Bahran, Y. Danon, M. Rapp, D. Williams, D. Barry, G. Leinweber, R. Block, J. Hoole, "A New High Resolution Neutron Transmission Detector at the RPI Gaerttner LINAC Laboratory", Submitted Proceedings of the Tenth International Topical Meeting on Nuclear Applications of Accelerators (AccApp 2011), Knoxville, TN, (2011).
[287] M. Herman, "Summary Document (Minutes) Presentations & Reports, CSEWG 2010". Available online http://www.nndc.bnl.gov/meetings/csewg2010.

APPENDIX A: MAXWELLIAN-AVERAGED 30-KEV CAPTURE

TABLE XLI: Maxwellian-averaged cross sections from ENDF/B-VII.0 [1], ENDF/B-VII.1, KADoNiS [36] and their ratios at kT=30 keV (C-calculated from BNL-325 data [133], T-theoretical data in KADoNiS).

Material	VII.0 (barns)	VII.1 (barns)	KADoNiS (barns)	VII.0/VII.1	KADoNiS/VII.1
1-H - 1	1.525E-4	1.525E-4±5.855E-6	2.540E-4±2.000E-5	1.000E+0	1.666E+0±1.312E-1
1-H - 2	1.998E-6	1.998E-6±1.265E-7	3.000E-6±2.000E-7	1.000E+0	1.502E+0±1.001E-1
1-H - 3					
2-He- 3	2.455E-8	2.126E-5	7.600E-6±6.000E-7	1.155E-3	3.575E-1±2.823E-2
2-He- 4					
3-Li- 6	3.275E-5	3.276E-5±3.181E-6		9.998E-1	
3-Li- 7	4.645E-5	4.645E-5±2.103E-5	4.200E-5±3.000E-6	9.999E-1	9.041E-1±6.458E-2
4-Be- 7					
4-Be- 9	1.128E-4	9.298E-6±1.860E-6	1.040E-5±1.600E-6	1.213E+1	1.118E+0±1.721E-1
5-B - 10	4.299E-4	4.299E-4±1.720E-4		9.999E-1	
5-B - 11	6.575E-5	6.575E-5±2.034E-5		1.000E+0	
6-C-0/6-C-12	1.344E-6	1.623E-5±3.246E-6	1.540E-5±1.000E-6	8.281E-2	9.488E-1±6.161E-2
7-N - 14	6.682E-5	6.683E-5	4.100E-5±6.000E-5^C	9.999E-1	6.135E-1±8.979E-1
7-N - 15	9.191E-6	9.190E-6±4.595E-6	5.800E-6±6.000E-7	1.000E+0	6.311E-1±6.529E-2
8-O - 16	1.692E-7	3.154E-5±3.249E-6	3.800E-5±4.000E-6	5.364E-3	1.205E+0±1.268E-1
8-O - 17	4.707E-6	4.708E-6		9.998E-1	
9-F - 19	4.362E-3	4.362E-3	3.200E-3±1.000E-4	1.000E+0	7.337E-1±2.293E-2
11-Na- 22	8.011E-3	8.011E-3		1.000E+0	
11-Na- 23	1.829E-3	1.829E-3±2.414E-4	2.100E-3±2.000E-4	1.000E+0	1.148E+0±1.094E-1
12-Mg- 24	3.793E-3	3.793E-3±7.183E-4	3.300E-3±4.000E-4	1.000E+0	8.701E-1±1.055E-1
12-Mg- 25	5.279E-3	5.279E-3±1.732E-3	6.400E-3±4.000E-4	1.000E+0	1.212E+0±7.577E-2
12-Mg- 26	8.645E-5	8.645E-5±1.625E-5	1.260E-4±9.000E-6	1.000E+0	1.457E+0±1.041E-1
13-Al- 27	3.303E-3	3.303E-3±5.615E-4	3.740E-3±3.000E-4	1.000E+0	1.132E+0±9.083E-2
14-Si- 28	3.608E-3	3.608E-3±7.998E-4	1.420E-3±1.300E-4	1.000E+0	3.936E-1±3.603E-2
14-Si- 29	7.755E-3	7.755E-3±8.328E-4	6.580E-3±6.600E-4	1.000E+0	8.485E-1±8.511E-2
14-Si- 30	4.432E-3	4.432E-3±1.514E-3	1.820E-3±3.300E-4	9.999E-1	4.106E-1±7.445E-2
15-P - 31	7.237E-3	7.238E-3	1.740E-3±9.000E-5	9.999E-1	2.404E-1±1.244E-2
16-S - 32	5.658E-3	5.658E-3	4.100E-3±2.000E-4	1.000E+0	7.246E-1±3.535E-2
16-S - 33	2.274E-3	2.274E-3	7.400E-3±1.500E-3	1.000E+0	3.255E+0±6.598E-1
16-S - 34	2.330E-4	2.330E-4	2.260E-4±1.000E-5	1.000E+0	9.701E-1±4.292E-2
16-S - 36	6.326E-4	6.327E-4	1.710E-4±1.400E-5	9.999E-1	2.703E-1±2.213E-2
17-Cl- 35	7.534E-3	7.529E-3	9.680E-3±2.100E-4	1.001E+0	1.286E+0±2.789E-2
17-Cl- 37	2.057E-3	2.041E-3	2.120E-3±7.000E-5	1.008E+0	1.039E+0±3.431E-2
18-Ar- 36	8.838E-3	8.838E-3	9.000E-3±1.500E-3^T	9.999E-1	1.018E+0±1.697E-1
18-Ar- 38	1.369E-4	1.369E-4	3.000E-3±3.000E-4^T	9.998E-1	2.191E+1±2.191E+0
18-Ar- 40	2.249E-3	2.249E-3	2.540E-3±1.000E-4	9.999E-1	1.129E+0±4.446E-2
19-K - 39	1.848E-2	1.056E-2	1.180E-2±4.000E-4	1.750E+0	1.117E+0±3.787E-2
19-K - 40	1.939E-2	1.939E-2	3.100E-2±7.000E-3^T	9.999E-1	1.599E+0±3.610E-1
19-K - 41	3.136E-2	2.029E-2±4.148E-3	2.200E-2±7.000E-4	1.545E+0	1.084E+0±3.449E-2
20-Ca- 40	5.142E-3	5.142E-3	5.730E-3±3.400E-4	1.000E+0	1.114E+0±6.612E-2
20-Ca- 42	1.240E-2	1.240E-2	1.560E-2±2.000E-3	1.000E+0	1.259E+0±1.613E-1
20-Ca- 43	3.526E-2	3.526E-2	5.100E-2±6.000E-3	1.000E+0	1.446E+0±1.702E-1
20-Ca- 44	7.738E-3	7.738E-3	9.400E-3±1.300E-3	1.000E+0	1.215E+0±1.680E-1
20-Ca- 46	1.859E-3	1.859E-3	5.300E-3±5.000E-4	1.000E+0	2.851E+0±2.690E-1
20-Ca- 48	1.079E-4	1.079E-4	8.700E-4±9.000E-5	1.000E+0	8.065E+0±8.343E-1
21-Sc- 45	6.835E-2	6.834E-2	6.900E-2±5.000E-3	1.000E+0	1.010E+0±7.316E-2
22-Ti- 46	2.039E-2	2.544E-2±3.096E-3	2.680E-2±3.200E-3	8.014E-1	1.053E+0±1.258E-1
22-Ti- 47	4.522E-2	4.864E-2±7.145E-3	6.440E-2±7.700E-3	9.297E-1	1.324E+0±1.583E-1
22-Ti- 48	3.303E-2	2.653E-2±1.507E-3	3.180E-2±5.100E-3	1.245E+0	1.199E+0±1.923E-1
22-Ti- 49	1.157E-2	1.582E-2±2.170E-3	2.210E-2±2.100E-3	7.315E-1	1.397E+0±1.328E-1
22-Ti- 50	3.105E-3	3.044E-3±4.119E-4	3.600E-3±4.000E-4	1.020E+0	1.183E+0±1.314E-1
23-V - 50		2.129E-2	5.000E-2±9.000E-2^T		2.348E+0±4.226E+0
23-V - 51		3.202E-2	3.800E-2±4.000E-3		1.187E+0±1.249E-1
24-Cr- 50	3.779E-2	3.825E-2±3.312E-3	4.900E-2±1.300E-2	9.880E-1	1.281E+0±3.399E-1
24-Cr- 52	8.657E-3	7.991E-3±3.995E-4	8.800E-3±2.300E-3	1.083E+0	1.101E+0±2.878E-1

TABLE XLI: Maxwellian-averaged cross sections (continued).

Material	**VII.0** (barns)	**VII.1** (barns)	**KADoNiS** (barns)	**VII.0/VII.1**	**KADoNiS/VII.1**
24-Cr- 53	3.139E-2	2.595E-2	5.800E-2±1.000E-2	1.210E+0	2.235E+0±3.854E-1
24-Cr- 54	7.693E-3	4.780E-3	6.700E-3±1.600E-3	1.609E+0	1.402E+0±3.347E-1
25-Mn- 55	3.099E-2	3.281E-2±2.664E-3	3.960E-2±3.000E-3	9.446E-1	1.207E+0±9.144E-2
26-Fe- 54	2.159E-2	2.159E-2±2.678E-3	2.960E-2±1.300E-3	9.999E-1	1.371E+0±6.021E-2
26-Fe- 56	1.151E-2	1.151E-2±1.179E-3	1.170E-2±5.000E-4	1.000E+0	1.017E+0±4.346E-2
26-Fe- 57	2.846E-2	2.845E-2±4.610E-3	4.000E-2±4.000E-3	1.000E+0	1.406E+0±1.406E-1
26-Fe- 58	1.973E-2	1.973E-2	1.350E-2±7.000E-4	9.999E-1	6.842E-1±3.548E-2
27-Co- 58	5.583E-2	2.020E-1		2.764E-1	
27-Co- 58M	6.437E-2	6.437E-2		1.000E+0	
27-Co- 59	3.442E-2	3.442E-2	3.960E-2±2.700E-3	1.000E+0	1.151E+0±7.845E-2
28-Ni- 58	4.001E-2	3.385E-2±3.318E-3	3.870E-2±1.500E-3	1.182E+0	1.143E+0±4.431E-2
28-Ni- 59	6.957E-2	6.957E-2	8.700E-2±1.400E-2^T	1.000E+0	1.251E+0±2.012E-1
28-Ni- 60	2.824E-2	2.674E-2±1.605E-3	2.990E-2±7.000E-4	1.056E+0	1.118E+0±2.618E-2
28-Ni- 61	7.173E-2	9.025E-2	8.200E-2±8.000E-3	7.948E-1	9.086E-1±8.864E-2
28-Ni- 62	5.143E-2	2.381E-2	2.230E-2±1.600E-3	2.160E+0	9.366E-1±6.720E-2
28-Ni- 64	2.199E-2	2.005E-2	8.000E-3±7.000E-4	1.097E+0	3.991E-1±3.492E-2
29-Cu- 63	7.145E-2	7.145E-2	5.560E-2±2.200E-3	1.000E+0	7.782E-1±3.079E-2
29-Cu- 65	3.913E-2	3.913E-2	2.980E-2±1.300E-3	1.000E+0	7.615E-1±3.322E-2
30-Zn- 64		6.098E-2	5.900E-2±5.000E-3		9.675E-1±8.199E-2
30-Zn- 65		1.677E-1	1.620E-1±2.700E-2^T		9.662E-1±1.610E-1
30-Zn- 66		3.641E-2	3.500E-2±3.000E-3		9.612E-1±8.239E-2
30-Zn- 67		1.157E-1	1.530E-1±1.500E-2		1.323E+0±1.297E-1
30-Zn- 68		2.075E-2	1.920E-2±2.400E-3		9.255E-1±1.157E-1
30-Zn- 70		1.171E-2	2.150E-2±2.000E-3^T		1.836E+0±1.708E-1
31-Ga- 69	1.184E-1	1.184E-1	1.390E-1±6.000E-3	9.997E-1	1.174E+0±5.066E-2
31-Ga- 71	1.223E-1	1.223E-1	1.230E-1±8.000E-3	1.000E+0	1.006E+0±6.542E-2
32-Ge- 70	8.913E-2	8.913E-2	8.800E-2±5.000E-3	1.000E+0	9.874E-1±5.610E-2
32-Ge- 72	5.295E-2	5.295E-2	7.300E-2±7.000E-3^T	1.000E+0	1.379E+0±1.322E-1
32-Ge- 73	2.096E-1	2.096E-1	2.430E-1±4.700E-2^T	1.000E+0	1.159E+0±2.243E-1
32-Ge- 74	4.540E-2	4.540E-2	3.760E-2±3.900E-3	1.000E+0	8.282E-1±8.591E-2
32-Ge- 76	1.700E-2	1.700E-2	2.150E-2±1.800E-3	1.000E+0	1.265E+0±1.059E-1
33-As- 74	1.361E+0	1.361E+0		9.999E-1	
33-As- 75	4.505E-1	4.500E-1	3.620E-1±1.900E-2	1.001E+0	8.045E-1±4.222E-2
34-Se- 74	2.083E-1	2.083E-1	2.710E-1±1.500E-2	1.000E+0	1.301E+0±7.202E-2
34-Se- 76	9.573E-2	9.573E-2	1.640E-1±8.000E-3	1.000E+0	1.713E+0±8.357E-2
34-Se- 77	4.447E-1	4.447E-1	4.180E-1±7.100E-2^T	9.999E-1	9.399E-1±1.596E-1
34-Se- 78	9.062E-2	9.062E-2	6.010E-2±9.600E-3	1.000E+0	6.632E-1±1.059E-1
34-Se- 79	4.145E-1	4.145E-1	2.630E-1±4.600E-2^T	1.000E+0	6.345E-1±1.110E-1
34-Se- 80	3.931E-2	3.931E-2	4.200E-2±3.000E-3	9.999E-1	1.068E+0±7.631E-2
34-Se- 82	3.110E-2	3.110E-2	9.000E-3±8.000E-2^T	1.000E+0	2.894E-1±2.573E+0
35-Br- 79	6.863E-1	6.863E-1	6.220E-1±3.400E-2	1.000E+0	9.063E-1±4.954E-2
35-Br- 81	2.286E-1	2.286E-1	2.390E-1±7.000E-3	1.000E+0	1.046E+0±3.063E-2
36-Kr- 78	3.800E-1	4.704E-1	3.210E-1±2.600E-2	8.078E-1	6.824E-1±5.527E-2
36-Kr- 80	2.944E-1	2.944E-1	2.670E-1±1.400E-2	1.000E+0	9.070E-1±4.756E-2
36-Kr- 82	1.027E-1	1.027E-1	9.000E-2±6.000E-3	1.000E+0	8.764E-1±5.843E-2
36-Kr- 83	2.668E-1	2.668E-1	2.430E-1±1.500E-2	9.998E-1	9.107E-1±5.621E-2
36-Kr- 84	2.637E-2	2.637E-2	3.800E-2±4.000E-3	1.000E+0	1.441E+0±1.517E-1
36-Kr- 85	1.223E-1	1.223E-1	5.500E-2±4.500E-2^T	9.997E-1	4.496E-1±3.678E-1
36-Kr- 86	5.064E-3	5.063E-3	3.400E-3±3.000E-4	1.000E+0	6.715E-1±5.925E-2
37-Rb- 85	2.816E-1	2.816E-1	2.340E-1±7.000E-3	9.999E-1	8.309E-1±2.486E-2
37-Rb- 86	3.164E-1	3.164E-1	2.020E-1±1.630E-1^T	9.999E-1	6.384E-1±5.151E-1
37-Rb- 87	2.325E-2	2.325E-2	1.570E-2±8.000E-4	1.000E+0	6.753E-1±3.441E-2
38-Sr- 84	3.188E-1	3.188E-1	3.000E-1±1.700E-2	1.000E+0	9.411E-1±5.333E-2
38-Sr- 86	6.145E-2	6.145E-2	6.400E-2±3.000E-3	1.000E+0	1.042E+0±4.882E-2
38-Sr- 87	8.049E-2	8.049E-2	9.200E-2±4.000E-3	1.000E+0	1.143E+0±4.970E-2
38-Sr- 88	5.214E-3	5.214E-3	6.130E-3±1.100E-4	1.000E+0	1.176E+0±2.110E-2
38-Sr- 89	1.446E-2	1.446E-2	1.900E-2±1.400E-2^T	1.000E+0	1.314E+0±9.682E-1
38-Sr- 90	1.459E-2	1.459E-2		9.997E-1	
39-Y - 89	1.700E-2	2.135E-2±1.843E-3	1.900E-2±6.000E-4	7.961E-1	8.897E-1±2.810E-2
39-Y - 90	5.568E-2	5.568E-2		1.000E+0	
39-Y - 91	8.776E-2	8.776E-2		1.000E+0	
40-Zr- 90	1.963E-2	1.891E-2±2.099E-3	1.930E-2±9.000E-4	1.038E+0	1.020E+0±4.759E-2
40-Zr- 91	6.487E-2	7.361E-2±1.281E-2	6.200E-2±3.400E-3	8.812E-1	8.422E-1±4.619E-2
40-Zr- 92	4.568E-2	4.543E-2±4.089E-3	3.010E-2±1.700E-3	1.006E+0	6.626E-1±3.742E-2
40-Zr- 93	1.009E-1	1.008E-1±2.176E-2	9.500E-2±1.000E-2	1.001E+0	9.428E-1±9.925E-2
40-Zr- 94	2.909E-2	2.900E-2±2.546E-3	2.600E-2±1.000E-3	1.003E+0	8.965E-1±3.448E-2
40-Zr- 95	1.392E-1	1.392E-1±2.578E-2	7.900E-2±1.200E-2^T	1.000E+0	5.675E-1±8.621E-2
40-Zr- 96	1.024E-2	1.025E-2±2.204E-3	1.070E-2±5.000E-4	9.991E-1	1.044E+0±4.879E-2
41-Nb- 93	2.662E-1	2.661E-1	2.660E-1±5.000E-3	1.000E+0	9.994E-1±1.879E-2
41-Nb- 94	3.172E-1	3.172E-1	4.820E-1±9.200E-2^T	9.999E-1	1.519E+0±2.900E-1
41-Nb- 95	4.027E-1	4.027E-1±9.785E-2	3.100E-1±6.500E-2^T	1.000E+0	7.699E-1±1.614E-1
42-Mo- 92	6.653E-2	6.914E-2±7.122E-3	7.000E-2±1.000E-2	9.622E-1	1.012E+0±1.446E-1
42-Mo- 94	1.097E-1	1.097E-1±1.481E-2	1.020E-1±2.000E-2	9.998E-1	9.296E-1±1.823E-1
42-Mo- 95	3.747E-1	3.756E-1±3.869E-2	2.920E-1±1.200E-2	9.976E-1	7.774E-1±3.195E-2
42-Mo- 96	1.035E-1	1.035E-1±1.346E-2	1.120E-1±8.000E-3	9.997E-1	1.082E+0±7.727E-2
42-Mo- 97	3.886E-1	3.886E-1±5.868E-2	3.390E-1±1.400E-2	1.000E+0	8.723E-1±3.603E-2
42-Mo- 98	9.503E-2	9.502E-2±4.751E-3	9.900E-2±7.000E-3	1.000E+0	1.042E+0±7.367E-2

TABLE XLI: Maxwellian-averaged cross sections (continued).

Material	**VII.0** (barns)	**VII.1** (barns)	**KADoNiS** (barns)	**VII.0/VII.1**	**KADoNiS/VII.1**
42-Mo- 99	4.795E-1	4.795E-1	2.400E-1±4.000E-2^T	9.999E-1	5.005E-1±8.341E-2
42-Mo-100	8.617E-2	8.617E-2±4.920E-3	1.080E-1±1.400E-2	1.000E+0	1.253E+0±1.625E-1
43-Tc- 99	9.094E-1	1.069E+0±9.197E-2	9.330E-1±4.700E-2	8.503E-1	8.724E-1±4.395E-2
44-Ru- 96	2.653E-1	2.653E-1	2.070E-1±8.000E-3	1.000E+0	7.803E-1±3.016E-2
44-Ru- 98	2.367E-1	2.367E-1	1.730E-1±3.600E-2^T	1.000E+0	7.309E-1±1.521E-1
44-Ru- 99	7.117E-1	7.118E-1	6.310E-1±9.900E-2^T	9.999E-1	8.865E-1±1.391E-1
44-Ru-100	2.035E-1	2.035E-1	2.060E-1±1.300E-2	9.999E-1	1.012E+0±6.387E-2
44-Ru-101	9.716E-1	9.716E-1±8.744E-2	9.960E-1±4.000E-2	1.000E+0	1.025E+0±4.117E-2
44-Ru-102	1.903E-1	1.903E-1±2.649E-2	1.510E-1±7.000E-3	1.000E+0	7.936E-1±3.679E-2
44-Ru-103	5.781E-1	5.781E-1±1.509E-1	3.430E-1±5.200E-2^T	9.999E-1	5.933E-1±8.994E-2
44-Ru-104	1.656E-1	1.656E-1±1.270E-2	1.540E-1±6.000E-3	1.000E+0	9.302E-1±3.624E-2
44-Ru-105	4.121E-1	4.122E-1		9.999E-1	
44-Ru-106	1.002E-1	1.002E-1±2.277E-2		9.997E-1	
45-Rh-103	8.026E-1	8.005E-1±6.828E-2	8.110E-1±1.400E-2	1.003E+0	1.013E+0±1.749E-2
45-Rh-105	8.276E-1	8.276E-1		1.000E+0	
46-Pd-102	4.591E-1	4.591E-1	3.690E-1±1.700E-2	1.000E+0	8.038E-1±3.703E-2
46-Pd-104	2.809E-1	2.809E-1	2.890E-1±2.900E-2	1.000E+0	1.029E+0±1.032E-1
46-Pd-105	1.185E+0	1.185E+0±1.502E-1	1.200E+0±6.000E-2	1.000E+0	1.013E+0±5.065E-2
46-Pd-106	2.369E-1	2.369E-1±4.999E-2	2.520E-1±2.500E-2	9.999E-1	1.064E+0±1.055E-1
46-Pd-107	1.296E+0	1.296E+0±1.835E-1	1.340E+0±6.000E-2	9.998E-1	1.034E+0±4.629E-2
46-Pd-108	2.090E-1	2.090E-1±4.619E-2	2.030E-1±2.000E-2	1.000E+0	9.713E-1±9.570E-2
46-Pd-110	1.567E-1	1.567E-1	1.460E-1±2.000E-2	1.000E+0	9.319E-1±1.277E-1
47-Ag-107	8.292E-1	8.292E-1	7.920E-1±3.000E-2	1.000E+0	9.552E-1±3.618E-2
47-Ag-109	7.786E-1	9.100E-1±1.432E-1	7.880E-1±3.000E-2	8.556E-1	8.659E-1±3.297E-2
47-Ag-110M	2.709E+0	2.709E+0		9.999E-1	
47-Ag-111	5.896E-1	5.896E-1		1.000E+0	
48-Cd-106	4.945E-1	4.964E-1	3.020E-1±2.400E-2	9.961E-1	6.083E-1±4.835E-2
48-Cd-108	3.984E-1	3.998E-1	2.020E-1±9.000E-3	9.965E-1	5.053E-1±2.251E-2
48-Cd-110	2.346E-1	2.349E-1	2.370E-1±2.000E-3	9.986E-1	1.009E+0±8.513E-3
48-Cd-111	9.224E-1	9.238E-1	7.540E-1±1.200E-2	9.985E-1	8.162E-1±1.299E-2
48-Cd-112	2.195E-1	2.179E-1	1.879E-1±1.700E-3	1.007E+0	8.624E-1±7.802E-3
48-Cd-113	6.265E-1	6.822E-1	6.670E-1±1.100E-2	9.183E-1	9.777E-1±1.612E-2
48-Cd-114	1.493E-1	1.497E-1	1.292E-1±1.300E-3	9.970E-1	8.628E-1±8.681E-3
48-Cd-115M	2.249E-1	2.249E-1	6.010E-1±2.000E-1^T	1.000E+0	2.672E+0±8.893E-1
48-Cd-116	9.022E-2	9.078E-2	7.480E-2±9.000E-4	9.938E-1	8.239E-1±9.914E-3
49-In-113	9.221E-1	9.221E-1	7.870E-1±7.000E-2	1.000E+0	8.535E-1±7.591E-2
49-In-115	7.714E-1	7.715E-1	7.060E-1±7.000E-2	9.999E-1	9.152E-1±9.074E-2
50-Sn-112	1.956E-1	1.956E-1	2.100E-1±1.200E-2	1.000E+0	1.074E+0±6.136E-2
50-Sn-113	6.708E-1	6.708E-1		1.000E+0	
50-Sn-114	1.532E-1	1.532E-1	1.344E-1±1.800E-3	1.000E+0	8.774E-1±1.175E-2
50-Sn-115	3.912E-1	3.912E-1	3.424E-1±8.700E-3	1.000E+0	8.753E-1±2.224E-2
50-Sn-116	1.003E-1	1.003E-1	9.160E-2±6.000E-4	1.000E+0	9.137E-1±5.985E-3
50-Sn-117	3.091E-1	3.091E-1	3.188E-1±4.800E-3	1.000E+0	1.031E+0±1.553E-2
50-Sn-118	6.530E-2	6.530E-2	6.210E-2±6.000E-4	9.999E-1	9.509E-1±9.188E-3
50-Sn-119	2.247E-1	2.247E-1	1.800E-1±1.000E-2	9.998E-1	8.009E-1±4.450E-2
50-Sn-120	3.798E-2	3.798E-2	3.620E-2±3.000E-4	1.000E+0	9.531E-1±7.899E-3
50-Sn-122	1.486E-2	1.486E-2	2.190E-2±1.500E-3	9.999E-1	1.474E+0±1.009E-1
50-Sn-123	3.602E-1	3.602E-1		9.999E-1	
50-Sn-124	1.182E-2	1.182E-2	1.200E-2±1.800E-3	9.999E-1	1.015E+0±1.523E-1
50-Sn-125	9.814E-2	9.814E-2	5.900E-2±9.000E-3^T	1.000E+0	6.012E-1±9.171E-2
50-Sn-126	1.081E-2	1.081E-2	1.000E-2±4.000E-3^T	9.998E-1	9.249E-1±3.700E-1
51-Sb-121	5.109E-1	5.109E-1	5.320E-1±1.600E-2	1.000E+0	1.041E+0±3.132E-2
51-Sb-123	3.210E-1	3.210E-1	3.030E-1±9.000E-3	1.000E+0	9.439E-1±2.804E-2
51-Sb-124	9.688E-1	9.688E-1		1.000E+0	
51-Sb-125	5.257E-1	5.257E-1	2.600E-1±7.000E-2^T	9.999E-1	4.945E-1±1.331E-1
51-Sb-126	7.352E-1	7.352E-1		1.000E+0	
52-Te-120	2.912E-1	2.912E-1	5.380E-1±2.600E-2	9.998E-1	1.847E+0±8.927E-2
52-Te-122	2.349E-1	2.349E-1	2.950E-1±3.000E-3	1.000E+0	1.256E+0±1.277E-2
52-Te-123	8.063E-1	8.063E-1	8.320E-1±8.000E-3	1.000E+0	1.032E+0±9.922E-3
52-Te-124	1.351E-1	1.351E-1	1.550E-1±2.000E-3	1.000E+0	1.147E+0±1.481E-2
52-Te-125	4.172E-1	4.172E-1	4.310E-1±4.000E-3	1.000E+0	1.033E+0±9.588E-3
52-Te-126	7.961E-2	7.961E-2	8.130E-2±1.400E-3	1.000E+0	1.021E+0±1.758E-2
52-Te-127M	8.866E-1	8.866E-1		1.000E+0	
52-Te-128	3.697E-2	3.697E-2	4.440E-2±1.300E-3	1.000E+0	1.201E+0±3.516E-2
52-Te-129M	7.481E-1	7.481E-1		1.000E+0	
52-Te-130	1.429E-2	1.429E-2	1.470E-2±2.800E-3	1.000E+0	1.029E+0±1.960E-1
52-Te-132	1.485E-2	1.485E-2		1.000E+0	
53-I -127	7.228E-1	7.229E-1±9.694E-2	6.350E-1±3.000E-2	9.999E-1	8.785E-1±4.150E-2
53-I -129	4.381E-1	4.381E-1±8.500E-2		9.999E-1	
53-I -130	6.874E-1	6.874E-1		1.000E+0	
53-I -131	2.629E-1	2.629E-1		9.999E-1	
53-I -135	7.019E-3	7.020E-3		9.999E-1	
54-Xe-123	1.802E+0	1.796E+0		1.004E+0	
54-Xe-124	1.150E+0	1.252E+0	6.440E-1±8.300E-2	9.187E-1	5.144E-1±6.630E-2
54-Xe-126	6.716E-1	6.716E-1	3.590E-1±5.100E-2	1.000E+0	5.346E-1±7.594E-2
54-Xe-128	2.826E-1	2.826E-1	2.625E-1±3.700E-3	9.999E-1	9.288E-1±1.309E-2
54-Xe-129	4.198E-1	4.198E-1	6.170E-1±1.200E-2	1.000E+0	1.470E+0±2.859E-2
54-Xe-130	1.518E-1	1.518E-1	1.320E-1±2.100E-3	9.997E-1	8.693E-1±1.383E-2

TABLE XLI: Maxwellian-averaged cross sections (continued).

Material	**VII.0** (barns)	**VII.1** (barns)	**KADoNiS** (barns)	**VII.0/VII.1**	**KADoNiS/VII.1**
54-Xe-131	3.060E-1	3.060E-1±4.161E-2	3.400E-1±6.500E-2^{T}	1.000E+0	1.111E+0±2.124E-1
54-Xe-132	4.727E-2	4.727E-2±1.117E-2	6.460E-2±5.300E-3	9.999E-1	1.367E+0±1.121E-1
54-Xe-133	1.273E-1	1.273E-1	1.270E-1±3.400E-2^{T}	1.000E+0	9.979E-1±2.672E-1
54-Xe-134	2.256E-2	2.256E-2±4.969E-3	2.020E-2±1.700E-3	9.998E-1	8.952E-1±7.534E-2
54-Xe-135	6.543E-2	6.543E-2		1.000E+0	
54-Xe-136	1.185E-3	1.185E-3	9.100E-4±8.000E-5	9.997E-1	7.677E-1±6.749E-2
55-Cs-133	5.114E-1	4.646E-1±5.528E-2	5.090E-1±2.100E-2	1.101E+0	1.096E+0±4.520E-2
55-Cs-134	1.156E+0	1.156E+0	7.240E-1±6.500E-2^{T}	1.000E+0	6.263E-1±5.623E-2
55-Cs-135	2.009E-1	2.009E-1±3.981E-2	1.600E-1±1.000E-2	1.000E+0	7.965E-1±4.978E-2
55-Cs-136	1.820E-1	1.820E-1		9.997E-1	
55-Cs-137	2.162E-2	2.162E-2		1.000E+0	
56-Ba-130	7.360E-1	7.360E-1	7.460E-1±3.400E-2	1.000E+0	1.014E+0±4.619E-2
56-Ba-132	4.559E-1	4.559E-1	3.970E-1±1.600E-2	9.999E-1	8.707E-1±3.509E-2
56-Ba-133	5.688E-1	5.688E-1		1.000E+0	
56-Ba-134	2.270E-1	2.270E-1	1.760E-1±5.600E-3	1.000E+0	7.753E-1±2.467E-2
56-Ba-135	4.839E-1	4.839E-1	4.550E-1±1.500E-2	1.000E+0	9.402E-1±3.100E-2
56-Ba-136	7.001E-2	7.001E-2	6.120E-2±2.000E-3	1.000E+0	8.742E-1±2.857E-2
56-Ba-137	5.869E-2	5.869E-2	7.630E-2±2.400E-3	1.000E+0	1.300E+0±4.089E-2
56-Ba-138	3.739E-3	3.739E-3	4.000E-3±2.000E-4	1.000E+0	1.070E+0±5.350E-2
56-Ba-140	1.030E-2	1.030E-2		1.000E+0	
57-La-138	3.132E-1	3.132E-1	4.190E-1±5.900E-2^{T}	1.000E+0	1.338E+0±1.884E-1
57-La-139	3.625E-2	3.625E-2±5.677E-3	3.240E-2±3.100E-3	9.999E-1	8.937E-1±8.551E-2
57-La-140	1.175E-1	1.175E-1		9.999E-1	
58-Ce-136	3.380E-1	3.380E-1	3.280E-1±2.100E-2	1.000E+0	9.704E-1±6.213E-2
58-Ce-138	2.080E-1	2.080E-1	1.790E-1±5.000E-3	1.000E+0	8.607E-1±2.404E-2
58-Ce-139	4.074E-1	4.074E-1	2.140E-1±1.200E-1^{T}	1.000E+0	5.253E-1±2.946E-1
58-Ce-140	7.739E-3	7.739E-3	1.100E-2±4.000E-4	1.000E+0	1.421E+0±5.169E-2
58-Ce-141	2.754E-1	2.754E-1±5.527E-2	7.600E-2±3.300E-2^{T}	1.000E+0	2.760E-1±1.198E-1
58-Ce-142	1.989E-2	1.989E-2	2.800E-2±1.000E-3	9.998E-1	1.407E+0±5.027E-2
58-Ce-143	1.142E-1	1.142E-1		1.000E+0	
58-Ce-144	2.423E-2	2.423E-2		9.999E-1	
59-Pr-141	1.090E-1	1.090E-1±1.096E-2	1.114E-1±1.400E-3	1.000E+0	1.022E+0±1.285E-2
59-Pr-142	3.612E-1	3.612E-1	4.150E-1±1.780E-1^{T}	1.000E+0	1.149E+0±4.928E-1
59-Pr-143	1.076E-1	1.076E-1	3.500E-1±8.600E-2^{T}	1.000E+0	3.254E+0±7.994E-1
60-Nd-142	3.344E-2	3.343E-2	3.500E-2±7.000E-4	1.000E+0	1.047E+0±2.094E-2
60-Nd-143	2.383E-1	2.383E-1±3.015E-2	2.450E-1±3.000E-3	9.999E-1	1.028E+0±1.259E-2
60-Nd-144	7.485E-2	7.485E-2	8.130E-2±1.500E-3	1.000E+0	1.086E+0±2.004E-2
60-Nd-145	4.128E-1	4.200E-1±4.633E-2	4.250E-1±5.000E-3	9.828E-1	1.012E+0±1.190E-2
60-Nd-146	9.852E-2	9.852E-2±1.133E-2	9.120E-2±1.000E-3	1.000E+0	9.257E-1±1.015E-2
60-Nd-147	8.336E-1	8.336E-1	5.440E-1±9.000E-2^{T}	1.000E+0	6.526E-1±1.080E-1
60-Nd-148	1.401E-1	1.401E-1±1.503E-2	1.470E-1±2.000E-3	1.000E+0	1.049E+0±1.428E-2
60-Nd-150	1.565E-1	1.565E-1	1.590E-1±1.000E-2	9.999E-1	1.016E+0±6.389E-2
61-Pm-147	1.047E+0	1.047E+0±1.980E-1	7.090E-1±1.000E-1	1.000E+0	6.772E-1±9.552E-2
61-Pm-148	1.701E+0	1.701E+0	2.970E+0±5.000E-1^{T}	1.000E+0	1.746E+0±2.940E-1
61-Pm-148M	7.210E+0	7.210E+0	2.453E+0±1.200E+0^{T}	1.000E+0	3.402E-1±1.664E-1
61-Pm-149	1.021E+0	1.021E+0	2.510E+0±7.500E-1^{T}	9.998E-1	2.458E+0±7.345E-1
61-Pm-151	1.024E+0	1.024E+0		1.000E+0	
62-Sm-144	8.767E-2	8.767E-2	9.200E-2±6.000E-3	1.000E+0	1.049E+0±6.844E-2
62-Sm-147	9.667E-1	9.667E-1	9.730E-1±1.000E-2	1.000E+0	1.007E+0±1.034E-2
62-Sm-148	2.449E-1	2.449E-1	2.410E-1±2.000E-3	1.000E+0	9.842E-1±8.168E-3
62-Sm-149	1.780E+0	1.780E+0±3.937E-1	1.820E+0±1.700E-2	1.000E+0	1.022E+0±9.550E-3
62-Sm-150	4.227E-1	4.227E-1	4.220E-1±4.000E-3	1.000E+0	9.984E-1±9.463E-3
62-Sm-151	2.874E+0	2.874E+0±8.487E-1	3.031E+0±6.800E-2	1.000E+0	1.055E+0±2.366E-2
62-Sm-152	4.583E-1	4.583E-1±5.651E-2	4.730E-1±4.000E-3	9.999E-1	1.032E+0±8.727E-3
62-Sm-153	9.111E-1	9.110E-1	1.095E+0±1.750E-1^{T}	1.000E+0	1.202E+0±1.921E-1
62-Sm-154	2.794E-1	2.794E-1	2.060E-1±9.000E-3	1.000E+0	7.374E-1±3.221E-2
63-Eu-151	3.568E+0	3.568E+0	3.478E+0±7.700E-2	1.000E+0	9.748E-1±2.158E-2
63-Eu-152	4.560E+0	4.560E+0	7.600E+0±1.200E+0^{T}	9.999E-1	1.667E+0±2.631E-1
63-Eu-153	2.464E+0	2.663E+0±6.139E-1	2.556E+0±4.600E-2	9.252E-1	9.597E-1±1.727E-2
63-Eu-154	3.470E+0	3.470E+0	4.420E+0±6.700E-1	9.999E-1	1.274E+0±1.931E-1
63-Eu-155	1.134E+0	1.134E+0±2.165E-1	1.320E+0±8.400E-2	1.000E+0	1.164E+0±7.410E-2
63-Eu-156	5.410E-1	5.410E-1		1.000E+0	
63-Eu-157	1.141E+0	1.141E+0		1.000E+0	
64-Gd-152	9.844E-1	9.844E-1±3.445E-2	1.049E+0±1.700E-2	1.000E+0	1.066E+0±1.727E-2
64-Gd-153	2.622E+0	2.622E+0±8.573E-1	4.550E+0±7.000E-1^{T}	1.000E+0	1.735E+0±2.670E-1
64-Gd-154	9.511E-1	9.511E-1±3.805E-2	1.028E+0±1.200E-2	1.000E+0	1.081E+0±1.262E-2
64-Gd-155	2.613E+0	2.613E+0±1.280E-1	2.648E+0±3.000E-2	1.000E+0	1.013E+0±1.148E-2
64-Gd-156	5.984E-1	5.984E-1±2.573E-2	6.150E-1±5.000E-3	1.000E+0	1.028E+0±8.355E-3
64-Gd-157	1.394E+0	1.396E+0±4.941E-2	1.369E+0±1.500E-2	9.988E-1	9.809E-1±1.075E-2
64-Gd-158	3.069E-1	3.069E-1±1.298E-2	3.240E-1±3.000E-3	9.999E-1	1.056E+0±9.774E-3
64-Gd-160	1.712E-1	1.712E-1±1.649E-2	1.540E-1±2.000E-2	9.999E-1	8.994E-1±1.168E-1
65-Tb-159	2.075E+0	2.075E+0	1.580E+0±1.500E-1	1.000E+0	7.616E-1±7.231E-2
65-Tb-160	2.389E+0	2.389E+0	3.240E+0±5.100E-1^{T}	9.998E-1	1.356E+0±2.134E-1
66-Dy-156	1.532E+0	1.532E+0	1.607E+0±9.200E-2	9.997E-1	1.049E+0±6.004E-2
66-Dy-158	1.115E+0	1.115E+0	1.060E+0±4.000E-1^{T}	1.000E+0	9.507E-1±3.588E-1
66-Dy-160	8.328E-1	8.328E-1	8.900E-1±1.200E-2	1.000E+0	1.069E+0±1.441E-2

TABLE XLI: Maxwellian-averaged cross sections (continued).

Material	**VII.0** (barns)	**VII.1** (barns)	**KADoNiS** (barns)	**VII.0/VII.1**	**KADoNiS/VII.1**
66-Dy-161	1.951E+0	1.951E+0	1.964E+0±1.900E-2	9.998E-1	1.006E+0±9.737E-3
66-Dy-162	4.544E-1	4.544E-1	4.460E-1±4.000E-3	9.999E-1	9.815E-1±8.802E-3
66-Dy-163	1.085E+0	1.085E+0	1.112E+0±1.100E-2	1.000E+0	1.025E+0±1.014E-2
66-Dy-164	2.168E-1	2.168E-1	2.120E-1±3.000E-3	1.000E+0	9.779E-1±1.384E-2
67-Ho-165	1.328E+0	1.329E+0	1.280E+0±1.000E-1	9.996E-1	9.635E-1±7.527E-2
67-Ho-166M	1.182E+0	1.182E+0		9.998E-1	
68-Er-162	8.679E-1	8.679E-1	1.624E+0±1.240E-1	1.000E+0	1.871E+0±1.429E-1
68-Er-164	1.924E+0	1.924E+0	1.084E+0±5.100E-2	9.999E-1	5.634E-1±2.651E-2
68-Er-166	6.976E-1	6.977E-1±7.214E-2	5.630E-1±5.600E-2	9.999E-1	8.070E-1±8.027E-2
68-Er-167	1.553E+0	1.554E+0±2.464E-1	1.425E+0±1.430E-1	9.996E-1	9.172E-1±9.204E-2
68-Er-168	3.022E-1	3.022E-1±3.430E-2	3.380E-1±4.400E-2	1.000E+0	1.119E+0±1.456E-1
68-Er-170	2.156E-1	2.156E-1±4.279E-2	1.700E-1±7.000E-3	1.000E+0	7.887E-1±3.247E-2
69-Tm-168		2.060E+0			
69-Tm-169		1.104E+0	1.129E+0±5.600E-2		1.022E+0±5.071E-2
69-Tm-170		1.622E+0	1.870E+0±3.300E-1^T		1.153E+0±2.035E-1
71-Lu-175	1.315E+0	1.315E+0	1.219E+0±1.000E-2	9.999E-1	9.269E-1±7.603E-3
71-Lu-176	1.540E+0	1.540E+0	1.639E+0±1.400E-2	1.000E+0	1.064E+0±9.092E-3
72-Hf-174	6.848E-1	9.496E-1	9.830E-1±4.600E-2	7.211E-1	1.035E+0±4.844E-2
72-Hf-176	4.571E-1	4.531E-1	6.260E-1±1.100E-2	1.009E+0	1.381E+0±2.427E-2
72-Hf-177	1.381E+0	1.387E+0	1.544E+0±1.200E-2	9.953E-1	1.113E+0±8.649E-3
72-Hf-178	3.044E-1	2.960E-1	3.190E-1±3.000E-3	1.028E+0	1.078E+0±1.014E-2
72-Hf-179	9.756E-1	9.788E-1	9.220E-1±8.000E-3	9.967E-1	9.420E-1±8.173E-3
72-Hf-180	1.741E-1	2.320E-1	1.570E-1±2.000E-3	7.503E-1	6.766E-1±8.619E-3
73-Ta-180		1.753E+0	1.465E+0±1.000E-1		8.359E-1±5.706E-2
73-Ta-181	7.923E-1	8.501E-1	7.660E-1±1.500E-2	9.321E-1	9.011E-1±1.765E-2
73-Ta-182	1.036E+0	1.036E+0	1.120E+0±1.800E-1^T	1.000E+0	1.081E+0±1.738E-1
74-W -180		5.598E-1±1.220E-1	6.600E-1±5.300E-2		1.179E+0±9.468E-2
74-W -182	3.025E-1	2.920E-1±1.139E-2	2.740E-1±8.000E-3	1.036E+0	9.384E-1±2.740E-2
74-W -183	5.278E-1	5.747E-1±2.552E-2	5.150E-1±1.500E-2	9.183E-1	8.961E-1±2.610E-2
74-W -184	2.218E-1	2.522E-1±1.689E-2	2.230E-1±5.000E-3	8.796E-1	8.844E-1±1.983E-2
74-W -186	1.820E-1	1.921E-1±4.860E-3	2.350E-1±9.000E-3	9.475E-1	1.223E+0±4.686E-2
75-Re-185	1.061E+0	1.168E+0	1.535E+0±6.200E-2	9.084E-1	1.314E+0±5.308E-2
75-Re-187	9.226E-1	1.015E+0	1.160E+0±5.700E-2	9.090E-1	1.143E+0±5.616E-2
77-Ir-191	1.271E+0	1.271E+0±1.144E-1	1.350E+0±4.300E-2	1.000E+0	1.062E+0±3.383E-2
77-Ir-193	1.118E+0	1.118E+0±1.264E-1	9.940E-1±7.000E-2	9.998E-1	8.889E-1±6.260E-2
79-Au-197	6.126E-1	6.127E-1±7.720E-3	5.820E-1±9.000E-3	9.999E-1	9.499E-1±1.469E-2
80-Hg-196	3.441E-2	3.441E-2	2.040E-1±8.000E-3	1.000E+0	5.929E+0±2.325E-1
80-Hg-198	1.613E-1	1.613E-1	1.730E-1±1.500E-2	1.000E+0	1.073E+0±9.301E-2
80-Hg-199	3.911E-1	3.911E-1	3.740E-1±2.300E-2	9.999E-1	9.562E-1±5.881E-2
80-Hg-200	1.277E-1	1.277E-1	1.150E-1±1.200E-2	1.000E+0	9.007E-1±9.398E-2
80-Hg-201	2.555E-1	2.555E-1	2.640E-1±1.400E-2	1.000E+0	1.033E+0±5.479E-2
80-Hg-202	8.530E-2	8.530E-2	6.320E-2±1.900E-3	9.999E-1	7.409E-1±2.227E-2
80-Hg-204	4.325E-2	4.325E-2	4.200E-2±4.000E-3	1.000E+0	9.711E-1±9.248E-2
81-Tl-203		1.704E-1	1.240E-1±8.000E-3		7.275E-1±4.694E-2
81-Tl-205		5.256E-2	5.400E-2±4.000E-3		1.027E+0±7.610E-2
82-Pb-204	7.242E-2	7.242E-2±2.897E-3	8.100E-2±2.300E-3	1.000E+0	1.118E+0±3.176E-2
82-Pb-206	1.359E-2	1.359E-2±4.349E-4	1.450E-2±3.000E-4	9.999E-1	1.067E+0±2.207E-2
82-Pb-207	8.259E-3	8.259E-3±8.259E-4	9.900E-3±5.000E-4	1.000E+0	1.199E+0±6.054E-2
82-Pb-208	6.553E-4	6.553E-4±3.277E-4	3.600E-4±3.000E-5	1.000E+0	5.493E-1±4.578E-2
83-Bi-209	3.345E-3	3.344E-3±6.020E-4	2.560E-3±3.000E-4	1.000E+0	7.654E-1±8.970E-2
88-Ra-223	5.987E-1	5.988E-1		9.999E-1	
88-Ra-224	2.258E-1	2.258E-1		9.998E-1	
88-Ra-225	6.502E-1	6.503E-1		9.998E-1	
88-Ra-226	4.459E-1	4.459E-1		1.000E+0	
89-Ac-225	1.551E+0	1.879E+0±5.674E-1		8.255E-1	
89-Ac-226	2.007E+0	2.224E+0±6.739E-1		9.024E-1	
89-Ac-227	8.546E-2	1.361E+0±3.673E-1		6.281E-2	
90-Th-227	1.388E+0	1.173E+0±6.415E-1		1.184E+0	
90-Th-228	4.268E-1	7.476E-1±1.914E-1		5.709E-1	
90-Th-229	1.396E+0	1.708E+0±4.099E-1		8.174E-1	
90-Th-230	2.107E-1	6.989E-1±1.679E-1		3.015E-1	
90-Th-231		1.539E+0±6.048E-1			
90-Th-232	4.848E-1	4.868E-1±7.545E-2		9.960E-1	
90-Th-233	5.706E-1	5.987E-1±2.874E-1		9.531E-1	
90-Th-234	4.301E-1	1.769E-1±5.963E-2		2.431E+0	
91-Pa-229		1.764E+0±2.162E+0			
91-Pa-230		6.925E-1±6.046E-1			
91-Pa-231	2.086E+0	2.086E+0		9.999E-1	
91-Pa-232	1.125E+0	4.309E-1±2.668E-1		2.611E+0	
91-Pa-233	2.245E+0	2.245E+0		1.000E+0	
92-U -230		4.149E-1±3.531E-1			
92-U -231		4.898E-1±4.684E-1			
92-U -232	7.671E-1	6.345E-1±1.948E-1		1.209E+0	
92-U -233	4.240E-1	4.240E-1±6.106E-2		9.999E-1	
92-U -234	5.641E-1	5.641E-1		1.000E+0	
92-U -235	6.938E-1	6.926E-1±2.244E-1		1.002E+0	
92-U -236	5.456E-1	5.505E-1±2.753E-2		9.910E-1	
92-U -237	4.532E-1	4.580E-1		9.894E-1	
92-U -238	4.014E-1	4.004E-1±6.166E-3		1.003E+0	

TABLE XLI: Maxwellian-averaged cross sections (continued).

Material	**VII.0** (barns)	**VII.1** (barns)	**KADoNiS** (barns)	**VII.0/VII.1**	**KADoNiS/VII.1**
92-U -239	8.416E-1	9.204E-1		9.144E-1	
92-U -240	3.171E-1	3.171E-1		1.000E+0	
92-U -241	8.838E-1	8.839E-1		9.998E-1	
93-Np-234		2.013E-1±1.843E-1			
93-Np-235	1.011E+0	2.002E+0±1.485E+0		5.051E-1	
93-Np-236	6.380E-1	4.184E-1±3.962E-1		1.525E+0	
93-Np-237	2.114E+0	2.114E+0±1.818E-1		9.998E-1	
93-Np-238	5.313E-1	5.218E-1±2.348E-1		1.018E+0	
93-Np-239	2.549E+0	1.644E+0±4.668E-1		1.551E+0	
94-Pu-236	3.325E-1	2.492E-1±1.119E-1		1.334E+0	
94-Pu-237	2.438E-1	3.741E-1±3.782E-1		6.518E-1	
94-Pu-238	9.023E-1	7.687E-1±7.840E-2		1.174E+0	
94-Pu-239	5.292E-1	5.278E-1±5.489E-2		1.003E+0	
94-Pu-240	6.847E-1	6.912E-1±2.765E-2		9.905E-1	
94-Pu-241	5.518E-1	5.518E-1±9.166E-2		9.999E-1	
94-Pu-242	5.825E-1	5.320E-1±1.703E-2		1.095E+0	
94-Pu-243	4.572E-1	4.572E-1		1.000E+0	
94-Pu-244	1.956E-1	3.269E-1±8.958E-2		5.983E-1	
94-Pu-246	2.518E+0	2.041E-1±7.818E-2		1.233E+1	
95-Am-240		5.794E-1±4.879E-1			
95-Am-241	2.493E+0	2.546E+0±7.639E-2		9.791E-1	
95-Am-242	5.468E-1	5.468E-1		1.000E+0	
95-Am-242M	6.526E-1	6.526E-1±3.263E-1		1.000E+0	
95-Am-243	2.098E+0	2.429E+0±2.216E-1		8.636E-1	
95-Am-244	8.809E-1	8.809E-1		1.000E+0	
95-Am-244M	8.532E-1	8.532E-1		1.000E+0	
96-Cm-240		1.043E+0±8.151E-1			
96-Cm-241	2.756E-1	2.292E-1±2.585E-1		1.202E+0	
96-Cm-242	3.337E-1	1.028E+0±2.478E-1		3.245E-1	
96-Cm-243	7.432E-1	4.560E-1±3.106E-1		1.630E+0	
96-Cm-244	8.797E-1	7.735E-1±2.027E-1		1.137E+0	
96-Cm-245	7.120E-1	5.968E-1±3.177E-1		1.193E+0	
96-Cm-246	6.534E-1	4.631E-1±1.176E-1		1.411E+0	
96-Cm-247	7.462E-1	4.295E-1±2.547E-1		1.737E+0	
96-Cm-248	3.076E-1	2.866E-1±7.279E-2		1.073E+0	
96-Cm-249	1.675E-1	1.896E-1±2.151E-1		8.832E-1	
96-Cm-250	1.395E-1	1.989E-1±6.829E-2		7.012E-1	
97-Bk-245		2.614E+0±1.146E+0			
97-Bk-246		1.076E+0±1.016E+0			
97-Bk-247		1.921E+0±7.760E-1			
97-Bk-248		1.198E+0±1.166E+0			
97-Bk-249	1.786E+0	1.572E+0±3.003E-1		1.136E+0	
97-Bk-250	6.798E-1	1.168E+0±1.299E+0		5.822E-1	
98-Cf-246		8.632E-1±4.526E-1			
98-Cf-248		5.802E-1±1.870E-1			
98-Cf-249	8.553E-1	7.448E-1±3.292E-1		1.148E+0	
98-Cf-250	4.373E-1	4.343E-1±9.771E-2		1.007E+0	
98-Cf-251	4.211E-1	5.564E-1±4.023E-1		7.568E-1	
98-Cf-252	4.044E-1	1.489E-1±4.946E-2		2.716E+0	
98-Cf-253	7.521E-2	8.886E-1±4.398E-1		8.464E-2	
98-Cf-254	9.138E-2	1.568E-1±9.142E-2		5.827E-1	
99-Es-251		1.574E+0±6.069E-1			
99-Es-252		4.542E-1±4.524E-1			
99-Es-253	4.324E-2	2.025E+0±1.115E+0		2.136E-2	
99-Es-254	6.582E-1	1.012E+0±5.978E-1		6.502E-1	
99-Es-254M		5.370E-1±5.254E-1			
99-Es-255	6.787E-1	2.163E+0±1.467E+0		3.138E-1	
100-Fm-255	3.296E-1	3.130E-1±3.922E-1		1.053E+0	